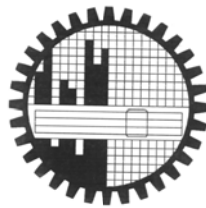


CONFINEMENT EFFECT OF FIBER REINFORCED  
POLYMER WRAPS ON CIRCULAR AND SQUARE  
CONCRETE COLUMNS.

MD. SHAHNEWAZ ISLAM CHOUDHURY



DEPARTMENT OF CIVIL ENGINEERING  
BANGLADESH UNIVERSITY OF ENGINEERING AND TECHNOLOGY  
DHAKA 1000, BANGLADESH

MARCH, 2012

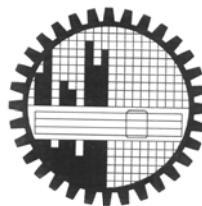
CONFINEMENT EFFECT OF FIBER REINFORCED  
POLYMER WRAPS ON CIRCULAR AND SQUARE  
CONCRETE COLUMNS.

A THESIS

SUBMITTED TO THE DEPARTMENT OF CIVIL ENGINEERING  
IN PARTIAL FULFILMENT OF THE REQUIREMENTS FOR THE DEGREE OF

MASTER OF SCIENCE IN CIVIL AND STRUCTURAL ENGINEERING

BY  
MD. SHAHNEWAZ ISLAM CHOUDHURY



DEPARTMENT OF CIVIL ENGINEERING  
BANGLADESH UNIVERSITY OF ENGINEERING AND TECHNOLOGY  
DHAKA 1000, BANGLADESH

MARCH, 2012

*TO MY  
PARENTS, FAMILY AND TEACHERS*

The thesis titled “**Confinement Effect of Fiber Reinforced Polymer Wraps on Circular and Square Concrete Columns**” submitted by Md. Shahnewaz Islam Choudhury, Student No. 100704302 (P), and Session: October 2007 has been accepted as satisfactory in partial fulfilment of the requirement for the degree of M.Sc. Engineering (Civil and Structural) on 28<sup>th</sup> March, 2012.

### **BOARD OF EXAMINERS**

---

**Dr. A.F.M. Saiful Amin**  
Professor  
Department of Civil Engineering  
BUET, Dhaka

Chairman  
(Supervisor)

---

**Dr. Md. Mujibur Rahman**  
Professor and Head  
Department of Civil Engineering  
BUET, Dhaka

Member  
(Ex-officio)

---

**Dr. Syed Ishtiaq Ahmad**  
Professor  
Department of Civil Engineering  
BUET, Dhaka

Member

---

**Dr. Md. Abdur Rahman Bhuiyan**  
Associate Professor  
Department of Civil Engineering  
CUET, Chittagong

Member  
(External)



## **DECLARATION**

It is hereby declared that, except where specific references are made, the work embodied in this thesis is the result of investigation carried out by the author under the supervision of Dr. A.F.M. Saiful Amin, Professor, Department of Civil Engineering, BUET.

Neither this thesis nor any part of it is concurrently submitted to any other institution in candidature for any degree.

---

Author

## ACKNOWLEDGEMENT

---

The author wishes to express his deepest gratitude to his supervisor Dr. A.F.M. Saiful Amin, Professor, Department of Civil Engineering, Bangladesh University of Engineering & Technology (BUET), for his constant guidance, continuous encouragements, generous help and unfailing enthusiasm to carry out the research. His active interest in this topic and valuable advice were the source where the author got deep inspiration.

The author owes his thanks to the members of the Board of Post Graduate Studies of the Department of Civil Engineering, BUET and also to the members of the committee of Advanced Studies and Research for kindly approving the research proposal and financing the experimental work reported in this thesis. The author is grateful to LaMaCo Sdn Bhd and Aziz & Company for their generous donation of confining materials used in the research.

The author would like express his gratefulness to Mr. Shameem Ahmed, Assistant Professor, Department of Civil Engineering, BUET for his cordial help in testing of specimens. Special thanks go to Md. Mashfiqul Islam, Assistant Professor, Department of Civil Engineering, AUST and Md. Abdulla, undergraduate student of the Department of Civil Engineering, BUET for their assistance in the research work. The author is also grateful to Mr. A.K.M. Jahangir Alam, Superintending Engineer, Engineering Office, BUET, for his kind support during the present study.

Special thanks also go to the staffs and technicians of the Concrete Laboratory and Structural Mechanics Laboratory of BUET for their cooperation in conducting difficult works related to specimen preparation and testing.

The author is grateful to his mother, Nur Negar Sultana and other members of his family for their deep support and love for him during his research work. Above all, he is grateful to the Almighty Allah for allowing him to bring this thesis to its satisfactory completion.

Effectiveness of confinement in concrete columns due to the variations of cross sectional geometry and sizes is studied by experiments. Confining pressures in the columns wrapped with fiber reinforced polymers (FRP) are engaged by the transverse dilation of concrete that in turn increases the axial load capacity. Concretes made of aggregates with higher porosity and lower density offer lower modulus of elasticity and higher Poisson's ratio. This property in turn increases larger dilation effect. However, the magnitude of dilation effect is further related to the stress field of concrete section under load. In this context, the curvature and size of the columns are varied to investigate the effect of geometric parameters i.e. radius of curvature, column side to corner radius ratio, FRP volumetric ratio and rigidity ratio on dilation.

To realize the experimental data, a total of 60 circular and 60 square short concrete columns made of stone, brick, recycled stone and recycled brick aggregate were cast and tested. Carbon-FRP (CFRP) and glass-FRP (GFRP) bonded to the surface of concrete with epoxy offered different confining effect on the specimens. Circular columns varied in their curvatures while the square columns had a constant curvature at the corners. Dilation effects of concrete are measured by using a simultaneous data acquisition system. The load and displacement histories of square and circular confined concrete columns obtained from the load cell of a computer controlled universal testing machine. The data are synthesized with the strain measurement results assembled from high speed (60 frames per second) video clips and high definition images. In this process, the confinement due to dilation of concrete for different aggregate types and cross-sections are evaluated and compared. To assess the Poisson's ratio in concrete with different aggregates, numerical trials on nonlinear finite element (FE) platform are conducted using ANSYS 10.0.

The dilation effect in brick aggregate concrete was found to be distinctly larger than the stone aggregate concrete. The Poisson's ratio of stone aggregate concrete was also evaluated convincingly to be lower than brick aggregate concrete, recycled stone aggregate concrete and recycled brick aggregate concrete by FE analysis and the values were estimated at 0.25, 0.35, 0.37 and 0.40, respectively. Dilation of concrete in square columns is found to be larger than circular columns. Axial capacity increases as the

dilation of concrete increases both for circular and square concrete columns made of different aggregates. The size and curvature effects on confinement are more pronounced for circular columns. There exists no such effect for square columns with the same corner radius except for ultimate axial strain of square columns. Results of FE simulations are found to be in reasonable conformities with the experimental result indicating validity of the FE models. The stress-strain model considering size and curvature of the columns, the Poisson's ratios, dilation characteristics and modulus of elasticity is proposed for brick, stone, recycled brick and recycled stone aggregate concrete. The proposed general models for square and circular columns have shown a good agreement with experimental results. ACI 440 model (2002), Lam and Teng's model (2003b), Kumutha et al. model (2007) and Wu and Wang model (2009) showed considerable similarities with the test results of square columns. ACI 440 model (2002) matched significantly with the test results for circular columns.

<b>Title</b>	<b>Page</b>
DECLARATION	v
ACKNOWLEDGEMENT	vi
ABSTRACT	vii
CONTENTS	ix
NOTATIONS AND SYMBOLS	xv
Chapter 1: INTRODUCTION	1
1.1 General	1
1.2 FRP confining system	1
1.3 Dilation effect and confinement in different prismatic sections	3
1.4 Limitations of available confinement models	6
1.5 Finite element models	7
1.6 Objective of research	7
1.7 Scope and methodology	8
Chapter 2: LITERATURE REVIEW	11
2.1 General	11
2.2 Materials used for confining concrete	11
2.2.1 Fiber reinforced polymer wraps	11
2.2.1.1 Glass fiber reinforced polymers (GFRP)	12
2.2.1.2 Carbon fiber reinforced polymers(CFRP)	15
2.2.1.3 Aramid fiber reinforced polymers(AFRP)	17
2.2.1.4 Other fibers	18
2.2.2 Resins	19

<b>Title</b>	<b>Page</b>
2.2.2.1 Epoxy resins	19
2.2.2.2 Vinylester resins	20
2.2.2.3 Phenolic resins	21
2.2.2.4 Polyurethane resins	22
2.2.2.5 Other polymer resins	22
2.2.3 Primers and putty	23
2.3 Dilation effect in concrete with different aggregates	25
2.4 Effect of curvature and size	25
2.5 Strength Models of FRP-confined concrete columns	28
2.5.1 Models for FRP confined circular columns	29
2.5.1.1 Saafi <i>et al.</i> (1999)	29
2.5.1.2 ACI 440 model (2002)	29
2.5.1.3 Lam and Teng's model (2003a)	31
2.5.1.4 Youssef et al. model (2007)	31
2.5.1.5 Wu and Wang's model (2009)	31
2.5.2 Models of FRP confined square columns	32
2.5.2.1 Mirmiran et al. model (1998)	32
2.5.2.2 Shehata et al. model (2002)	32
2.5.2.3 Lam and Teng's model (2003b)	33
2.5.2.4 Kumutha et al. model (2007)	34
2.5.2.5 Al-Salloum's model (2007)	34
2.6 Finite element modeling	35
 Chapter 3: MATERIALS	 37
3.1 General	37
3.2 Properties of concrete	37
3.2.1 Portland cement	37

<b>Title</b>	<b>Page</b>
3.2.2 Aggregates	37
3.2.2.1 Fine aggregates	38
3.2.2.2 Coarse aggregates	38
3.2.3 Water	40
3.3 Properties of FRP	40
3.3.1 CFRP wraps	40
3.3.2 GFRP wraps	42
3.4 Properties of adhesives and primers	43
 Chapter 4: EXPERIMENTAL PROGRAM AND DATA ACQUISITION	 46
4.1 General	46
4.2 Size and geometry of specimen	46
4.3 Geometric parameters affecting confinement	49
4.3.1 Radius of curvature	49
4.3.2 Column side to corner radius ratio	51
4.3.3 FRP volumetric ratio	52
4.3.4 Rigidity ratio	54
4.4 Sample size	54
4.5 Specimen preparation	54
4.5.1 Casting and sampling	54
4.5.2 Curing of concrete	55
4.5.3 Surface Preparation	56
4.5.4 Installation of FRP and lapping	56
4.6 Testing and data acquisition	58
4.7 Data correction and synthesis	60
4.8 Specimen designations and legends	61

<b>Title</b>	<b>Page</b>
Chapter 5: EXPERIMENTAL RESULTS AND DISCUSSION	63
5.1 General	63
5.2 Failure patterns	63
5.2.1 Circular columns	63
5.2.2 Square columns	64
5.3 Confinement due to dilation of concrete	65
5.4 Axial capacity enhancement	70
5.5 Effect of geometric parameters	76
5.5.1 Effect of radius of curvature	76
5.5.2 Effect of column side to corner radius ratio	78
5.5.3 Effect of FRP volumetric ratio	81
5.5.4 Effect of Rigidity ratio	85
Chapter 6: FINITE ELEMENT MODELING	88
6.1 General	88
6.2 Dilation due to Poisson's effect	88
6.3 Finite Element (FE) model Formation	89
6.3.1 Element type	89
6.3.2 Real constants	90
6.3.3 Material properties	90
6.3.4 FE mesh	92
6.3.5 Boundary conditions and loading	95
6.3.6 Results and discussion	96
6.3.6.1 Effect of radius of curvature	97
6.3.6.2 Effect of column side to corner radius ratio	105
6.3.6.3 Effect of FRP volumetric ratio	111
6.3.7 Stress contours: simulations and experiments	122



<b>Title</b>	<b>Page</b>
Chapter 7: STRESS-STRAIN MODEL	125
7.1 General	125
7.2 Model for confined compressive strength of concrete	126
7.2.1 Equation for confined circular concrete columns	128
7.2.2 Equation for confined square concrete columns	134
7.3 Validation of the models	141
 Chapter 8: CONCLUSION	 154
8.1 General	154
8.2 Failure patterns	154
8.3 Stress-strain behaviour	155
8.3.1 Dilation of concrete	155
8.3.2 Axial capacity enhancement	156
8.4 Confinement effectiveness affected by geometric parameters	157
8.4.1 Effect of radius of curvature	157
8.4.2 Effect of column side to corner radius ratio	157
8.4.3 Effect of FRP volumetric ratio	158
8.4.4 Effect of rigidity ratio	158
8.5 Finite element modeling	158
8.6 Stress-strain models	159
8.7 Scope of future studies	160
 REFERENCES	 161
 APPENDIX A.1 Failure patterns of brick aggregate concrete columns	 166
APPENDIX A.2 Failure patterns of stone aggregate concrete columns	171
APPENDIX A.3 Failure patterns of recycled brick aggregate concrete columns	176

<b>Title</b>		<b>Page</b>
APPENDIX A.4	Failure patterns of recycled stone aggregate concrete columns	181
APPENDIX B	Stress-strain behaviours	186
APPENDIX C	Validation of the models	194
APPENDIX D.1	Test results of circular concrete columns	200
APPENDIX D.2	Test results of square concrete columns	202

## NOTATIONS AND SYMBOLS

---

$f'_c$	=	Compressive strength of concrete
$f'_{c0}$	=	Unconfined compressive strength of concrete column
$f'_{cc}$	=	Confined compressive strength of concrete column
$\epsilon_c$	=	Compressive strain of concrete
$\epsilon_{c0}$	=	Unconfined compressive strain of concrete column
$\epsilon_{cc}$	=	Confined compressive strain of concrete column
$f_{frp}$	=	Tensile strength of FRP in the hoop direction
$E_{frp}$	=	Elastic modulus of FRP in the hoop direction
$t$	=	Total thickness of FRP
$d$	=	Diameter of the confined concrete core
$\epsilon_j$	=	Hoop tensile strain of FRP at failure
$\epsilon_{frp}$	=	Ultimate tensile strain
$\epsilon_{h,rupt}$	=	Actual hoop rupture strain
$k_e$	=	Strain efficiency factor of FRP
$k_1$	=	Confinement effectiveness coefficient
$f_l$	=	Effective lateral confining pressure
$k_c$	=	Enhancement factor of concrete strength
$f_{l,j1}$	=	Larger values of confinement pressure due to the composite jacket in the x and y directions
$f_{l,j2}$	=	Smaller values of confinement pressure due to the composite jacket in the x and y directions
$h$	=	Depth of the column section
$b$	=	Breadth of the column section
$f_j$	=	Stress of the FRP jacket/wrap
$k_s$	=	Shape factor that accounts for the effect of nonuniform confinement
$D$	=	Diameter of an equivalent circular column
$\rho_f$	=	FRP volumetric ratio
$\epsilon_{fe}$	=	Effective value for nominal hoop rupture strain in the FRP jacket
$\rho_g$	=	Ratio of the area of longitudinal steel reinforcement to the cross-sectional area of a compression member
$\sigma_j$	=	FRP stress due to confinement
$k_i$	=	Reduction factor
$A_g$	=	Gross area of the column section

$f_{l\max}$	=	Maximum effective lateral confinement stress
$\kappa_a$	=	Efficiency factor determined as the ratio of the effectively confined cross-sectional area to the gross area
$E_c$	=	Elastic modulus of the original uncracked concrete
$\varepsilon_{cu}$	=	Ultimate compressive strain of concrete
$\varepsilon'_{cc}$	=	Confined compressive strain of concrete
$k_2$	=	Strain enhancement coefficient
$f'_{cc}/f'_{c0}$	=	Strengthening ratio or confinement effectiveness
$f_l/f'_{c0}$	=	Actual confinement ratio
$\varepsilon_{cc}/\varepsilon_{c0}$	=	Strain enhancement ratio

## 1.1 General

Use of fiber reinforced polymer (FRP) confinement in circular columns for strength enhancement is older than that in the noncircular columns. The majority of past studies, therefore on FRP encasement of concrete are focused on the performance of columns having circular cross sections. The present experimental information on the performance of square or rectangular cross sections has increased over the recent years. However, it is limited in the context of studying effectiveness of confinement due to the variations of cross section and sizes (Mirmiran et. al. 1998). Thus, the application of FRP wraps for retrofitting noncircular columns still remains in its developmental stages. This indicates the necessity of having more information on testing and analysis to explore its prospects and promises.

## 1.2 FRP confining system

The main objectives of confinement are: (i) to prevent the concrete cover from spalling, (ii) to provide lateral support to the longitudinal reinforcement and (iii) to enhance concrete strength and deformation capacities. Confinement is generally applied to members in compression, with the aim of enhancing their load carrying capacity or, in cases of seismic upgrading, to increase their ductility. Section enlargement is one of the methods used in retrofitting concrete members. Enlargement is the placement of reinforced concrete jacket around the existing structural member to achieve the desired section properties and performance. The main disadvantages of such system are the increase in the column size obtained after the jacket is constructed and the need to construct a new formwork (Al-Salloum 2007). Steel jacketing has been proven to be an effective technique to enhance the seismic performance of old bridge columns. The steel jacket is manufactured in two shell pieces and welded in the field around the column. However, this method requires difficult welding work and, in a long term, the potential problem of corrosion remains unsolved (Al-Salloum 2007). Several advantages are

observed in using FRP wraps compared to the most common other techniques based on the use of steel reinforcements such as: the high-mechanical properties of the material (tensile strength and elasticity modulus) compared with its lightness; its insensitivity to corrosion; the ease of applying the reinforcing material, etc. (Campione 2006). FRP, as opposed to steel that applies a constant confining pressure after yield, has an elastic behavior up to failure and therefore exerts its (passive) confining action on concrete columns under axial load in a different way with respect to steel. In Figure 1.1 it can be seen that, at a certain value of the normalized axial concrete strain, the steel reaches yielding and then, from that point on, it exerts a constant lateral (confining) pressure, while FRP exerts a continuously increasing confining action (Lam and Teng 2006).

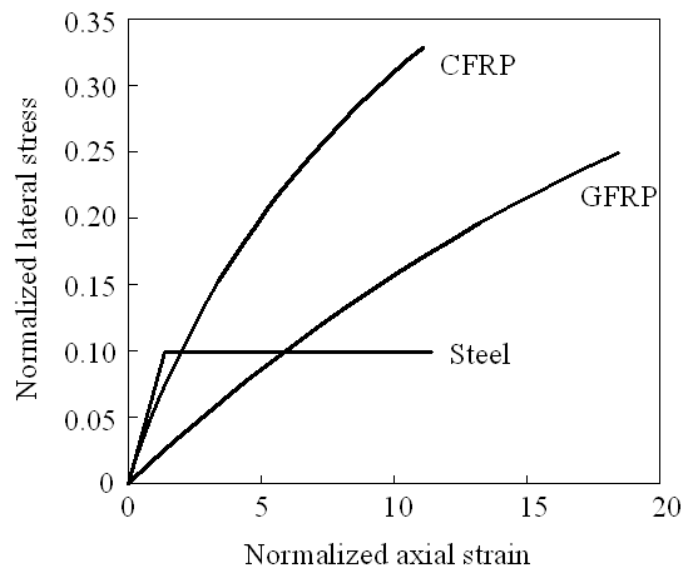


Figure 1.1: Comparison of confinement actions of steel and FRP materials (Lam and Teng 2006).

When the FRP hoop reinforcement is added to the exterior of the column, the apparent compressive strength of the concrete is increased. This apparent increase in the concrete strength is due to the confining effect of the FRP, which encircles and wraps the column completely. This increased concrete strength, known as the confined compressive strength  $f'_{cc}$  occurs only after the concrete in the column has begun to crack and hence dilate. This typically occurs after the internal transverse reinforcing steel has yielded. By arresting the cracked concrete from displacing laterally, the FRP serves to confine the concrete and allow it to carry additional compressive stress. Thus it gets additionally deformed in axial direction and so that the compression steel yields. Compression steel of eccentrically loaded unconfined reinforced concrete does not yield usually (Maaddawy 2009) before failure of concrete. Additional strength of concrete due to FRP confinement increases the moment capacity by making the compression reinforcement yielding. The

Whitney stress block is used to represent the nonlinear stress–strain relationship of the concrete at failure in the compression zone (Bank 2006).

Utilizing composite systems for confinement of concrete, a transfer of tensile stresses from concrete to the composite system is realized. The confining system changes the characteristic loading – strain behavior of concrete applying it a confining pressure. The maximum efficiency of confining systems using FRP materials is reached in case of columns with circular cross-section and is explained by the fact that the entire section of the column is involved into the confinement effect. The confining pressure is uniformly distributed on the entire cross-section of the element. In case of columns with noncircular cross section only a part of it is subjected to the confining effect, and that part is known as the highly confined area or active area.

Columns confined with FRP begin to take additional load until the rupture of FRP wrap. FRP wrap is a competitive choice for strengthening or retrofitting of concrete columns that are deficient in axial capacity.

### **1.3 Dilation effect and confinement in different prismatic sections**

Confining pressures in the columns wrapped with FRP are engaged by the transverse dilation of concrete that in turn increases the axial load capacity (Mirmiran and Shahawy 1997a). The key requirement for the accurate prediction of the axial capacity of FRP-confined concrete is the level of strain in the FRP at failure which is dictated by the rupture of confinement jacket. It is recognized that the circumferential (hoop) strain in the FRP rupture at failure is less than the ultimate tensile strain of a flat coupon of the same material (Lam and Teng 2004, Pessiki 2001, Shahawy et. al. 2000, Xiao and Wu, 2000). Such reduction of the capacity has been attributed to (1) curvature of FRP, (2) cracked concrete causing nonuniform deformation, (3) strains in the overlapping zone being less than the regions without an overlap, (4) multiaxial state of stresses in an FRP jacket, i.e. tension in the hoop direction but compression in the axial direction. It is because of either direct loading of the jacket or the transfer of axial loading from concrete to the FRP jacket through bond and friction (Lam and Teng 2004). The strain efficiency of the FRP, which is defined as the ratio of hoop strain in the FRP wrap at failure to the rupture strain of flat tensile coupons. This is the most important parameter for the design. In concrete columns with circular cross-section, the confining effectiveness is optimal since the geometrical configuration allows fibers to be effective on the entire concrete cross section

(Figure 1.2). At that time confining pressures are engaged by the transverse dilation of concrete (Lam and Teng 2003a, 2003b).

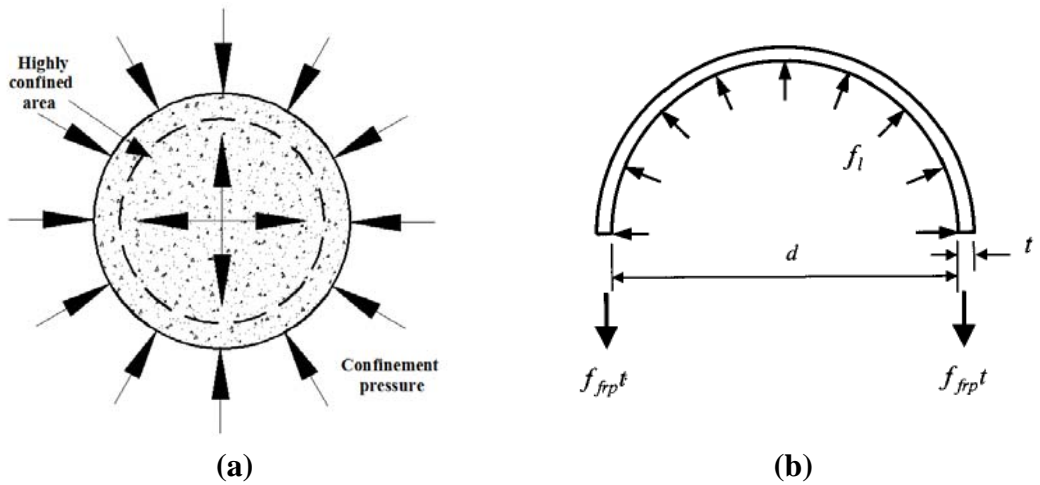


Figure 1.2: Confining action of FRP in circular column (a) confined concrete, (b) free body diagram of FRP wrap.

Prismatic cross sections behave differently, as it is well recognized that the confining pressure is high at the corners and low along the flat sides (Figure 1.3). Therefore the cross section is only partially confined (Lam and Teng 2003a, 2003b, Luca 2011, Mander 1988). Confining of a noncircular cross section still enhances concrete strength and ultimate strain, but the effectiveness is not as significant as that on a circular cross section.

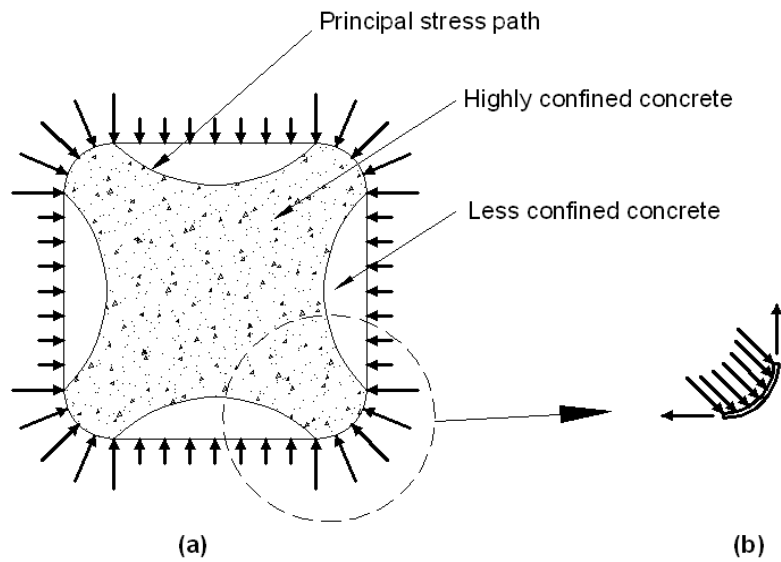


Figure 1.3: Confining action of FRP in square column (a) confined concrete, arrows are scaled down at sides to indicate a reduced confinement (b) free body diagram of FRP wrap at corner.



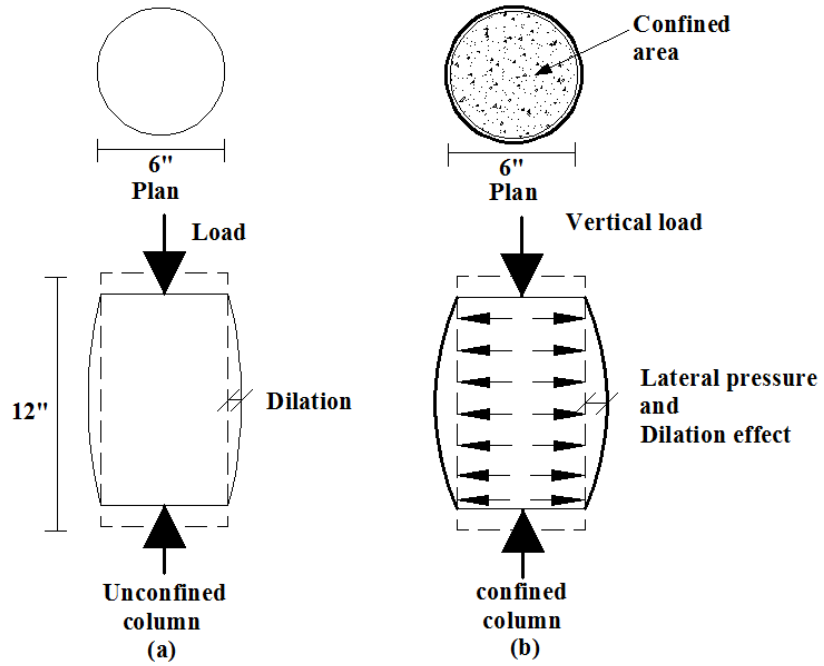


Figure 1.4: Short circular columns and effect of confinement (a) unconfined, (b) confined under load.

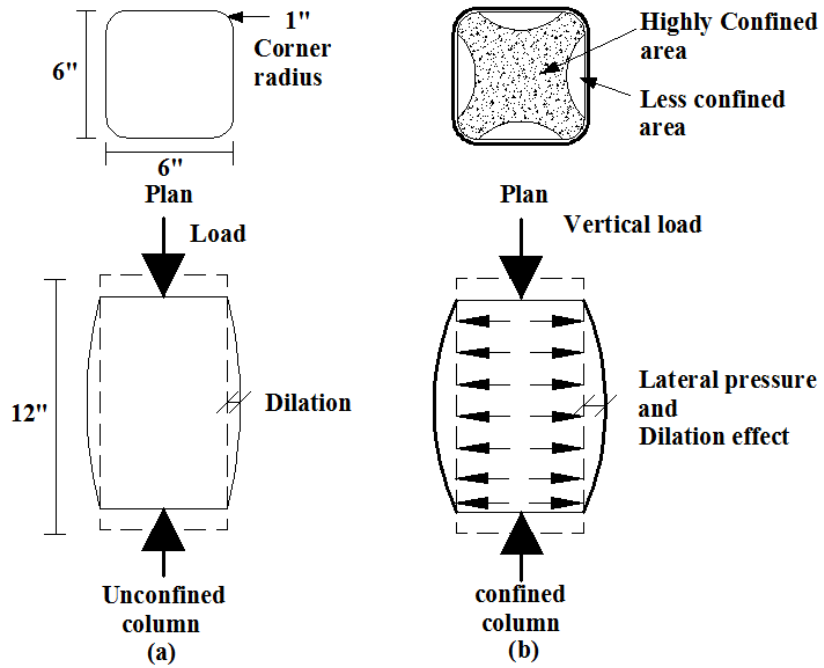


Figure 1.5: Short square columns and effect of confinement (a) unconfined, (b) confined under load.

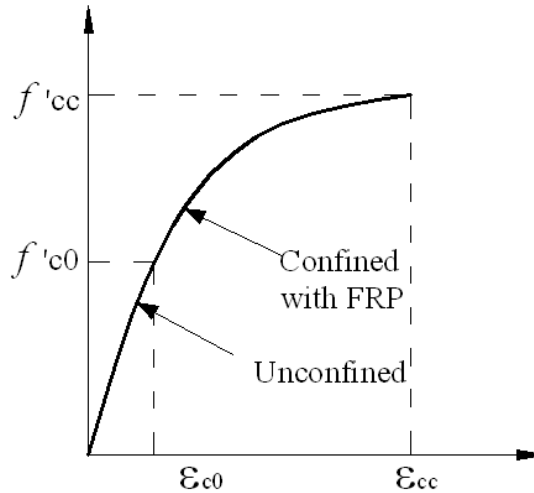


Figure 1.6: Schematic diagram of stress-strain behaviours of unconfined and confined concrete column. The stress-strain path of confined columns is same upto unconfined compressive strength.

Figure 1.4, 1.5 and 1.6 shows the possibility of testing the short plain concrete column specimens of different curvature and size in unconfined and confined conditions to understand the fundamental mechanism of confinement for different aggregate types.

#### 1.4 Limitations of available confinement models

A number of studies have been conducted and several analytical models are proposed for predicting confined compressive strength (Luca 2011, Mirmiran and Shahawy 1997b, Parvin and Wang 2001, Samaan 1998). However, these models widely diverge in predicting values. Furthermore, results from small scale test specimens are used in developing such models embed obvious limitations as the FRP wrap. This is significantly stiffer to concrete specimen than is feasible or necessary for practical retrofit applications (Pessiki 2001). Furthermore, no single investigation on size effect allowing the extrapolation of small scale experiment to full scale applications is presented in available literature (Pessiki 2001, Carey and Harries 2005). Matthys et al. (2006) reports test results of a few large size concrete columns. This shows the agreement of their behavior with the confinement models proposed by (Spoelstra and Monti 1999, Toutanji 1999) but wide disagreements with other well known models (Lam and Teng 2003a, 2003b). Due to uncertainty in the behavioral prediction, the load carrying capacities predicted by existing guidelines differ widely from one another (ACI 440.2R-08 2008, CSA-S806-02 2002, ISIS M04 2001). The safety margin of these guidelines may be of interest to the practicing engineers (Chaallal et. al. 2006). Furthermore, it is necessary to validate the

models for concretes of lower strengths as of the case encountered in rehabilitation of weak structures (Chaallal et. al. 2006).

Therefore, it is of fundamental interest to generate test results and build a test database to assess and to compare different compressive strength models for FRP confined concrete and testing their applicability for local materials of Bangladesh origin.

## **1.5 Finite element models**

Some previous researchers have reported their finite-element models for concrete columns confined by FRP sheets, (Karabinis et al. 2008), (Mirmiran et al. 2000), (Malvar et al. 2004), (Mukherjee et al. 2004) and proved that the FEM can be used to simulate the behaviors of the columns. Malvar et al. (2004) analyzed circular and square concrete columns confined by aramid, carbon and glass FRP composites using the finite-element method (FEM) to compare with the test data which showed good agreement.

## **1.6 Objective of research**

- a) To investigate the effectiveness of the FRP confinement defined by geometric parameters i.e. radius of curvature, column side to corner radius ratio, FRP volumetric ratio and rigidity ratio in relation to the square and circular concrete columns of different sizes.
- b) To investigate the contribution of carbon fiber reinforced polymer (CFRP) and glass fiber reinforced polymer (GFRP) wraps in generating passive confining pressure on the concrete for axial capacity enhancement in relation to the square and circular concrete columns of different sizes.
- c) To investigate the adequacy of the available analytical models in predicting confined compressive strengths under axial load in representing the test data in relation to the square and circular concrete columns of different sizes.
- d) To identify the unknown pertinent parameters of circular and square unconfined and confined concrete columns made of different aggregates (crushed stone, crushed brick, recycled stone and recycled brick) using finite element method.

## 1.7 Scope and methodology

This may be considered as primary efforts in generating a test database in Bangladesh context. The experimental information, comparison and validation are important to build confidence on the analytical models that implicitly accounts for the lateral dilation of concrete and its interaction with FRP jacket. This information founds the basis of proposing the strain efficiency factors for CFRP and GFRP. This will also open up the ways for implementation of the analytical models in a finite element code for simulation at the design desk. This is the most important design tool for the construction industry to use advanced materials and hybrid systems in civil infrastructure. Therefore, the research not only sheds light on the behavior of hybrid columns in general, but also has direct application in the current retrofitting projects in the country.

Extensive tests have been conducted on different sized concrete columns having circular and square cross sections. In order to vary the confining pressures, two kinds of FRP; namely CFRP and GFRP are used. The effect of dilation in concrete with different aggregates and flat coupon tests results from FRP manufacturer are considered together to determine the confinement modulus and strain efficiency factors. Each specimen is tested under uniaxial compression in a computer controlled universal testing machines to obtain the ultimate crushing loads. The load and displacement histories are recorded.

In this process, the ultimate tensile strain in FRP acting to confine the concrete in the hoop direction are investigated and compared for non-slender different sizes of square and circular confined concrete columns subjected to uniaxial compression. The lateral dilation of columns under uniaxial compression are measured both in confined and unconfined concretes. The measurements are taken by using a simultaneous data acquisition system. The load and displacement histories of square and circular confined concrete columns obtained from the load cell of a computer controlled universal testing machine. This is synthesized with the strain measurement results assembled from image analysis of High Definition (60 frames per second) video clips and images. In this process, the confinement due to dilation of concrete for different aggregate types and cross-sections are evaluated and compared. The unconfined columns specimens are tested in the same test setup for comparisons.

To realize the experimental data, an experimental program involving the testing of 120 short unreinforced concrete column specimens is outlined. The heights to width ratio (1:2) of the columns are kept constant to nullify the slenderness effect, if any. Four types

of coarse aggregates; e.g. crushed stone (CS), crushed brick (CB), recycled stone (RS) and recycled brick (RB) having same gradation are used in this research program. The sizes of the coarse aggregates are 25mm passing-19mm retained, 19mm passing-12mm retained and 12mm passing-6mm retained of ratio 1.24:1.67:1. The mix ratio is 1:2:4 and the water-cement ratio is 0.5. Two basic geometric shapes with three different sizes of specimen have been studied. The circular concrete columns are 100, 150 and 200 mm in diameter and 200, 300 and 400 mm in height respectively with the same aspect ratio but radius of curvature are increased with height of the columns. Again the square concrete columns are 100 x 100 x 200mm, 150 x 150 x 300mm and 200 x 200 x 400 mm with the same aspect ratio and a constant radius of curvature is maintained.

To reduce the stress concentration and to avoid the damage to the FRP jacket, the steel moulds are prepared with 25mm corner radius for the square concrete columns (Lam and Teng 2003a). All the specimens are cast according to standard laboratory procedures and are cured for at least 28 days. The total numbers of 40 specimens are wrapped with carbon fiber reinforced polymer (CFRP) composites and 40 specimens are wrapped with glass fiber reinforced polymer (GFRP) composites using wet lay-up technique and the rest 40 specimens are tested as control specimen. The test results of 24 square concrete columns having dimension of 150 x 150 x 300mm including 8 control specimen, 8 confined with CFRP and 8 confined with GFRP obtained from tests that are conducted from previous research work (Islam 2011).

Nonlinear finite element solid models of confined and unconfined square concrete columns are used from a previous research work (Islam 2011). To simulate the responses based on observed uniaxial behaviour of unconfined and confined concrete columns of symmetric cross-section, finite element (FE) models are constructed using ANSYS 10.0 (2005). To this end, the concrete is modeled both as unconfined and confined concrete to study the confining effect and stress-strain responses. The analytical model helped in predicting confined compressive strengths under axial load. The objectives of the FE models are to verify the results with the experimental measurements and also to estimate the hoop strain in confined concrete considering differences in dilational behaviour due to aggregates and confinements. The Poisson's ratio of the brick aggregate concrete, stone aggregate concrete, recycled aggregate concrete and recycled brick aggregate concrete is optimized by numerous test runs using ANSYS 10.0. The values of Poisson's ratio are varied from 0.25 to 0.4 for the FE models for different concrete. For a particular value of Poisson's ratio the experimental axial stress-strain curve matches with the FE model curve which conform the Poisson's ratio for that particular type of concrete. The confined

compressive strengths of concrete to predict stress fields and stress concentrations around the cross section and throughout the height of the analytical model are studied in this research.

## **2.1 General**

Confinement of reinforced Concrete (RC) columns by means of Fiber Reinforced Polymer (FRP) jackets has been extensively studied, in particular the behavior of confined elements of circular cross section because the confinement of circular columns provides circumferentially uniform confining pressure to the radial expansion of the compression member. Some of investigations focused on size effect analysis of confined concrete cylinders have concluded that the scale of cylinders does not significantly affect the normalized axial stress strain behavior. Furthermore, the most of existing studies are based on small scale specimens and limited studies are found for the case of large scale specimens. The size effect of FRP confined concrete columns is often conflicted and therefore demands further investigations.

## **2.2 Materials used for confining concrete**

### **2.2.1 Fiber reinforced polymer wraps**

The fiber phase of an FRP composite material consists of thousands of individual micrometer diameter individual filaments. In the large majority of fiber forms used in FRP products for structural engineering, these fibers are indefinitely long and are called continuous. This is to differentiate them from short fibers of length 10 to 50 mm (0.5 to 2 in.) that are used in the spray-up process for boat building and consumer products or in reinforced cementitious materials [known as glass-reinforced cements (GRCs) or fiber reinforced cementitious (FRC) composites]. Continuous fibers are used at a relatively high volume percentage (from 20 to 60%) to reinforce the polymer resin: thus the term fiber reinforced polymer (FRP) comes up. The classification of fiber reinforced polymers based on application is shown in Figure 2.1.

The mechanical properties of the fibers are typically orders of magnitude greater than those of the polymer resins that these reinforce; however, due to the filamentary nature these cannot be used as stand-alone construction materials and must be used in a synergistic fashion with polymer resins to realize the superior mechanical properties.

### 2.2.1.1 Glass fiber reinforced polymers (GFRP)

Glass fibers are used in a multitude of FRP products for structural engineering, from FRP reinforcing bars for concrete, to FRP strengthening fabrics, to FRP structural profile shapes. Glass is an amorphous inorganic compound of primarily metallic oxides that is produced in fibrous form in a number of standard formulations or types. Silica dioxide (SiO<sub>2</sub>) is the largest single compound in all glass formulations, constituting from 50 to 70% by weight of the glass. Different grades of glass fiber are identified by letter nomenclature. A borosilicate glass known as E-glass (electrical glass) because of its high electrical resistivity is used to produce the vast majority of glass fiber used in FRP products for structural engineering (Figure 2.2). A-glass (window glass) and C-glass (corrosion resistant, also known as AR-glass or alkali resistant glass) are used to produce specialized products for use in structural engineering. S-glass (structural or high-strength glass) is used to produce the high performance fibers used primarily in the aerospace industry.

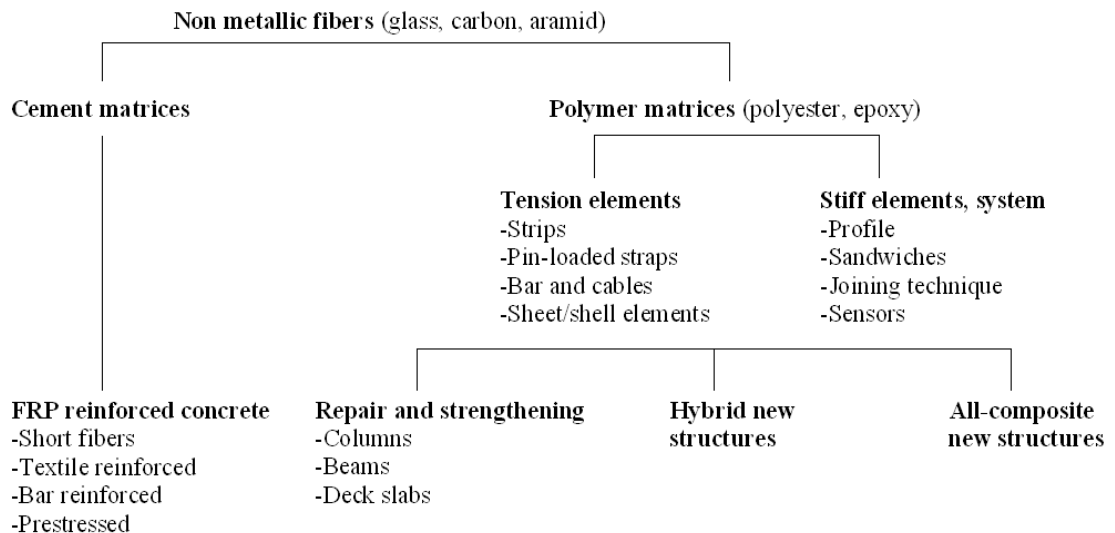


Figure 2.1: Classification of fiber reinforced polymers based on application



The diameter of an individual glass fiber or filament ranges from approximately 3 to 24  $\mu\text{m}$  (0.00118 to 0.00945 in.). The 17  $\mu\text{m}$  (0.0067 in) diameter fiber is most commonly used for FRP products for structural engineering. Microscopic view of glass fiber failed in compression of column and direct tension is shown in Figure 2.3. A glass fiber has a distinctive bright white color to the naked eye. Glass is usually considered to be an isotropic material. Approximate properties of commonly used grades of glass fibers are given in Table 2.1. Values presented in Table 2.1 are intended as a guide and should not be used in design calculations. Glass fibers are produced at melt temperatures of about 1400°C (2550°F). Individual filaments are produced with a surface coating called a sizing that serves to protect the filaments when these are formed into a bundle or a strand.

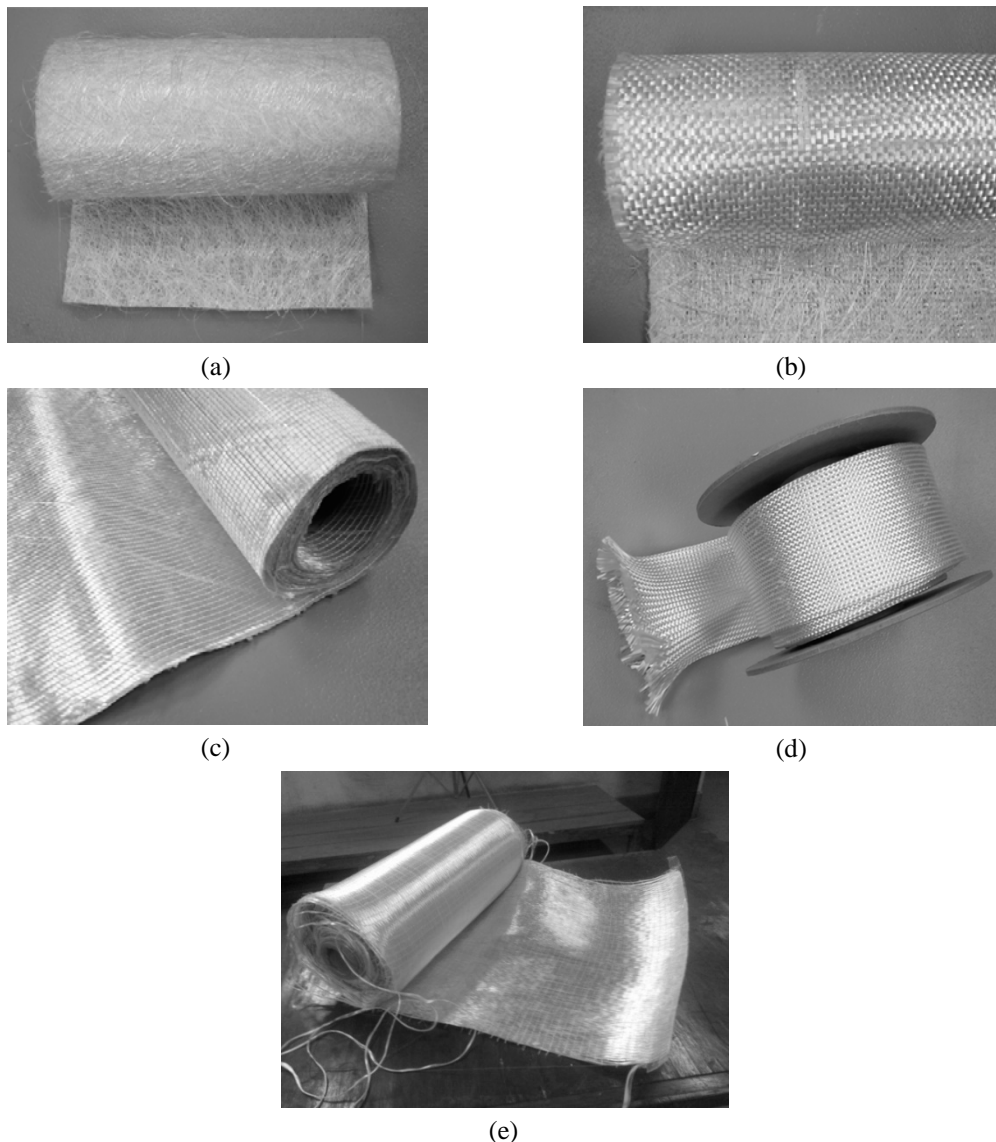


Figure 2.2: (a) E-glass continuous filament mat (b) woven glass roving combination fabric (c) stitched glass fiber fabric (d) glass fiber braided sleeve (e) GFRP wrap used in this research.

Table 2.1 Approximate Properties of Common Grades of Glass Fibers

Grade of Glass Fiber	Density [g/cm <sup>3</sup> (lb/in <sup>3</sup> )]	Tensile Modulus [GPa (Msi)]	Tensile Strength [MPa (ksi)]	Max. Elongation (%)
E	2.57 (0.093)	72.5 (10.5)	3400 (493)	2.5
A	2.46 (0.089)	73 (10.6)	2760 (400)	2.5
C	2.46 (0.089)	74 (10.7)	2350 (340)	2.5
S	2.47 (0.089)	88 (12.8)	4600 (667)	3.0

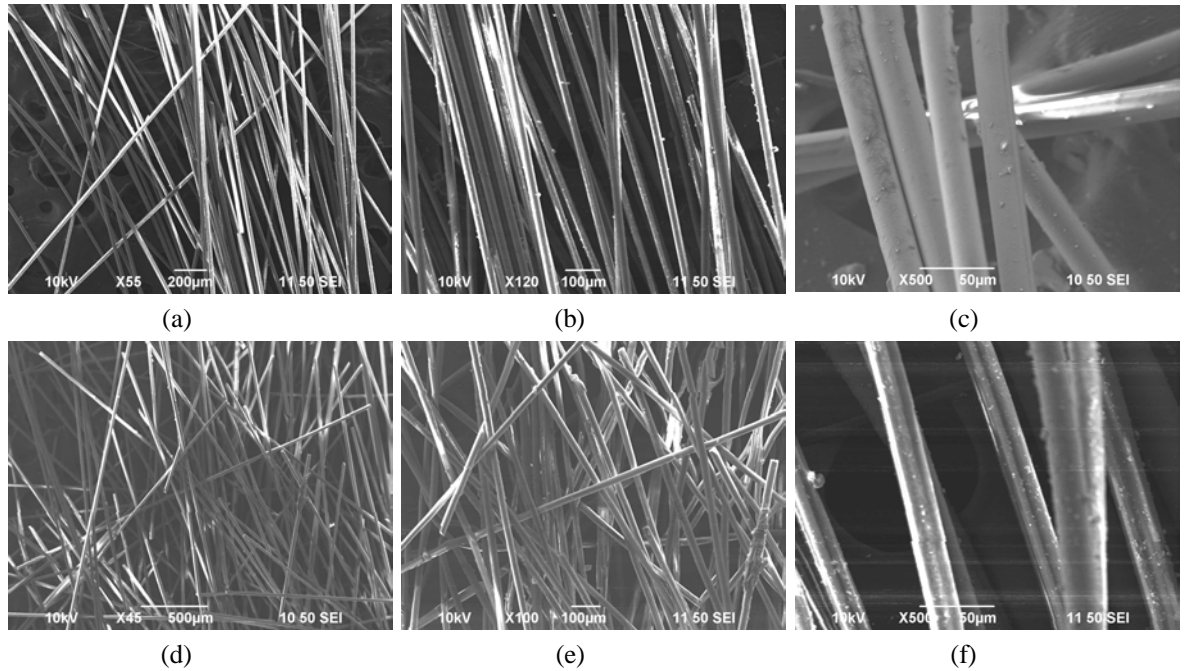


Figure 2.3: Microscopic view of glass fiber or filament after failure (a), (b), (c) filaments failed in hoop tension (d), (e), (f) failed in direct tension.

The sizing also contains coupling agents, usually silanes, that are specially formulated to enhance bonding between the glass fiber and the particular polymer resin being used when making a glass reinforced FRP composite material. Today, most commercially available glass fibers can be obtained with sizings that are compatible with the three major thermosetting resin systems used in structural engineering: epoxy, polyester, and vinylester. The commonly used term fiberglass is generally used to refer to the glass fiber reinforced polymer composite material itself and not solely to the glass fiber constituent material. When referring to the fibrous reinforcement alone, the term glass fiber is preferred. Glass fibers are particularly sensitive to moisture, especially in the presence of salts and elevated alkalinity, and need to be well protected by the resin system used in the FRP part. Glass fibers are also susceptible to creep, rupture and lose strength under sustained stresses (Bank 2006). The endurance limit of glass fibers is

generally lower than 60% of the ultimate strength. Glass fibers are excellent thermal and electrical insulators (hence, the extensive use in buildings and the electric power industry as insulation materials) and are the most inexpensive of the high-performance fibers.

### **2.2.1.2 Carbon fiber reinforced polymer (CFRP)**

Carbon fibers are used in structural engineering applications today in FRP strengthening sheets and fabrics, in FRP strengthening strips, and in FRP prestressing tendons. Carbon fiber is a solid semicrystalline organic material consisting on the atomic level of planar two-dimensional arrays of carbon atoms. The two-dimensional sheetlike array is usually known as the graphitic form; hence, the fibers are also known as graphite fibers (the three-dimensional array is well known as the diamond form). Carbon fiber is produced in grades known as standard modulus, intermediate modulus, high strength, and ultrahigh modulus (SM, IM, HS, UHM) Carbon fibers have diameters from about 5 to 10  $\mu\text{m}$  (0.00197 to 0.00394 in.). Microscopic view of glass fiber failed in compression of column and direct tension is shown in Figure 2.4. Carbon fiber has a characteristic charcoal-black color (Figure 2.5). Due to the two dimensional atomic structure, carbon fibers are considered to be transversely isotropic, having different properties in the longitudinal direction of the atomic array than in the transverse direction. The longitudinal axis of the fiber is parallel to the graphitic planes and gives the fiber its high longitudinal modulus and strength. Approximate properties of common grades of carbon fibers are given in Table 2.2.

Carbon fiber is produced at high temperatures [1200 to 2400°C (2200 to 4300°F)] from three possible precursor materials: a natural cellulosic rayon textile fiber, a synthetic polyacrylonitrile (PAN) textile fiber, or pitch (coal tar). Pitch-based fibers, produced as a by-product of petroleum processing, are generally lower cost than PAN- and rayon-based fibers. As the temperature of the heat treatment increases during production of the carbon fiber, the atomic structure develops more of the sheet like planar graphitic array, giving the fiber higher and higher longitudinal modulus. For this reason, early carbon fibers were also known as graphite fibers. The term carbon fiber is used to describe all carbon fibers used in structural engineering applications. The term graphite fiber is still used in the aerospace industry; however, this term is slowly dying out. Similar to glass fibers, carbon fibers need to be sized to be compatible with a resin system. Historically, carbon fibers have been used primarily with epoxy resins, and suitable sizings for epoxy

resin systems are readily available. Nowadays, carbon fibers are being used with vinylester and blended vinylester–polyester resins for FRP profiles and FRP strengthening strips. Sizing for carbon fibers for polyester and vinylester resins are not as common. Care must be taken when specifying a carbon fiber for use with a nonepoxy resin system to ensure that the fiber is properly sized for the resin system used.

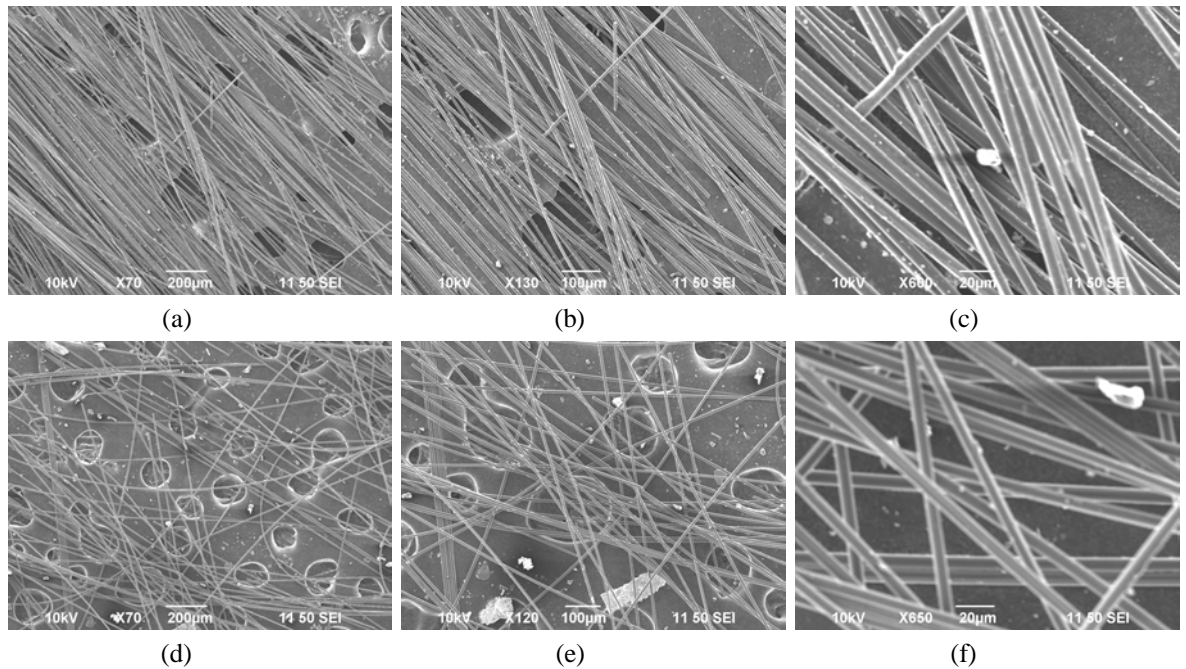
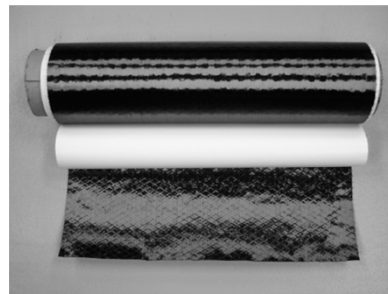


Figure 2.4: Microscopic view of carbon fiber or filament after failure (a), (b), (c) filaments failed in hoop tension (d), (e), (f) failed in direct tension.

Carbon fibers are very durable and perform very well in hot and moist environments and when subjected to fatigue loads. Carbon fibers do not absorb moisture and have a negative or very low coefficient of thermal expansion in the longitudinal direction, giving them excellent dimensional stability. Carbon fibers are, however, thermally and electrically conductive. Care must be taken when these are used in contact with metallic materials, as a galvanic cell can develop due to the electropotential mismatch between the carbon fiber and most metallic materials. Some research has suggested that this can lead to degradation of the polymer resin in the FRP composite, especially in the presence of chlorides and to corrosion of the metallic material.

Table 2.2 Approximate Properties of Common Grades of Carbon Fibers

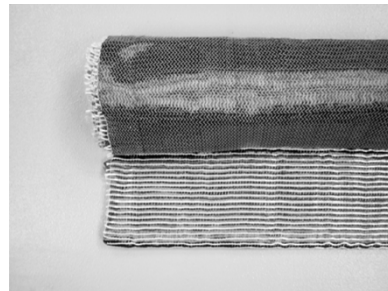
Grade of Carbon Fiber	Density [g/cm <sup>3</sup> (lb/in <sup>3</sup> )]	Tensile Modulus [GPa (Msi)]	Tensile Strength [MPa (ksi)]	Max. Elongation (%)
Standard	1.7 (0.061)	250 (36.3)	3700 (537)	1.2
High strength	1.8 (0.065)	250 (36.3)	4800 (696)	1.4
High modulus	1.9 (0.068)	500 (72.5)	3000 (435)	0.5
Ultrahigh modulus	2.1 (0.076)	800 (116.0)	2400 (348)	0.2



(a)



(b)



(c)



(d)

Figure 2.5: (a) Carbon fiber tow sheet (b) carbon fiber tow on a spool (c) Carbon fiber fabric with an aramid weft fiber (d) CFRP wrap used in this research.

### 2.2.1.3 Aramid fiber reinforced polymer (AFRP)

Aramid fibers were used to produce first-generation FRP prestressing tendons in the 1980s in Europe and Japan; however, few manufacturers still produce aramid fiber FRP reinforcing bars or tendons. Aramid fabrics are occasionally used in FRP strengthening applications to wrap columns and as sparse-volume weft (fill) fibers in unidirectional glass or carbon fabrics for FRP strengthening. Aramid fibers consist of aromatic polyamide molecular chains. These were first developed, and patented, by DuPont in 1965 under the trade name Kevlar. A combination of the relatively high price, difficulty in processing, high moisture absorption (up to 6% by weight), low melting temperatures [around 425°C (800°F)], and relatively poor compressive properties have made them

less attractive for FRP parts for structural engineering applications. The advantages include extremely high tenacity and toughness, and consequently, these are used in many industrial products, either in bare fabric form or as reinforcements for FRP composites where energy absorption is required, such as in bulletproof vests (body armor), helmets, and automotive crash attenuators. These have a distinctive yellow color and are similar in cost to carbon fibers. Like carbon fibers, these have a negative coefficient of thermal expansion in the fiber longitudinal direction. These are the lightest of the high performance fibers, having a density of around  $1.4 \text{ g/cm}^3$  ( $0.051 \text{ lb/in}^3$ ). Depending on the type of aramid fiber, the fiber longitudinal tensile strength ranges from 3400 to 4100 MPa (500 to 600 ksi), and its longitudinal tensile modulus ranges from 70 to 125 GPa (10,000 to 18,000 ksi).

#### **2.2.1.4 Other fibers**

Other fibers that are now in the development phase for use in FRP products for structural engineering include thermoplastic ultrahighmolecular-weight (UHMW) polyethylene fibers and polyvinyl alcohol (PVA) fibers. PVA fibers have been used in FRP bars and FRP strengthening sheets in Japan. UHMW short fibers are being used in the development of ductile fiber-reinforced cements (FRCs) but have not yet been used in FRP products for structural engineering. Inorganic basalt fibers, produced in Russia and the Ukraine, may see future applications in FRP products in structural engineering, due to the superior corrosion resistance and similar mechanical properties to glass fibers. Thin steel wires have been developed for use in FRP strengthening fabrics with either polymer or cementitious binders. Natural fibers such as hemp, sisal, and flax, as well as bamboo fibers, have been used in experimental applications to produce FRP composites, but no commercial FRP products are available that contain these fibers at this time. It is anticipated that FRP products in structural engineering that will be developed in the first half of the twenty-first century will probably use more of these natural fibers as sustainability and recyclability become more important drivers in the construction industry.

## 2.2.2 Resins

### 2.2.2.1 Epoxy resins

Epoxy resins are used in many FRP products for structural engineering applications. Most carbon fiber–reinforced precured FRP strips for structural strengthening are made with epoxy resins. In addition, epoxy resin adhesives are used to bond precured FRP strips to concrete (and other materials) in the FRP strengthening process. Epoxy resins are also used extensively in FRP strengthening applications, where the epoxy resin is applied to the dry fiber sheet or fabric in the field and then cured in situ, acting as both the matrix for the FRP composite and as the adhesive to attach the FRP composite to the substrate. When applied to dry fiber sheets or fabrics, the epoxy resins are often referred to saturants. Epoxy resins have also been used to manufacture FRP tendons for prestressing concrete and FRP stay cables for bridges. These are not used extensively to produce larger FRP profiles, due to the higher costs and the difficulty entailed in processing large pultruded FRP parts. An epoxy resin contains one or more epoxide (or oxirane) groups that react with hydroxyl groups. Most common are the reaction products of bisphenol A and epichlorohydrin, called bis A epoxies, or those made from phenol or alkylated phenol and formaldehyde and called novolacs. The resins are cured (or hardened) with amines, acid anhydrides, (Lewis acids) by condensation polymerization and not, like polyesters, by free-radical chain polymerization. The epoxy resin and the curing agent (or hardener) are supplied in two parts and are mixed in specific proportions (usually about 2 to 3 parts to 1 part by weight) just prior to use to cause the curing reaction (Figure 2.6). The first epoxy resin was produced by Schlack in 1939 (Bank 2006).



Figure 2.6: Epoxy resins used to bond FRP with concretes (part A and B).

Epoxy resins are particularly versatile and can be formulated in a range of properties to serve as matrix materials for FRP composites or to serve as adhesives. The epoxies used as the resins in FRP parts for structural engineering belong to the same family as the more familiar epoxies currently used in a variety of structural engineering applications, such as for concrete crack injection, as anchors for concrete, and for bonding precast concrete elements. Epoxy resins are known to have excellent corrosion resistance and to undergo significantly less shrinkage than polyester or vinylester resins when cured. Consequently, these are less prone to cracking under thermal loads. Epoxy resins have been developed for high-temperature applications of 180°C (350°F) and higher and have been the thermosetting resins of choice in the aerospace industry for the last 50 years. Epoxies based on bisphenol A resins cost about \$1.10 per pound (\$2.4 per kilogram); those based on the novolac resins cost about \$2.00 per pound (\$4.4 per kilogram) (2004 costs). The density of epoxy resin is about 1.05 g/cm<sup>3</sup> (0.038 lb/ in<sup>3</sup>). Epoxy resins can be cured at room temperature or at high temperature. In many aerospace applications, epoxy resin composites are postcured at elevated temperatures to raise the glass transition temperatures and to improve the physical and mechanical properties. The glass transition temperature of an epoxy is therefore highly formulation and cure temperature–dependent and can range from 40°C up to 300°C (100 to 570°F). Epoxy resins usually are clear to yellowish or amber in color.

#### **2.2.2.2 Vinylester resins**

Vinylester resins developed in the last 20 years, vinylester resins have become attractive polymer resins for FRP products for structural engineering due to the good properties, especially the corrosion resistance and the ease of processing (Bank 2006). Today, vinylester resins are used to make the majority of FRP rebars sold in the world and are also used widely in FRP pultruded profiles. Most manufacturers of pultruded profiles make profiles of identical shapes in both a polyester and a vinylester resin series. Vinylester resins have also been used to make FRP strengthening strips and FRP rods for near-surface-mounting applications. These are generally replacing polyester resins in FRP products in structural engineering, due to the superior environmental durability in alkaline environments.

A vinylester resin is a hybrid of an epoxy and an unsaturated polyester resin and is sometimes referred to as an epoxy vinylester resin or a modified epoxy resin. It is an



unsaturated polymer that is produced from an epoxy and an acrylic ester monomer. When it is dissolved in styrene, it reacts with the styrene monomer in the same way as an unsaturated polyester does and cures by free-radical chain polymerization with a peroxide catalyst. Consequently, it tends to have many of the desirable physical properties of an epoxy resin and many of the desirable processing properties of a polyester resin. The two major groups of epoxies used to produce vinylester resins are bisphenol A and novolac epoxies (Bank 2006).

Vinylester resins can be filled and pigmented. These have densities from 1.05 to 1.10 g/cm<sup>3</sup> (0.038 to 0.042 lb/ in<sup>3</sup>) and glass transition temperatures from 40 to 120°C (100 to 250°F). These can be cured at room temperatures or at elevated temperatures. The cost of vinylester resins range from \$1.20 to \$1.60 per pound (\$2.60 to \$3.50 per kilogram, 2004 costs), making them more expensive than general-purpose unsaturated polyester resin. Vinylester resins have a color similar to that of polyester resins, ranging from clear to greenish.

### **2.2.2.3 Phenolic resins**

Phenolic resins are the oldest and most widely used thermosetting resins; however, these have only recently been used for FRP products for structural engineering, due to the difficulty of reinforcing them and curing them by condensation polymerization. These were first developed by Leo Baekeland in the early 1900s and called Bakelite when filled with wood flour (Seymour, 1987). Until the 1980s these had to be cured at high temperatures from 150 to 300°C (300 to 570°F). These are used extensively in the production of plywood and other engineered wood products. These are being introduced into FRP products for structural engineering because these have superior fire resistance, and these char and release water when burned. These can be filled and reinforced; however, these are difficult to pigment and have a characteristic brownish color. The costs are similar to that of low performance polyesters, about \$0.60 per pound (\$1.30 per kilogram) (2004 costs). The density is around 1.50 to 2.0 g/cm<sup>3</sup> (0.054 to 0.072 lb/ in<sup>3</sup>). These have glass transition temperatures from 220 to 250°C (430 to 480°F). At this time these are used in a limited number of FRP products, particularly in walkway gratings for offshore platforms and in FRP strengthening strips for timber structures.

#### **2.2.2.4 Polyurethane resins**

Thermosetting polyurethane resins have recently been introduced into the market as structural resins. These were first produced in the 1930s by Otto Bayer and consist of long-chain urethane molecules of isocyanate and hydroxyl-containing molecules (polyols). These have been used extensively in the thermoplastic formulation to produce insulation and structural polymer foam materials for decades. Only recently have these been produced in high-density forms that can be used in resin molding and pultrusion operations. Polyurethane resins have high toughness and when used with glass fibers produce composites with high transverse tensile and impact strengths. The cost is approximately the same as that of high-performance vinylester resins. Polyurethane resins do not require styrene to polymerize as do unsaturated polyester and vinylester resins.

#### **2.2.2.5 Other polymer resins**

Thermoplastic resin systems such as polyethylene terephthalate (PET, a saturated polyester), polypropylene, and nylon have been used in a very limited fashion to produce FRP parts for structural engineering. Thermoplastic composites based on polyether ether ketone (PEEK), polyphenylene sulfide (PPS), and polyimide (PI) thermoplastic resins, as well as many others, are being used extensively in the high temperature aerospace composites market. The attractiveness of using thermoplastic resin systems in structural engineering is due to the ability to be heated, softened, and reformed, which may give the parts the potential to be joined by local heating processes, akin to welding of metals. In addition, these are generally less expensive than thermosetting resins and are recyclable. However, these are difficult to process and generally have lower strength and stiffness than thermosets. These do, however, have higher elongations than thermosets (up to 20%), making them tougher and more ductile. A comparison of the properties of thermosetting resins for FRP products for structural engineering is given in Table 2.3.

FRP products produced for use in structural engineering can include significantly more ingredients than just the primary constituents: fibers and polymer resins. Fibers are produced with surface coatings called sizings and are supplied in many different strand and broadgood forms. Resins can contain fillers, catalysts, accelerators, hardeners, curing agents, pigments, ultraviolet stabilizers, fire retardants, mold release agents, and

other additives. These have different functions, from causing the resin to polymerize to helping the processing to modifying the final properties of the FRP part.

Table 2.3: Approximate Properties of Thermosetting Polymer Resins

	Density [g/cm <sup>3</sup> (lb/in <sup>3</sup> )]	Tensile Modulus [GPa (Msi)]	Tensile Strength [MPa (ksi)]	Max. Elongation (%)
Polyester	1.2 (0.043)	4.0 (0.58)	65 (9.4)	2.5
Epoxy	1.2 (0.043)	3.0 (0.44)	90 (13.1)	8.0
Vinylester	1.12 (0.041)	3.5 (0.51)	82 (11.9)	6.0
Phenolic	1.24 (0.045)	2.5 (0.36)	40 (5.8)	1.8
Polyurethane	varies	2.9 (0.42)	71 (10.3)	5.9

### 2.2.3 Primers and putty

For FRP strengthening applications, the epoxy resin is usually sold in a packaged system together with the fiber sheet or fabric and additional surface primers and putties, which are also epoxy based. These packaged epoxies are typically formulated by FRP strengthening system manufacturers to be compatible with the fabrics and sheets and to be of the appropriate viscosity to be used in the field (either as a saturating resin or as an adhesive). These epoxies are typically unfilled systems that are clear to yellow or amber color (Figure 2.7). Many manufacturers pigment the brand-name epoxy resin formulations so that these are identifiable. Green, blue, and gray systems are common. These have a fairly low viscosity of around 500 to 1000 cP, similar to that of 10weight motor oil. These are easily rolled with paint rollers. But due to the lower viscosity, these tend to run and drip if over applied, making the installation process somewhat messy, especially in overhead applications.

Primer should be applied to all areas on the concrete surface where the FRP system is to be placed (Figure 2.8). The primer should be placed uniformly on the prepared surface at the manufacturer's specified rate of coverage. The applied primer should be protected from dust, moisture, and other contaminants before applying the FRP system. If the concrete is damaged (e.g., due to corrosion), it must first be repaired. Protrusions must be ground down. The surface must be dried and a primer must be applied to seal the concrete.

Putty should be used in an appropriate thickness and sequence with the primer as recommended by the FRP manufacturer. The system-compatible putty, which is

typically a thickened resin-based paste, should be used only to fill voids and smooth surface discontinuities before the application of other materials. Rough edges or trowel lines of cured putty should be ground smooth before continuing the installation. Before applying the saturating resin or adhesive, the primer and putty should be allowed to cure as specified by the FRP system manufacturer. If the putty and primer are fully cured, additional surface preparation may be required before the application of the saturating resin or adhesive. Surface preparation requirements should be obtained from the FRP system manufacturer.

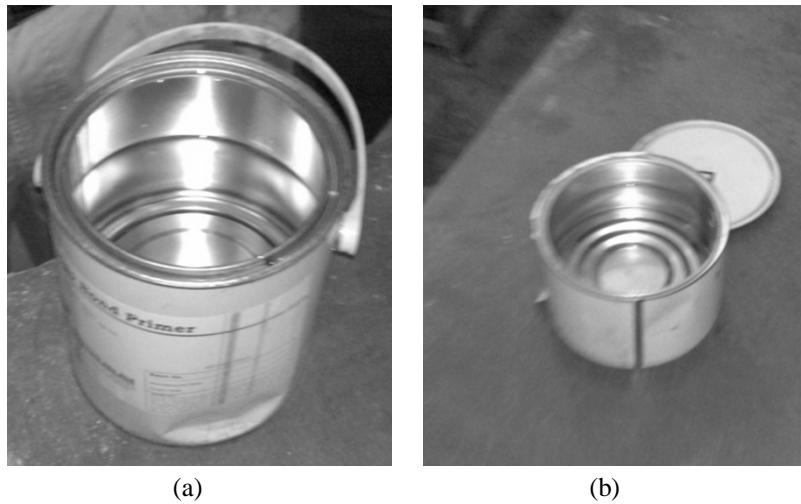


Figure 2.7: Primers used to apply on concrete surface before FRP wrapping.



Figure 2.8: Columns prepared for primer coating and FRP wrapping

### **2.3 Dilation effect in concrete with different aggregates**

It is well known that concrete expands laterally before failure. If the lateral expansion is prevented, a substantial concrete strength and deformation enhancements can be gained. Thus, the expected enhancement in the axial load capacity of the columns wrapped with FRP depends on two factors; (1) the confinement effect of the externally bonded transverse fibers, and (2) the direct contribution of longitudinally aligned fibers.

Islam (2011) found experimentally that the dilation effect in brick aggregate concrete is found distinctly larger than the stone aggregate concrete. He also found that the Poisson's ratio of stone aggregate concrete is convincingly lower than brick aggregate concrete, recycled brick aggregate concrete and recycled stone aggregate concrete using finite element analysis. The values of Poisson's ratio of the concretes were estimated at 0.25, 0.35, 0.37 and 0.40, respectively. But he only considered 150 x 150 x 300mm size square concrete columns. From this direct observation he suggests that the confinement effect due to dilation of brick and recycled aggregate concretes are higher than stone aggregate concretes. But confinement due to dilation not only depends on the Poisson's ratio of the concretes but also depends on the geometric parameters i.e. radius of curvature, column side to corner radius ratio, FRP volumetric ratio and stiffness ratio, which is different in circular and square concrete columns. For that reason, more investigations need to be done to get an accurate result useful in the confined concrete structures design.

### **2.4 Effect of curvature and size**

The factors that greatly influence the stress-strain relation are the concrete characteristics (modulus of elasticity, strength and Poisson ratio), the modulus of elasticity and strength of the composite, the cross section geometry (circular, square or rectangular) and column curvature and size. In the case of rectangular cross section the degree of rectangularity affect the stress-strain curve, while in both square and rectangular cross sections the curve is also influenced by the radius of curvature to which the corners of the section are rounded off, in order to avoid the breakage of the fibers.

Wang and Wu (2011) described that in recent years, the size effect for FRP-confined concrete short columns has been considered by Thériault et al. (2004), who tested such columns confined by Glass Fiber Reinforced Polymer (GFRP) and Carbon Fiber Reinforced Polymer (CFRP) and concluded that the size effect on the compressive

strength is clearly evident in very small specimens with 50mm diameter. Silva and Rodrigues (2006) demonstrated that the increasing size of the specimen significantly reduced the compressive strength of CFRP confined concrete cylinders if the thickness of CFRP is not increased. Jia and Cheng (2003) observed that the size effect existed in the enhancement in load carrying capacity of concrete cylinders because of external CFRP wrapping. Lin and Li (2003) and Masia et al. (2004) experimentally confirmed the size effect of FRP confined concrete columns with circular or square sections. However, several researchers have reported conflicting results. Lorenzis et al. (2002) concluded that the size of CFRP confined concrete cylinders have a weak influence on the compressive strength. Carey and Harries (2005) did not observe the size effect when a relatively high level of confinement is provided. Gu et al. (2006) found that the size effect is not obvious when the diameter of CFRP confined concrete cylinder is larger than 100 mm. In addition, Zhu et al. (2005) observed that the size of GFRP confined concrete cylinders did not appear to have a significant effect on the confinement or the overall axial compression response.

Wang and Wu (2011) observed size effect of FRP confined concrete short columns experimentally. Ninety-nine confined concrete short columns wrapped with aramid FRP (AFRP) jackets and 36 unconfined concrete short columns with circular and square sections are tested under axial compressive testing. They concluded that the size of a specimen have a significant effect on the strength of AFRP confined concrete short columns, lesser effect on the axial stress-strain curves and slight effect on the failure modes.

Mirmiran et al. (1998) found experimentally that for length-to-diameter ratios within the range of 2:1 to 5:1, changes in strength or ductility of FRP confined concrete columns are insignificant. They also concluded that shape of cross section can directly impact the confinement effectiveness of the jacket and square sections are less effective than their circular counterparts. They considered fixed diameter and side length of circular and square concrete columns of different size but they cannot consider the curvature effect.

Mohsen et al. (2009) fabricated and tested six control and 49 CFRP confined circular short RC columns of 450 mm, 600 mm, 750 mm and 900 mm in length and 150 mm in diameter to failure and they found that the ultimate capacity and ductility increase with the increase in volumetric ratio of CFRP and unconfined strength of concrete. In addition, they also concluded that the size effect exists and the confinement effectiveness is more

pronounced for columns with low  $f_{co}$  and  $\rho_f$  but they can't increase the radius of curvature.

Rochette and Labossiere (2000) concluded that for a given number of wraps around a section, the confinement effect is directly related to the shape of the section and the most effective confinement are obtained for circular sections. They also concluded that the section corners should always be rounded off sufficiently to prevent premature failure by punching of the fibers in the FRP.

Pessiki et al. (2001) have presented the results of an experimental investigation of the axial behavior of small scale circular and square plain concrete specimens and large-scale circular and square reinforced concrete columns confined with fiber reinforced polymer (FRP) composite jackets, subject to monotonic, concentric axial loads. Improvements in the axial load-carrying and deformation capacities of FRP jacketed concrete members over unjacketed members are reported. Factors influencing the axial stress-strain behavior of FRP confined concrete, such as transverse dilation and effectively confined regions and their relationship to jacket properties, are identified and discussed. But the dilation of variably confined concrete, including the effect curvature and size jacket stiffness is not considered.

Chaallal et al. (2006) found experimentally that for the given FRP jacket, the increase of the column size results in a decrease of the FRP volumetric ratio and therefore, in a decrease of the confined concrete strength. Chaallal et al. (2006) also concluded that as the modulus of elasticity of the FRP increases, the confined concrete strength also increases.

Shehata et al. (2002) tested 54 short concrete column externally confined by CFRP wrapping and investigated the behavior of confined short column models with different cross section geometry and degree of confinement. They found experimentally that the efficiency of the confinement is very sensitive to the column cross section geometry (circular, square and rectangular) but they cannot increase the curvature and size.

Yeh and Chang (2004) concluded that the normalized column axial strength and ductility increase with increasing CFRP volumetric ratio, but decrease with increasing column side to corner radius ratio ( $D/r$ ) and column side aspect ratio ( $B/D$ ). For columns with the same corner radius and CFRP volumetric ratio, the normalized column axial strength and ductility decrease with increasing column size ( $D$ ). There are no size effects on

normalized strength and ductility for columns with the same CFRP volumetric ratio, column side to corner radius ratio ( $D/r$ ) and column side aspect ratio ( $B/D$ ).

Akogbe et al. (2011) tested 24 concrete cylinders with different sizes, small specimens with a diameter of 100 mm and a height of 200 mm, medium specimens with a diameter of 200 mm and a height of 400 mm, and big specimens with a diameter of 300 mm and a height of 600 mm. They concluded that no size effect is observed on axial compressive strength of CFRP confined concrete cylinders, a bit lower strength obtained in the case of big confined specimens can be explained by scattered strength value of plain concrete specimens.

In the past studies columns made of only stone aggregate concretes were investigated. Effect of curvature of the columns were investigated by changing only the geometric shape i.e. circular and non-circular (square and rectangular) keeping the size (height) constant. In case of size effect, the sizes of the columns were varied with keeping the curvature unchanged. For that reason, the curvature and the size of the columns are varied simultaneously to investigate the curvature and size effect in this research work.

## 2.5 Strength Models of FRP-confined concrete columns

Several of the existing strength models for FRP-confined concrete take the following general form:

$$\frac{f'_{cc}}{f'_{c0}} = 1 + k_1 \left( \frac{f_l}{f'_{c0}} \right) \quad (2.1)$$

where  $f'_{cc}$  and  $f'_{c0}$  = compressive strength of confined and unconfined concrete columns, respectively;  $f_l$  = lateral confining pressure; and  $k_1$  = is the confinement effectiveness coefficient. This form is first proposed by Richart et al. (1928) for actively confined concrete with a value of 4.1 for  $k_1$ . Richart et al. (1929) subsequently showed that the model is also suitable for steel confined concrete. Fardis and Khalili (1982) suggested that Richart et al.'s (1928) model could be directly used for FRP-confined concrete. The expression of Eq. (2.1) is the general form adopted by the majority of the existing strength models for FRP confined concrete columns. Numerous strength models have been developed by fitting experimental data to the general form; and the confinement effectiveness coefficient  $k_1$  is derived either as a constant, as a function of the effective lateral confining pressure  $f_l$ , or as a function of  $f_l / f'_{c0}$ . In circular concrete column, the confining pressure is constant in the whole cross section (Wu and Wang, 2009). For



application to FRP-confined concrete,  $f_l$  can be related to the amount and strength of the FRP by

$$f_l = \frac{2f_{frp}t}{d} = \frac{2E_{frp}\varepsilon_j t}{d} \quad (2.2)$$

where  $f_{frp}$ =tensile strength of FRP in the hoop direction;  $E_{frp}$ =elastic modulus of FRP in the hoop direction;  $t$ =total thickness of FRP;  $d$ =diameter of the confined concrete core; and  $\varepsilon_j$ = hoop tensile strain of FRP at failure. An important aspect of the behavior of uniformly confined concrete is that at the rupture of FRP, the hoop strain reached in jacket,  $\varepsilon_j$ , is considerably smaller than the ultimate tensile strain obtained from flat coupon tensile tests,  $\varepsilon_{frp}$ . Lam and Teng (2003a) suggested that, in the development of confinement models,  $\varepsilon_j$  should be taken as the actual hoop rupture strain,  $\varepsilon_{h,rupt}$ , which is measured in the FRP jacket rather than  $\varepsilon_{frp}$ . The actual hoop rupture strain,  $\varepsilon_{h,rupt}$ , can be related to the FRP ultimate tensile strain,  $\varepsilon_{frp}$ , through an efficiency factor,  $k_\varepsilon$ , as given by  $\varepsilon_{h,rupt} = k_\varepsilon \varepsilon_{frp}$ . The value of  $k_\varepsilon$  has been shown to vary with the type of FRP, and an average value of 0.586 has been recommended for carbon FRP confined circular columns, based on an analysis of 52 CFRP specimens in the database collected by Lam and Teng (2003a).

## 2.5.1 Models for FRP confined circular columns

### 2.5.1.1 Saafi *et al.* (1999)

Saafi et al. (1999) have used regression analysis based on their experimental results to derive an expression to predict the ultimate strength. CFRP- and GFRP-confined concrete tubes are tested. The confined strength expression recommended by Saafi et al. (1999) is given by:

$$\frac{f'_{cc}}{f'_{c0}} = 1 + 2.2 \left( \frac{f_l}{f'_{c0}} \right)^{0.84} \quad (2.3)$$

where  $f_l$  is calculated using Eq. (2.2)

### 2.5.1.2 ACI 440 model (2002)

The ACI 440 model (ACI 2002) adopts the following which is originally proposed by Mander et al. (1988) for steel confined concrete columns

$$\frac{f'_{cc}}{f'_{c0}} = -1.254 + 2.254 \sqrt{1 + \frac{7.94k_s f_l}{f'_{c0}}} - 2 \frac{k_s f_l}{f'_{c0}} \quad (2.4)$$

In this model, the confining pressure is given as

$$f_l = \frac{\rho_f \varepsilon_{fe} E_{frp}}{2} \quad (2.5)$$

in which  $\rho_f$ =FRP volumetric ratio, and can be determined by

$$\rho_f = \frac{4nt}{d} \quad (2.6)$$

for circular sections

$$\rho_f = \frac{2nt(b+h)}{bh} \quad (2.7)$$

for noncircular sections. The nominal hoop rupture strain in the FRP jacket is assumed to be equal to an effective value,  $\varepsilon_{fe}$ , and it is specified that for RC column members that are completely wrapped by the FRP system around the cross section, the maximum strain used for the design should be limited to 0.4%, that is

$$\varepsilon_{fe} = 0.004 \leq 0.75 \varepsilon_{frp} \quad (2.8)$$

The shape factor for square and rectangular sections can be determined by

$$k_s = 1 - \frac{(b-2r)^2 + (h-2r)^2}{3bh(1-\rho_g)} \quad (2.9)$$

where  $\rho_g$ =ratio of the area of longitudinal steel reinforcement to the cross-sectional area of a compression member but for circular section the shape factor  $k_s$  is considered as 1. The confining effect of FRP jackets should be assumed to be negligible for rectangular sections with aspect ratios ( $b/h$ ) exceeding 1.5 or face dimensions ( $b$  or  $h$ ) exceeding 900 mm, unless testing demonstrates their effectiveness (Wu and Wang, 2009).

### 2.5.1.3 Lam and Teng's model (2003a)

Lam and Teng (2003a) have developed a model based on a large test database assembled from an extensive survey of existing studies. The model is based on observation that a linear relationship exists between the confined strength and the lateral confining pressure from the FRP. The proposed equation is given by:

$$\frac{f'_{cc}}{f'_{c0}} = 1 + 1.3 \left( \frac{f_l}{f'_{c0}} \right) \quad (2.10)$$

where  $f_l$  is calculated using Eq. (2.2)

### 2.5.1.4 Youssef et al. model (2007)

This model adopts different forms for the ascending and the descending branches of the stress-strain curves, given as

$$\frac{f'_{cc}}{f'_{c0}} = 1 + 2.25 \left( \frac{f_l}{f'_{c0}} \right)^{1.25} \quad (2.11)$$

for ascending curves, where  $f_l$  is calculated using Eq. (2.2)

$$\frac{f'_{cc}}{f'_{c0}} = 1 + 3.0 \left( \frac{4E_{frp} \varepsilon_{jt}}{f'_{c0}} \right)^{1.25} \quad (2.12)$$

for descending curves.

### 2.5.2.5 Wu and Wang's model (2009)

This model takes the form

$$\frac{f'_{cc}}{f'_{c0}} = 1 + 2.23 \rho^{0.73} \left( \frac{f_l}{f'_{c0}} \right)^{0.96} \quad (2.13)$$

where  $\rho =$  corner radius ratio, which is defined as  $2r/b$ . This model can be degenerated into two special cases, for circular columns and sharp cornered square columns when  $\rho = 1$  and  $0$ . In this model the lateral confining pressure  $f_l$  is calculated by

$$f_l = \frac{2f_{frp}t}{b} = \frac{2E_{frp}\varepsilon_{frp}t}{b} \quad (2.14)$$

where  $b$  is considered the diameter of circular column.

## 2.5.2 Models for FRP confined square columns

### 2.5.2.1 Mirmiran et al. model (1998)

The model proposed by Mirmiran et al. (1998) is given by

$$\frac{f'_{cc}}{f'_{c0}} = 1 + k_1 k_s \left( \frac{f_l}{f'_{c0}} \right) \quad (2.15)$$

In this equation, the confinement effectiveness coefficient  $k_1$  is adopted as  $k_1 = 6.0f_l^{-0.3}$ , and the shape factor is defined as  $k_s = 2r/D$ , in which  $D =$  diameter of an equivalent circular column and equated to the side length of a square column or the longer side length in the case of a rectangular section (Wu and Wang, 2009). The lateral confining pressure  $f_l$  is calculated by replacing  $d$  in Eq. (2.2) with  $D$ , and the FRP strain,  $\varepsilon_j$ , is taken as the ultimate tensile strain,  $\varepsilon_{frp}$ . Therefore, its final form is given by

$$\frac{f'_{cc}}{f'_{c0}} = 1 + 6.0 \left( \frac{2r}{D} \right) \left( \frac{f_l}{f'_{c0}} \right)^{0.7} \quad (2.16)$$

### 2.5.2.2 Shehata et al. model (2002)

The equation for the average confined concrete strength of square columns is simply given as

$$\frac{f'_{cc}}{f'_{c0}} = 1 + 0.85 \left( \frac{f_l}{f'_{c0}} \right) \quad (2.17)$$

The lateral confining pressure  $f_l$  in Eq. (2.17) is calculated by  $\varepsilon_f = \varepsilon_{frp}$  and replacing  $d$  in Eq. (2.2) with  $b$ , the breath of the square column cross section (Wu and Wang, 2009).

### 2.5.2.3 Lam and Teng's model (2003b)

This model takes the form

$$\frac{f'_{cc}}{f'_{c0}} = 1 + 3.3 \left( \frac{A_e}{A_c} \right) \left( \frac{f_l}{f'_{c0}} \right) \quad (2.18)$$

where the value of the confinement effectiveness coefficient  $k_1$  of 3.3 is obtained by calculating the confining pressure  $f_l$  in Eq. (2.2) with  $\varepsilon_f = \varepsilon_{h,rupt}$  and replacing  $d$  with an equivalent diameter  $D$  that is defined as the diagonal distance of the section, i.e.,  $D = \sqrt{(h^2 + b^2)}$ . The stress-strain model is shown in Figure 2.1. The shape factor  $k_s$  is taken into account by the effective confinement area ratio of  $A_e / A_c$  that is given by

$$\frac{A_e}{A_c} = 1 - \frac{(b/h)(h-2r)^2 + (h/b)(b-2r)^2}{3A_g(1-\rho_g)} \quad (2.19)$$

where  $A_g$  = gross area of the column section and can be evaluated as

$$A_g = bh - (4 - \pi)r^2 \quad (2.20)$$

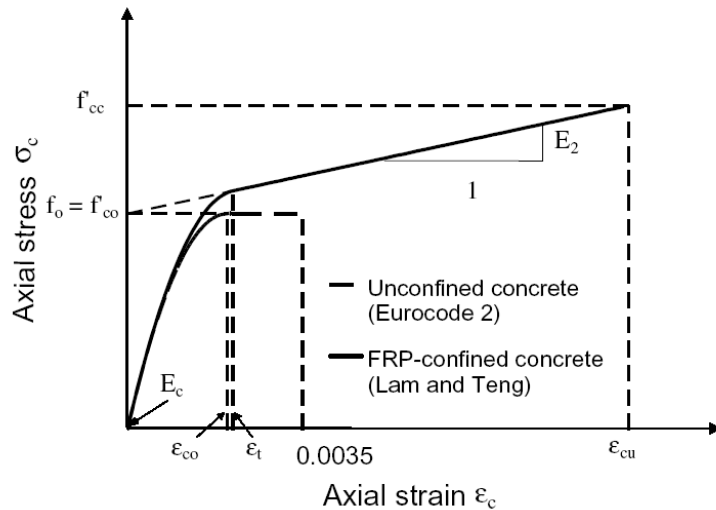


Figure 2.1: Lam and Teng's stress-strain model for FRP-confined concrete.

#### 2.5.2.4 Kumutha et al. model (2007)

This model takes the form

$$\frac{f'_{cc}}{f'_{c0}} = 1 + 0.93 \left( \frac{f_l}{f'_{c0}} \right) \quad (2.21)$$

In this equation, the value of  $k_1 k_s$  is found to be a constant of 0.93 from a regression analysis. The lateral confining pressure  $f_l$  provided by FRP is calculated as

$$f_l = \frac{\rho_f f_{frp}}{2} \quad (2.22)$$

with the FRP volumetric ratio  $\rho_f$  given by Eq. (2.14)

#### 2.5.2.5 Al-Salloum's model (2007)

In the model proposed by Al-Salloum (2007), the shape factor  $k_s$  is expressed as a function of the breadth of the section  $b$  and the corner radius  $r$ , as given by

$$k_s = 1 - \frac{2(1 - 2r/b)^2}{3[1 - (4 - \pi)(r/b)^2]} \quad (2.23)$$

As the shape factor  $k_s$  takes into account the effective confined area of the section, it is suggested that another factor of  $b/D$  that accounts for the nonuniformity of the confining pressure be included, where  $D$ =diagonal length of the square columns and can be calculated by  $D = \sqrt{2}b - 2r\sqrt{2-1}$ . The confinement effectiveness coefficient  $k_1$  is taken as 3.14, which is the average value of 2.98 and 3.3, as proposed by Lam and Teng (2003a), respectively (Wu and Wang, 2009). Therefore, the model is expressed as

$$\frac{f'_{cc}}{f'_{c0}} = 1 + 3.14 k_s \left( \frac{b}{D} \right) \left( \frac{f_l}{f'_{c0}} \right) \quad (2.24)$$

Since the 1980, efforts are given to obtain a reliable and accurate model for confined concrete. Most of these investigations considered mechanical response of circular columns to propose numerous models. However, relatively few studies addressed square columns that suffer the non-uniform distribution of the confinement stress across the cross section. It is worth noting that a model for accurate prediction of the stress-strain relation of composite confined concrete is rather complex to obtain due to the number of

variables that affect it. For that reason simple models are predicted for the strength of FRP-confined concrete columns considering different size and curvature for using in the design desk.

## **2.6 Finite element modeling**

Wu et al. (2009) presented a three-dimensional nonlinear finite element circular model with a Drucker–Prager plasticity model for the concrete core and an elastic model for the AFRP is developed by using the finite-element code ANSYS (2005). The finite-element code ANSYS provides various elements for materials with different characteristics (ANSYS 2005). In the finite-element model developed by Wu et al. (2009), the concrete core is modeled with an eight-noded SOLID65 element, which is a 3D solid element. The SOLID65 is capable of cracking in tension, crushing in compression and accommodating plastic deformations. The AFRP sheets are modeled with a four-noded SHELL41 element, which is 3D shell element having membrane (in-plane) stiffness but no bending (out-of-plane) stiffness. In this paper, no slip between SOLID65 and SHELL41 is considered. And the SHELL41 element is set as tension only, which acts like a cloth, in that tension loads will be supported but compression loads will cause the element to wrinkle.

Hajsadeghi and Alaei (2010) devoted to investigate the behavior of square RC columns confined with FRP wraps using ANSYS software. A total of four prisms of size 150 x 300 x 500mm and 210 x 210 x 500mm are simulated by the FE model and the results are compared with the experimental test results reported in literature. Very good agreement is found between the model results and the test results. Concrete, steel reinforcement (including longitudinal and transverse) and FRP are modeled using SOLID65, LINK8, and SHELL41 elements of ANSYS software, respectively. Any slip between concrete, steel reinforcement and FRP is ignored. SOLID45 elements are used for the steel plates at the support and the loading areas as rigid bodies. Considering that FRP only resists tensile stresses, “tension-only” option of SHELL41 is activated. The loading of all specimens is controlled by force.

Square shaped plain concrete columns of size 150 x 150 x 300mm with rounded corners of 25mm radius are modeled using ANSYS 10.0 by Islam (2011). The corners of the model are defined by keypoints. The corners are rounded by defining the keypoints at the intermediate points of the curved line. Then the 8 noded SOLID65 elements are created

using volume modeling approach. Considering a displacement control loading system, displacement is applied to the nodes of the upper surface of the columns at vertically downward direction. The displacement value is determined by multiplying the initial height (150mm) with the ultimate strain of the columns obtained from the load cell of universal testing machine (UTM).



### **3.1 General**

Concretes with four aggregate types and two types/grades of fiber reinforced polymers are used in this study. The aggregates are crushed brick (CB), crushed stone (CS), recycled brick (RB) and recycled stone (RS) aggregates. The aggregates are of same gradation produced by crushing in the same crushing machine. The concrete mix ratio is maintained 1:2:4 and the water-cement ratio are maintained at 0.5. Four types of aggregate are used because of investigating and comparing the confinement effect of FRP wrap on concrete made of different aggregate with different sizes of square and circular confined concrete columns subjected to uniaxial compression which is depends on the dilation effect of four types of aggregate concretes. This chapter presents the properties of the used materials.

### **3.2 Properties of concrete**

#### **3.2.1 Portland cement**

All cement used for the casting of concrete columns is ordinary Portland cement conforming to the requirements of the ASTM. Different types of concrete columns are cast with same brand of cement. All cement for casting purposes are delivered from the same shipment and stored of the laboratory. The storage cements are carefully protected against moisture and exposure to air.

#### **3.2.2 Aggregates**

Aggregates comprise about 85% volume of concrete. Aggregate used for concrete are chemically inert, strong, hard, durable, limited porosity and free from adverse coating

clay lumps, coal, coal residues and organic or other impurities that may cause corrosion of the reinforcement or may impair the strength or durability of concrete.

According to size aggregates are of 2 types, fine aggregates (size < ASTM sieve no. 4) and coarse aggregates (size > ASTM sieve no. 4).

### 3.2.2.1 Fine aggregates

Fine aggregates are natural sand and free from coagulated lump, alkaline or acidic reaction and other deleterious matters. Sand is normally dredged from river beds and stream in the dry season when the river bed is dry or when there is not much flow in the river. According to the size and source there are two types of sands are available in Bangladesh such as sylhet sand and local sand. Sylhet sand is used in this research as fine aggregate which is bought from Narayanganj. Sylhet sands are available from the eastern part of the Bangladesh and are obtained from the bed of flowing river. Sylhet sands are reddish in colour and the fineness modulus (FM) is 2.5-2.9. Sylhet sand is composed of angular grains which are coarser than any other sand. The basic engineering properties of fine aggregates are given in Table 3.1.

Table 3.1: Properties of fine aggregates

Type of fine aggregate	Bulk specific gravity (SSD)	Bulk specific gravity (OD)	Bulk unit wt. (SSD) kg/m <sup>3</sup> (lb/ft <sup>3</sup> )	Fineness modulus
Sylhet sand	2.58	2.54	1520 (95)	2.62

### 3.2.2.2 Coarse aggregates

In this research four types of coarse aggregates; e.g. crushed stone (CS), crushed brick (CB), recycled stone (RS) and recycled brick (RB) having same gradation are used (Figure 3.1). The stone aggregates and bricks are bought from Narayanganj, Bangladesh. The stone and brick concrete cylinders after compressive strength test from BUET Concrete Laboratory are taken as recycled concrete. After crushing aggregates are graded in ASTM standard sieves to attain a specific gradation. The basic engineering properties of coarse aggregates are given in Table 3.2. Again from Table 3.2 it is found that the Los Angeles Abrasion values (LAA) are generally higher in brick and recycled aggregates than the stone aggregates due to higher porosity and lower unit weight of brick and

recycled aggregates. Mix proportions of aggregates of sizes used in this research are given in Table 3.3.

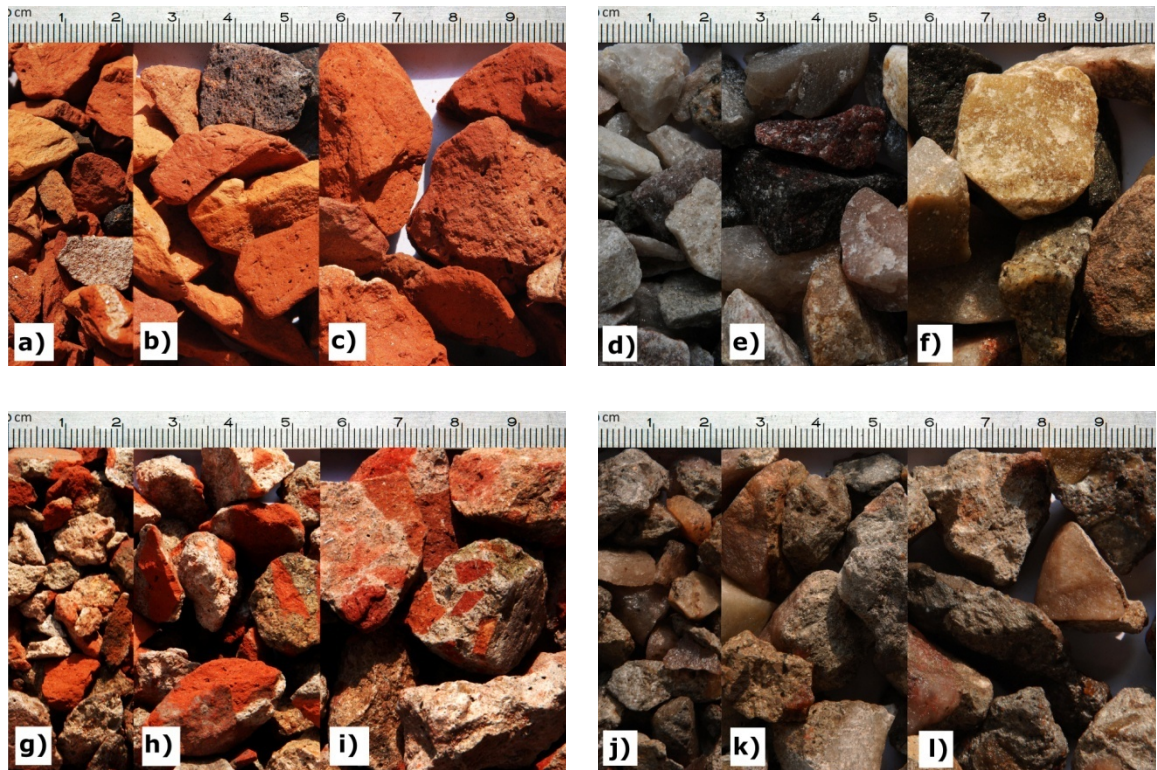


Figure 3.1: Types of aggregate used in the experiment (a), (b), (c) are brick aggregates, (d), (e), (f) are stone aggregates, (g), (h), (i) are recycled brick aggregates and (j), (k), (l) are recycled stone aggregates. Here (a), (d), (g), (j) are 1/2 inch passing and 1/4 inch retained, (b), (e), (h), (k) are 3/4 inch passing and 1/2 inch retained and (c), (f), (i), (l) are 1 inch passing and 3/4 inch retained.

Table 3.2: Properties of coarse aggregates

Type of coarse aggregate (ID)	LAA* value (%)	Absorption capacity (%)	Bulk specific gravity (OD)	Bulk specific gravity (SSD)	Unit wt. kg/m <sup>3</sup> (lb/ft <sup>3</sup> )
Stone (CS)	29.5	0.8	2.6	2.6	1568 (98)
Brick (CB)	38.0	14.4	1.7	2.0	936 (60)
Recycled Stone (RS)	38.1	5.8	2.2	2.4	1223 (76)
Recycled Brick (RB)	40.8	12.4	1.9	2.1	1000 (62)

\*Los Angeles Abrasion value.

Table 3.3: Mix proportions of coarse aggregate

Particle size		Mix proportion (by weight)
Passing through	Retained on	
25 mm	19 mm	1.24
19 mm	12 mm	1.67
12 mm	6 mm	1

### **3.2.3 Water**

Water is an important ingredient of concrete as it actively participates in the chemical reaction with cement. It has been estimated that on an average 23% of water by weight of cement is required for chemical reaction with Portland cement compound, which is known as bound water. A certain quantity of water is embedded within the gel-pores. This water is known as gel water. It can be said that bound water and gel water are complimentary to each other. It has been estimated that about 15 percent by weight of cement is required to fill up the gel-pores. Therefore a total 38 percent of water by weight of cement is required for the complete chemical reactions and occupy the space within gel-pores. In this research the water-cement ratio is maintained at 0.5 for all types of concrete. The slump is maintained 25 mm to 37 mm (1-1.5 in). However the moisture contents of the aggregates are duly taken care of by adjusting the water to be added during mixing.

## **3.3 Properties of FRP**

### **3.3.1 CFRP wraps**

Carbon fiber Build Seal<sup>®</sup> is a fabric sheet of longitudinal oriented, continuous carbon fiber filaments which are held in position by a lightweight, open mesh, glass scrim (Figure 3.2). Build Seal<sup>®</sup> CFFS Extra has robust handling and rapid wet-out characteristics which make it ideal for on-site strengthening of structural of buildings, bridges, beams, columns and marine structures. Additionally, Build Seal<sup>®</sup> CFFS Extra is compatible with all commonly used resin systems which can be applied using a variety of wetout/resin infusion techniques. The physical properties of carbon fibers provided by manufacturer are given in Table 3.4.

Carbon fiber is produced by the controlled oxidation, carbonization and graphitization of carbon-rich organic precursors which are already in fiber form. The most common precursor is polyacrylonitrile (PAN), because it gives the best carbon fiber properties, but fibers can also be made from pitch or cellulose. Variation of the graphitization process produces either high strength fibers (at 2,600°C) or high modulus fibers (at 3,000°C) with other types in between. Once formed, the carbon fiber has a surface treatment applied to improve matrix bonding and chemical sizing which serves to protect it during handling. The engineering properties of CFRP provided by manufacturer are given in Table 3.5.

The flat coupon test results of carbon fibers done by the manufacturers are given in Table 3.6.

Key properties of the CFRP are high strength, high thermal conductivity, light weight, electrical conductivity, excellent fatigue resistance, excellent corrosion resistance, low friction and wear, low thermal expansion, resistance to high temperatures, good creep and damping properties, transparent to x-rays.

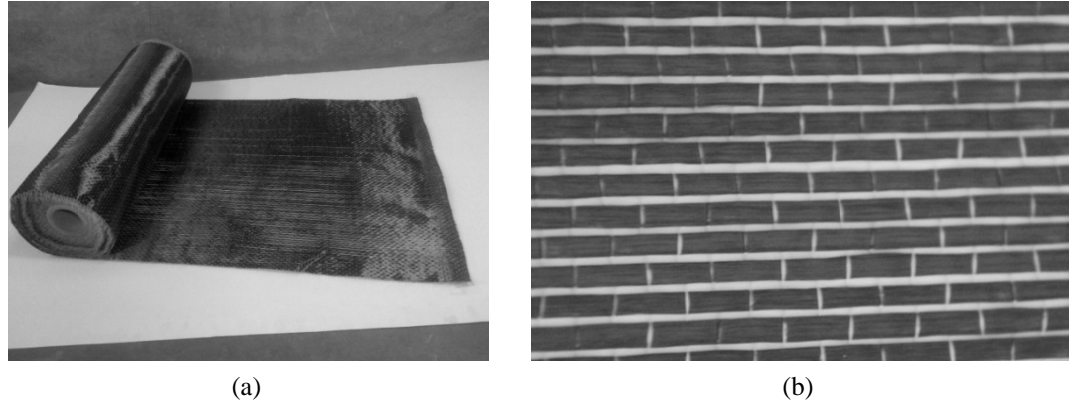


Figure 3.2: FRP wraps for confinement of short plain concrete columns (a) CFRP wrap (b) close look of CFRP fibers

Table 3.4: Physical properties of CFRP

Products grade	Extra 200	
Carbon fiber weight	200	g/m <sup>2</sup>
Glass scrim weight	10	g/m <sup>2</sup>
Total product weight	210	g/m <sup>2</sup>
Roll width	500	mm
Sheet thickness	0.117	mm
Typical binder/size content	3.0	%

Table 3.5: Specification properties of carbon fiber fabric sheet

Typical of carbon fiber properties	SI units		US units	
Tensile strength	4,900	MPa	710,500	psi
Tensile modulus	230	GPa	32.80 x 10 <sup>6</sup>	psi
Ultimate elongation	1.80	%	1.80	%
Density	1.79	g/cm <sup>3</sup>	0.0646	lb/in <sup>3</sup>
Cross-sectional area per filament	0.43	mm <sup>2</sup>	6.63 x 10 <sup>-4</sup>	in <sup>2</sup>
Approximate yield (12k)	1.31	m/g	1,950	ft/lb
Filament shape	Round		Round	
Filament diameter	6.7	μm	0.265	mil
Weight/length	0.765	g/m	42.8 x 10 <sup>-6</sup>	lb/in

Table 3.6: Flat Coupon Test results of CFRP wrap

Flat coupon test for carbon fiber and resin Test parameters	Test method	SI units	
Tensile strength	ASTM D3039	3,100 ±50	MPa
Tensile modulus	ASTM D3039	160±05	GPa
Flexural strength	ASTM D790	1,850 ±52	MPa
Flexural modulus	ASTM D790	131 ±05	GPa
ILS/SBSS	ASTM D2344	128 ±05	MPa
No. of piles		3	Nos.
Fiber volume		±72	%
Resin volume (Epoxy)		±28	%
Elongation @ break (Calc.)		1.61	%

### 3.3.2 GFRP wraps

Glass fiber Build Wrap<sup>®</sup> is a fabric sheet of longitudinal oriented, continuous glass fiber filaments which are held in position by a lightweight, open mesh, glass scrim (Figure 3.3). Build Wrap<sup>®</sup> has robust handling and rapid wet-out characteristics which make it ideal for on-site strengthening of structural of buildings, bridges, beams, columns and marine structures. Additionally, Build Wrap<sup>®</sup> is compatible with all commonly used resin systems which can be applied using a variety of wet-out/resin infusion techniques. The physical properties of carbon fibers provided by manufacturer are given in Table 3.7.

Key properties of GFRP are high modulus, high thermal conductivity, light weight, electrical conductivity, excellent fatigue resistance, excellent corrosion resistance, low friction and wear, low thermal expansion, resistance to high temperatures, good creep and damping properties, transparent to x-rays. The engineering properties of GFRP provided by manufacturer are given in Table 3.8.

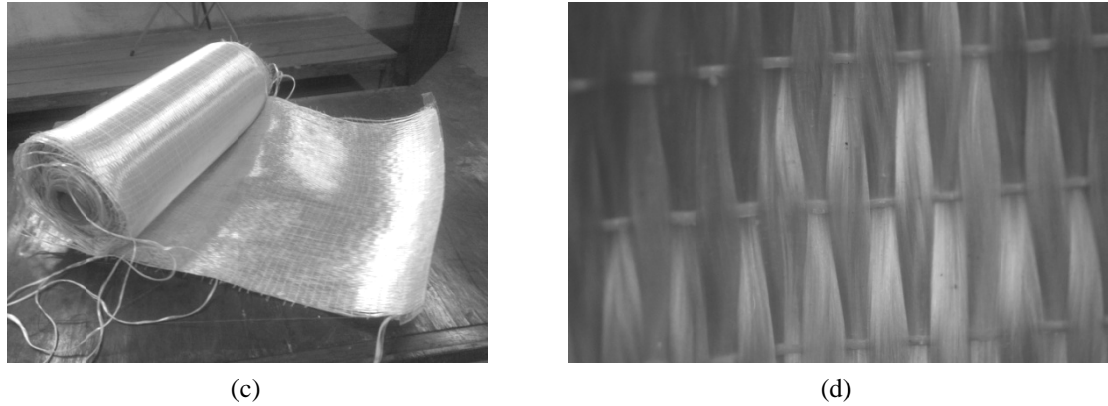


Figure 3.3: FRP wraps for confinement of short plain concrete columns (a) GFRP wrap (b) close look of GFRP fibers.

Table 3.7: Physical properties of GFRP wrap

Products grade	Build Wrap® G920
Glass Fiber Weight	920 g/m <sup>2</sup>
Glass Scrim Weight	20 g/m <sup>2</sup>
Total Product Weight	940 g/m <sup>2</sup>
Roll Width	500 mm
Roll Length	40 meter
Sheet Thickness	0.376 mm
Total Roll Weight	18.80 kg

Table 3.8: Specification properties of glass fiber

Typical of Fiber Properties	SI / Units		US / Units	
Tensile Strength	2,300	MPa	333,500	psi
Tensile Modulus	76	GPa	10.84 x 10 <sup>6</sup>	psi
Ultimate Elongation	2.80	%	2.80	%
Density	2.56	g/cm <sup>3</sup>	0.0923	lb/in <sup>3</sup>

### 3.4 Properties of adhesives and primers

Epo Bond CF Resin is Epoxy Solvent Free (Bisphenol-F). It has two components; these are Part A & Part B (Figure 3.4). It is suitable for applied on overhead or vertical or horizontal surfaces. A low speed (300 to 500 rpm) electric drill fitted with a paint mixer is used to mix these components for at least 3 minutes until the mix is uniform and free to flow. As the pot life of this epoxy is only 60 minutes, resin or polyurethane resin is applied within this time. The engineering properties of Epoxy Resin (Epo Bond CF Paste) and Epo Bond Primer provided by manufacturer are given in Tables 3.9-3.10.



Figure 3.4: Epo Bond CF Resin (provided by manufacturer).

Table 3.9: Epoxy Resin (Epo Bond CF Paste) properties of specification

Epoxy resin properties of specification	(Paste form: high viscosity solvent free)
Compressive strength	50 N/mm <sup>2</sup>
Flexural strength	37 N/mm <sup>2</sup>
Tensile strength	80 N/mm <sup>2</sup>
Bonding strength	Excellent bond to structural
Tension elongation at break	6%
Solid volume	100% High Solid Resin
Viscosity at 25 °C	25000 (±550) mPa.s
Density at 25 °C	0.97 g/cu. cm
Pot life at 25 °C	> 45 minutes until 60 minutes
Cure time at 25 °C	As pot life test method
Specific gravity	970 g/liter
Flash point	> 200 °C
Tear resistance	Excellent on External & Internal Layer
Abrasion resistance	10 sec/1000 cycle, 0.01% Peeling off on Top Surfaces
Fire resistance	Burning Test, Good Conditions of Class 0
Toxicity	Essentially non-toxic in cured fabricated panel
Coverage thickness	0.75 kg/m <sup>2</sup> to 2.00 kg/m <sup>2</sup>
Stability under heat	70 °C
Glass transition temp	90 °C
Shore A hardness	None
Shore D hardness	82-86%
Packing	5 kg/pail (Part A/2.95 kg & Part B/2.05 kg)



Table 3.10: Epo Bond Primer properties of specification

Properties of specification	Test results of cured coating
Compressive strength	48 N/mm <sup>2</sup>
Flexural strength	36 N/mm <sup>2</sup>
Tensile strength	72 N/mm <sup>2</sup>
Bonding strength	Excellent bond to structural
Tension elongation at break	2%
Solid volume	100% High solid resin
Viscosity at 25 °C	3500 (±250) MPa.s
Density at 25 °C	1.02 g/cu. cm
Pot life at 25 °C	> 25 minutes until 60 minutes
Cure time at 25 °C	Dust-dry time: 1.5 hours , full cured: 4 hours
Specific gravity	1020 g/liter
Flash point	> 200 °C
Tear resistance	Excellent on external & internal layer
Abrasion resistance	10 sec/1000 cycle, 0.01% peeling off on top surfaces
Fire resistance	Burning test, good conditions of class 0
Coverage thickness	0.15 kg/m <sup>2</sup> to 0.50 kg/m <sup>2</sup>
Stability under heat	70 °C
Glass transition temp	90 °C
Shore A hardness	None
Shore D hardness	75%
Packing	5.00 kg/pail

**EXPERIMENTAL PROGRAM AND DATA ACQUISITION**

---

**4.1 General**

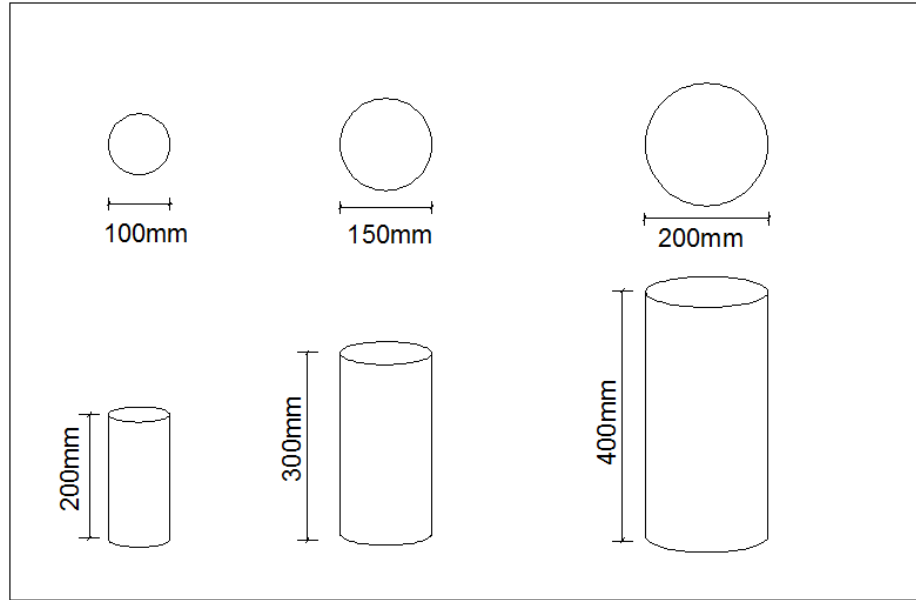
The specimens are designed as full-scale models due to the need for testing larger and more realistic column sections. All specimens are unreinforced short concrete columns. One third of the specimens are wrapped with Carbon Fiber Reinforced Polymer (CFRP) composites while the other third Glass Fiber Reinforced Polymer (GFRP) composites to investigate the effect of confinement of different sizes of concrete column. The rest columns are kept unconfined as control specimens. Two basic geometric types, i.e. circular and square columns are studied. All the CFRP and GFRP fabrics, adhesives and primers are provided by the genuine Manufacturers. This chapter presents the geometric parameters, experimental plan, specimen preparation methodology, data acquisition philosophy and details of laboratory procedure.

**4.2 Size and geometry of specimen**

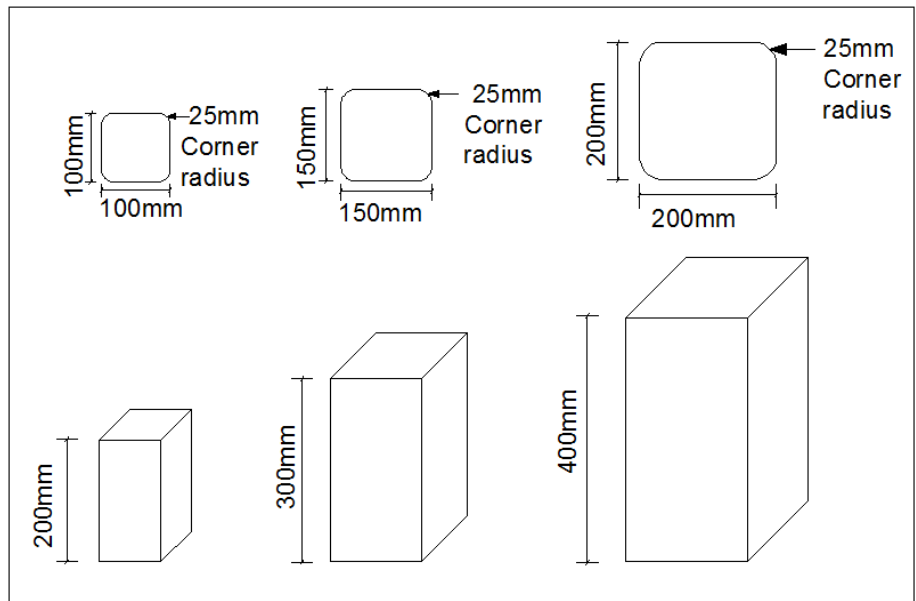
The circular concrete columns are 100 mm, 150 mm and 200 mm in diameter and 200 mm, 300 mm and 400 mm in height respectively with the same aspect ratio (Figure 4.1a). Again the square concrete columns are 100 mm x 100 mm x 200mm, 150 mm x 150 mm x 300 mm and 200 mm x 200 mm x 400mm but with the same aspect ratio (Figure 4.1b). Size and geometry of the specimen are summarized in Table 4.1. ACI 440.2R-08 recommends that the corners of rectangular cross sections should be rounded to a minimum 0.5 in. (13 mm) radius to prevent stress concentrations in the FRP confined system. If the corner of square cross section rounded manually, these may create uneven curvature and may not be uniform in all the columns. For this reason specially prepared steel molds with rounded corners (25 mm radius) are used to cast all the columns to attain similar confinement at the corners and to avoid any damage on FRP wrap due to stress concentration. Steel moulds for square and circular concrete columns of different size are shown in Figure 4.2.

Table 4.1 Size and Geometry of the specimens

Shape	Aggregate types	Number of specimens	Nominal dimension Length x Diameter/ Side (mm)	
Circular	Crushed brick	6	200x100	
		6	300x150	
		3	400x200	
		6	200x100	
		6	300x150	
		3	400x200	
	Recycled brick	6	200x100	
		6	300x150	
		3	400x200	
		Recycled stone	6	200x100
			6	300x150
			3	400x200
Square	Crushed brick	6	200x100x100	
		6	300x150x150	
		3	400x200x200	
		6	200x100x100	
		Crushed stone	6	300x150x150
			3	400x200x200
	6		200x100x100	
	Recycled brick	6	300x150x150	
		3	400x200x200	
		Recycled stone	6	200x100x100
			6	300x150x150
			3	400x200x200



(a) Circular columns



(b) Square columns

Figure 4.1: Column geometries.



(a) Square moulds



(b) Circular moulds

Figure 4.2: Steel moulds for square and circular concrete columns

### 4.3 Geometric parameters affecting confinement

The parameters considered in this study are radius of curvature, column side to corner radius ratio, FRP volumetric ratio and rigidity ratio which are affecting the confinement due to dilation of concrete.

#### 4.3.1 Radius of curvature

Radius of curvature is the radius of an approximating circle passing through points on the curve. Figure 4.3 shows that small radius provides high curvature and large radius provides low curvature. Radius of curvature of circular concrete columns is increased with height but for square concrete columns, a constant radius of curvature is maintained

for different height with the same aspect ratio (Figure 4.4). Radius of curvature of circular concrete columns are 50mm,75mm and 100mm but for square concrete columns it is 25mm with 200mm, 300mm and 400mm height respectively.

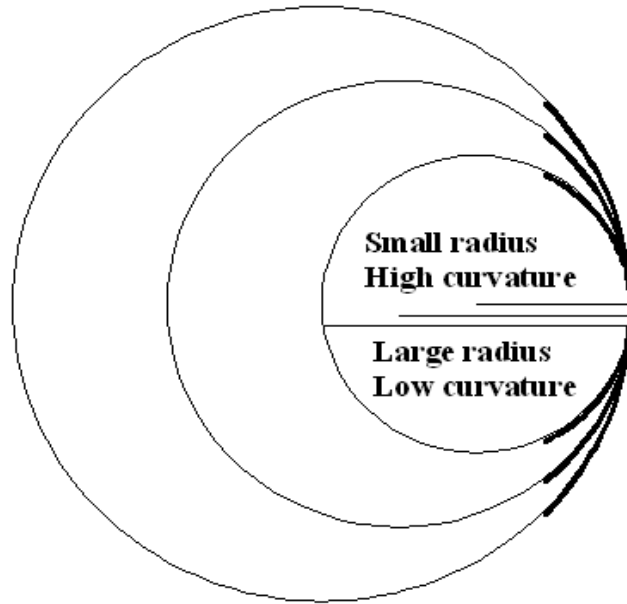


Figure 4.3: Radius of curvature.

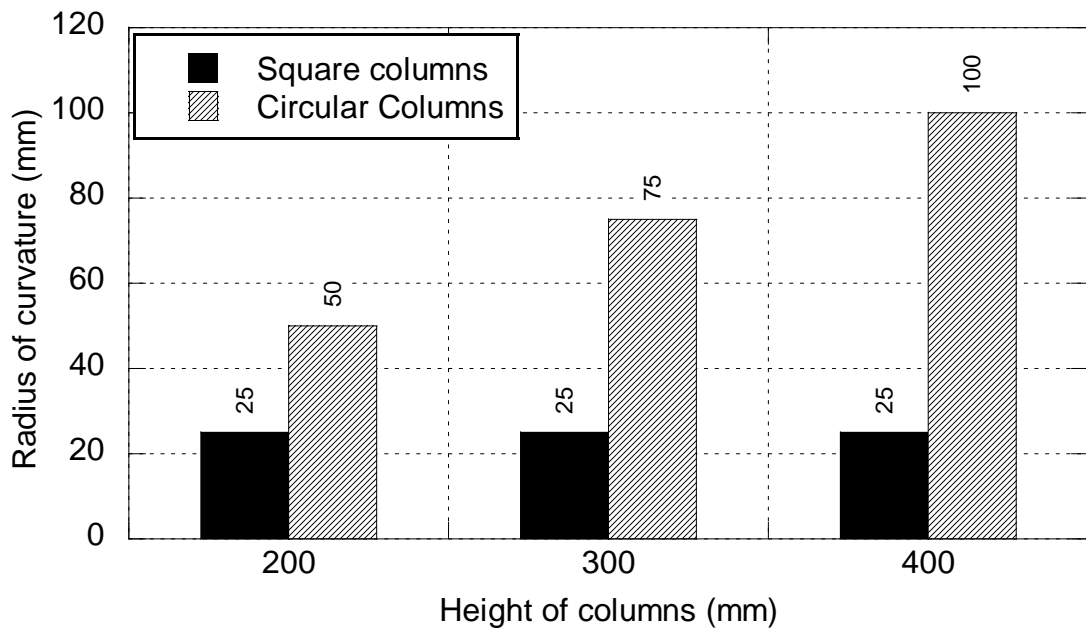


Figure 4.4: Evaluation of radius of curvature with height of circular and square concrete columns.

### 4.3.2 Column side to corner radius ratio

Column side to corner radius ratio is the ratio of the column side to the radius of the rounded corner of non-circular columns, i.e.  $B/r$  (Figure 4.5). Column side to corner radius ratio are 4, 6 and 8 with respect to 200mm, 300mm and 400mm size square concrete columns which is clearly shown in Figure 4.6.

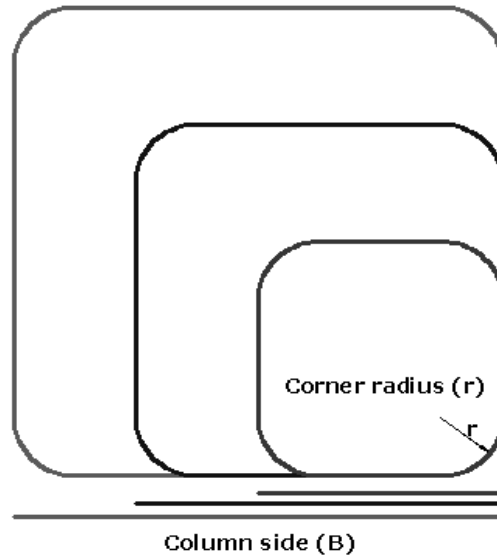


Figure 4.5: column side to corner radius ratio of square concrete columns.

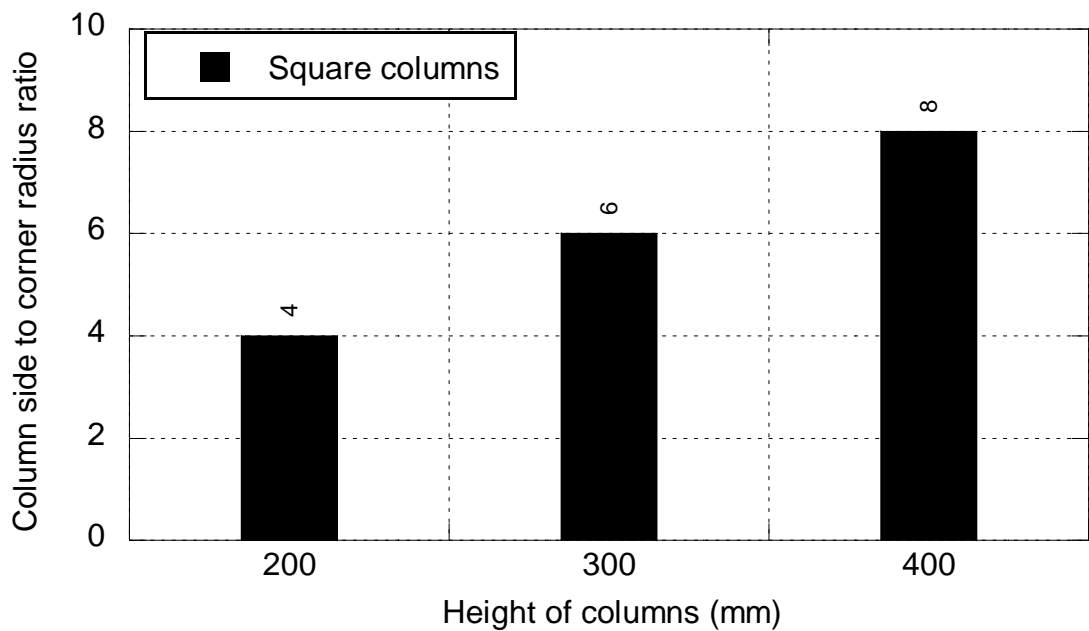


Figure 4.6: Evaluation of column side to corner radius ratio with height of square concrete columns.

### 4.3.3 FRP volumetric ratio ( $\rho_{frp}$ )

FRP volumetric ratio is defined as the area of the FRP wrap to the area of the cross section i.e.  $A_f / A_c$  (Figure 4.7). The FRP volumetric ratio for circular column is calculated as the following formula (Teng et al. 2002):

$$\rho_{frp} = \frac{\pi d n t_f}{\pi d^2 / 4} \quad (4.1)$$

where  $d$  = diameter of the circular column,  $n$  = number of FRP layers,  $t_f$  = thickness of one layer FRP in mm.

The FRP volumetric ratio for square column is calculated as the following formula:

$$\rho_{frp} = \frac{2\pi + 4(b - 50)nt_f}{b^2 - 536.5} \quad (4.2)$$

where  $b$  = side of the square column,  $n$  = number of FRP layers,  $t_f$  = thickness of one layer FRP in mm.

The CFRP volumetric ratio are considered 0.255%, 0.216%, 0.179% and 0.468%, 0.312%, 0.234% for square and circular concrete columns respectively. Again for GFRP volumetric ratio the values are 0.819%, 0.695%, 0.577% and 1.5%, 1%, 0.752% for square and circular concrete columns. Figure 4.8 and Figure 4.9 shows that CFRP and GFRP volumetric ratio are decreased with increasing column height both for square and circular concrete columns.

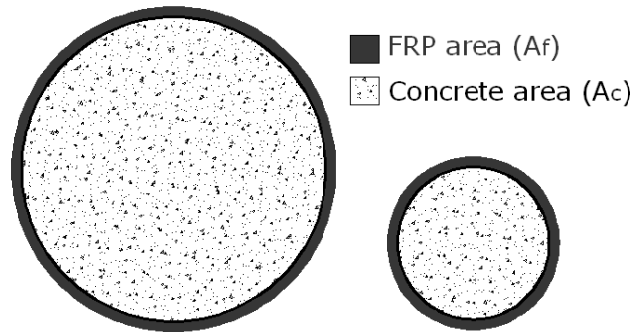


Figure 4.7: FRP volumetric ratio of circular and square concrete columns.



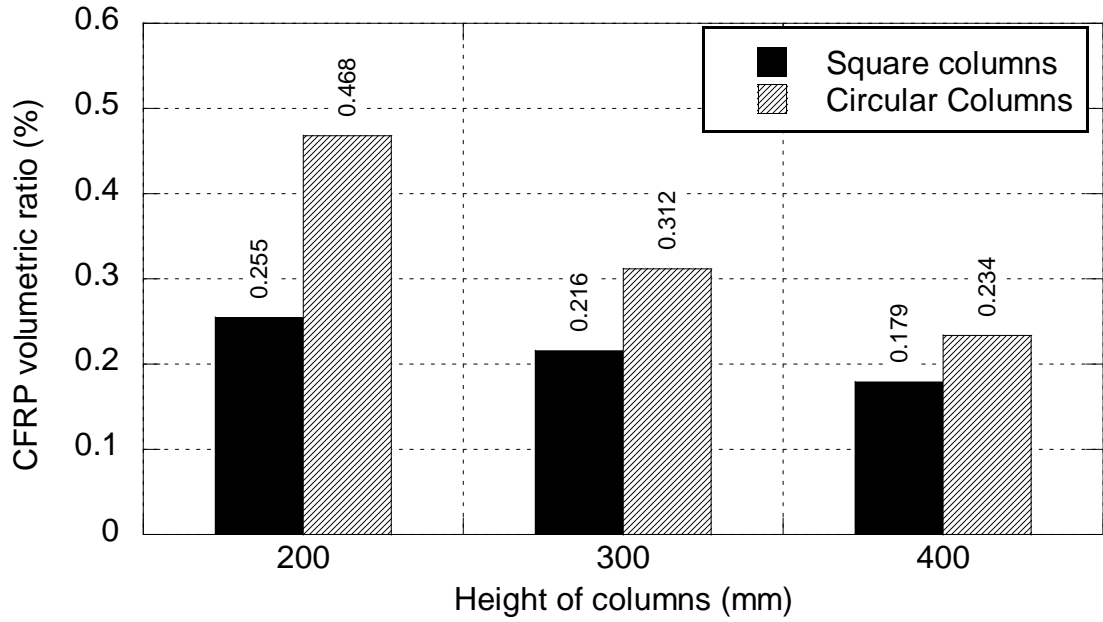


Figure 4.8: Evaluation of CFRP volumetric ratio with height of circular and square concrete columns.

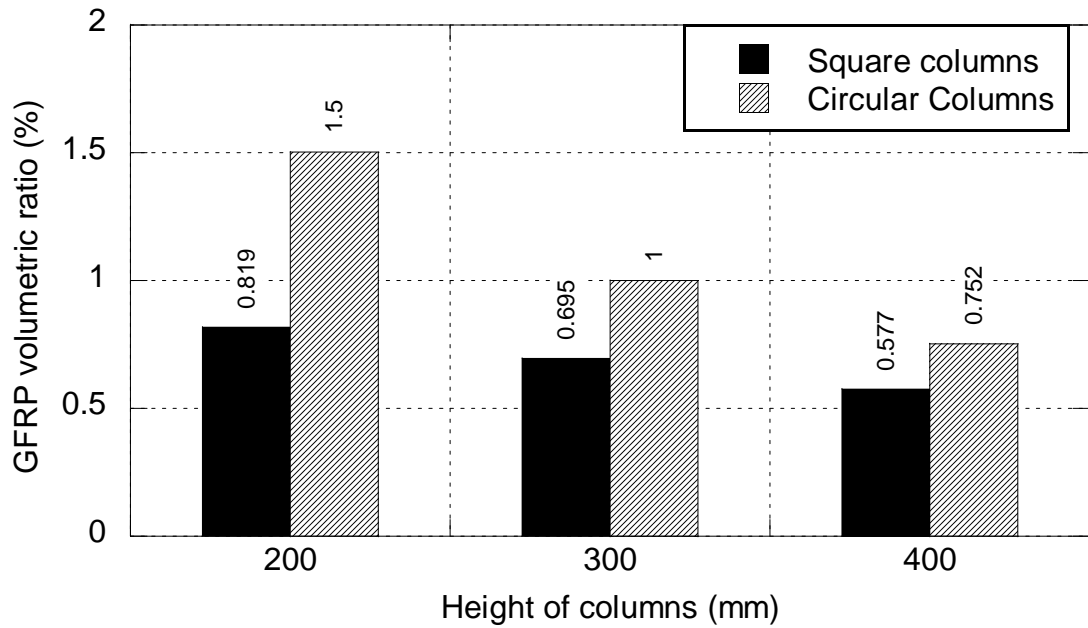


Figure 4.9: Evaluation of GFRP volumetric ratio with height of circular and square concrete columns.

#### 4.3.4 Rigidity ratio

The gain in strength depends not only on the number of FRP layers but also on the properties of concrete. The confining effect depends on two principal factors, the first being the deformability of the concrete, which is inversely proportional to its stiffness, and the second being the stiffness of the confining jacket in the lateral direction. The ratio of the FRP jacket's stiffness in the lateral direction to the short column axial stiffness  $E_c A_c$  is calculated using the following formula (Chaallal et al. 2003 ):

$$\text{Rigidity ratio} = \frac{E_f A_f}{E_c A_c} \quad (4.3)$$

where  $E_f$  = Modulus of Elasticity of FRP,  $E_c$  = Modulus of Elasticity of concrete,  $A_f$  = Area of FRP,  $A_c$  = Area of concrete columns.

The modulus of elasticity of the concrete is derived from the stress-strain diagram of the experimental results.

#### 4.4 Sample size

A total of 120 circular and square concrete columns are cast to investigate and compare the confinement effect of concrete confined with CFRP and GFRP wraps for three different sizes. Out of 120 columns, 40 columns are wrapped with carbon fiber reinforced polymer (CFRP) composites and 40 columns are wrapped with glass fiber reinforced polymer (GFRP) composites and the rest 40 columns are tested as control specimen. As there are 4 types of concrete, i.e. stone aggregate concrete, brick aggregate concrete, recycled stone aggregate concrete and recycled brick aggregate concrete, 6 columns are cast by each type of concrete.

#### 4.5 Specimen preparation

##### 4.5.1 Casting and sampling

All different size and shape of concrete columns are cast using the same mixer machine. The concrete is cast and compacted in layers using mechanical vibrator (Figure 4.10). The columns are stripped of the moulds after about 24 hours of casting and are given

specimen designation as per type of concrete and type of confining wrap. Same mix ratio, w/c ratio and slump are maintained for all kind of concrete casting (Figure 4.11).



Figure 4.10: concrete compacted in layers using mechanical vibrator



Figure 4.11: Circular and square moulds filled with fresh concrete

#### 4.5.2 Curing of concrete

Concrete columns are cured with water for 28 days in the curing tank. Water used for curing is met by the requirements of the specifications for water used for mixing concrete.

#### 4.5.3 Surface Preparation

Standard FRP installation recommends that after curing, all the columns are removed from the curing tank and left to dry in air to bring the surface moistures below 4%. All the dusts and alkalis of the columns surface are cleaned and removed by rubbing with sand paper. The fins at the mold joints of the column specimen are removed with grinding machine (Figure 4.12). The dusts are cleaned by using brooms and brushes.



Figure 4.12: Columns after surface preparation. Uneven surfaces are made even using grinding machine.

#### 4.5.4 Installation of FRP and lapping

After cleaning the concrete column surfaces from dust, low viscosity Epo Bond CF<sup>®</sup> Primer is applied on the concrete surface. The primer has two components; Part A and Part B which is mixed with a ratio about 3:2. A low speed (300 to 500 rpm) electric drill fitted with a paint mixer is used to mix these components for at least 3 minutes until the mix is uniform and free to flow. As the pot life of this epoxy is only 60 minutes, resin or polyurethane resin is applied within this time on the concrete surface at a rate  $0.20 \text{ kg/m}^2$

using a roller and left for 1/2 hour for curing (Figure 4.13). After that Epo Bond CF<sup>®</sup> Paste is applied on the FRP sheets at a rate 0.25 kg/m<sup>2</sup> for CFRP and 0.50 kg/m<sup>2</sup> for GFRP which is a high solid Epoxy based or Polyurethane based resin. This adhesive is prepared by mixing its two components Part A and Part B with a ratio about 3:2. It is applied on the FRP fabrics using a roller to begin the saturation of the sheet and left for 1/2 hour to 4 hours for curing depending on whether temperature. After saturation the FRP sheets are wrapped on the concrete columns. The fiber is oriented to the hoop direction (Figure 4.14). The lapping is 25% of columns perimeter or 1 face extra is maintained for all the columns. Hand pressure is applied to squeeze out air pockets and to press against the preceding layers to ensure sound adhesion between the two. Proper orientation of fibers is visually checked. Another coat of Epo Bond CF<sup>®</sup> Paste is applied over the FRP sheet of the columns.

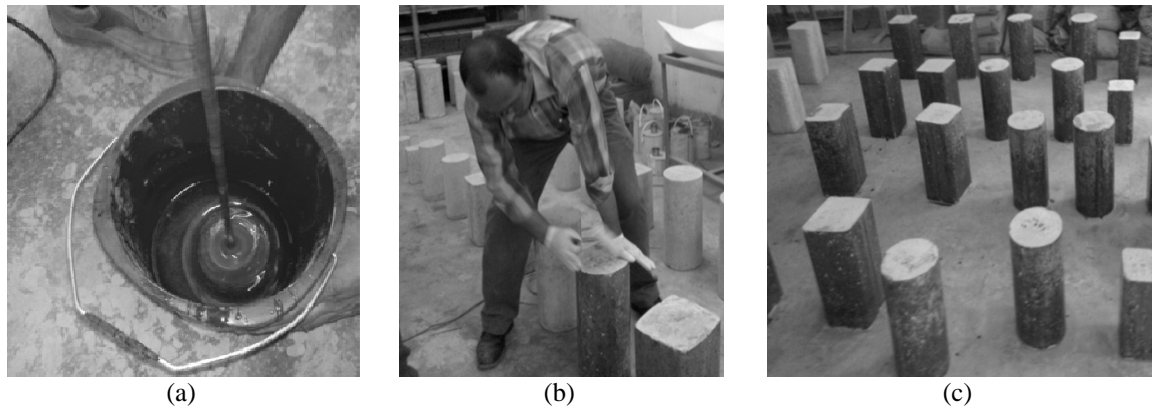


Figure 4.13: Preparation of primer (a) Mixing of Part A and B of primer; thickening for prime coat application with a mechanical mixer operating at 500 rpm at 3 minutes, (b) application of primers on the columns, (c) primer coated columns (surface are darkened by the prime coat)





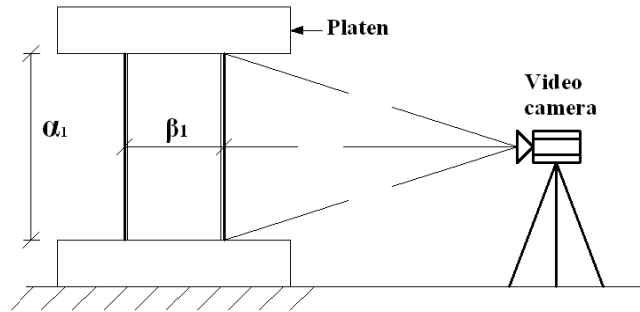
(c)

Figure 4.14: (a) Saturation of GFRP sheet with epoxy resin, (b) Wrapping of column with CFRP sheet, (c) CFRP confined columns prepared for testing

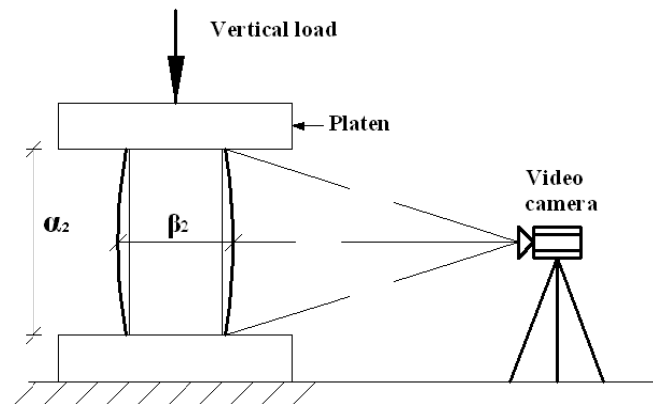
#### 4.6 Testing and data acquisition

All 120 concrete columns are tested using a 2000 kN universal testing machine at Structural Mechanics Laboratory of Bangladesh University of Engineering and Technology. The machine is also equipped with sophisticated computer control and data acquisition system. The specimens are tested under pure axial compression and the loading rate maintained is 0.21 MPa/s under displacement control mode according to ASTM C39. The time required for each testing of CFRP and GFRP confined square columns is 120-130 second but for circular columns it is 220-250 seconds for CFRP confined concrete columns and 280-300 seconds for GFRP confined concrete columns. Rubber pad is used at the top and bottom of the column to minimize the edge effect and to distribute the pressure uniformly on the concrete contact surface.

Axial load and vertical displacement data are recorded from the load cell of a computer controlled universal testing machine. Using these data the axial stress-strain curves are plotted. But the lateral dilation of both confined and unconfined concrete columns are measured by analyzing the image histories obtained from High Definition (60 frames per second) video camera (Figure 4.15 and 4.16). After that an image analysis technique are employed. The load and displacement histories obtained from the load cell of a computer controlled universal testing machine is synthesized with the lateral strain measurement results gathered from image analysis of High Definition video clips and images. In this process, lateral strain, Poisson's effect and the confinement due to dilation of concrete for different aggregates are measured.



(a)



(b)

$\alpha_1 - \alpha_2 = \text{Vertical Contraction}$   
 $\beta_2 - \beta_1 = \text{Lateral Expansion (Dilation)}$



(c)

Figure 4.15: Simultaneous data acquisition system (a) unloaded condition, (b) loaded condition (c) experimental setup.

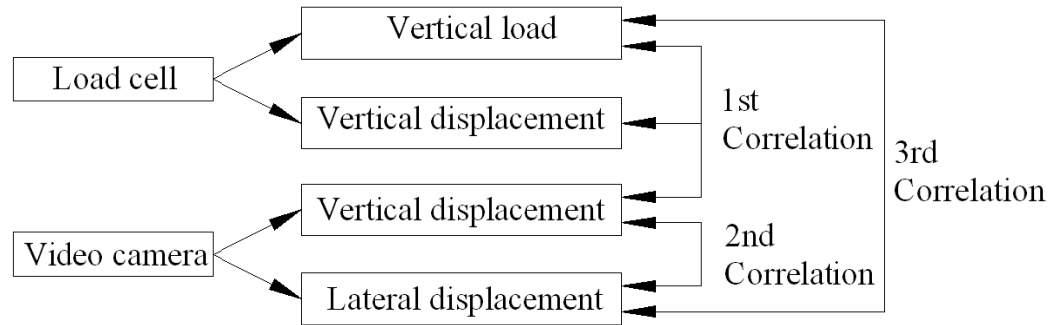


Figure 4.16: Data acquisition scheme

#### 4.7 Data correction and synthesis

Due to the large displacement of rubber pad all the load displacement curves are found to be affected at the initial segment of the curves. But rubber pad is used to minimize the edge effect and to distribute the pressure uniformly on the uneven surface at the contact area of concrete with the platen. For that reason the curves started in a parabolic shape instead of linear. So the axial load displacement data is corrected by removing the displacement part due to the rubber pad and then plotted again for all 120 columns (Figure 4.17 and 4.18).

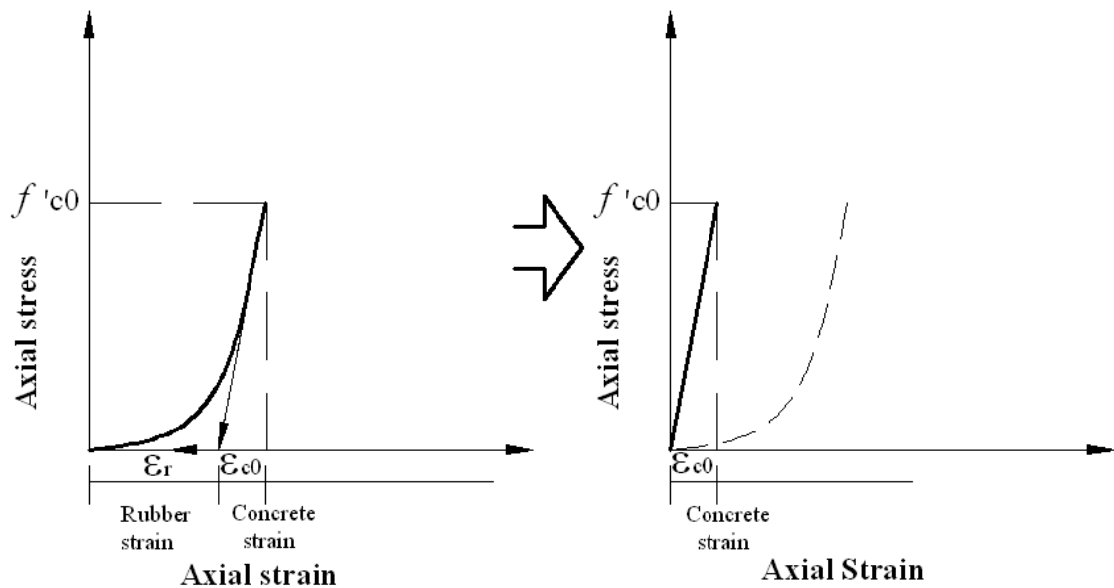


Figure 4.17: Stress-strain behaviour of unconfined concrete (a) affected by displacement due to rubber pad (b) after correction



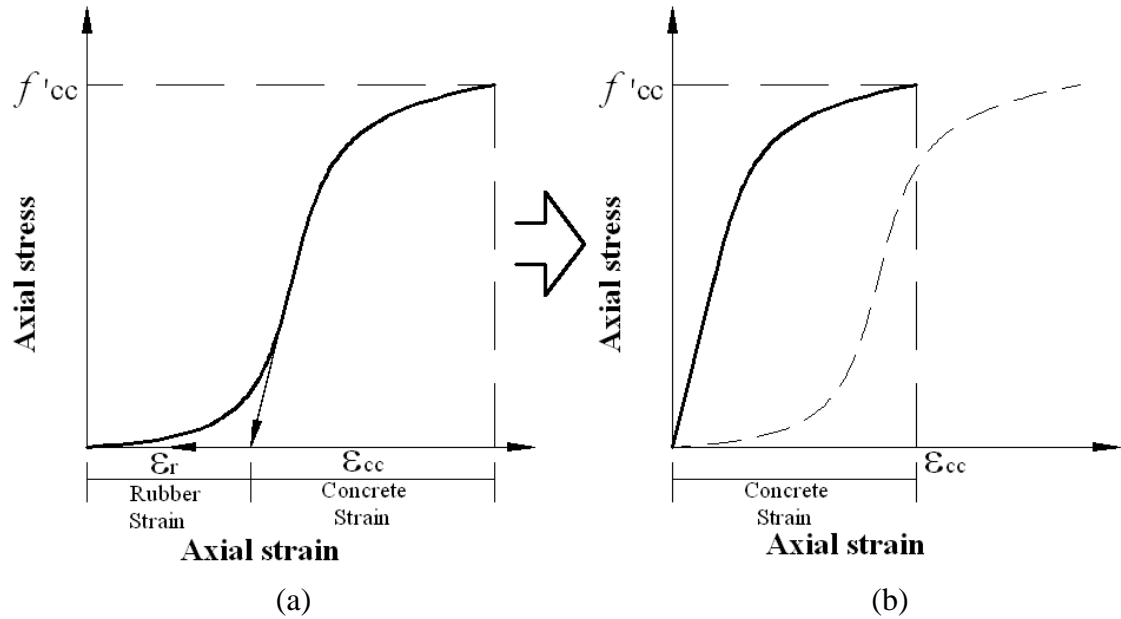


Figure 4.18: Stress-strain behaviour of confined concrete (a) affected by displacement due to rubber pad (b) after correction

#### 4.8 Specimen designations and legends

A special designation is used for all the columns. The designation system provides the information of type of concrete used, shape of column, size of column, confining condition (unconfined or confined) and type of FRP used in confinement. The legends used in the curves also have significant characteristics. The specimen designations and legends are shown in Figures 4.19 and 4.20. The system has been used throughout the text of this dissertation.

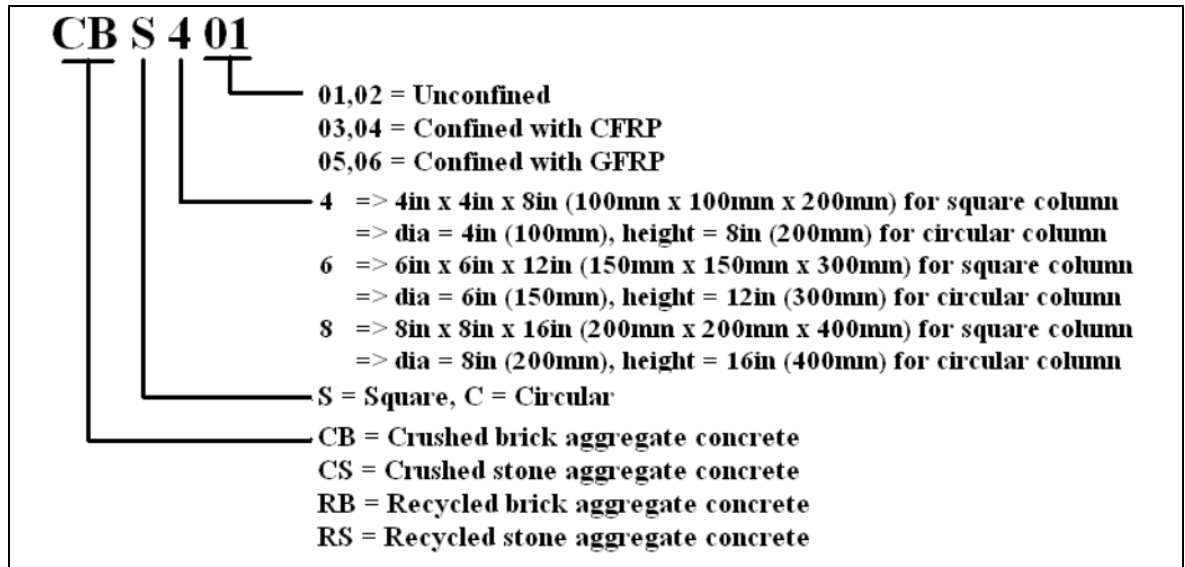


Figure 4.19: Specimen designation

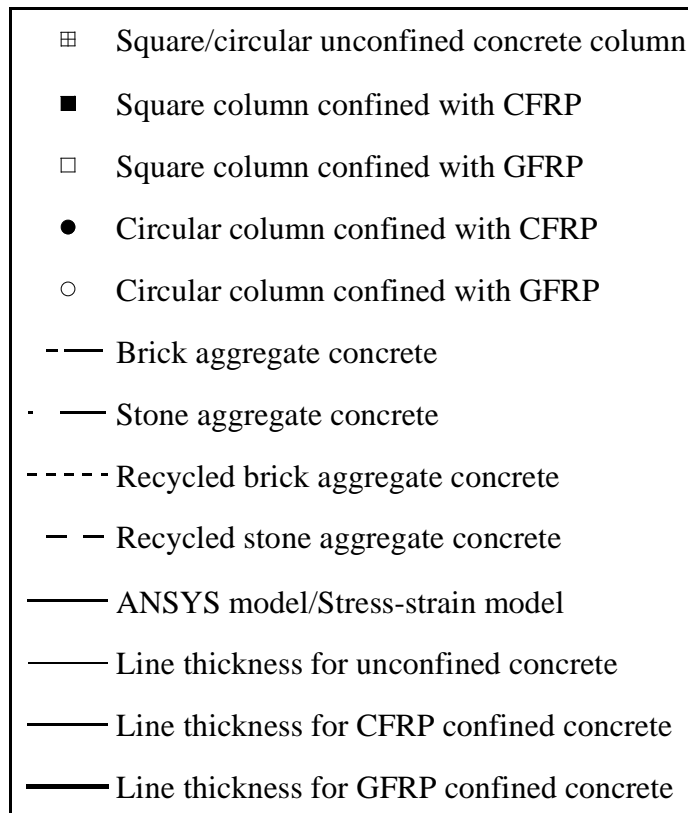


Figure 4.20: Legends used in the figures.

**EXPERIMENTAL RESULTS AND DISCUSSION**

---

**5.1 General**

The behaviors of FRP-confined concrete under compressive loads are compared for different geometries, shape of cross section (circular and square) and different type of fibers. To this end, parameters representing geometry and confinement have been varied to observe their effect on axial capacity enhancement. This chapter discusses the failure patterns and the confining effect of CFRP and GFRP wrapped circular and square concrete columns made of brick, stone, recycled brick and recycled stone concrete on the basis of test results of different geometry.

**5.2 Failure patterns**

FRP-wrapped specimens failed under axial compression primarily due to rupture of fiber in tension developed along the hoop direction. Failure is occurred in a sudden and explosive way and is preceded by typical creeping sounds. The failure patterns of the unconfined and confined columns of different shapes are given in Tables 5.1-5.4 of Appendix A.1-A.4. It is also observed from the tests that failure of GFRP-jacketed specimens was more ductile than specimens with CFRP confinement. Progressive cracking sounds are heard during the tests for GFRP specimens before failure, showing a more progressive failure than that observed, for CFRP-jacketed specimens.

**5.2.1 Circular columns**

Performance of the circular columns under axial load is consistent. Prior to the failure, cracking noises are heard, indicating the start of stress transfer from the dilated concrete to the FRP jacket. The failure is gradual and ended suddenly with noise of explosion. It is characterized by crushing of concrete followed by rupturing the FRP laminates at the middle portion of the specimen. The rupture started at mid-height (Figure 5.1). The

explosive nature of the failure indicates the release of tremendous amount of energy as a result of the uniform confining stress provided by the jacket. Inspections of the broken samples are shown good contact between the jacket and the concrete indicating that no debonding took place at any stage throughout the loading process. It is concluded that column size does not have an obvious influence on the failure modes of CFRP and GFRP confined circular columns are shown in Tables 5.1-5.4 of Appendix A.1-A.4.

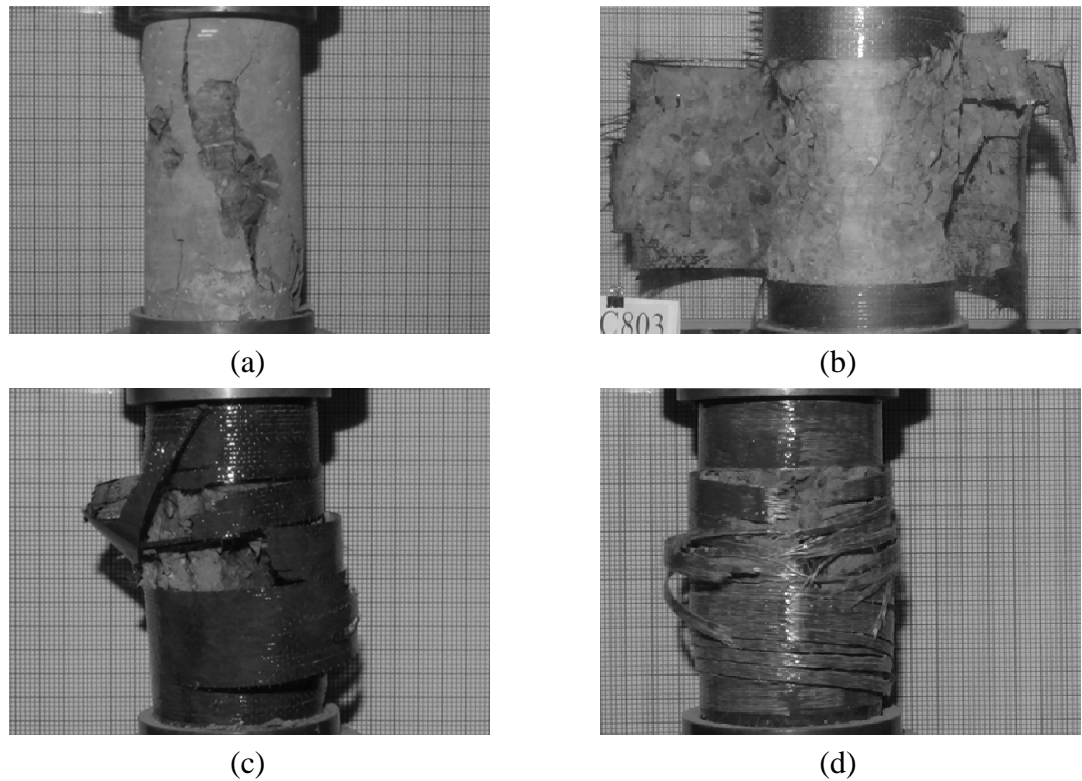


Figure 5.1: Failure patterns of circular columns (a) failed by shear, (b) CFRP rapture at middle, (c) bursting of CFRP and (d) bursting of GFRP at middle.

### 5.2.2 Square columns

Most of the unconfined square columns are failed by vertical splitting. Depending on maximum sustained vertical loads, the confined columns failed either through bursting or crushing. The failure of confined square concrete columns took place at one of the corners near bottom to mid height of the specimen (Figure 5.2). The failure is gradual and less explosive than that of the circular columns. This proves the fact that confining forces created by a square jacket tends to be concentrated at the corners. For this reason, the rounding of the square column corners provides a uniform confining stress. A few

failures at the top of the column are also found by the rapture of FRP and crushing of concrete. Thus it is concluded that all sizes of square columns failed due to stress concentration at or near corner (Appendix A.1-A.4).

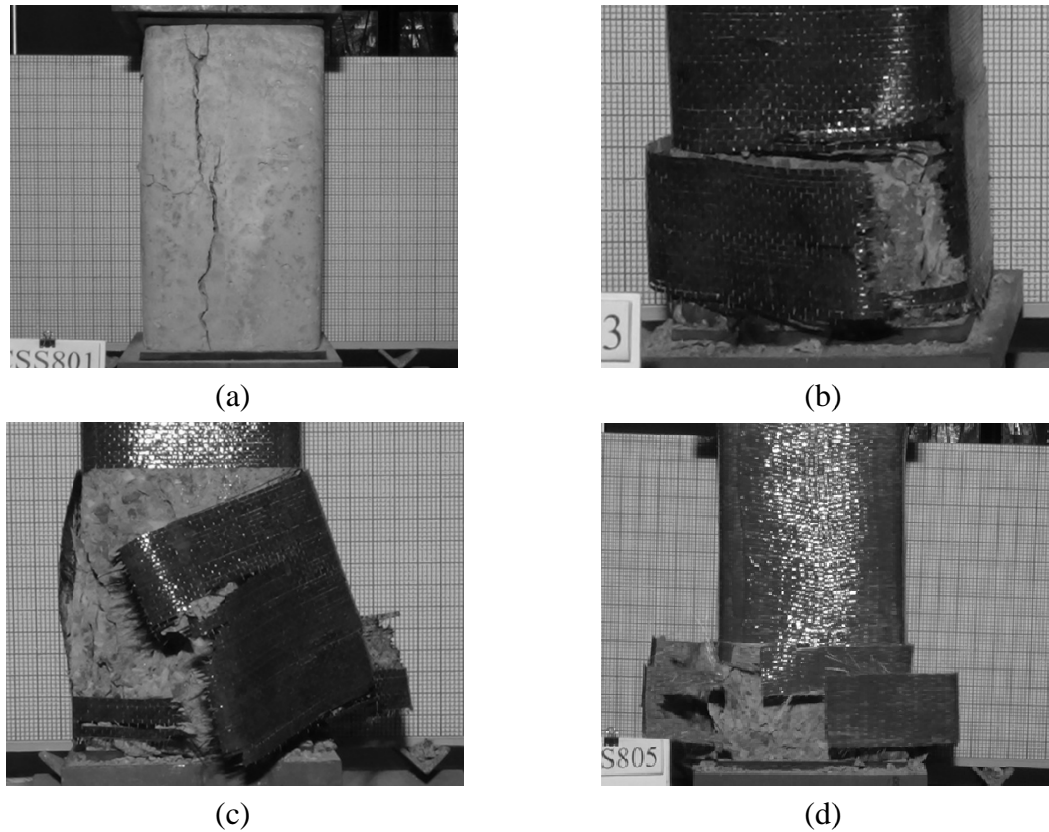


Figure 5.2: Failure patterns of square columns (a) failed by vertical splitting, (b) CFRP rapture at the bottom, (c) bursting of CFRP and (d) bursting of GFRP at the bottom.

### 5.3 Confinement due to dilation of concrete

Confinement in the form of transverse reinforcement is known to contain and delay the damage process by restraining the dilation (lateral expansion) of concrete. The nature of such a confinement mechanism is passive because the FRP confinement only becomes effective when the concrete dilates adequately due to Poisson's effect. As such, confining pressure is engaged as a result of the lateral dilation of the axially loaded column. The bilinear behavior (Samaan et. al. 1998) until rupture of FRP materials results in an increased level of confinement throughout the load history. The method of providing confinement has a number of implications for the design of column rehabilitation. Jacket

stiffness must be sufficient to develop the required confining pressure at relatively low transverse strains.

Initially, as loading begins, no confinement is provided. At low load levels, confined concrete behavior will not differ from that of unconfined concrete. As the load level increases, transverse dilation of the concrete first takes up any slack in the jacket and then engages confining pressure by generating hoop strains in the jacket. If the jacket is flexible, however, very small confining stresses are generated, resulting in small increases in concrete strength and deformation capacity and a stress-strain response similar to that of unconfined concrete. In such a case, significant confining pressure are achieved only after large post-peak dilations have occurred, resulting in a second peak on the axial stress-strain response. A stiff jacket is, therefore, desirable.

The level of concrete confinement is also significantly affected by column geometry. While the entire section of an FRP wrapped circular column becomes fully confined, considerable dilation of the section is necessary before the flat sides of a jacket are able to provide confinement to a square column. Due to the relatively small strain capacity of FRP materials, the jacket are typically ruptured at its corners before the sides of the jacket can afford any significant confinement.

Dilation occurred in all types of concrete columns. The amount of dilation depends on type of concrete and also type of FRP wrap. The elongation of CFRP and GFRP are 1.8% and 2.4% respectively. In almost all type of concrete columns the dilation is found higher in GFRP confined concrete than CFRP confined concrete due to the thickness of the FRP jackets. Figure 5.3 shows that for 100 mm diameter circular concrete column made of brick aggregate, stone aggregate, recycled brick and recycled stone aggregate the axial capacity increases as the dilation of concrete increases. It is clear from Figure 5.3 that dilation of brick aggregate concrete is higher compared to other aggregate concrete. Similarly for 150 mm and 200 mm diameter circular concrete columns the axial capacity increases as the dilation of concrete increases except for 6 inch high recycled brick aggregate concrete columns (Figure 5.4-5.5) due to the limitation of strain measurement technique. Again for square concrete columns with the same corner radius, the axial capacity increases as the dilation of concrete increases except for 8 inch high brick aggregate concrete columns (Figure 5.6-5.8) due to the limitation of strain measurement technique, variation is found in some cases. Thus it is concluded that the confinement effect and the axial load carrying capacities are increased significantly due to dilation.

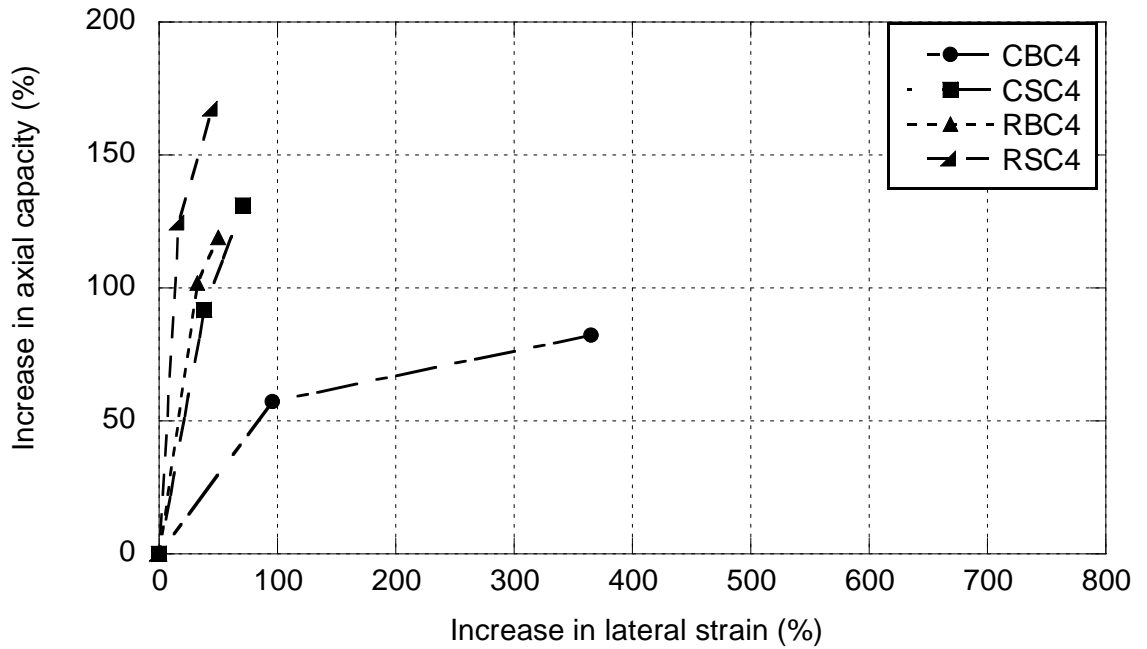


Figure 5.3: Confinement effect of 100 mm diameter circular column due to dilation of concrete.

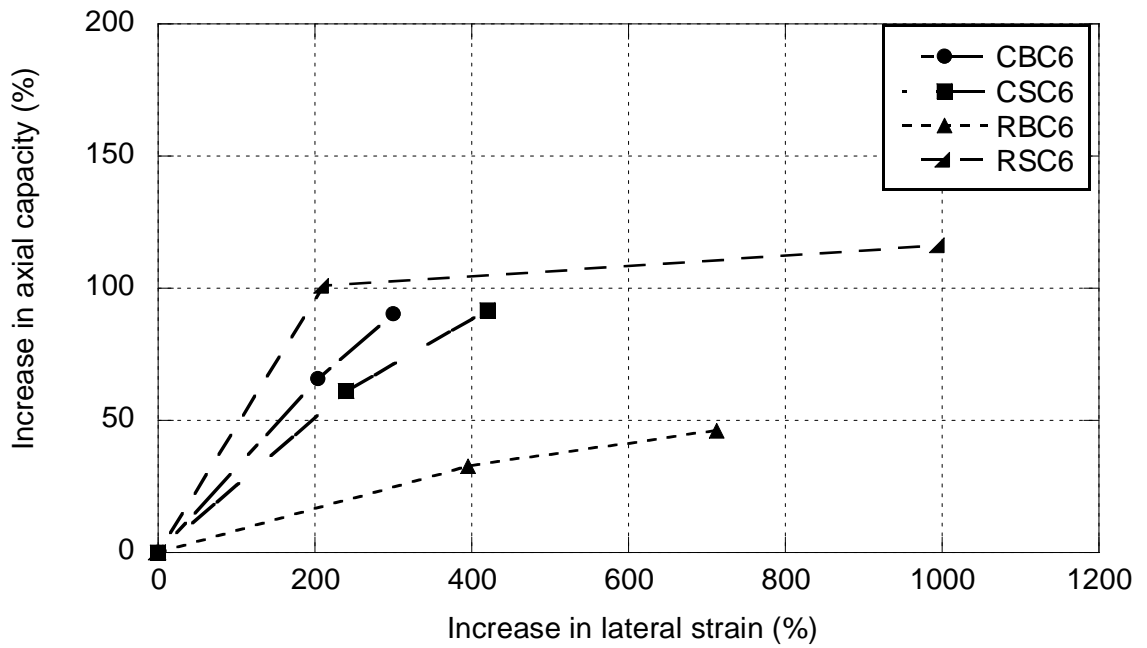


Figure 5.4: Confinement effect of 150 mm diameter circular column due to dilation of concrete.

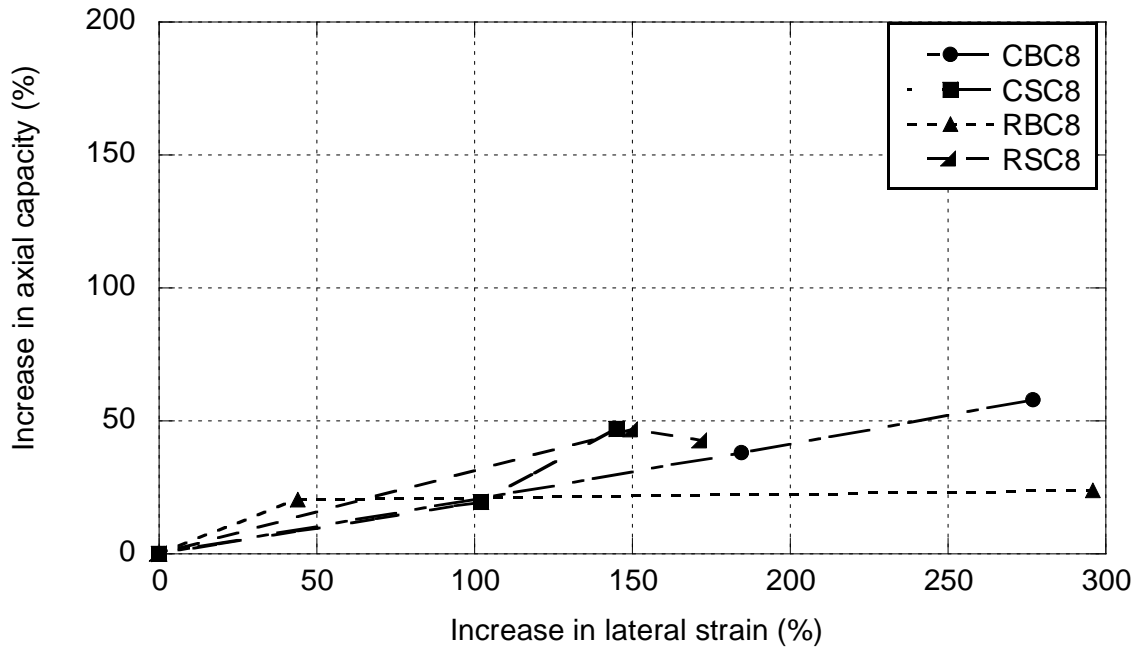


Figure 5.5: Confinement effect of 200 mm diameter circular column due to dilation of concrete.

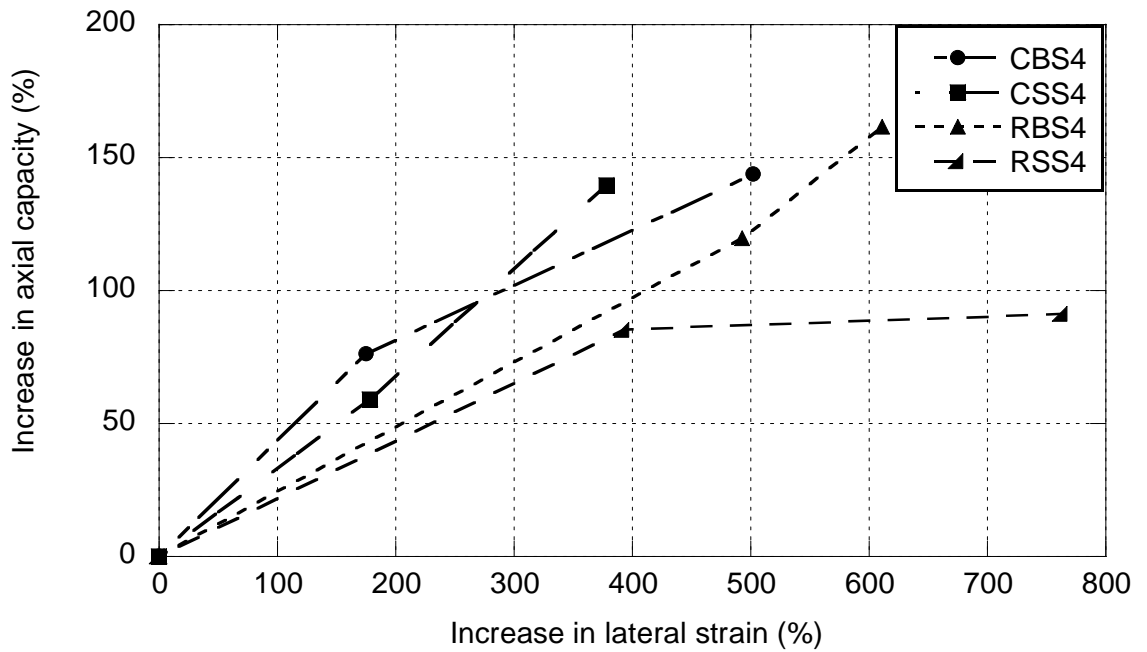


Figure 5.6: Confinement effect of 100 mm x 100 mm size square column due to dilation of concrete.



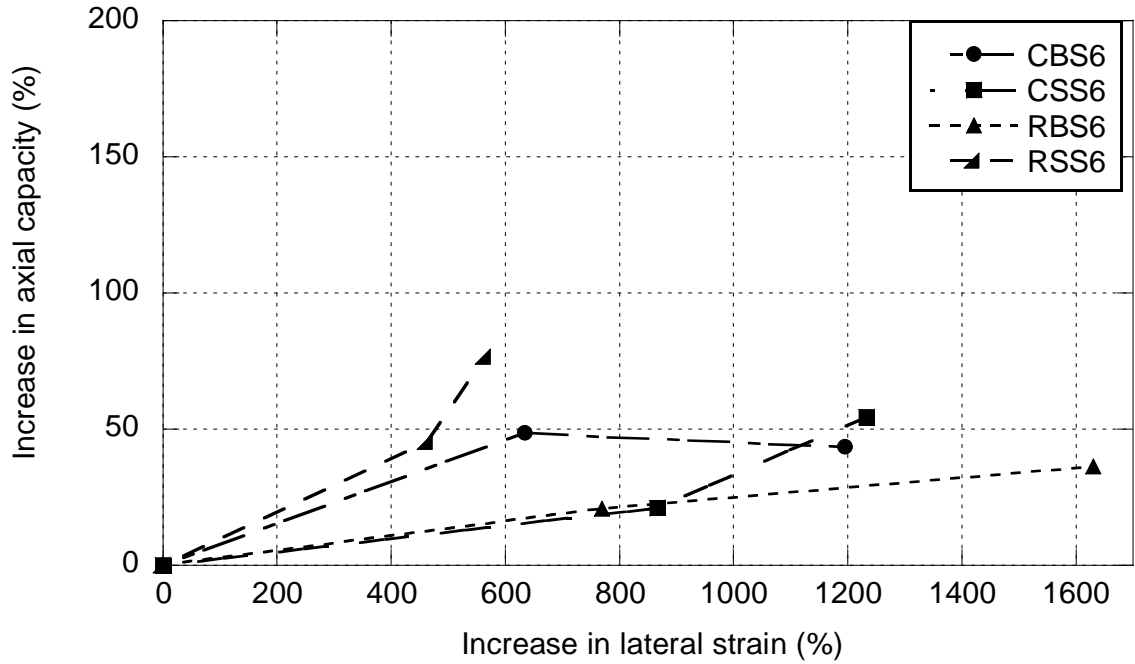


Figure 5.7: Confinement effect of 150 mm x 150 mm size square column due to dilation of concrete.

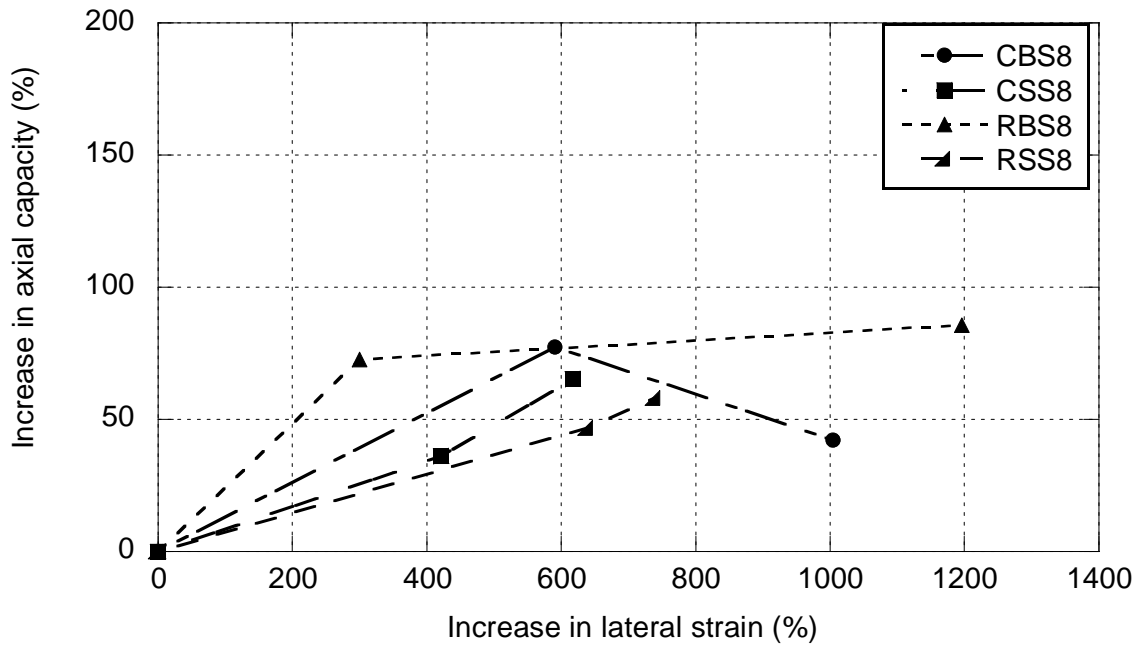


Figure 5.8: Confinement effect of 200 mm x 200 mm size square column due to dilation of concrete.

Figures 5.9-5.12 and Figures 5.13-5.20 of Appendix B show the dilation effect in brick, stone, recycled brick and recycled stone aggregate concretes of different shape and sizes of columns. For all columns, the dilation of square confined concrete columns is found to

be higher compared to circular confined columns. For 4 inch high circular and square concrete columns, the dilation of brick aggregate concrete square column is typically 47% and 35% higher than circular confined concrete column due to CFRP and GFRP confinement, respectively (Figure 5.9). Similarly, for stone, recycled brick and recycled stone aggregate concretes these values are typically 30% and 17%, 5% and 8%, 113% and 106%, respectively (Figure 5.10 to Figure 5.12). Again for 6 inch high circular and square concrete columns, the dilation of brick, stone and recycled brick aggregate concrete square column is typically 114% and 187%, 184% and 156%, 75% and 113% higher than circular confined concrete column due to CFRP and GFRP confinement respectively (Figures 5.13-5.15 of Appendix B). The columns made of recycled stone aggregate concrete this value is typically 281% for CFRP confinement but for GFRP confinement the dilation for both square and circular column is found nearly the same (Figure 5.16 of Appendix B). Again for 8 inch high circular and square concrete columns, the dilation of brick, stone, recycled brick and recycled stone aggregate concrete square column is typically 115% and 159%, 21% and 28%, 268% and 201%, 38% and 54% higher than circular confined concrete column due to CFRP and GFRP confinement respectively (Figures 5.17-5.20 of Appendix B). Confinement of columns by means of FRP jackets is done by containing the dilation of concrete by wrapping of fibers in the hoop direction of concrete columns. In circular columns the confinement due to dilation is uniform throughout the cross section but for square concrete columns stress concentration at the corners fails to resist further dilation and larger dilation occurs in the square concrete columns compared to circular columns.

#### **5.4 Axial capacity enhancement**

The axial compressive strength of concrete member is increased by providing confinement with an FRP jacket. Confining a concrete member is accomplished by orienting the fibers transverse to the longitudinal axis of the member. In this orientation, the transverse or hoop fibers are similar to conventional spiral or tie reinforcing steel. FRP jackets provide passive confinement to the compression member. For this reason, intimate contact between the FRP jacket and the concrete member is critical. FRP axial strengthening of square columns can be achieved by providing adequate corner rounding which is very advantageous for confinement. It is clear from these figures (Figures 5.9-5.12 and Figures 5.13-5.20 of Appendix B) that the path of the initial slope of the stress-strain curves for the unconfined and confined concrete columns are same upto unconfined compressive strength. The compressive strength increases due to confinement which is

termed as the confined compressive strength. When the concrete reaches the compressive strength, internal cracks starts to form and concrete begins to dilate. Due to dilation, confining pressure develops in the FRP wrap which resist the concrete from falling apart. The phenomenon enhances the load carrying capacity of the column.

For all columns, the axial capacity of circular confined concrete columns is found to be higher compared to square confined columns in Figures 5.9-5.12 and Figures 5.13-5.20 of Appendix B. For 4 inch high circular and square concrete columns, the axial strength of brick aggregate concrete circular column is typically 90% and 93% higher than square confined concrete column due to CFRP and GFRP confinement respectively (Figure 5.9). Similarly, for stone, recycled brick and recycled stone aggregate concretes these values are typically 167% and 109%, 133% and 71%, 143% and 126% respectively (Figures 5.10-5.12). Again for 6 inch high circular and square concrete columns, the axial strength of brick, stone and recycled brick and recycled stone aggregate concrete circular column is typically 86% and 105%, 91% and 93%, 105% and 100% , 70% and 75% higher than square confined concrete column due to CFRP and GFRP confinement respectively (Figures 5.13-5.16 of Appendix B). Again for 8 inch high circular and square concrete columns, the axial strength of brick, stone, recycled brick and recycled stone aggregate concrete circular column is typically 57% and 46%, 70% and 71%, 42% and 30%, 58% and 48% higher than square confined concrete column due to CFRP and GFRP confinement respectively (Figures 5.17-5.20 of Appendix B). The axial load capacity of stone aggregate concrete is found to be increased greater than other concretes for both CFRP and GFRP confinement. So it is found that, the increase of axial load capacity of square columns is significantly lower compared to circular columns. This may be explained by the distribution of confining pressure in circular and square columns. For circular columns, the confining pressure is uniform, and is a function of hoop strength of the jacket. Instead in the cases of square sections with a small amount of FRP, the peak stress is similar to that of unconfined concrete, indicating the fact that the confining action is mostly limited at the corners, producing a confining pressure not sufficient to overcome the effect of concrete degradation. It is clear from Figures 5.9-5.12 and Figures 5.13-5.20 of Appendix B that the increase in strength provided by confinement is very sensitive to the cross section geometry and the amount of this increase drops sharply as the geometry deviates.

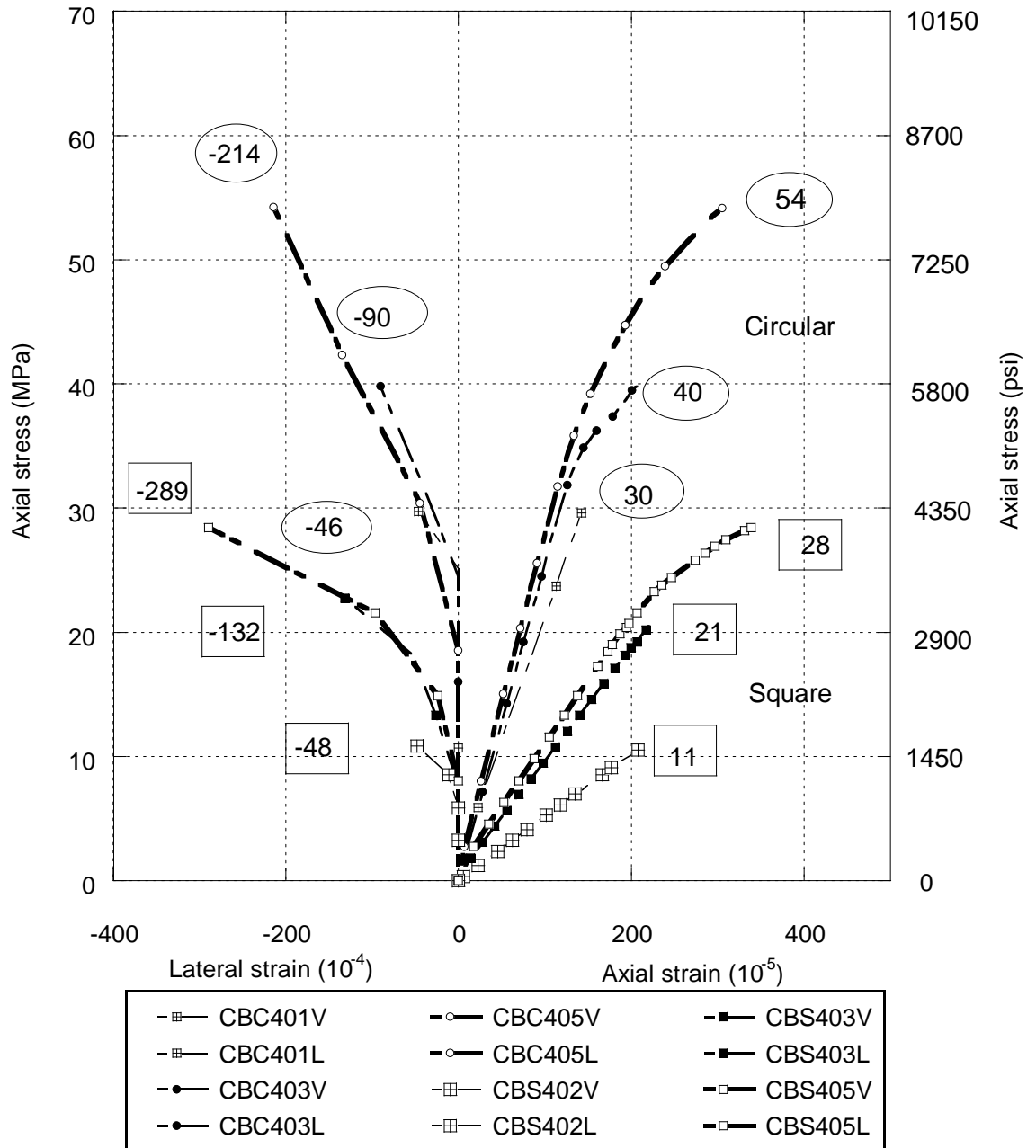


Figure 5.9: Stress-strain behaviours of unconfined and confined circular and square columns made of brick aggregate concrete. Numbers appear in the circles and squares are peak axial stress and peak lateral strain of circular and square columns respectively (MPa).  $\square$  Unconfined column,  $\bullet$  CFRP confined circular column,  $\circ$  GFRP confined circular column,  $\blacksquare$  CFRP confined square column,  $\square$  GFRP confined square column.

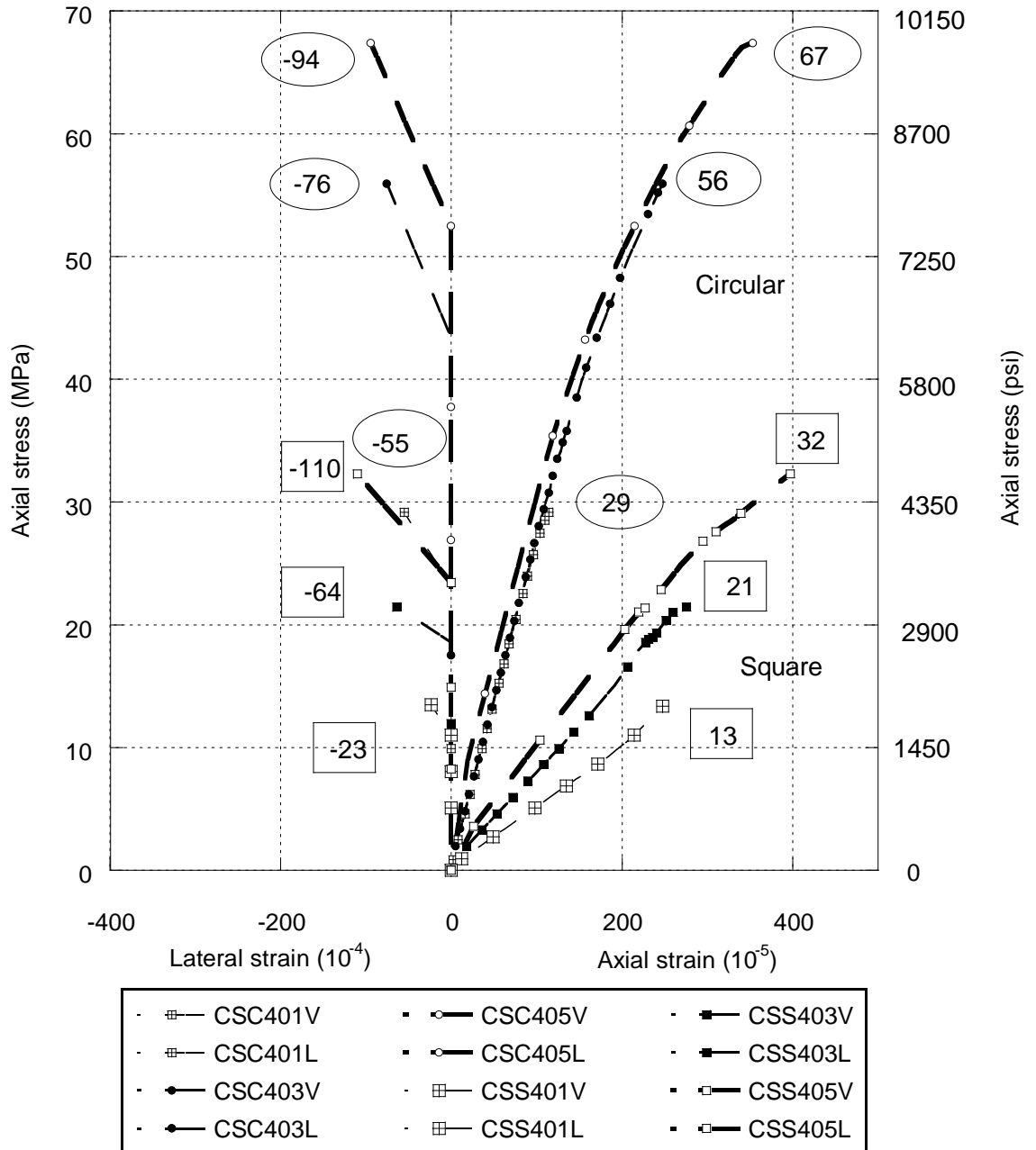


Figure 5.10: Stress-strain behaviours of unconfined and confined circular and square columns made of stone aggregate concrete. Numbers appear in the circles and squares are peak axial stress and peak lateral strain of circular and square columns respectively (MPa).  $\square$  Unconfined column,  $\bullet$  CFRP confined circular column,  $\circ$  GFRP confined circular column,  $\blacksquare$  CFRP confined square column,  $\square$  GFRP confined square column.

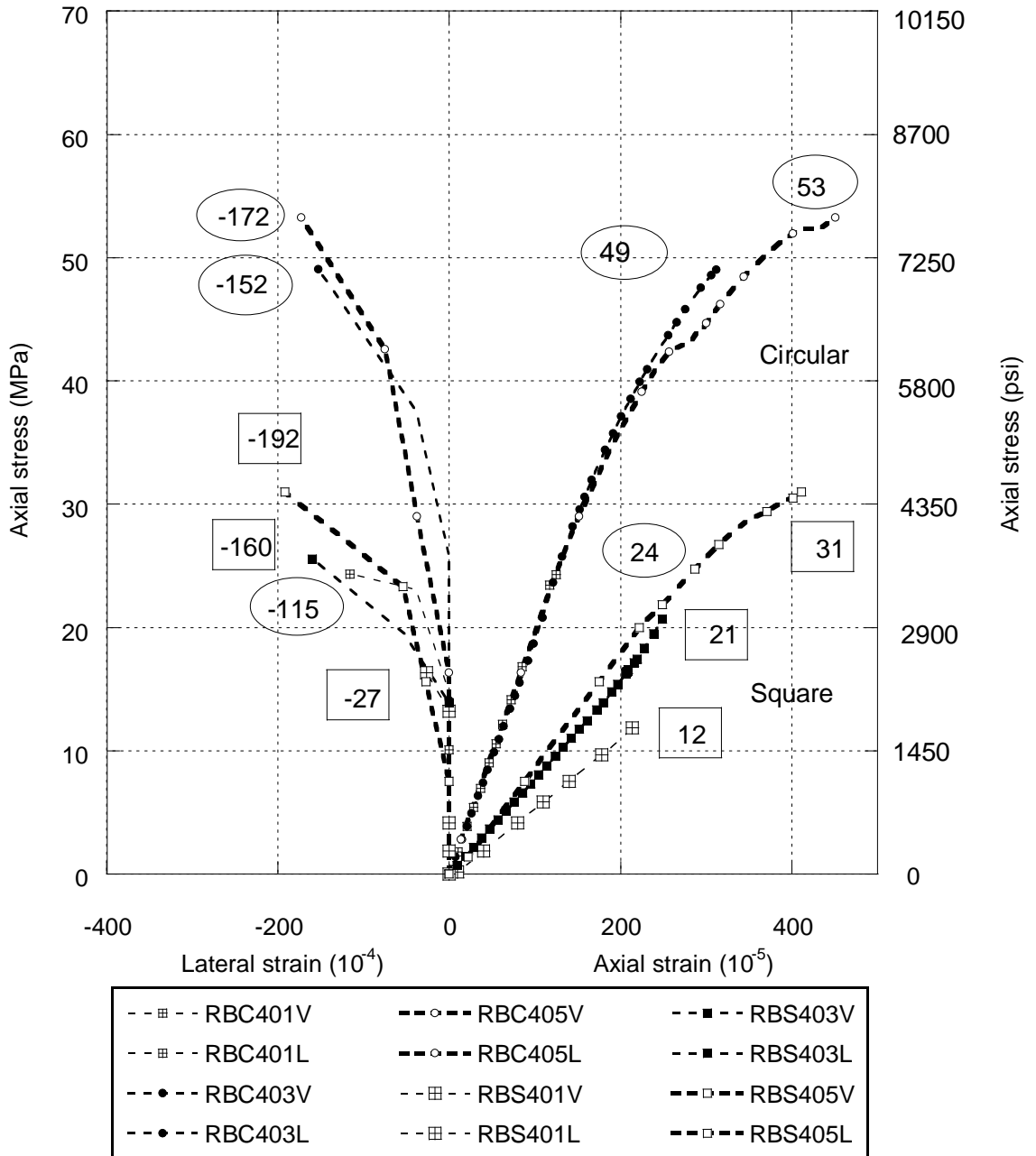


Figure 5.11: Stress-strain behaviours of unconfined and confined circular and square columns made of recycled brick aggregate concrete. Numbers appear in the circles and squares are peak axial stress and peak lateral strain of circular and square columns respectively (MPa).  $\square$  Unconfined column,  $\bullet$  CFRP confined circular column,  $\circ$  GFRP confined circular column,  $\blacksquare$  CFRP confined square column,  $\square$  GFRP confined square column.

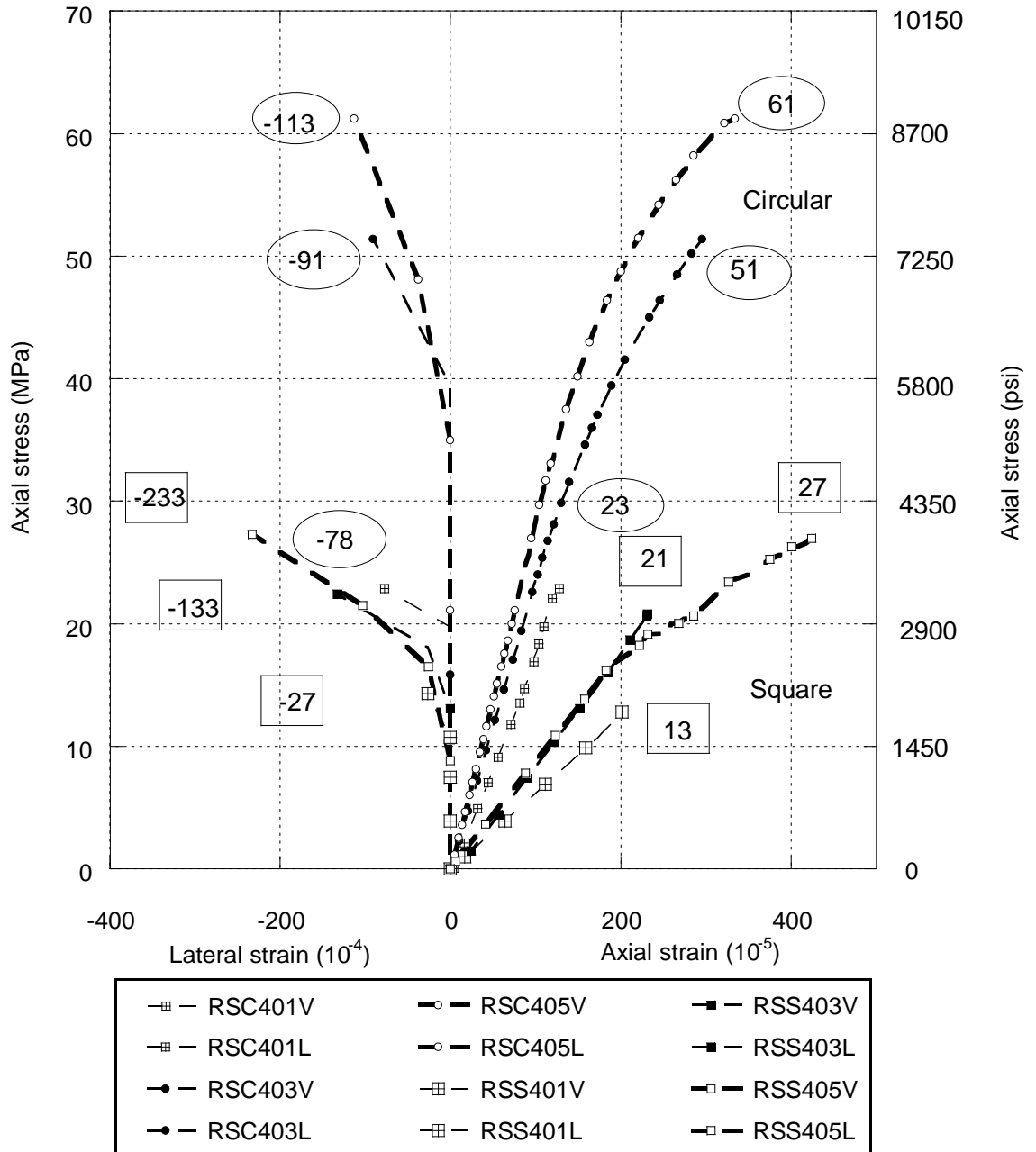


Figure 5.12: Stress-strain behaviours of unconfined and confined circular and square columns made of recycled stone aggregate concrete. Numbers appear in the circles and squares are peak axial stress and peak lateral strain of circular and square columns respectively (MPa).  $\boxplus$  Unconfined column,  $\bullet$  CFRP confined circular column,  $\circ$  GFRP confined circular column,  $\blacksquare$  CFRP confined square column,  $\square$  GFRP confined square column.

## 5.5 Effect of geometric parameters

### 5.5.1 Effect of radius of curvature

The effects of radius of curvature to the compressive strength and ultimate axial strain of the CFRP and GFRP confined circular concrete columns made of brick, stone, recycled brick and recycled stone aggregate concrete are shown in Figures 5.21-5.24. Inspection of Figures 5.21- 5.24 reveal that Compressive strength and ultimate axial strain of CFRP and GFRP confined circular columns decreases with increase of radius of curvature for all types of concrete due to the curvature effect. Also Mandal et al. (2005) observed that the increase of column diameter, namely from 150 mm to 250 mm, caused a significant reduction in the strength of the cylinders.

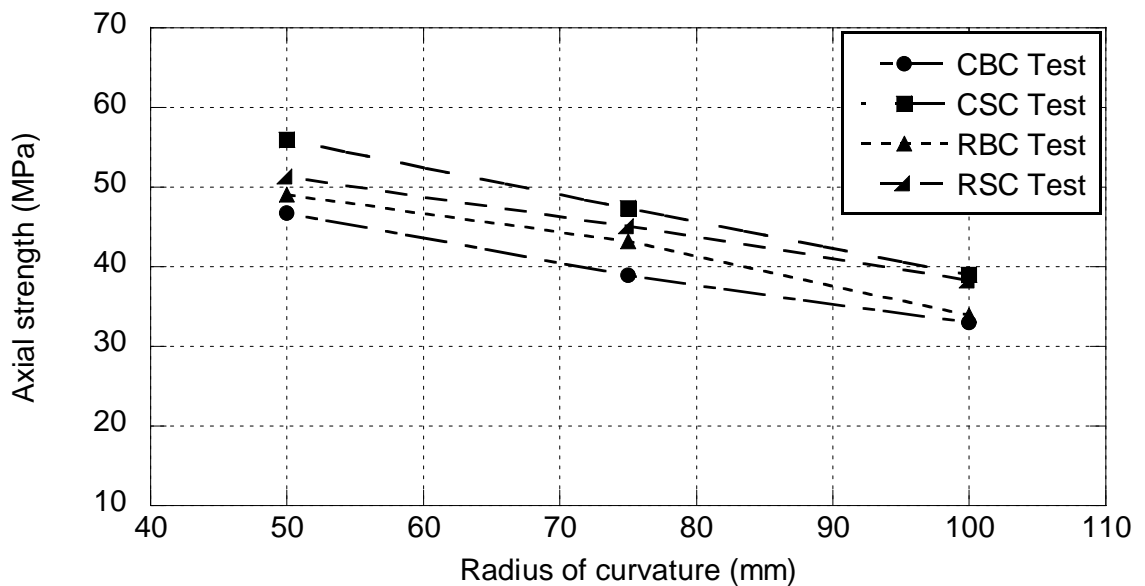


Figure 5.21: Compressive strengths of CFRP confined circular columns made of brick, stone, recycled brick and recycled stone aggregate concrete with 50, 75, and 100 mm in radius of curvature.



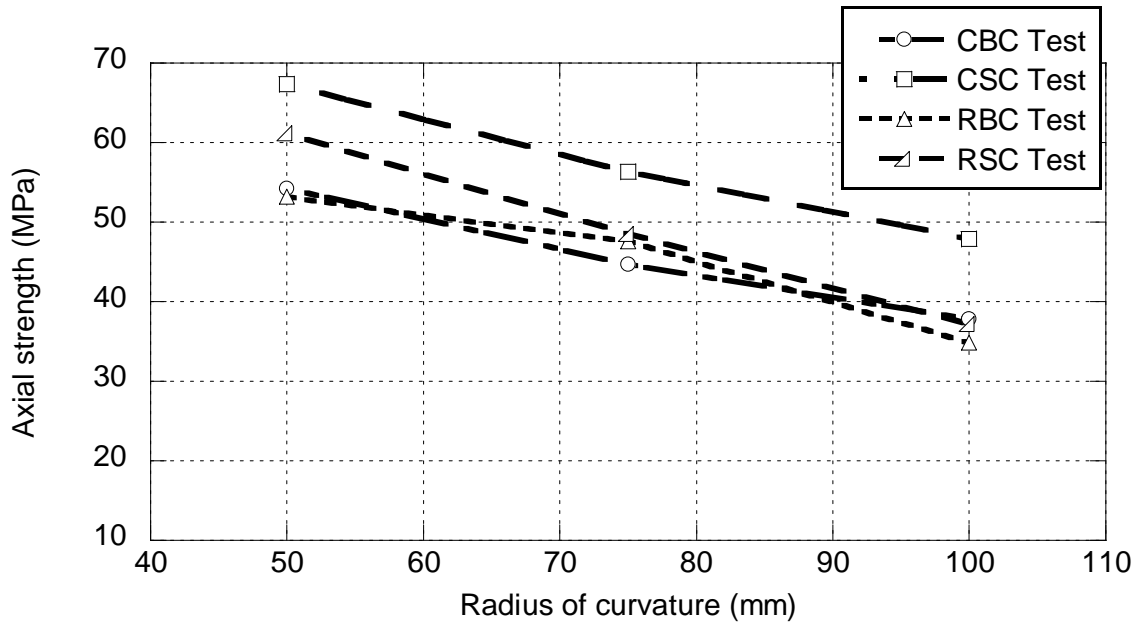


Figure 5.22: Compressive strengths of GFRP confined circular columns made of brick, stone, recycled brick and recycled stone aggregate concrete with 50, 75, and 100 mm in radius of curvature.

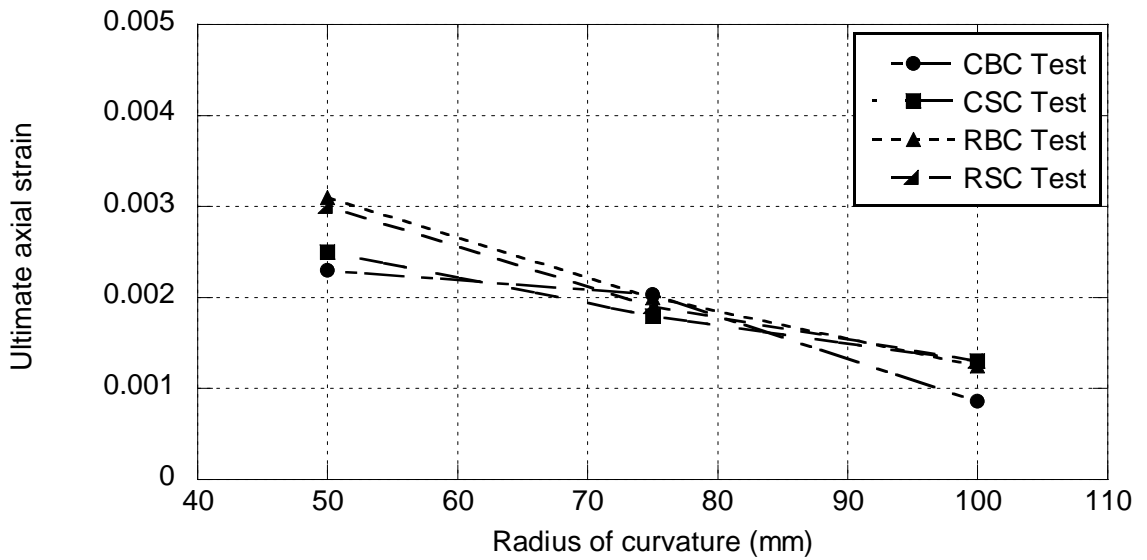


Figure 5.23: Ultimate axial strain of CFRP confined circular columns made of brick, stone, recycled brick and recycled stone aggregate concrete with 50, 75, and 100 mm in radius of curvature.

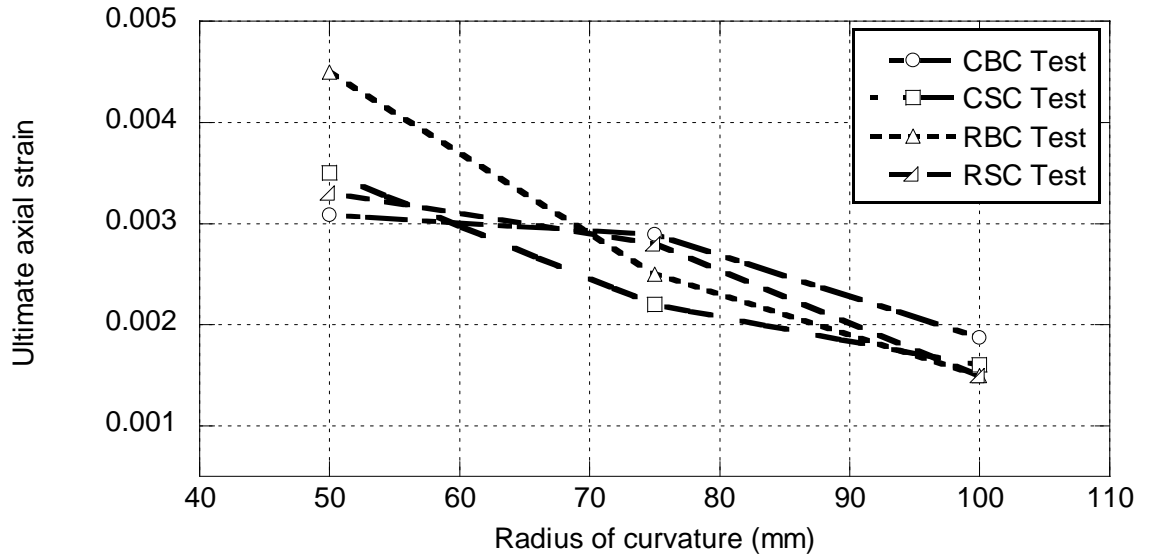


Figure 5.24: Ultimate axial strain of GFRP confined circular columns made of brick, stone, recycled brick and recycled stone aggregate concrete with 50, 75, and 100 mm in radius of curvature.

### 5.5.2 Effect of column side to corner radius ratio (B/r)

The effects of column side to corner radius ratio curvature to the compressive strength and ultimate axial strain of the CFRP and GFRP confined circular concrete columns made of brick, stone, recycled brick and recycled stone aggregate concrete are shown in Figures 5.25-5.28. For the CFRP and GFRP confined square concrete columns with same corner radius ( $r = 25$  mm), there is no size effect to exist in axial strength but ultimate axial strain decreases with the increase of column side to corner radius ratio for brick, recycled brick and recycled stone aggregate concrete except for stone aggregate concrete due to the limitation of strain measurement technique are shown in Figures 5.25-5.28.

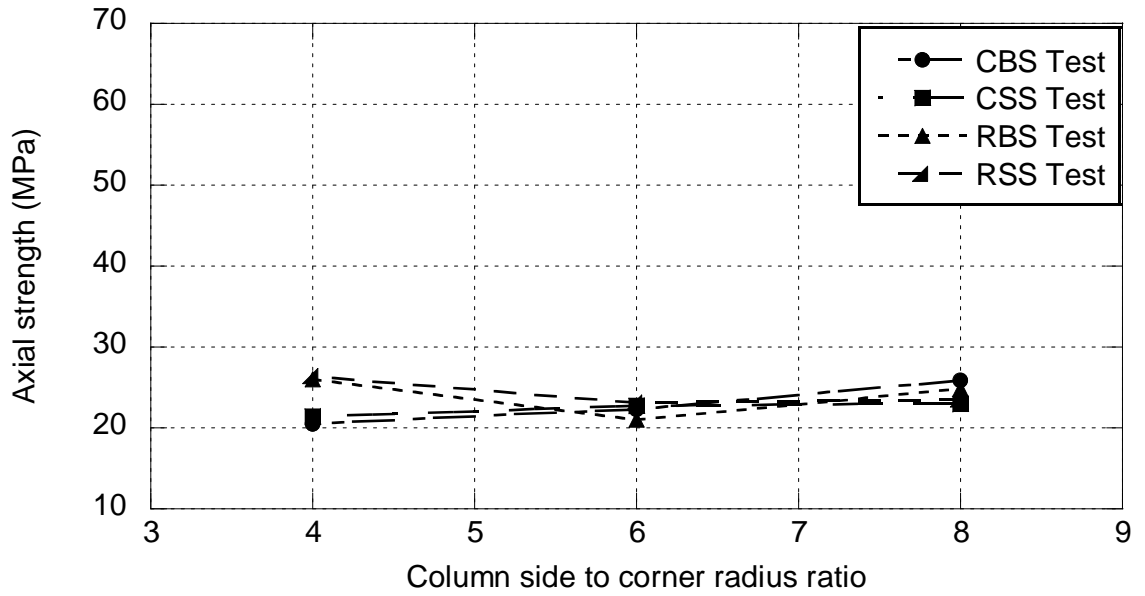


Figure 5.25: Compressive strengths of CFRP confined square columns made of brick, stone, recycled brick and recycled stone aggregate concrete with different column side to corner radius ratio.

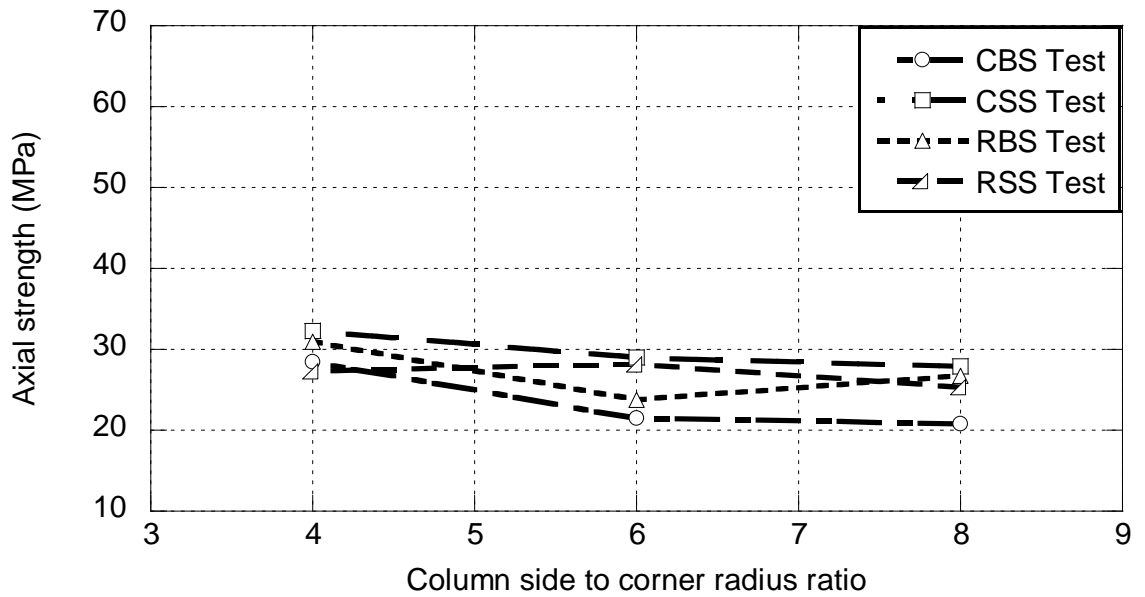


Figure 5.26: Compressive strengths of GFRP confined square columns made of brick, stone, recycled brick and recycled stone aggregate concrete with different column side to corner radius ratio.

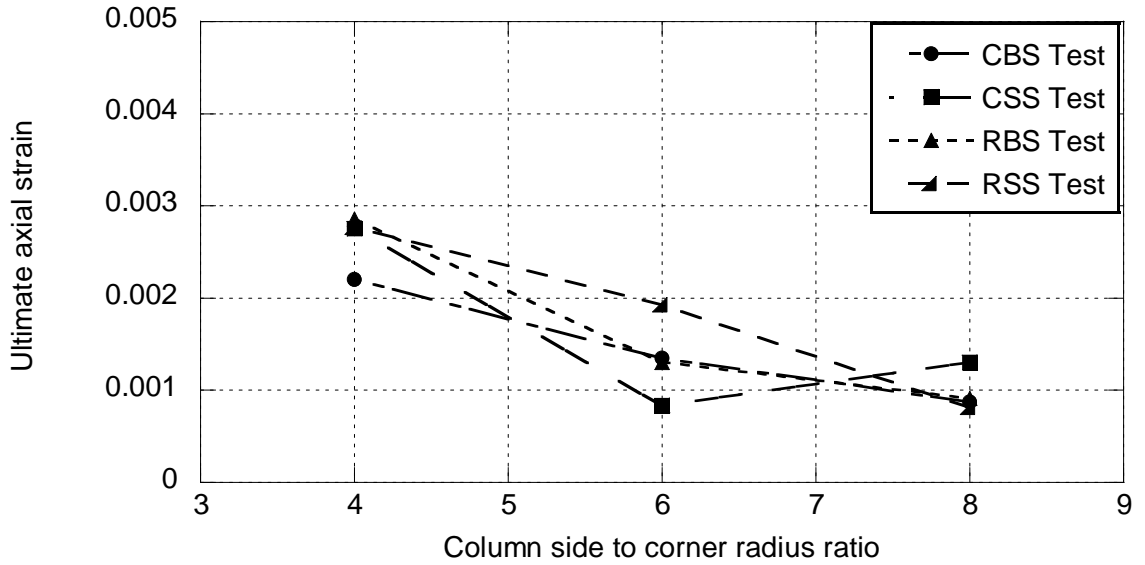


Figure 5.27: Ultimate axial strain of CFRP confined square columns made of brick, stone, recycled brick and recycled stone aggregate concrete with different column side to corner radius ratio.

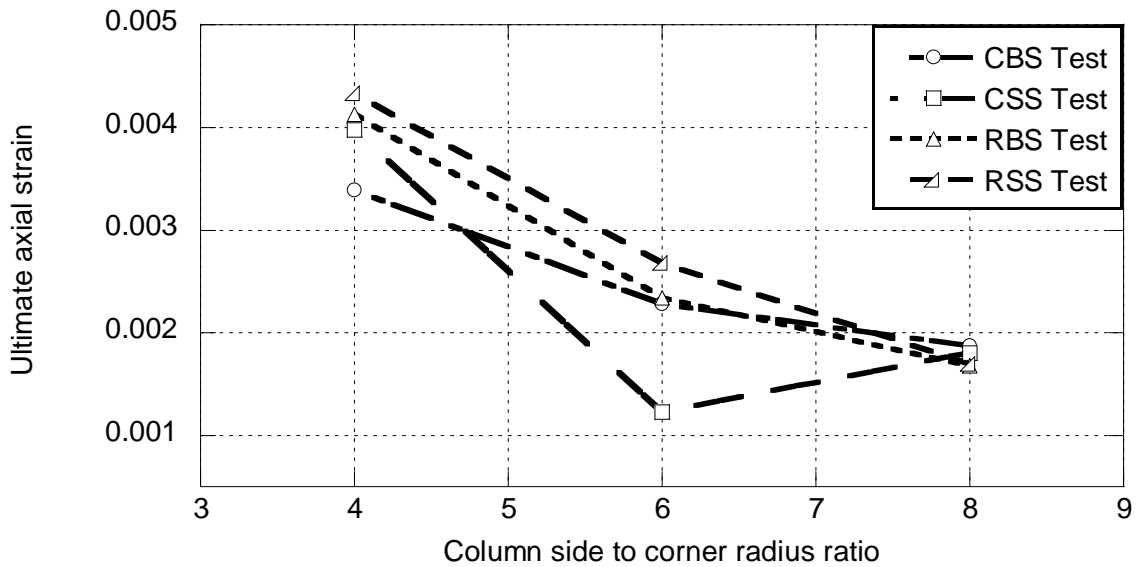


Figure 5.28: Ultimate axial strain of GFRP confined square columns made of brick, stone, recycled brick and recycled stone aggregate concrete with different column side to corner radius ratio.

### 5.5.3 Effect of FRP volumetric ratio ( $\rho_f$ )

The CFRP and GFRP volumetric ratio of different types of concrete circular and square columns are calculated by using Eq. 4.1 and 4.2 respectively. The effect of CFRP and GFRP volumetric ratio to the compressive strength and ultimate axial strain of the confined circular and square concrete columns made of brick, stone, recycled brick and recycled stone aggregate concrete are shown in Figures 5.29- 5.36. As shown in Figures 5.29-5.32 the compressive strength and ultimate axial strain of the CFRP and GFRP confined circular concrete columns increases as the CFRP and GFRP volumetric ratio increases for all types of concrete. With the same corner radius ( $r = 25\text{mm}$ ), there is no size effect to exist on the axial strength but ultimate axial strain increases with the increase of FRP volumetric ratio of the square concrete columns for brick, recycled brick and recycled stone aggregate concrete except for stone aggregate concrete due to the limitation of strain measurement technique are shown in Figures 5.33 - 5.36.

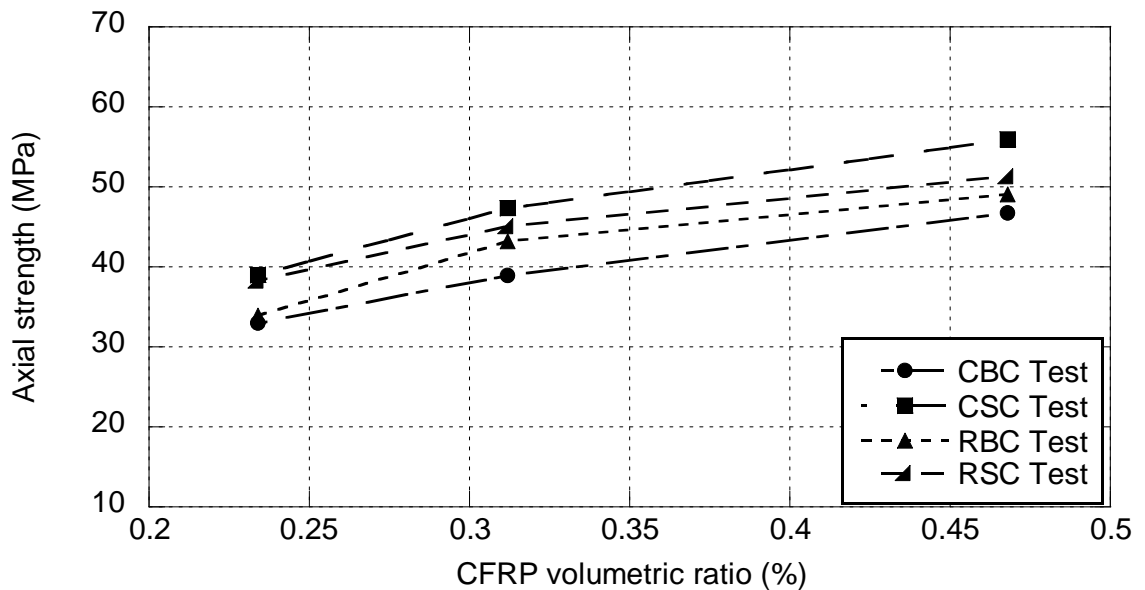


Figure 5.29: Axial strength of CFRP confined circular columns made of brick, stone, recycled brick and recycled stone aggregate concrete with different volumetric ratio.

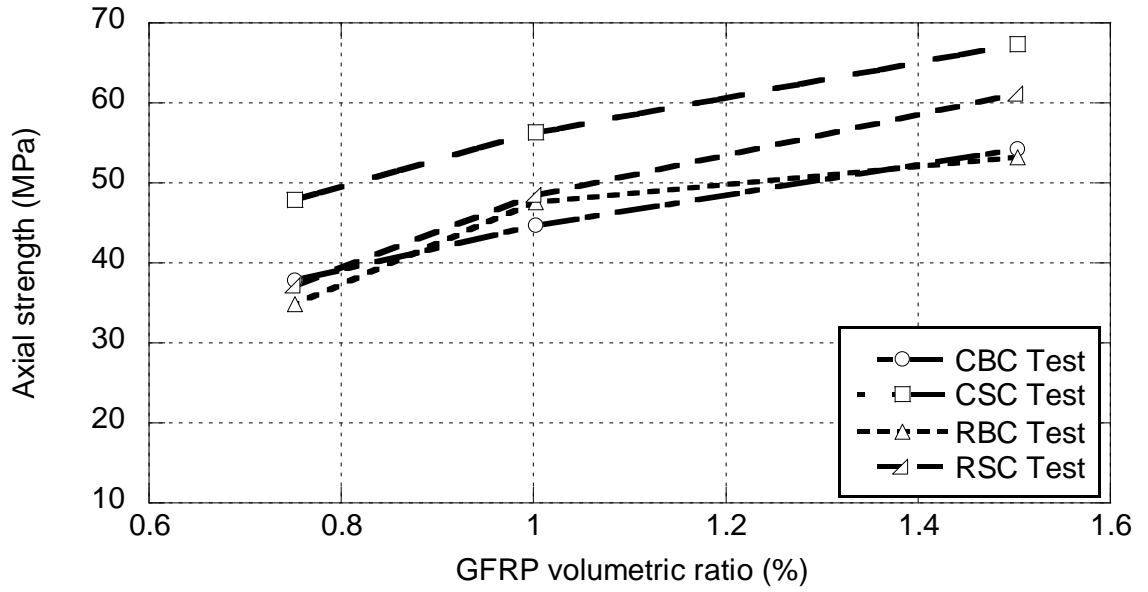


Figure 5.30: Axial strength of GFRP confined circular columns made of brick, stone, recycled brick and recycled stone aggregate concrete with different volumetric ratio.

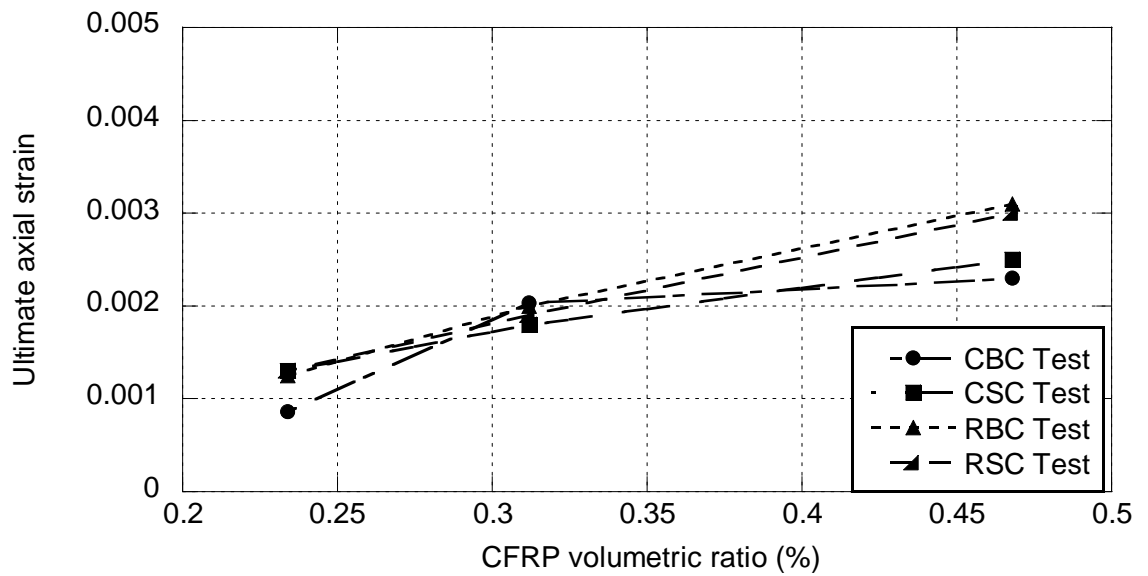


Figure 5.31: Ultimate axial strain of CFRP confined circular columns made of brick, stone, recycled brick and recycled stone aggregate concrete with different volumetric ratio.

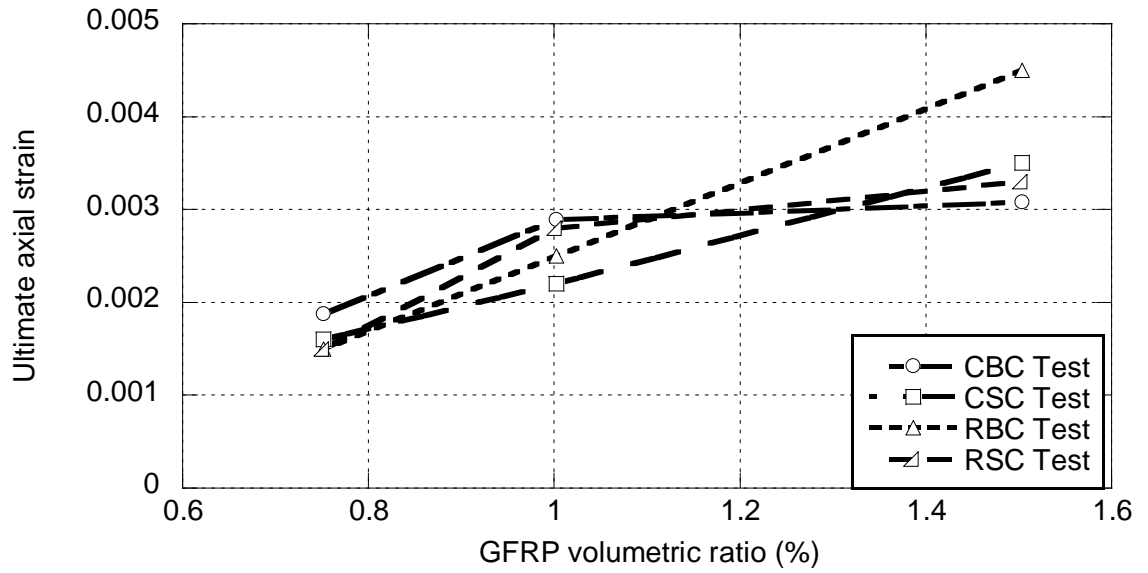


Figure 5.32: Ultimate axial strain of GFRP confined circular columns made of brick, stone, recycled brick and recycled stone aggregate concrete with different volumetric ratio.

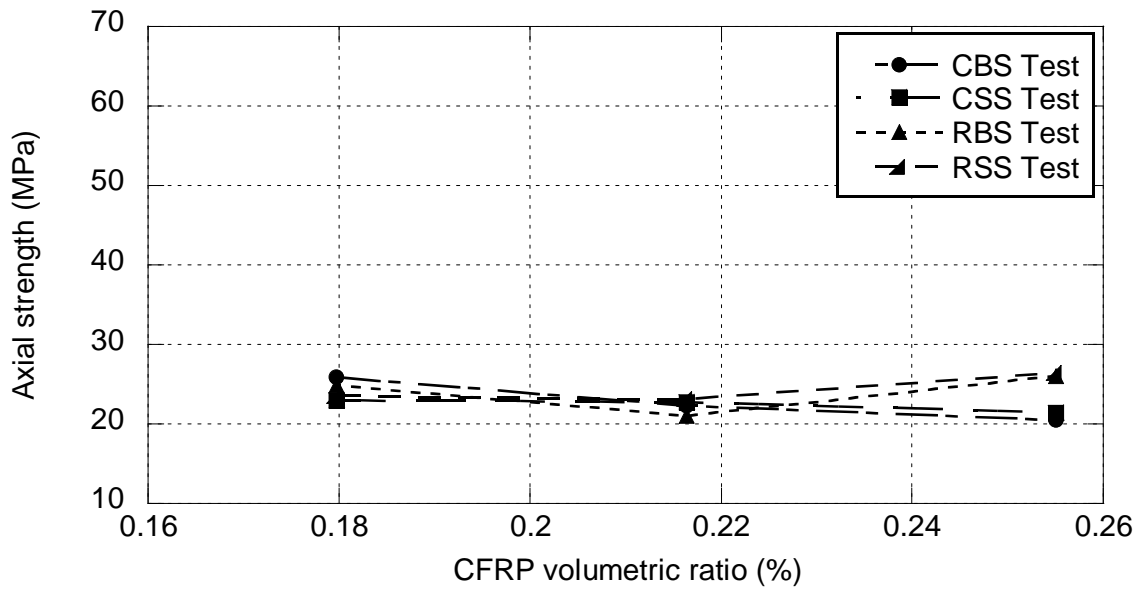


Figure 5.33: Axial strength of CFRP confined square columns made of brick, stone, recycled brick and recycled stone aggregate concrete with different CFRP volumetric ratio.

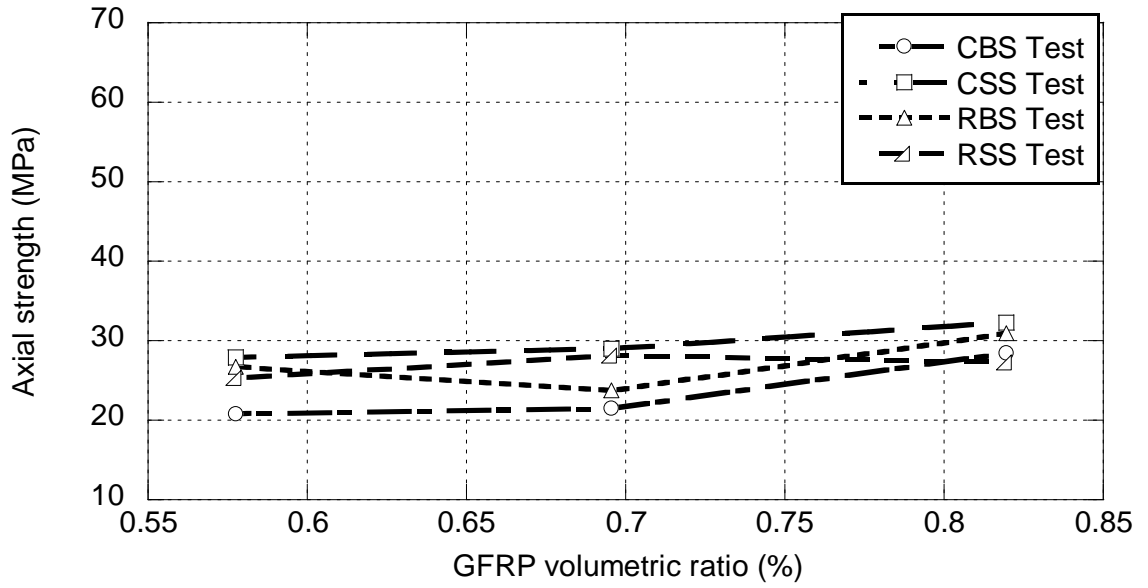


Figure 5.34: Axial strength of GFRP confined square columns made of brick, stone, recycled brick and recycled stone aggregate concrete with different GFRP volumetric ratio.

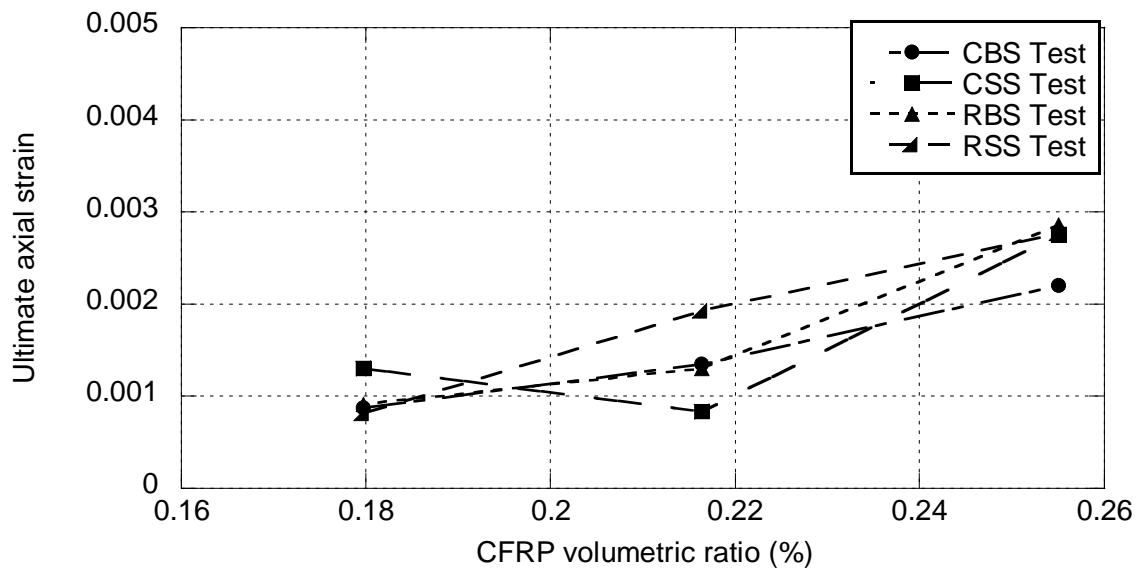


Figure 5.35: Ultimate axial strain of CFRP confined square columns made of brick, stone, recycled brick and recycled stone aggregate concrete with different CFRP volumetric ratio.



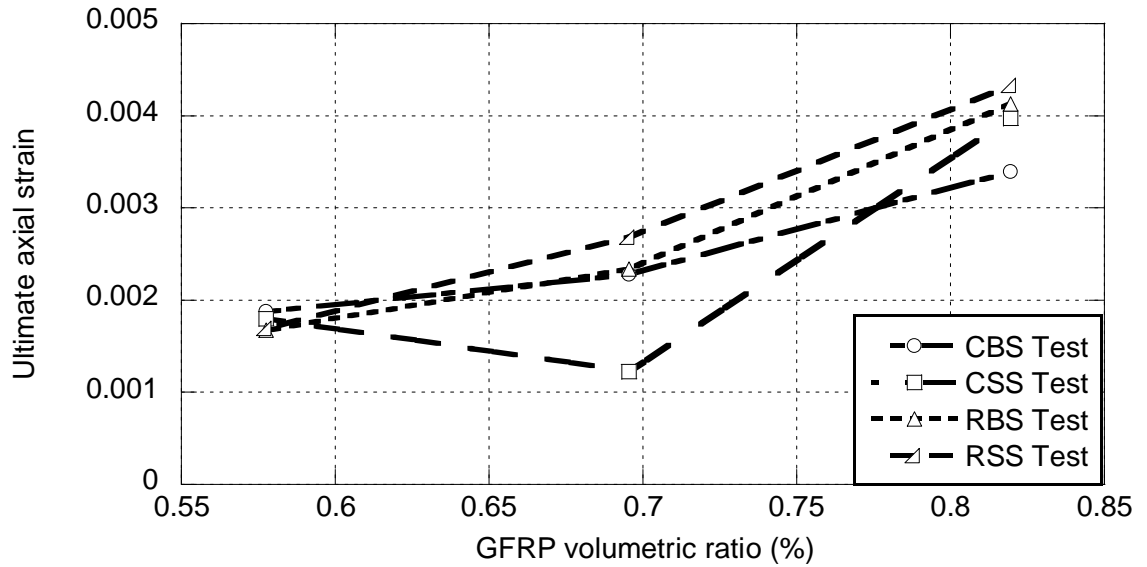


Figure 5.36: Ultimate axial strain of GFRP confined square columns made of brick, stone, recycled brick and recycled stone aggregate concrete with different GFRP volumetric ratio.

#### 5.5.4 Effect of Rigidity ratio

The CFRP and GFRP stiffness to the column stiffness of different types of concrete circular and square columns are calculated by using Eq. 4.3. From Figures 5.37 - 5.40, it can be observed that the compressive strength of the CFRP and GFRP confined circular and square concrete columns clearly depends on the rigidity ratio of the lateral stiffness of the FRP jacket to the axial stiffness of the column rather than solely on the concrete strength. As shown in Figures 5.37-5.38 the compressive strength of the CFRP and GFRP confined circular concrete columns increases as the rigidity ratio increases for all types of concrete. But CFRP and GFRP confined square concrete columns with the same corner radius ( $r = 25\text{mm}$ ), there is no size effect to exist on the axial strength for all types of concrete are shown in Figures 5.39 - 5.40.

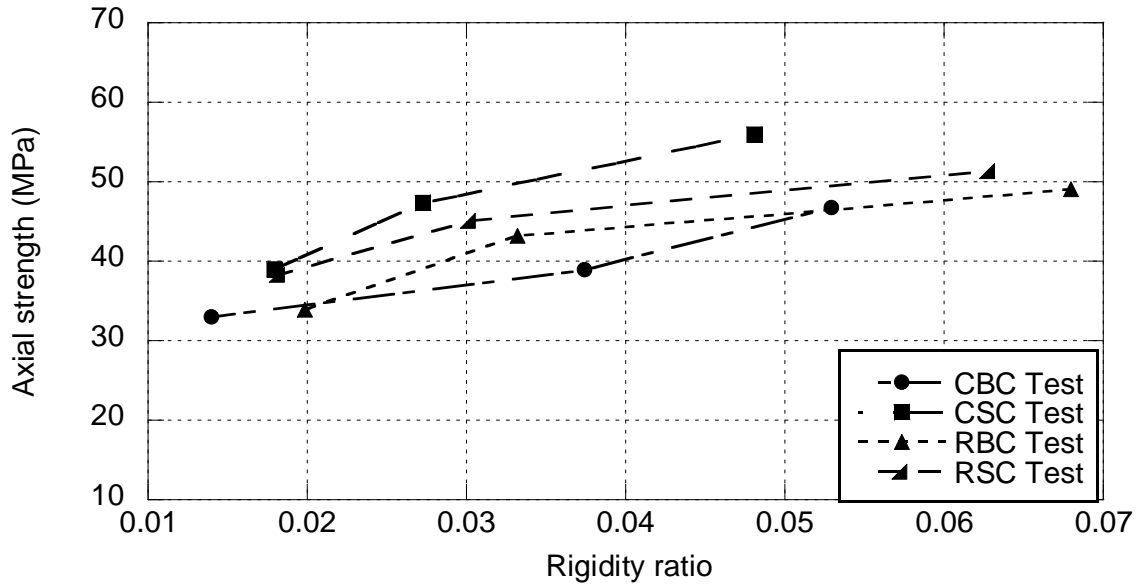


Figure 5.37: Axial strength of CFRP confined circular columns made of brick, stone, recycled brick and recycled stone aggregate concrete with rigidity ratio.

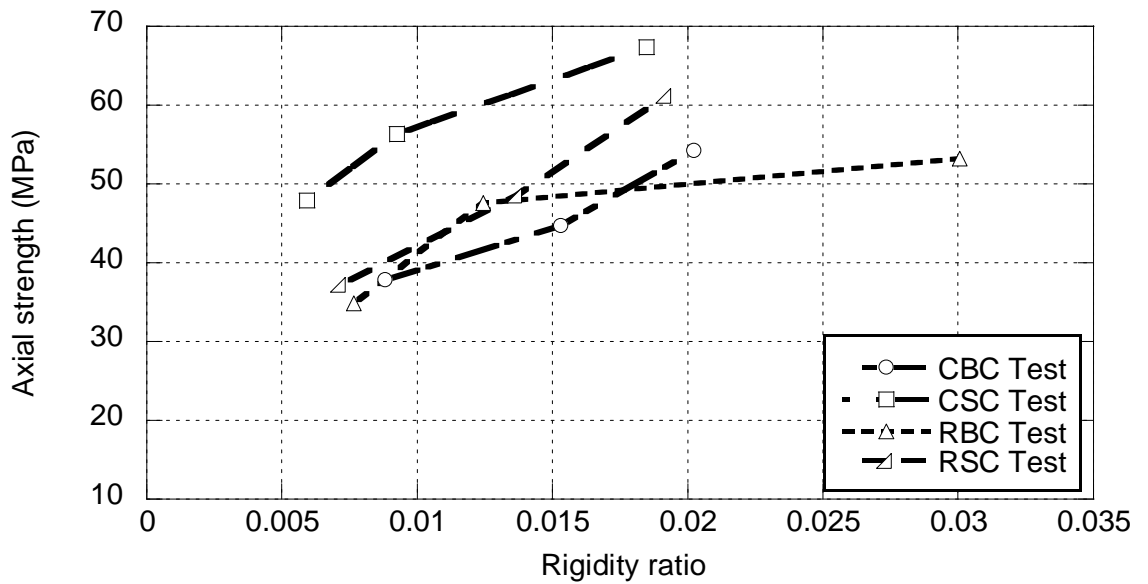


Figure 5.38: Axial strength of GFRP confined circular columns made of brick, stone, recycled brick and recycled stone aggregate concrete with rigidity ratio.

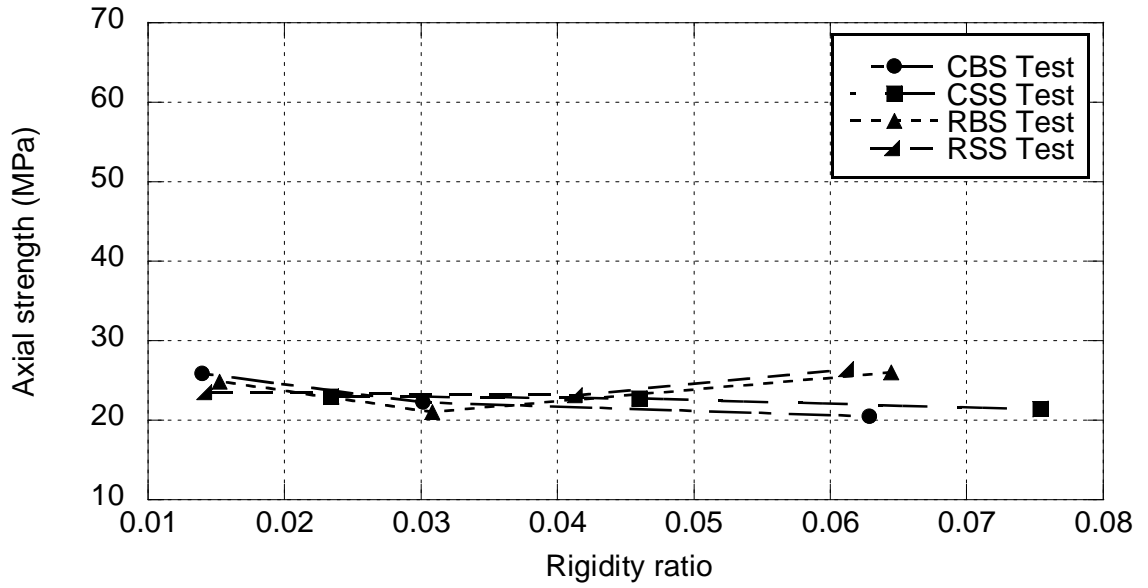


Figure 5.39 Axial strength of CFRP confined square columns made of brick, stone, recycled brick and recycled stone aggregate concrete with rigidity ratio.

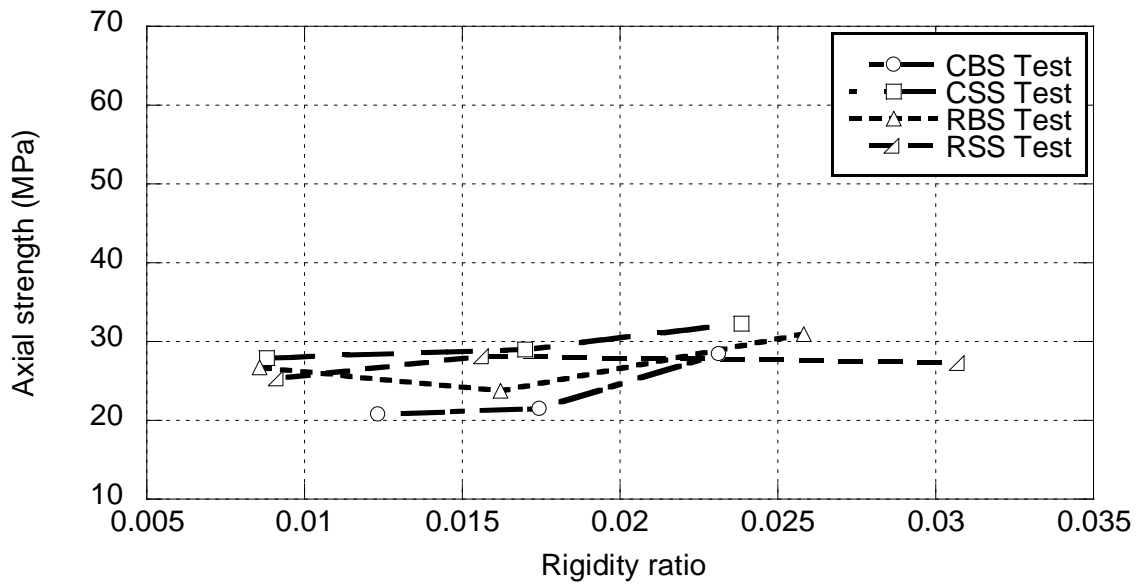


Figure 5.40: Axial strength of GFRP confined square columns made of brick, stone, recycled brick and recycled stone aggregate concrete with rigidity ratio.

## 6.1 General

In order to understand the behavior of design of concrete confined with FRP, the mechanical properties need to be studied. Designing FRP confined concrete requires analytical tools that predict the level of performance enhancement for the concrete core. Confinement model - a model predicting the strength and ductility has to be developed. A number of studies are conducted to evaluate the confinement effectiveness of FRP, taking into account the mechanism of fiber composites as well as the 3-D stresses in concrete core. Confinement of columns is a three-dimensional phenomenon that cannot readily be reduced into two-dimensions. When studying the ductility of confined and unconfined normal concrete columns, it is important to accurately incorporate the behavior of concrete. This factor is important as the concrete shows unique dilation characteristics when confined with linear-elastic and non-yielding materials such as FRP. For obtaining accurate results, a Finite Element Method can be approached. The objectives of the FE models are to verify the numerical results with the experimental measurements. In this work, a finite element model of FRP confined concrete column is developed and validated by existing experimental results. The models are simulated using ANSYS 10.0 (2005) finite element software.

## 6.2 Dilation due to Poisson's effect

Dilation due to Poisson's effect of concrete influences the confinement mechanism of FRP significantly. Akhtaruzzaman and Hasnat (1983) concluded that modulus of elasticity and the Poisson's ratio of the concrete varies with the different type of aggregate. Modulus of elasticity can be measured from the axial stress-strain curve obtained from the load cell. Four types of concrete made of brick, stone, recycled brick and recycled stone having same gradation are used in this work. For that reason, Poisson's ratio of the concrete varies with the different type of aggregate. Islam (2011) concluded that for stone, brick, recycled stone and recycled brick aggregate concrete the

Poisson's ratio are 0.25, 0.35, 0.37 and 0.40 respectively. For that reason the Poisson's ratio of different concrete used in this research are summarized in Table 6.1.

Table 6.1: Poisson's ratio of different concrete

Concrete type	Poisson's ratio
Stone aggregate concrete	0.25
Brick aggregate concrete	0.35
Recycled stone aggregate concrete	0.37
Recycled brick aggregate concrete	0.40

### 6.3 Finite Element (FE) model Formation

Two types of Methods are recommended ANSYS 10.0 to create a model, such as graphical user interface (GUI) or command prompt line input. In this research, GUI are used to create the models.

#### 6.3.1 Element type

For the modeling of unconfined and confined concrete columns, a 3-D reinforced concrete solid element SOLID 65 is used. It can be used with or without reinforcing bars. The solid is capable of cracking in tension and crushing in compression. The element is defined by eight nodes having three degrees of freedom at each node: translations in x, y, z directions. The most important aspect of this element is the treatment of nonlinear material properties. The concrete is capable of cracking (in three orthogonal directions), crushing, plastic deformation, and creep. The rebar are capable of tension and compression, but not shear. They are also capable of plastic deformation and creep. The geometry and coordinate system is shown in the Figure 6.1.

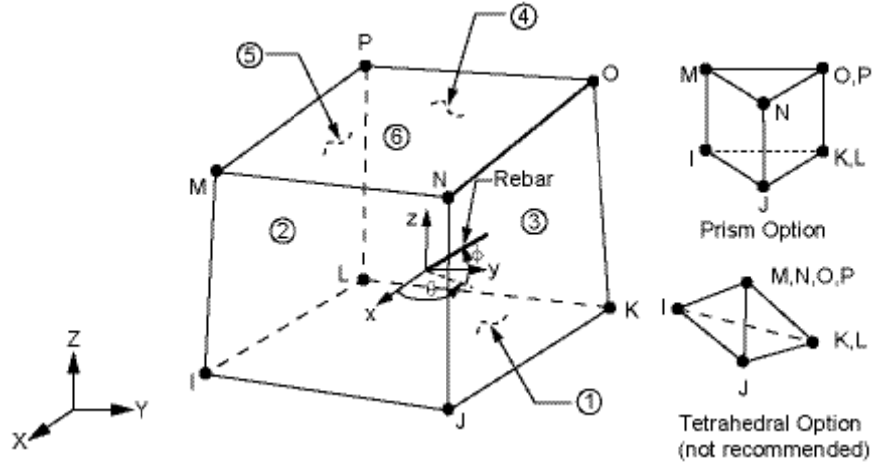


Figure 6.1: SOLID 65 element geometry and coordinate system (ANSYS 10.0)

### 6.3.2 Real constants

The real constants for the unconfined and confined circular and square concrete column models are shown in Table 6.2. The models are considered plain concrete having no reinforcement for modeling the uniaxial behaviour.

Table 6.2 Real constants for SOLID65 element

Real constant set	Element type	Constants			
		Real constants for rebar 1	Real constants for rebar 2	Real constants for rebar 3	
1	SOLID65	Material number	0	0	0
		Volume ratio	0	0	0
		Orientation angle	0	0	0
		Orientation angle	0	0	0

### 6.3.3 Material properties

For concrete, ANSYS requires some input data to be defined as a model properties, such as elastic modulus ( $E_c$ ), ultimate uniaxial compressive strength ( $f'_c$ ), ultimate uniaxial tensile strength (modulus of rupture,  $f_r$ ), Poisson's ratio ( $\nu$ ) and compressive uniaxial stress-strain relationship. Both the unconfined and confined concrete columns are modeled in the same principle. The modulus of elasticity is applied according to the initial slope of the stress-strain curves. Respective stress-strain relationships for unconfined and confined concretes as realized from test data are used as input.

ANSYS requires 9 constants to be defined as the material properties to model the concrete element as per William and Warnke (1975) failure criterion. These constants are:

1. Shear transfer coefficients for an open crack
2. Shear transfer coefficients for a closed crack
3. Uniaxial tensile cracking stress
4. Uniaxial crushing stress (positive)
5. Biaxial crushing stress (positive)
6. Ambient hydrostatic stress state for use with constants 7 and 8
7. Biaxial crushing stress (positive) under the ambient hydrostatic stress state (constant 6)
8. Uniaxial crushing stress (positive) under the ambient hydrostatic stress state (constant 6)
9. Stiffness multiplier for cracked tensile condition.

Typical shear transfer coefficients range from 0.0 to 1.0, with 0.0 representing a smooth crack (complete loss of shear transfer) and 1.0 representing a rough crack (no loss of shear transfer). The shear transfer coefficients for open and closed cracks are determined using the work of Kachlakev et al. (2001) as a basis. Convergence problems occurred when the shear transfer coefficient for the open crack dropped below 0.2. No deviation of the response occurs with the change of the coefficient. Therefore, the coefficient for the open crack is set to 0.3 (Table 6.3). The uniaxial cracking stress is based upon the modulus of rupture which is usually being 8-15% of the compressive strength of concrete. It is assumed 10% of the compressive strength in the FE models. Table 6.3 shows the values of constant for the model.

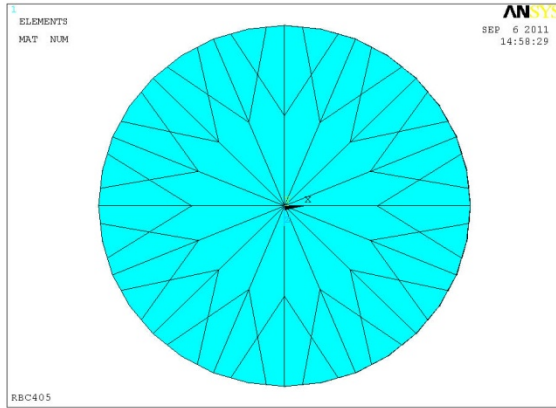
Table 6.3: Material properties of concrete

Material number	Element type	Material properties (Concrete)	
1	SOLID65	ShrCf-Op	0.3
		ShrCf-CI	1
		UnTensSt	$0.1f'_{co}$
		UnCompSt	-1
		BiCompSt	0
		HydroPrs	0
		BiCompSt	0
		UnTensSt	0
		TenCrFac	0

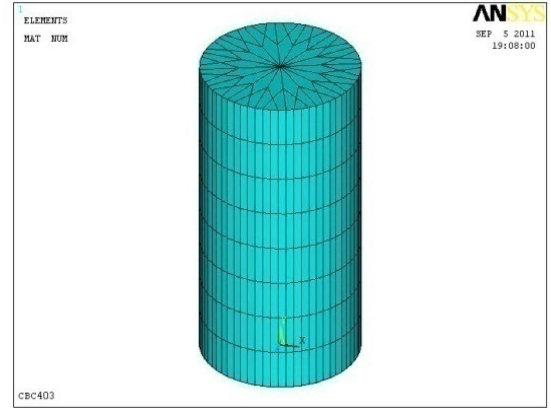
#### **6.3.4 FE mesh**

Two basic geometric shapes with three different sizes of specimen are modeled. The circular plain concrete columns are 100, 150 and 200 mm in diameter and 200, 300 and 400 mm in height respectively with the same aspect ratio. Again the square plain concrete columns are 100 x 100 x 200 mm, 150 x 150 x 300 mm and 200 x 200 x 400 mm with rounded corners of 25mm radius. In this research work 60 out of 120 columns are modeled using ANSYS 10. The edges of the models are defined by the keypoints. Eight noded SOLID65 elements are created using volume modeling approach. The generated model is meshed using mapped mesh which helps in controlling the number of elements. The fewer the number of elements, the coarse, the mesh is. Refinement of the mesh increases the accuracy of the simulation also increasing the analysis effort. The mesh sizes are varied with the dimension of the model. For 100, 150 and 200 mm in diameter and 200, 300 and 400 mm in height respectively circular columns, the mesh sizes along the longitudinal direction are 8, 10 and 12 respectively. Similarly for 100 x 100 x 200 mm, 150 x 150 x 300 mm and 200 x 200 x 400 mm sized square concrete columns the mesh sizes along the longitudinal direction are 8, 10 and 12 respectively. Element attributes are assigned to the respective elements. Typical meshing of the circular and square concrete columns models is shown in Figure 6.2 and Figure 6.3.

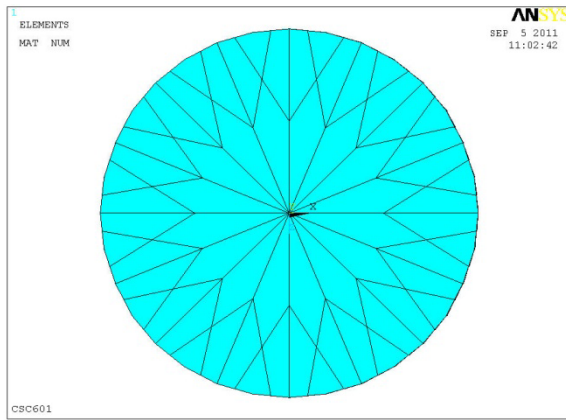




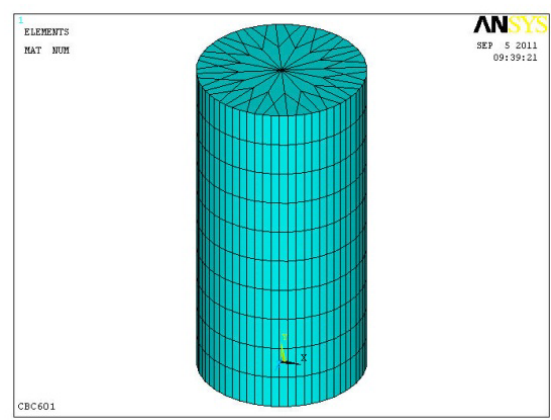
(a)



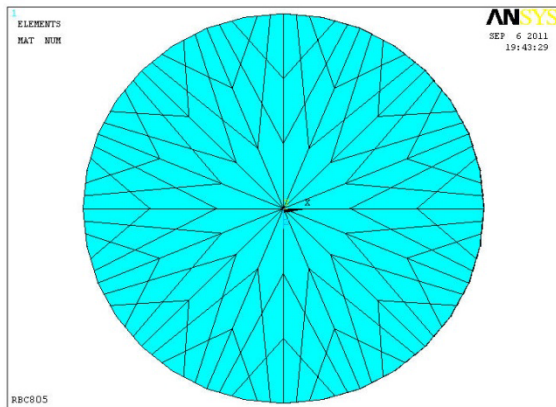
(b)



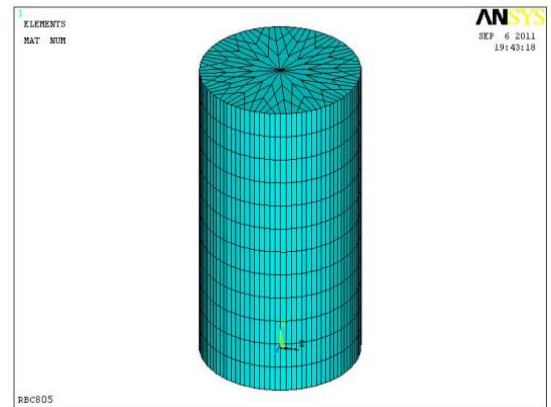
(c)



(d)

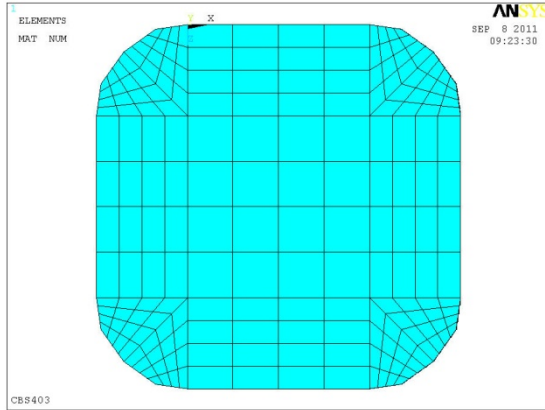


(e)

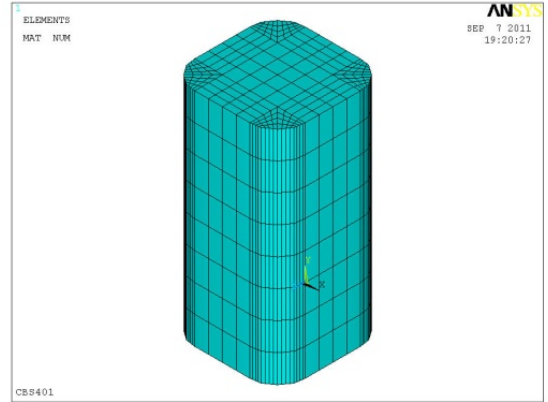


(f)

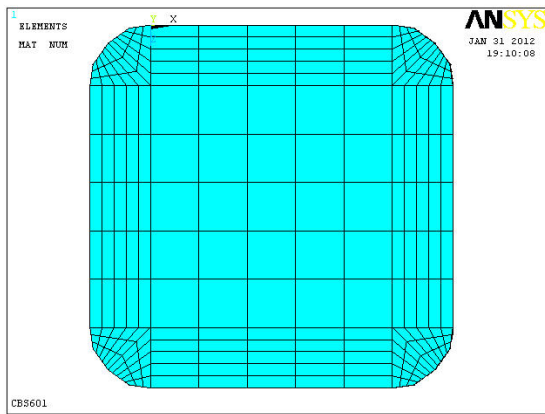
Figure 6.2: Typical meshing of circular plain concrete column (a), (c) and (e) plan view of the 100, 150 and 200 mm in diameter meshed circular columns, (b), (d) and (f) oblique view of the 100, 150 and 200 mm in diameter meshed circular columns.



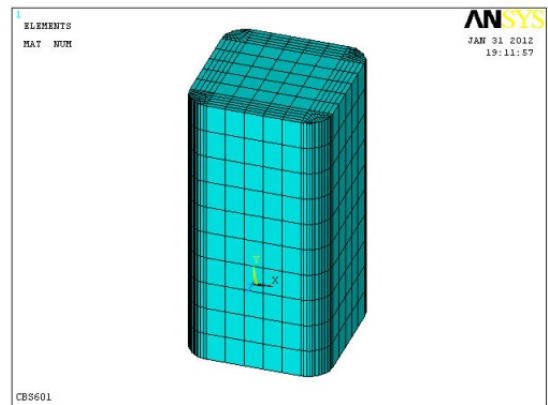
(a)



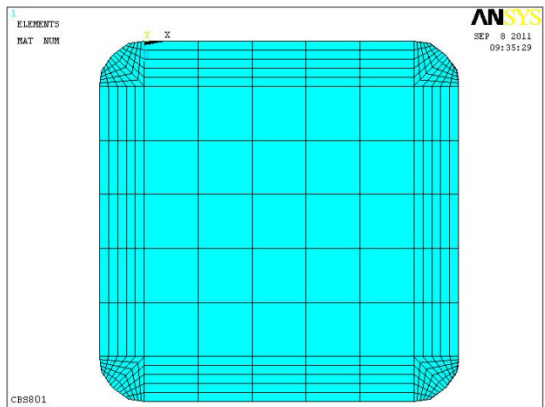
(b)



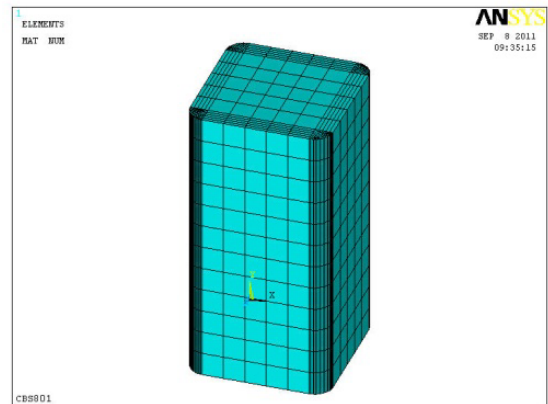
(c)



(d)



(e)

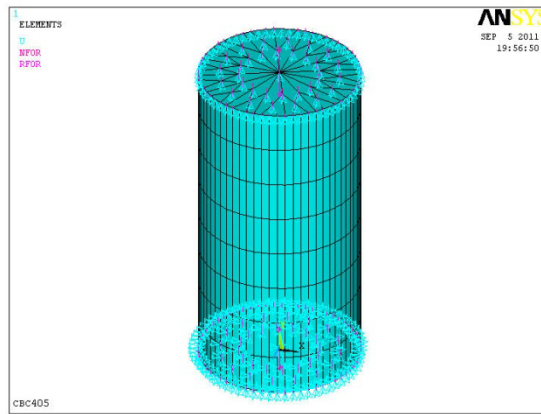


(f)

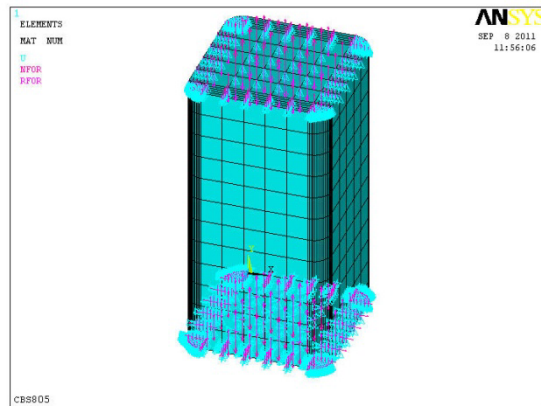
Figure 6.3: Typical meshing of square plain concrete column (a), (c) and (e) meshing of 100 x 100 x 200 mm, 150 x 150 x 300 mm and 200 x 200 x 400 mm sized square columns, fine mesh at the corners and sides and coarse mesh at the middle (b), (d) and (f) oblique view of the 100 x 100 x 200 mm, 150 x 150 x 300 mm and 200 x 200 x 400 mm sized meshed square column.

### 6.3.5 Boundary conditions and loading

In all cases, the bottom of the columns is constrained at X, Y and Z direction (Figure 6.4) so that no degree freedom is allowed there to simulate the boundary condition for the uniaxially loaded columns. For each model, a nonlinear analysis is conducted considering both material and geometric nonlinear behavior are shown in Table 6.4 and 6.5. The loading process is divided into many incremental steps, in which an incremental axial displacement is applied to the top surface of each column and all nodes on the top face are tied together so that a uniform compressive displacement could be exerted. The displacement value is determined by multiplying the initial height with the ultimate strain of the column obtained from the load cell of universal testing machine (UTM). Every increment would be iterated until convergence is met with respect to the criteria of force and displacement.



(a)



(b)

Figure 6.4: Loading and boundary condition of the FE model (a) circular column (b) square column

Table 6.4: Commands used to control nonlinear analysis, output, nonlinear algorithm and advanced nonlinear analyses

Option	Criteria	Value/selection
Basic	Analysis option	Small displacement static
	Time Control: Time at end of load step	500
	Automatic time stepping	Program chosen
	Time increment	Activated
	Substep size	0.5
	Max. substep size	0.5
	Min. substep size	0.5
Solution	Write items to result files	All solution items
	Frequency	Write every substep
	Equation solver	Sparse direct
Nonlinear	Restart control: No. of restart files to write	1
	Frequency	Write every substep
	Line search	Off
	DOF solution predictor	Program chosen
	Equilibrium iterations: Maximum no. of iterations	100
	Cut back control: limits on physical values to perform bisections	
	Equivalent plastic strain	0.15
	Explicit creep ratio	0.1
	Implicit creep ratio	0
	Incremental displacement	10000000
	Points per cycle	13
	Cut back according to predicted number of iterations	Activated
	Advanced nonlinear	Termination criteria:
Program behaviour upon nonconvergence		Terminate but do not exit
Limits on physical values to stop analysis:		
Nodal DOF solution		0
Cumulative iteration		0
Elapsed time		0
CPU time	0	

Table 6.5: Convergence criteria parameters

Set convergence criteria		
Label	F	U
Reference value	Calculated	Calculated
Tolerance	0.005	0.05
Norm	L2	L2
Minimum reference	N/A	N/A

### 6.3.6 Results and discussion

The output of ANSYS results consists of the nodal displacement, element stress and element strain. The results are found to be in reasonable similarities with the experimental test result indicating validity of the FE models. So the Poisson's ratio of the brick aggregate concrete, stone aggregate concrete, recycled brick aggregate concrete and recycled stone aggregate concrete used in this research which is obtained from Islam (2011) thesis appears to be reliable. In this research, these Poisson's ratios are used for 60 circular and square concrete columns of three different sizes. This analysis gives a better theoretical understanding and helps in achieving an accurate confinement model.

The comparison between experimental results and nonlinear finite element analysis results are shown in Figure 6.5 to Figure 6.20. The detail of comparison is described as follows.

### 6.3.6.1 Effect of radius of curvature

The effects of radius of curvature to the axial strength and ultimate axial strain of the CFRP and GFRP confined circular columns made of brick, stone, recycled brick and recycled stone aggregate are shown in Figure 6.5 to Figure 6.20. For brick aggregate CFRP and GFRP confined concrete circular columns shown in Figures 6.5-6.8, the axial strength and ultimate axial strain decreases with increasing radius of curvature. This is because the FRP volumetric ratio decreases as the cross sectional size increases if the numbers of layers are not increased. As it can be seen in Figures 6.5 - 6.8, the agreement between nonlinear finite element results (solid lines) and experimental results (markers) is satisfactory but due to the limitation of strain measurement technique, variation is found in some cases.

Similarly for stone, recycled brick and recycled stone aggregate CFRP and GFRP confined concrete circular columns shown in Figures 6.9 - 6.20, it can be seen that the axial strength and ultimate axial strain also decreases with increasing radius of curvature and again the agreement between nonlinear finite element results (solid lines) and experimental results (markers) is very satisfactory.

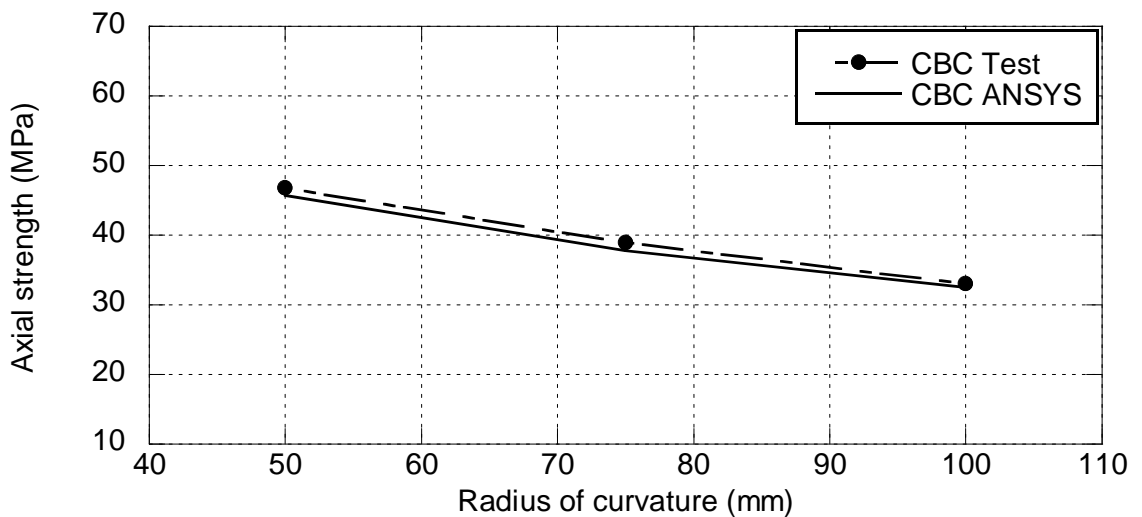


Figure 6.5: Comparisons for effect of column size on axial strength between experiment and ANSYS results for brick aggregate CFRP confined circular concrete columns.

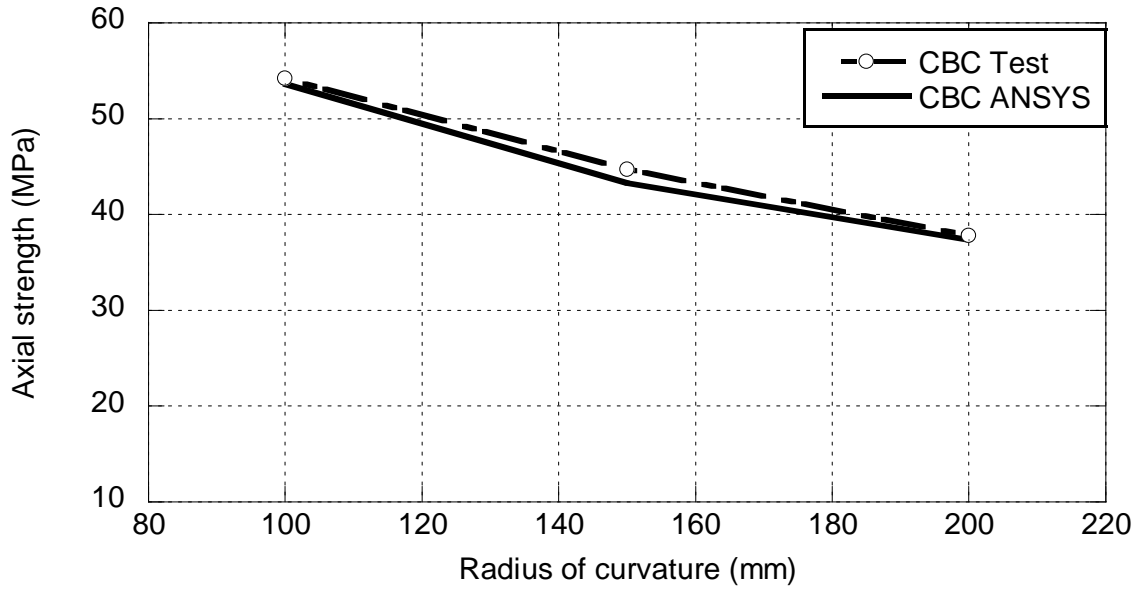


Figure 6.6: Comparisons for effect of column size on axial strength between experiment and ANSYS results for brick aggregate GFRP confined circular concrete columns.

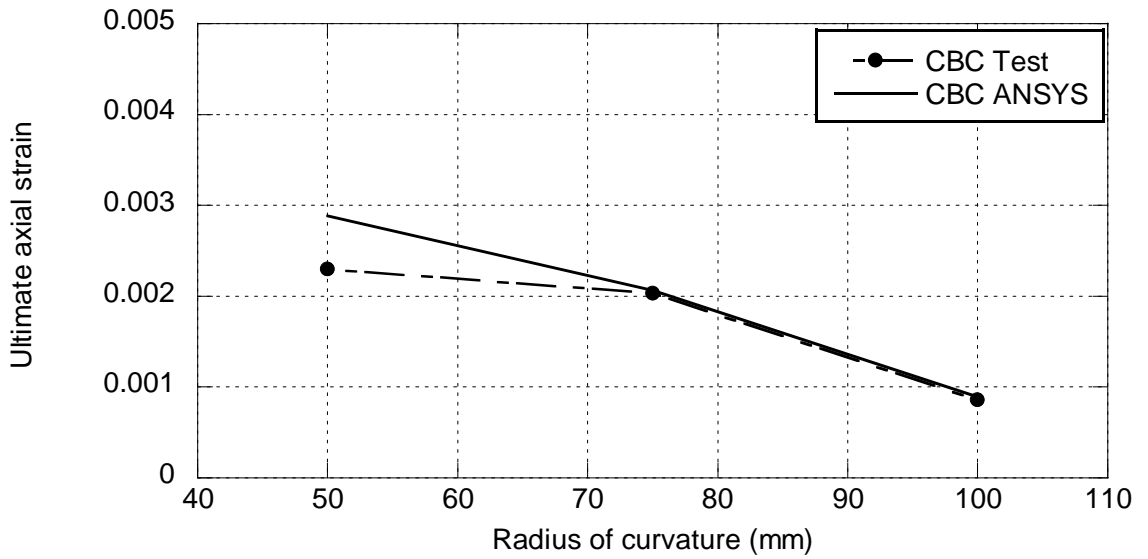


Figure 6.7: Comparisons for effect of column size on ultimate axial strain between experiment and ANSYS results for brick aggregate CFRP confined circular concrete columns.

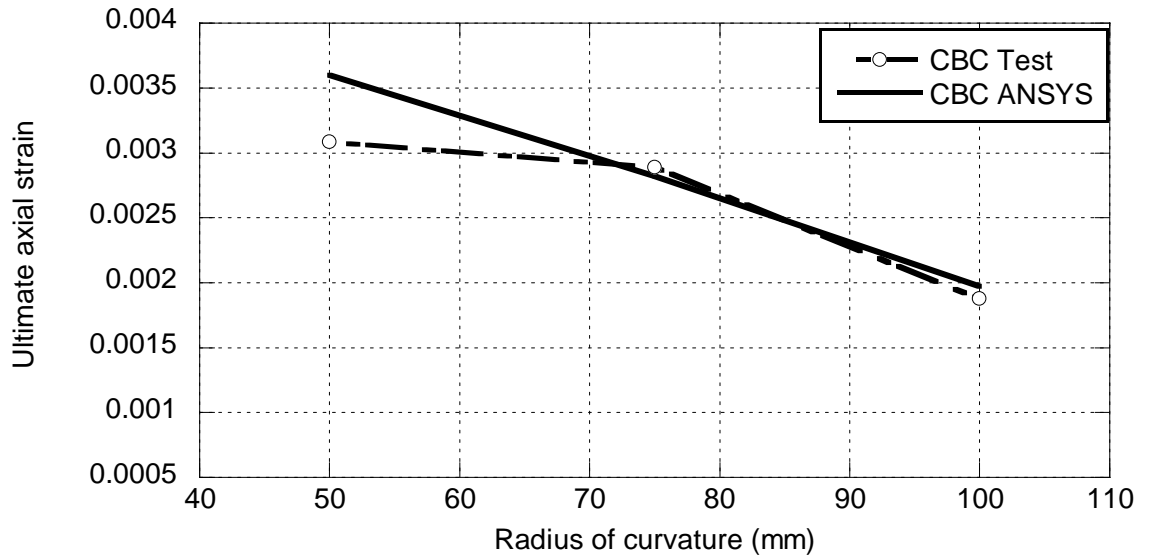


Figure 6.8: Comparisons for effect of column size on ultimate axial strain between experiment and ANSYS results for brick aggregate GFRP confined circular concrete columns.

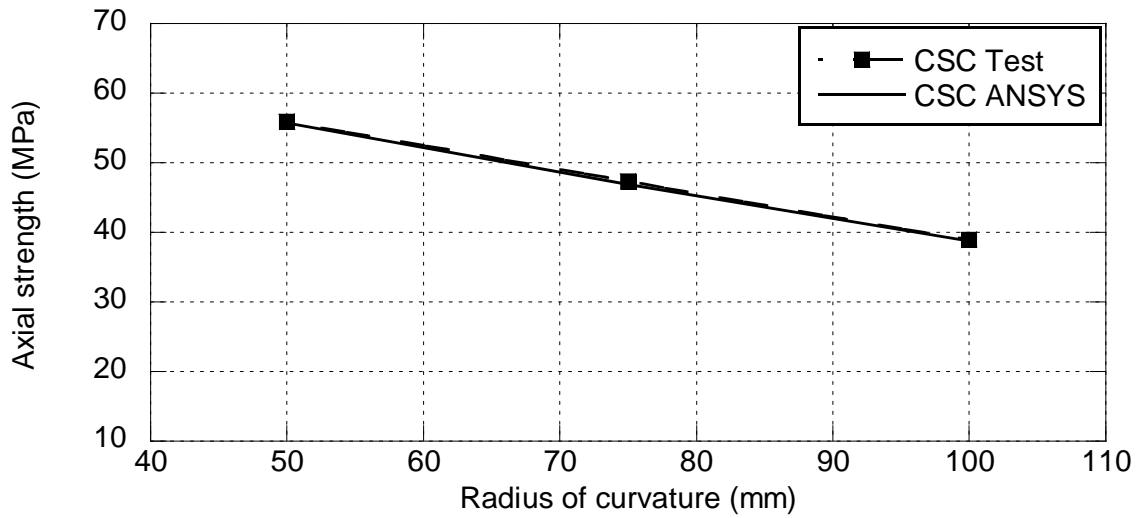


Figure 6.9: Comparisons for effect of column size on axial strength between experiment and ANSYS results for stone aggregate CFRP confined circular concrete columns.

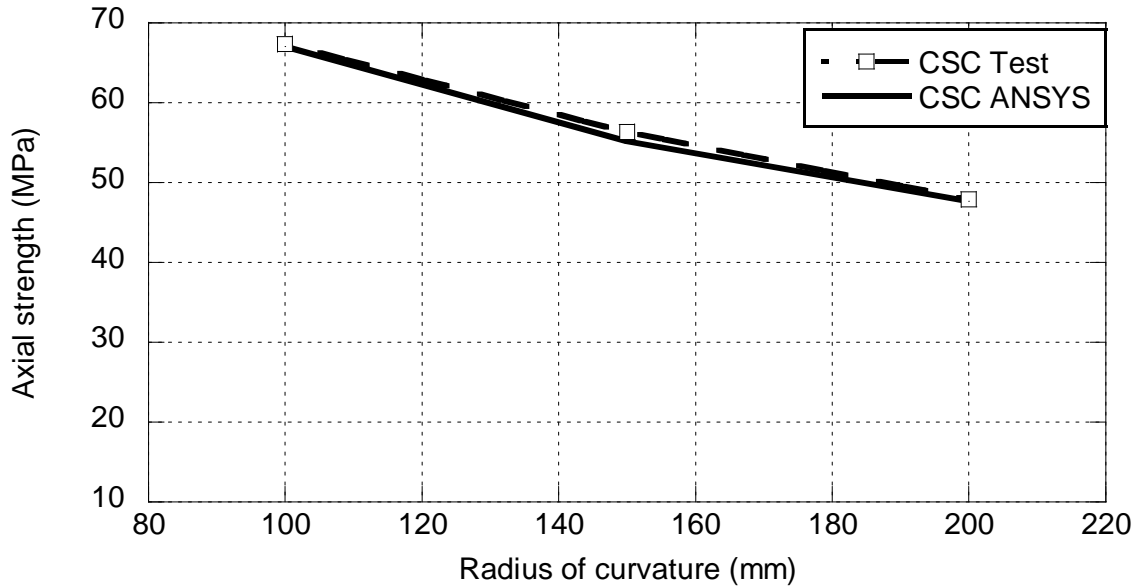


Figure 6.10: Comparisons for effect of column size on axial strength between experiment and ANSYS results for stone aggregate GFRP confined circular concrete columns.

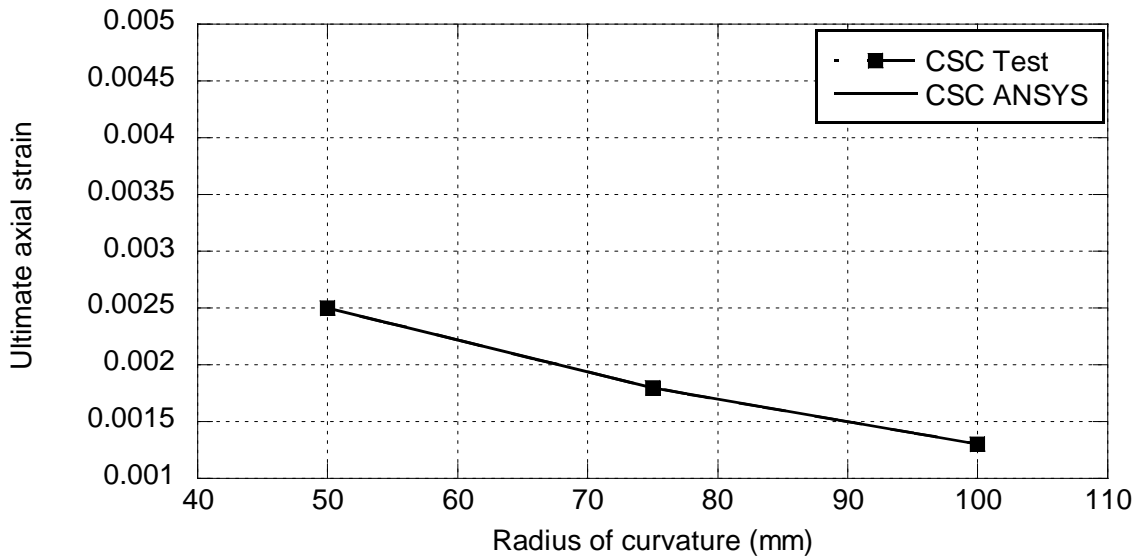


Figure 6.11: Comparisons for effect of column size on ultimate axial strain between experiment and ANSYS results for stone aggregate CFRP confined circular concrete columns.



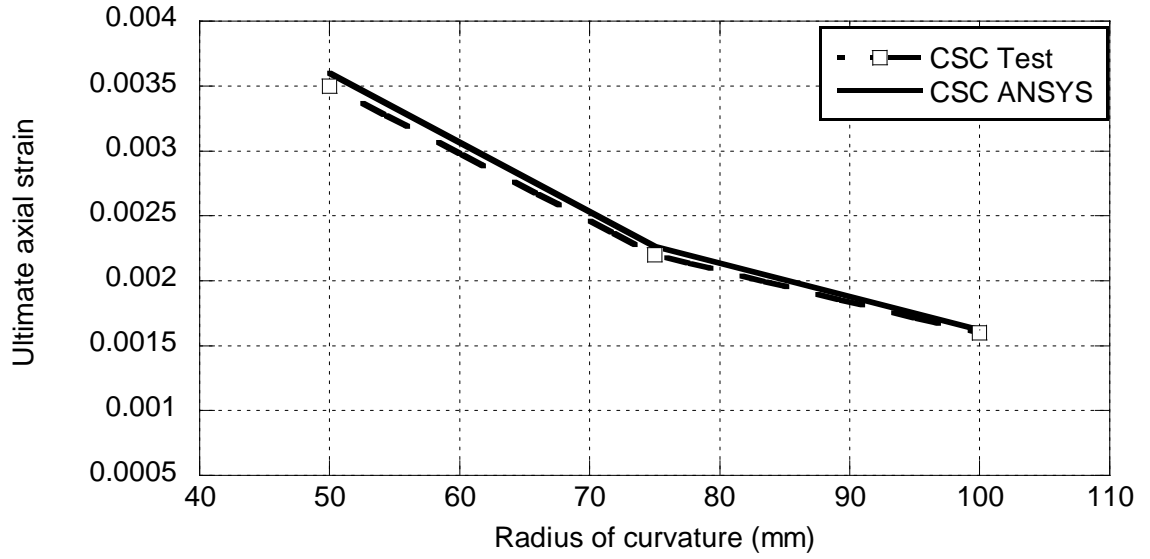


Figure 6.12: Comparisons for effect of column size on ultimate axial strain between experiment and ANSYS results for stone aggregate GFRP confined circular concrete columns.

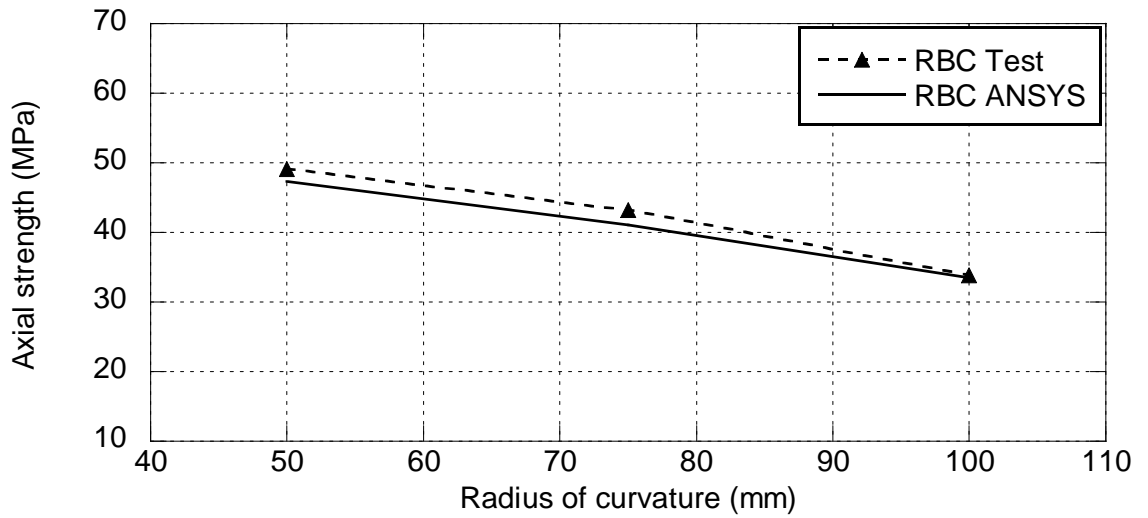


Figure 6.13: Comparisons for effect of column size on axial strength between experiment and ANSYS results for recycled brick aggregate CFRP confined circular concrete columns.

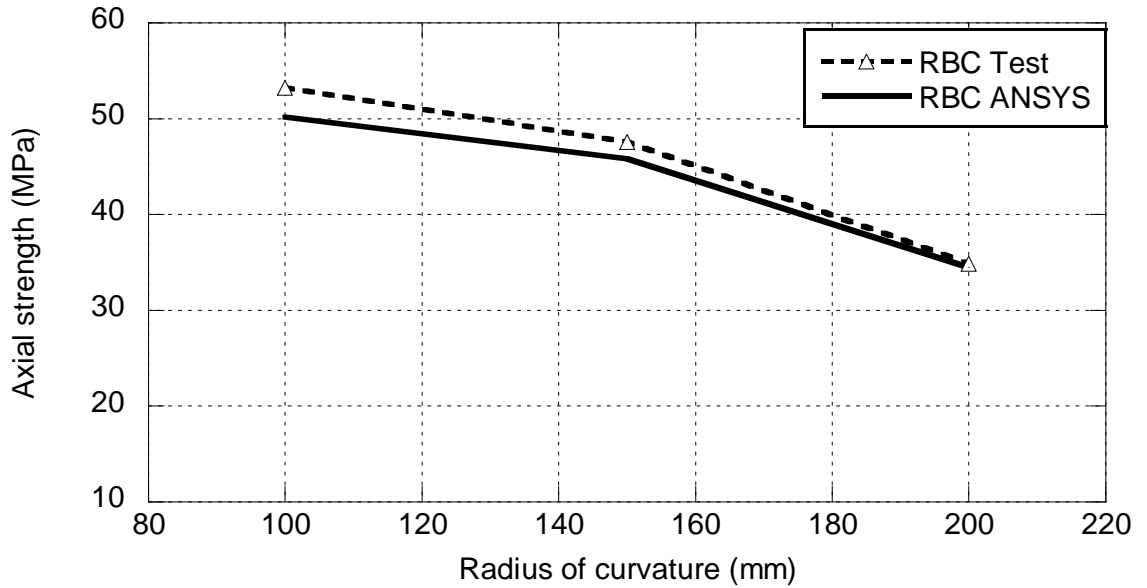


Figure 6.14: Comparisons for effect of column size on axial strength between experiment and ANSYS results for recycled brick aggregate GFRP confined circular concrete columns.

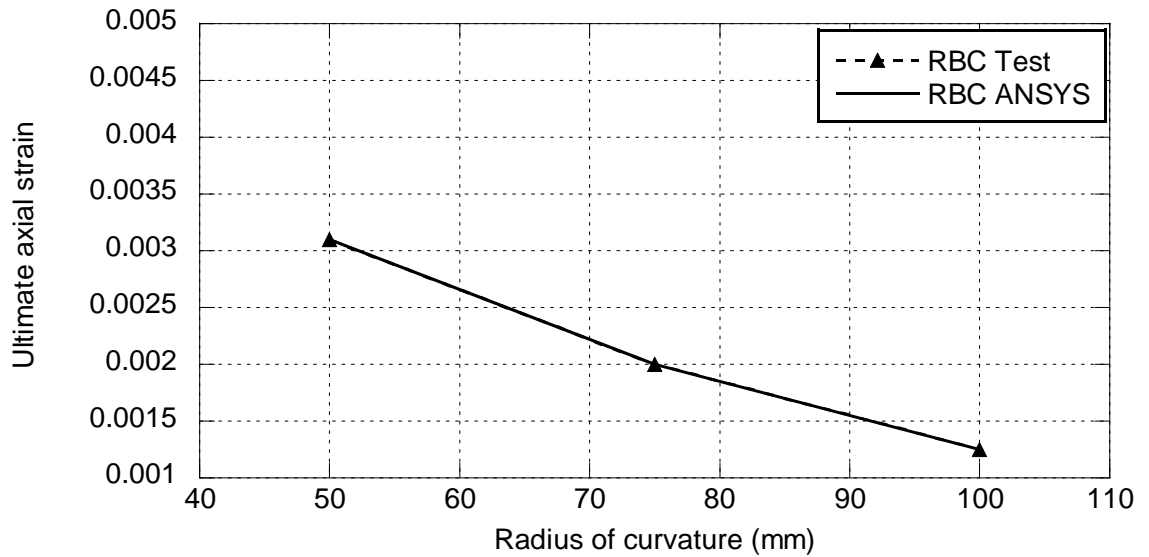


Figure 6.15: Comparisons for effect of column size on ultimate axial strain between experiment and ANSYS results for recycled brick aggregate CFRP confined circular concrete columns.

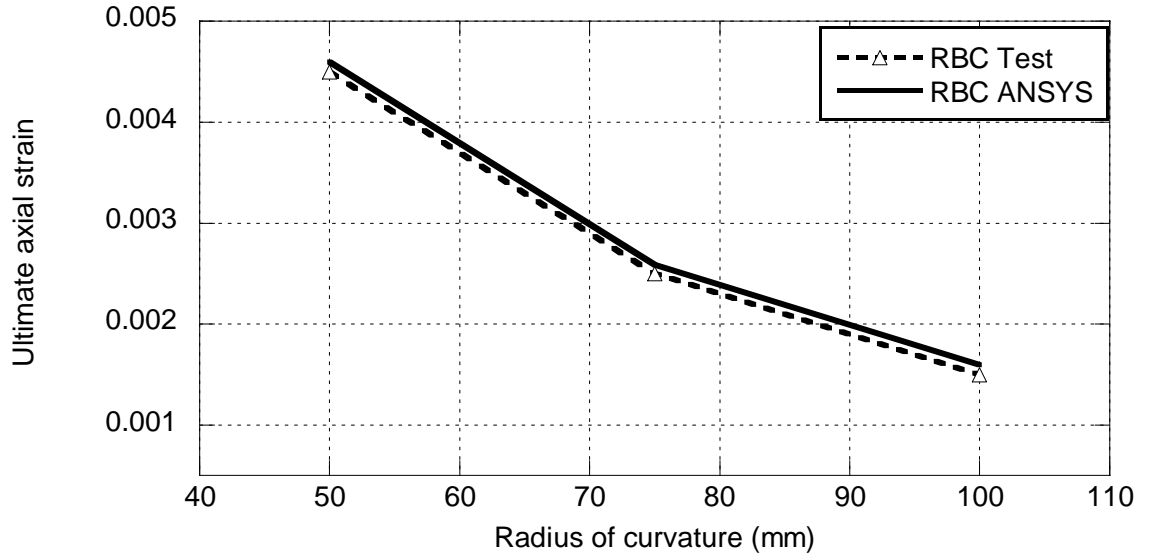


Figure 6.16: Comparisons for effect of column size on ultimate axial strain between experiment and ANSYS results for recycled brick aggregate GFRP confined circular concrete columns.

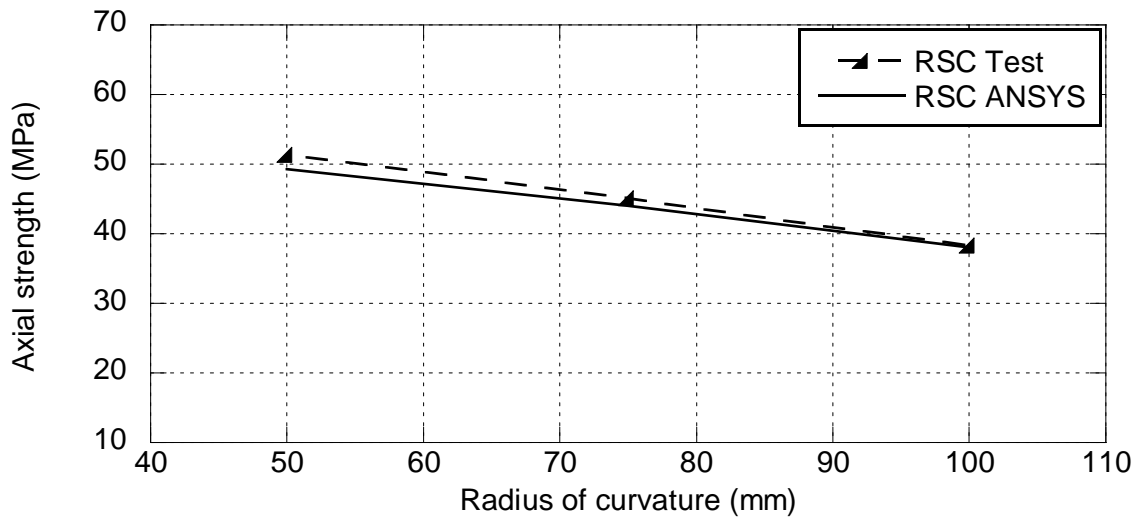


Figure 6.17: Comparisons for effect of column size on axial strength between experiment and ANSYS results for recycled stone aggregate CFRP confined circular concrete columns.

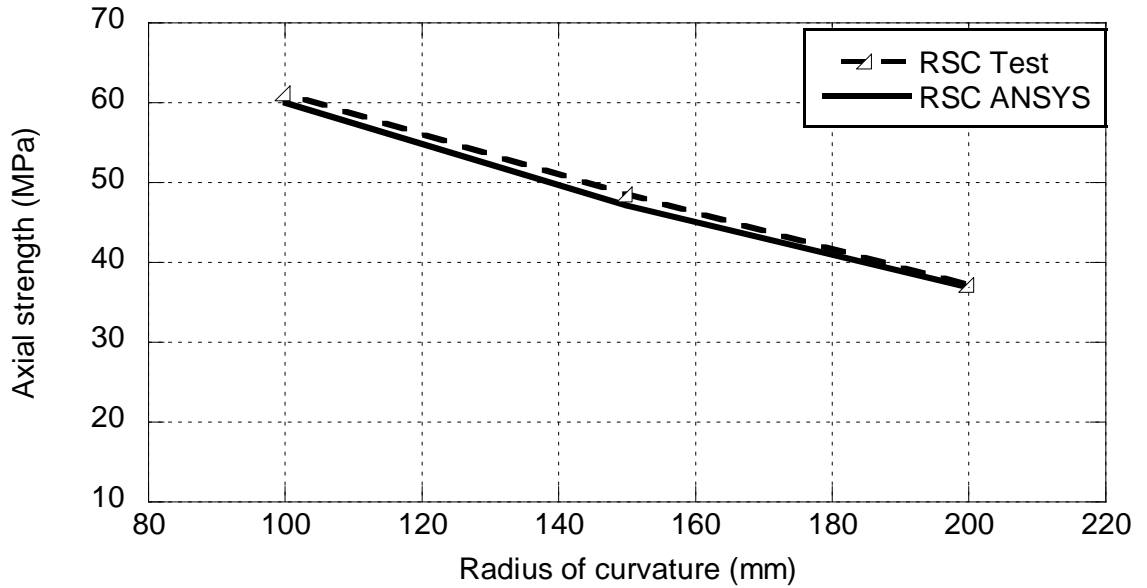


Figure 6.18: Comparisons for effect of column size on axial strength between experiment and ANSYS results for recycled stone aggregate GFRP confined circular concrete columns.

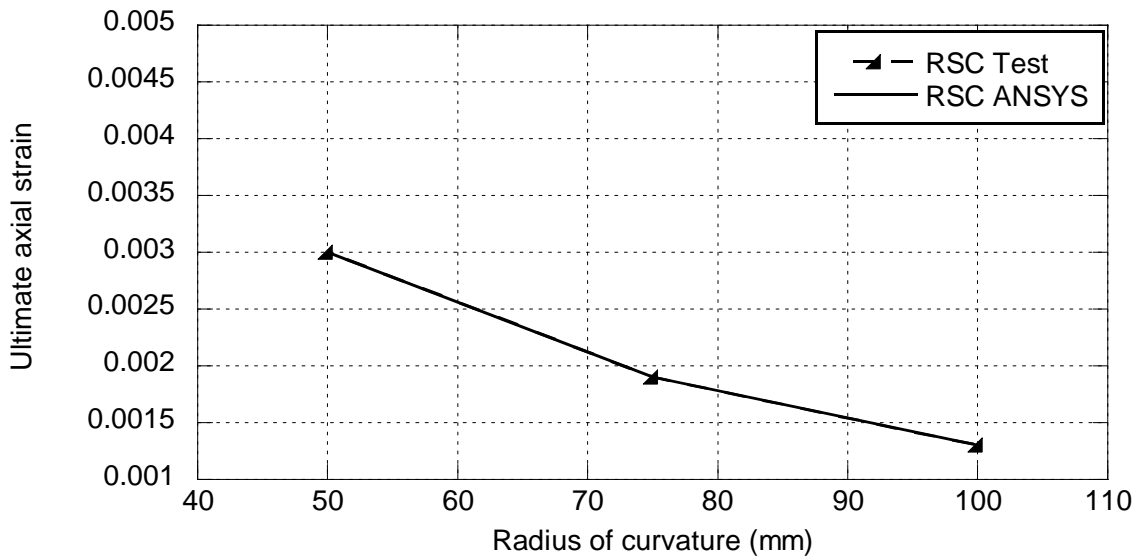


Figure 6.19: Comparisons for effect of column size on ultimate axial strain between experiment and ANSYS results for recycled stone aggregate CFRP confined circular concrete columns.

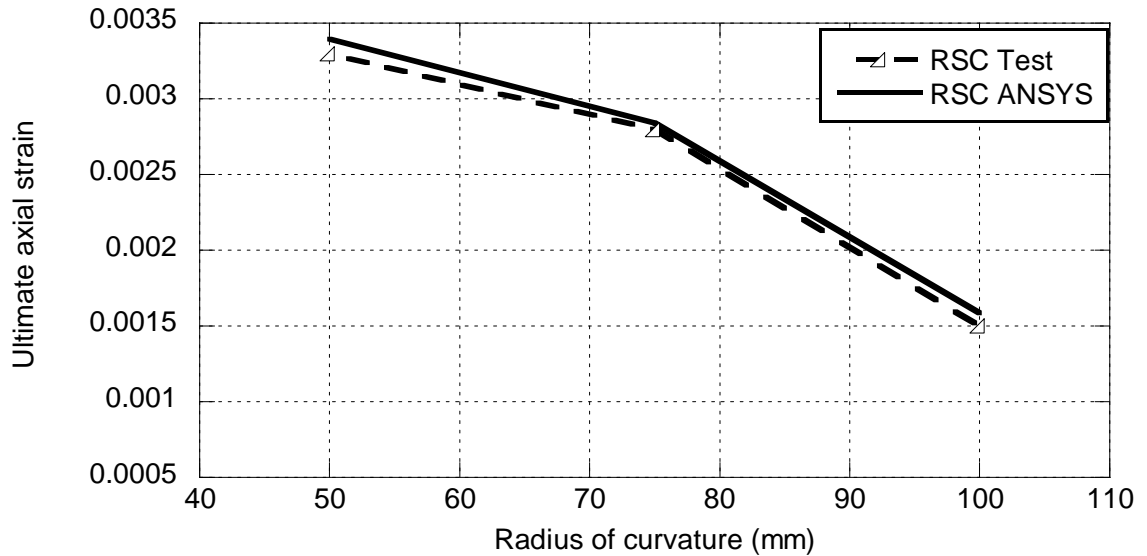


Figure 6.20: Comparisons for effect of column size on ultimate axial strain between experiment and ANSYS results for recycled stone aggregate GFRP confined circular concrete columns.

### 6.3.6.2 Effect of column side to corner radius ratio

The effects of column side to corner radius ratio to the axial strength and ultimate axial strain of the CFRP and GFRP confined square concrete columns made of brick, stone, recycled brick and recycled stone aggregate are shown in Figures 6.21-6.36. As shown in Figures 6.21-6.24, for brick aggregate CFRP and GFRP confined square columns with the same corner radius ( $r = 25$  mm), there is no size effect to exist in axial strength but ultimate axial strain slightly decreases with increasing column side to corner radius ratio. As it can be seen in Figures 6.21-6.24, the agreement between nonlinear finite element results (solid lines) and experimental results (markers) is very satisfactory.

Similarly for stone, recycled brick and recycled stone aggregate CFRP and GFRP confined square concrete columns shown in Figures 6.25 - 6.36, it can be seen that there is no size effect to exist in axial strength and ultimate axial strain decreases with increasing column side to corner radius ratio but for stone aggregate concrete variation is found in some cases due to the limitation of strain measurement technique. Again the agreement between nonlinear finite element results (solid lines) and experimental results (markers) is satisfactory.

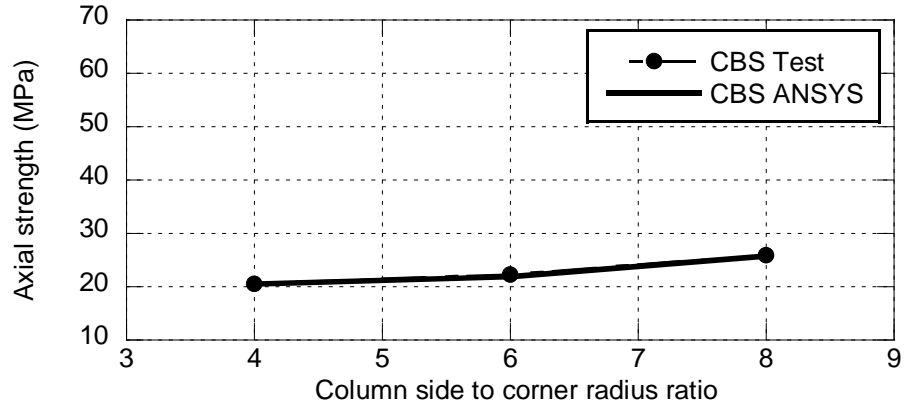


Figure 6.21: Comparisons for effect of column size on axial strength between experiment and ANSYS results for brick aggregate CFRP confined square concrete columns.

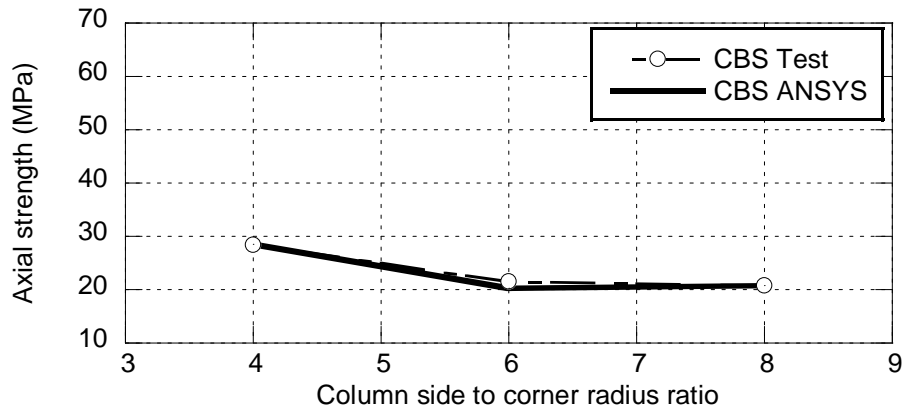


Figure 6.22: Comparisons for effect of column size on axial strength between experiment and ANSYS results for brick aggregate GFRP confined square concrete columns.

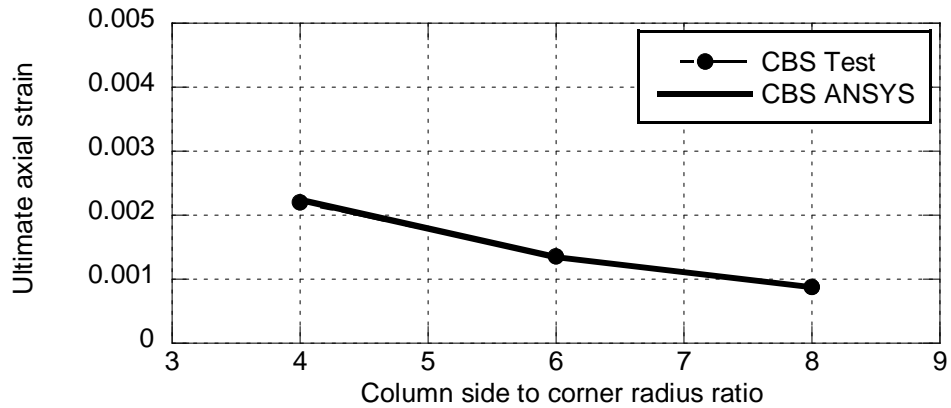


Figure 6.23: Comparisons for effect of column size on ultimate axial strain between experiment and ANSYS results for brick aggregate CFRP confined square concrete columns.

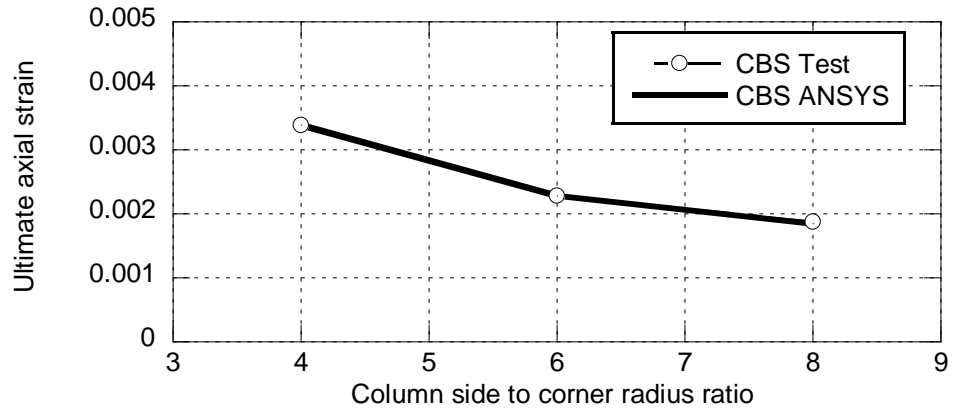


Figure 6.24: Comparisons for effect of column size on ultimate axial strain between experiment and ANSYS results for brick aggregate GFRP confined square concrete columns.

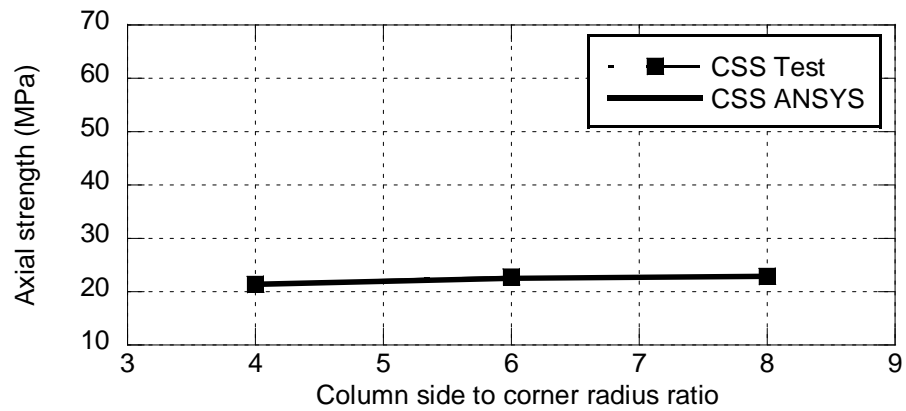


Figure 6.25: Comparisons for effect of column size on axial strength between experiment and ANSYS results for stone aggregate CFRP confined square concrete columns.

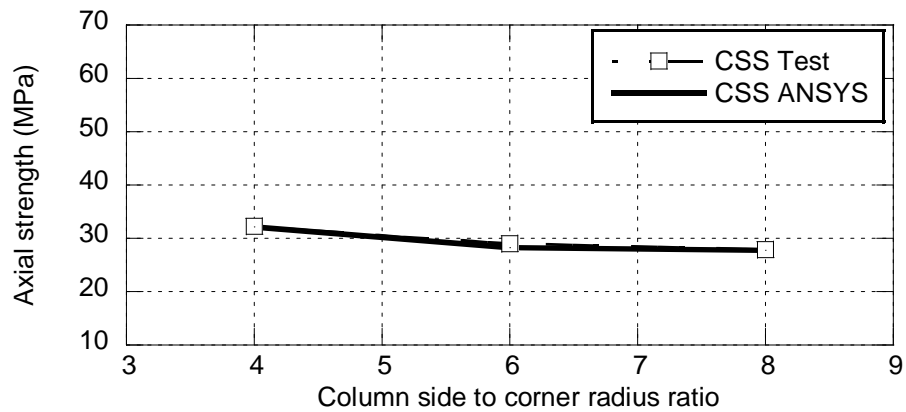


Figure 6.26: Comparisons for effect of column size on axial strength between experiment and ANSYS results for stone aggregate GFRP confined square concrete columns.

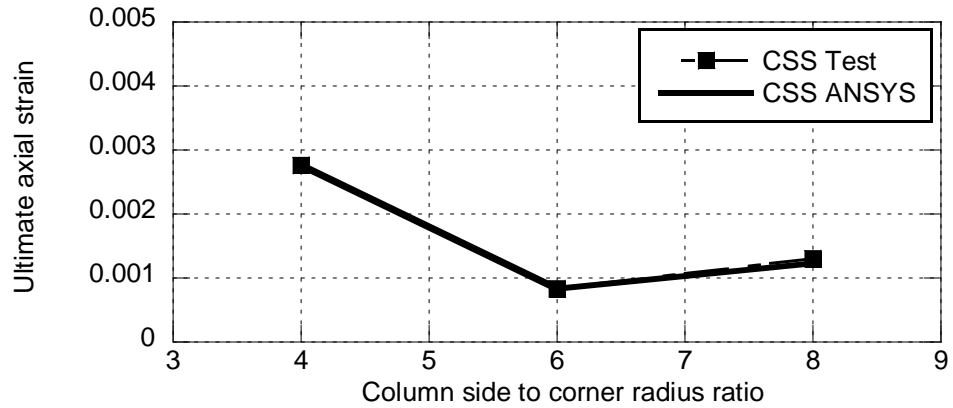


Figure 6.27: Comparisons for effect of column size on ultimate axial strain between experiment and ANSYS results for stone aggregate CFRP confined square concrete columns.

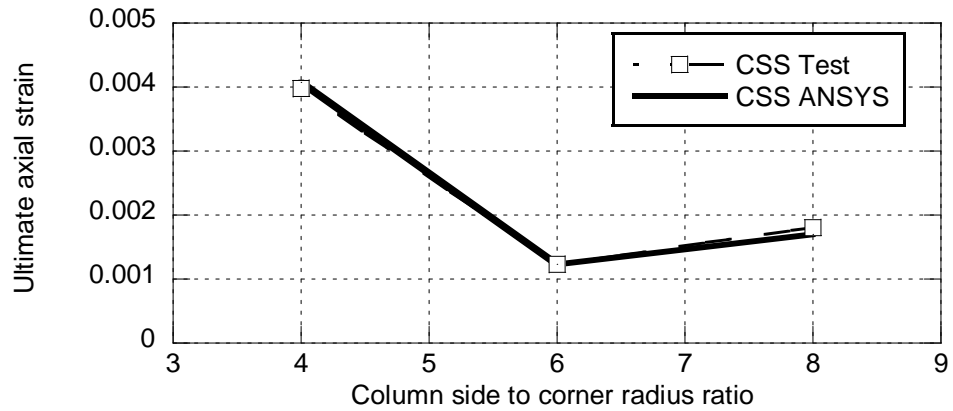


Figure 6.28: Comparisons for effect of column size on ultimate axial strain between experiment and ANSYS results for stone aggregate GFRP confined square concrete columns.

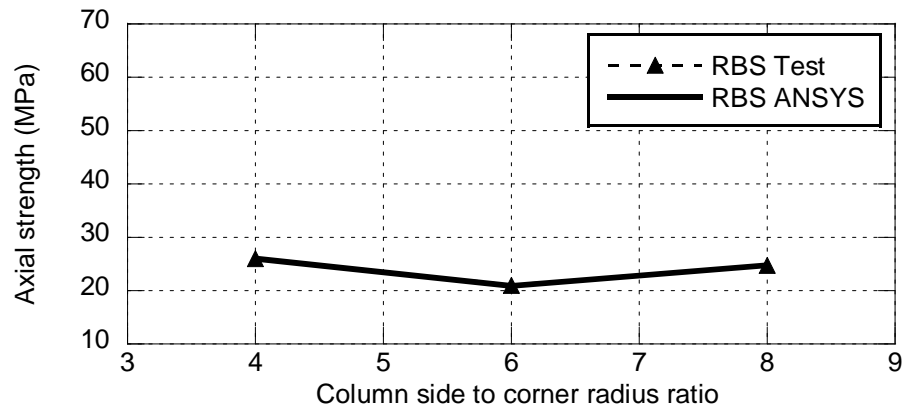


Figure 6.29: Comparisons for effect of column size on axial strength between experiment and ANSYS results for recycled brick aggregate CFRP confined square concrete columns.



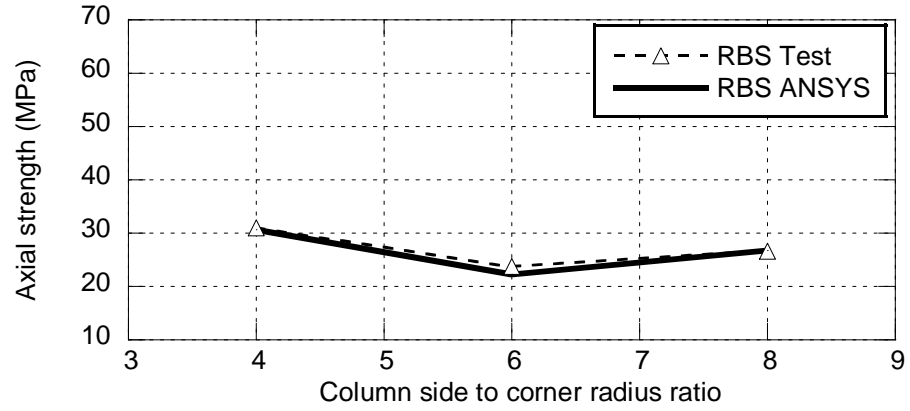


Figure 6.30: Comparisons for effect of column size on axial strength between experiment and ANSYS results for recycled brick aggregate GFRP confined square concrete columns.

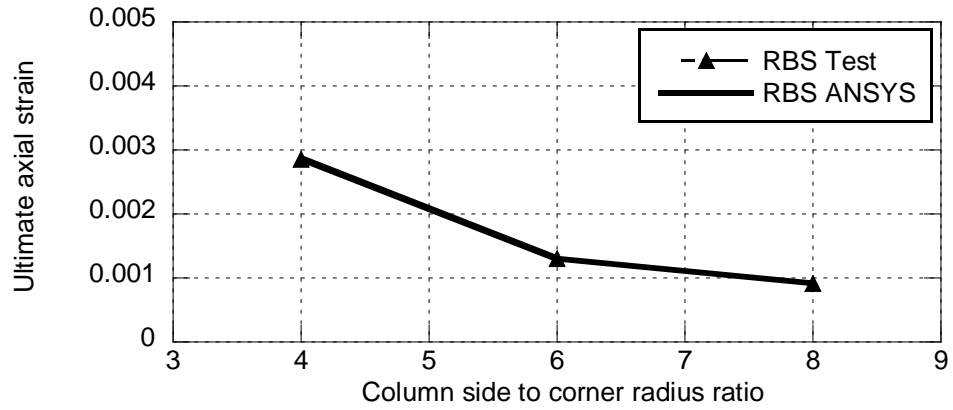


Figure 6.31: Comparisons for effect of column size on ultimate axial strain between experiment and ANSYS results for recycled brick aggregate CFRP confined square concrete columns.

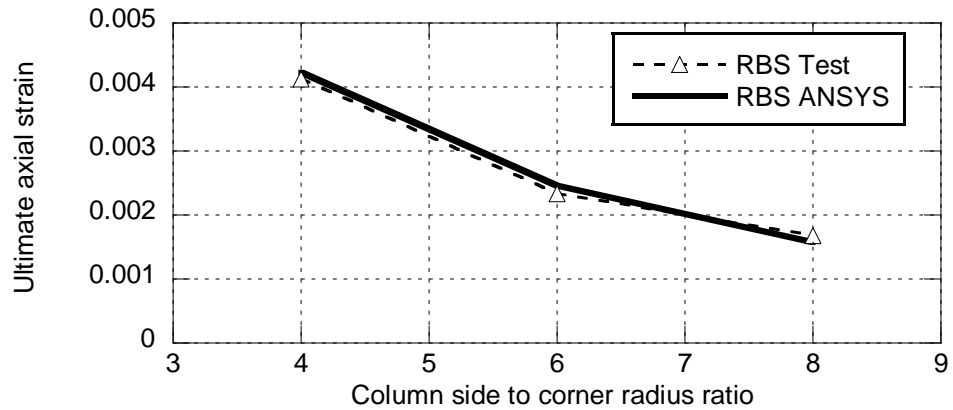


Figure 6.32: Comparisons for effect of column size on ultimate axial strain between experiment and ANSYS results for recycled brick aggregate GFRP confined square concrete columns.

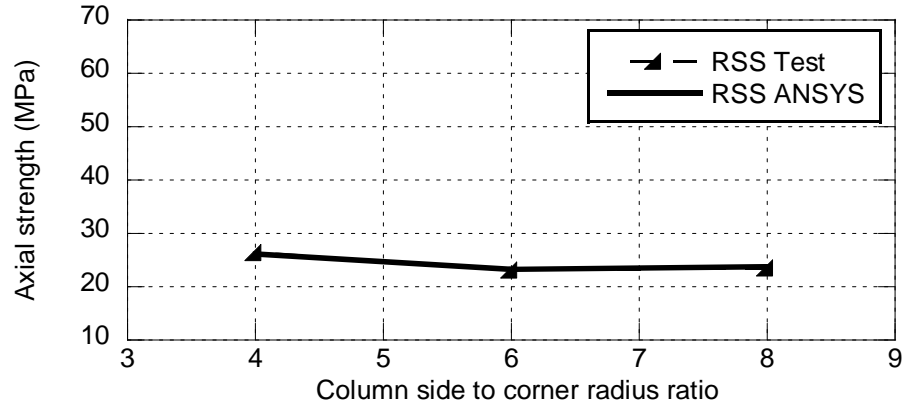


Figure 6.33: Comparisons for effect of column size on axial strength between experiment and ANSYS results for recycled stone aggregate CFRP confined square concrete columns.

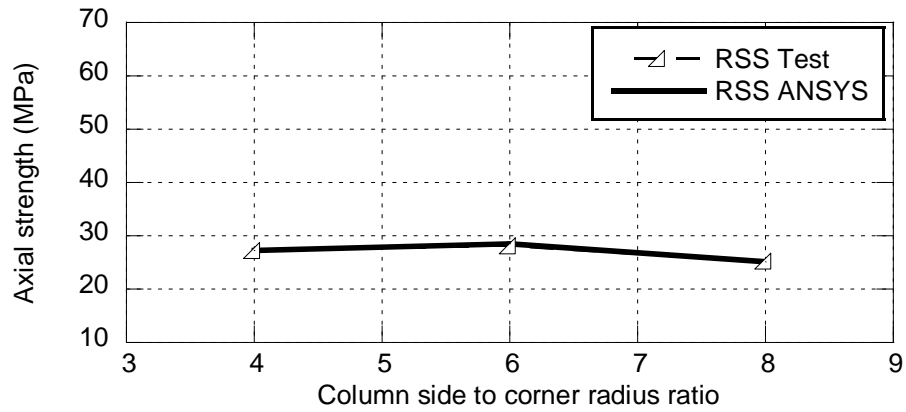


Figure 6.34: Comparisons for effect of column size on axial strength between experiment and ANSYS results for recycled stone aggregate GFRP confined square concrete columns.

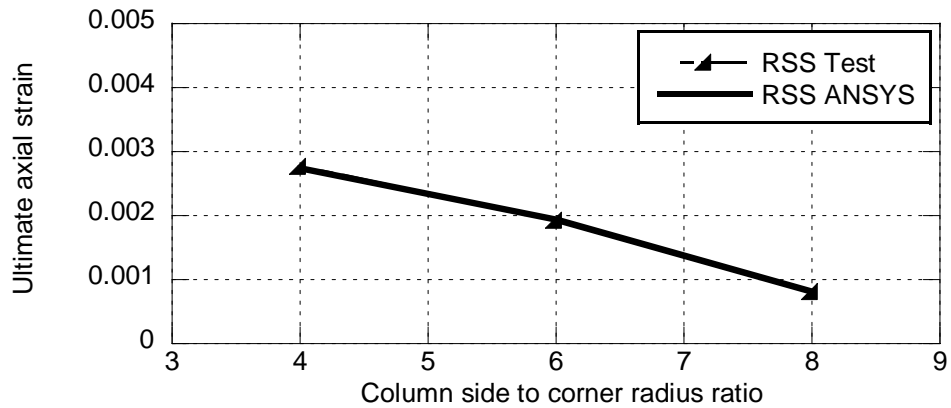


Figure 6.35: Comparisons for effect of column size on ultimate axial strain between experiment and ANSYS results for recycled stone aggregate CFRP confined square concrete columns.

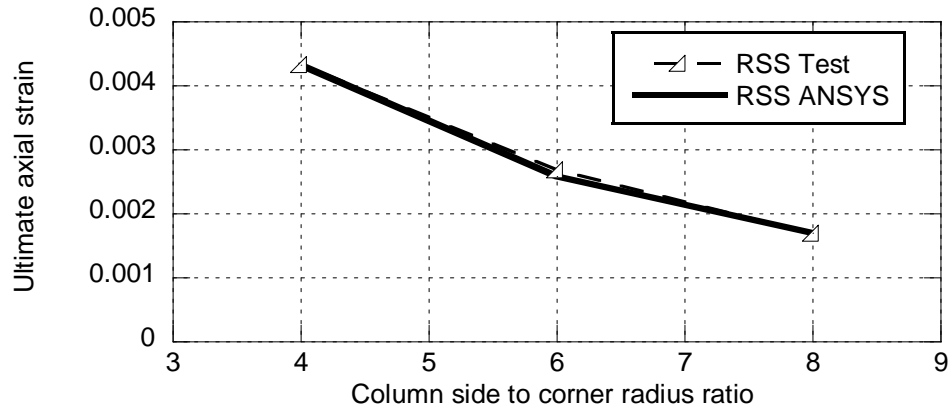


Figure 6.36: Comparisons for effect of column size on ultimate axial strain between experiment and ANSYS results for recycled stone aggregate GFRP confined square concrete columns.

### 6.3.6.3 Effect of FRP volumetric ratio

FRP volumetric ratio depends upon the number of layers of FRP, thickness of each FRP layer and the ratio of circumference to cross-sectional area. The effects of CFRP and GFRP volumetric ratio to the compressive strength and ultimate axial strain of confined columns made of brick, stone, recycled brick and recycled stone aggregate are shown in Figures 6.37 - 6.68. For CFRP and GFRP confined circular concrete columns made of brick aggregate concrete shown in Figures 6.37 - 6.40, the compressive strength and ultimate axial strain increases as the CFRP and GFRP volumetric ratio increases but variation is found in some cases due to the limitation of strain measurement technique. As it can be seen in Figures 6.37-6.40, the agreement between nonlinear finite element results (solid lines) and experimental results (markers) is satisfactory.

Similarly for CFRP and GFRP confined circular columns made of stone, recycled brick and recycled stone aggregate concrete shown in Figures 6.41-6.52, the compressive strength and ultimate axial strain increases with increasing the CFRP and GFRP volumetric ratio and again the agreement between nonlinear finite element results (solid lines) and experimental results (markers) is very satisfactory.

For square columns with the same corner radius ( $r = 25$  mm), there is no effects in axial strength and ultimate axial strain increases as the CFRP and GFRP volumetric ratio increases but due to the limitation of strain measurement technique variation is found in some cases as shown in Figures 6.53 - 6.68 for all types of aggregate. Again it can be

seen in Figures 6.53 - 6.68, the agreement between nonlinear finite element results (solid lines) and experimental results (markers) are very satisfactory.

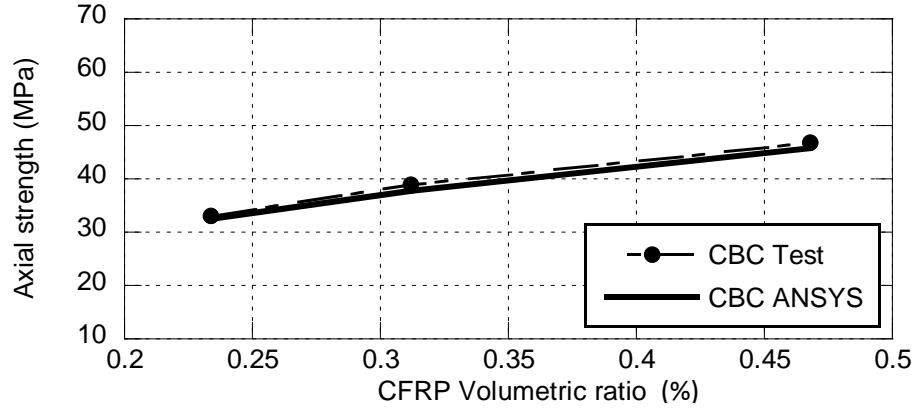


Figure 6.37: Comparisons for effect of volumetric ratio on axial strength between experiment and ANSYS results for brick aggregate CFRP confined circular concrete columns.

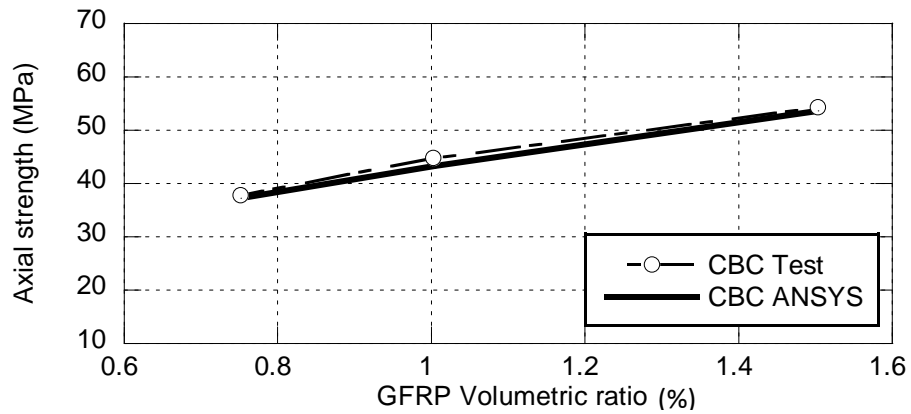


Figure 6.38: Comparisons for effect of volumetric ratio on axial strength between experiment and ANSYS results for brick aggregate GFRP confined circular concrete columns.

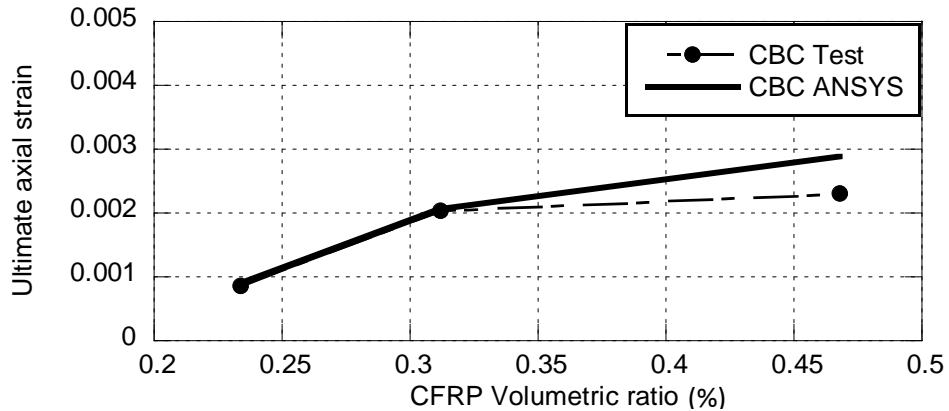


Figure 6.39: Comparisons for effect of volumetric ratio on ultimate axial strain between experiment and ANSYS results for brick aggregate CFRP confined circular concrete columns.

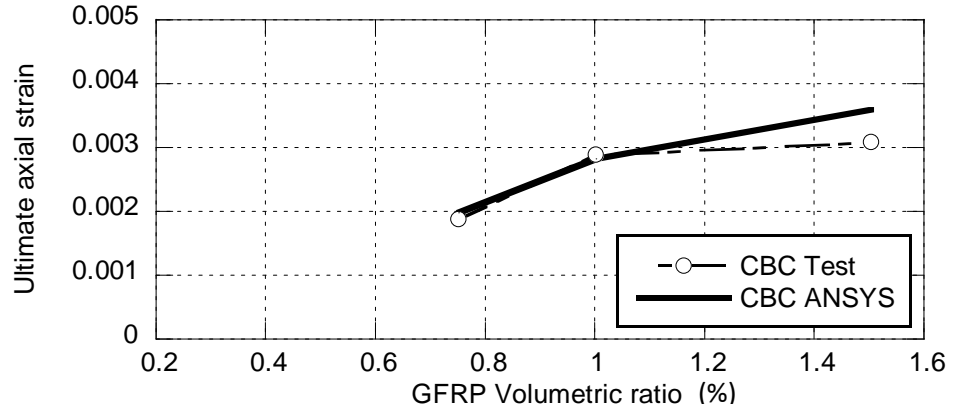


Figure 6.40: Comparisons for effect of volumetric ratio on ultimate axial strain between experiment and ANSYS results for brick aggregate GFRP confined circular concrete columns.

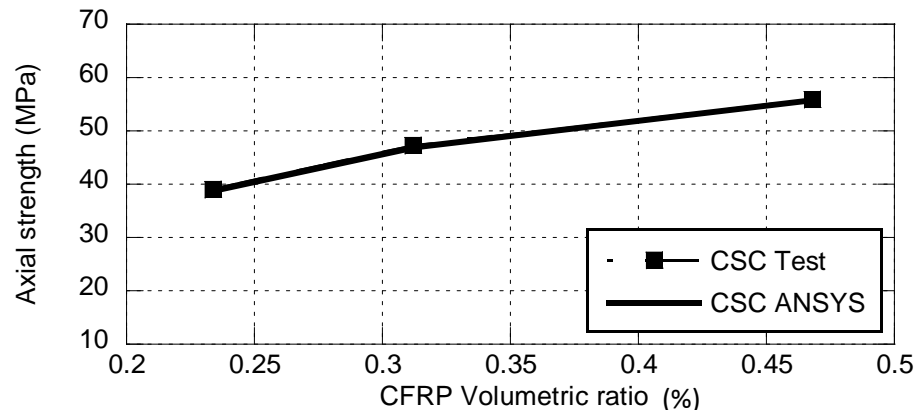


Figure 6.41: Comparisons for effect of volumetric ratio on axial strength between experiment and ANSYS results for stone aggregate CFRP confined circular concrete columns.

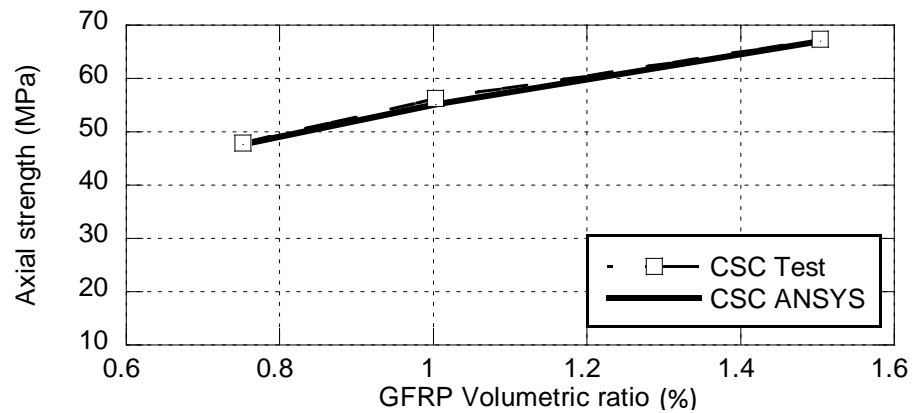


Figure 6.42: Comparisons for effect of volumetric ratio on axial strength between experiment and ANSYS results for stone aggregate GFRP confined circular concrete columns.

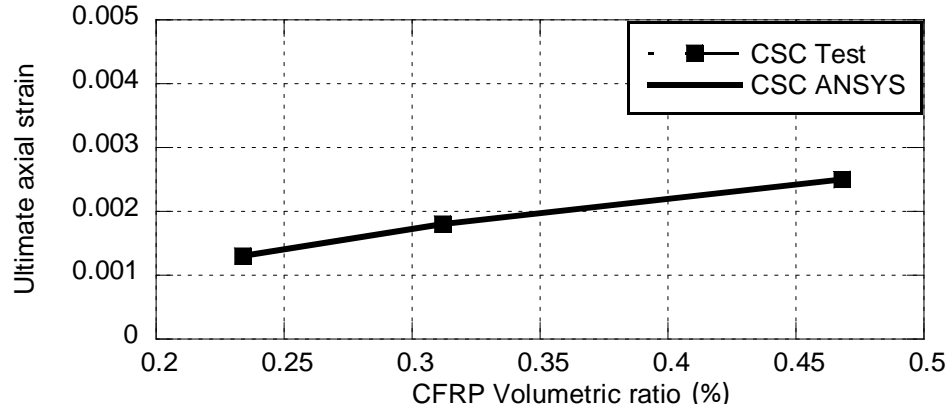


Figure 6.43: Comparisons for effect of volumetric ratio on ultimate axial strain between experiment and ANSYS results for stone aggregate CFRP confined circular concrete columns.

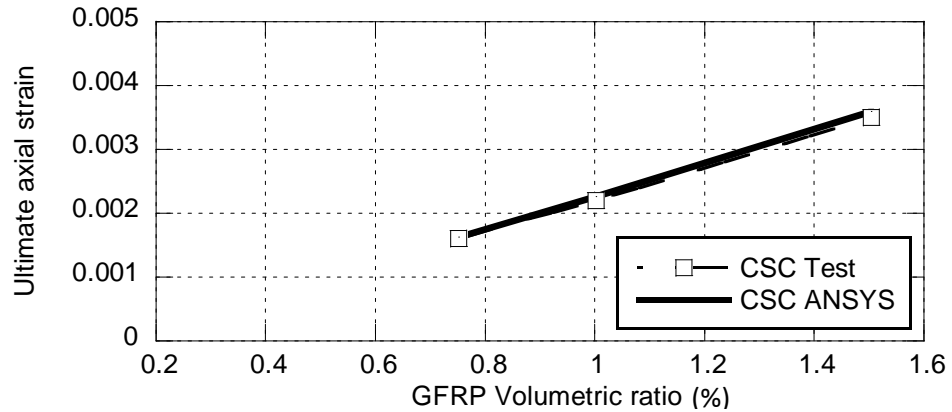


Figure 6.44: Comparisons for effect of volumetric ratio on ultimate axial strain between experiment and ANSYS results for stone aggregate GFRP confined circular concrete columns.

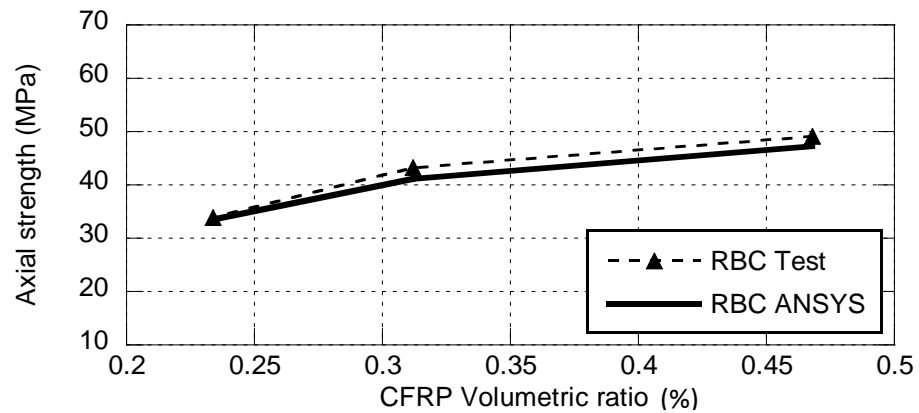


Figure 6.45: Comparisons for effect of volumetric ratio on axial strength between experiment and ANSYS results for recycled brick aggregate CFRP confined circular concrete columns.

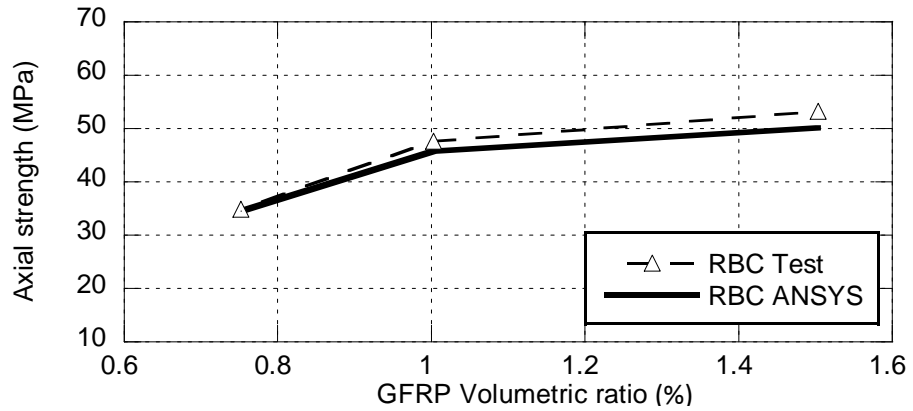


Figure 6.46: Comparisons for effect of volumetric ratio on axial strength between experiment and ANSYS results for recycled brick aggregate GFRP confined circular concrete columns.

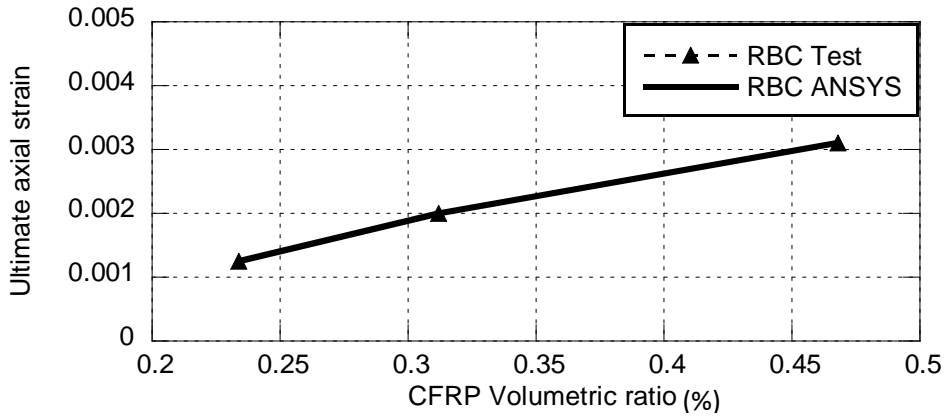


Figure 6.47: Comparisons for effect of volumetric ratio on ultimate axial strain between experiment and ANSYS results for recycled brick aggregate CFRP confined circular concrete columns.

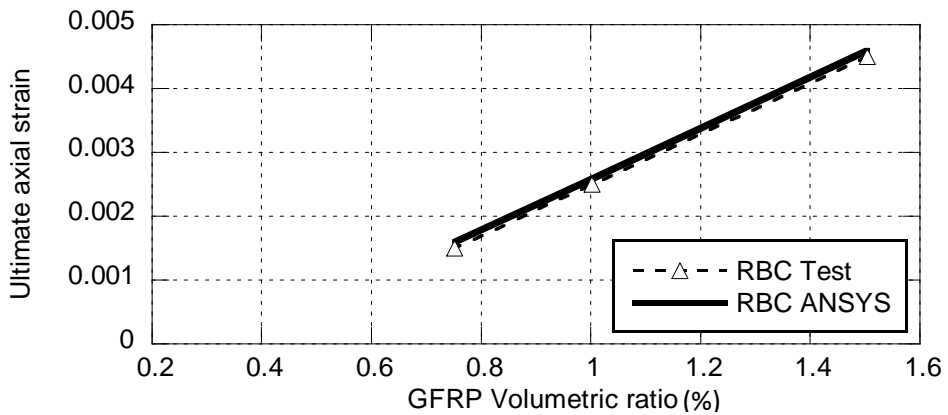


Figure 6.48: Comparisons for effect of volumetric ratio on ultimate axial strain between experiment and ANSYS results for recycled brick aggregate GFRP confined circular concrete columns.

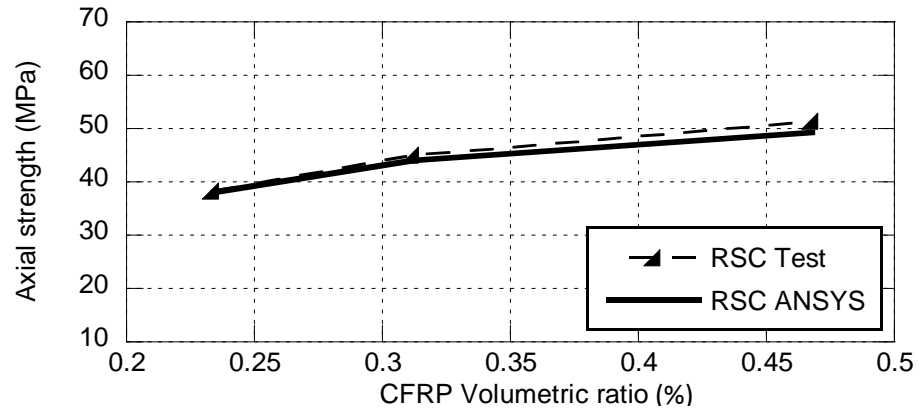


Figure 6.49: Comparisons for effect of volumetric ratio on axial strength between experiment and ANSYS results for recycled stone aggregate CFRP confined circular concrete columns.

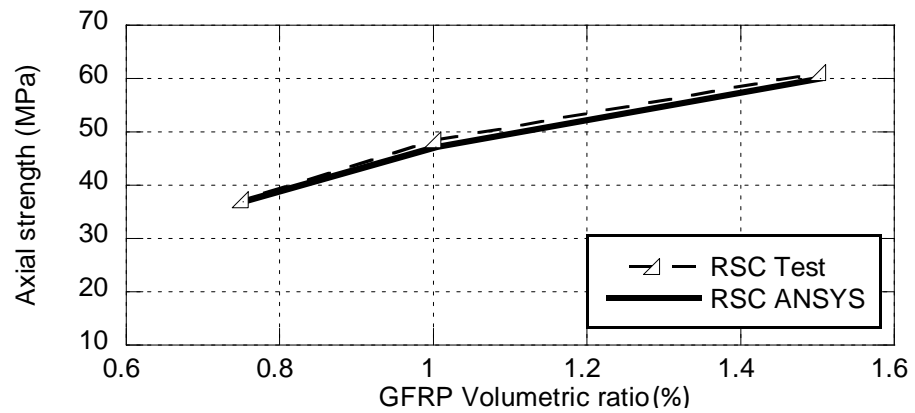


Figure 6.50: Comparisons for effect of volumetric ratio on axial strength between experiment and ANSYS results for recycled stone aggregate GFRP confined circular concrete columns.

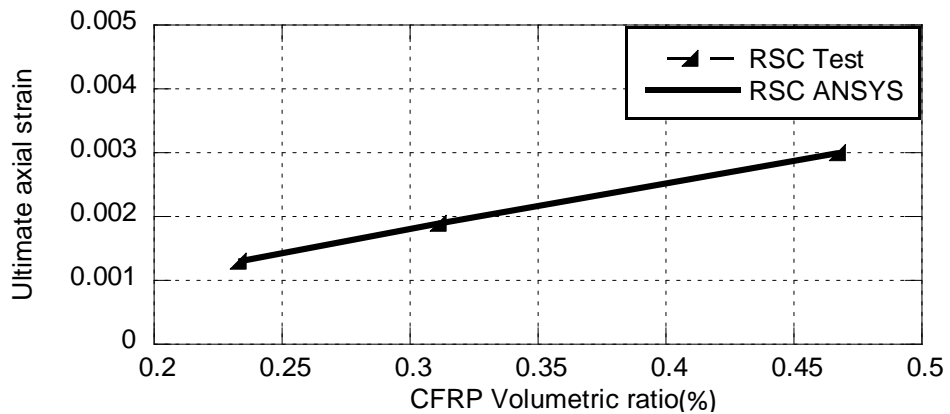


Figure 6.51: Comparisons for effect of volumetric ratio on ultimate axial strain between experiment and ANSYS results for recycled stone aggregate CFRP confined circular concrete columns.



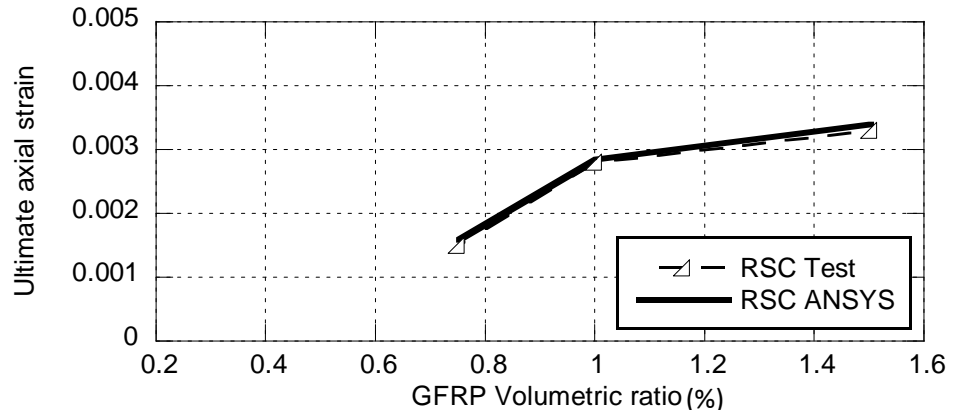


Figure 6.52: Comparisons for effect of volumetric ratio on ultimate axial strain between experiment and ANSYS results for recycled stone aggregate GFRP confined circular concrete columns.

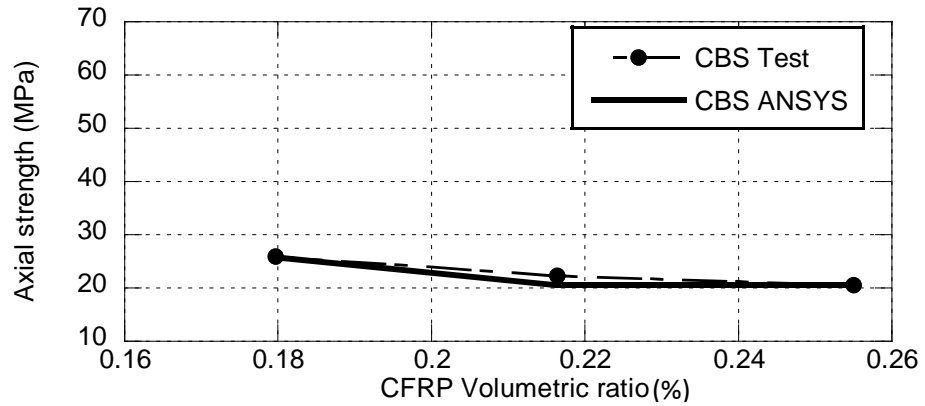


Figure 6.53: Comparisons for effect of volumetric ratio on axial strength between experiment and ANSYS results for brick aggregate CFRP confined square concrete columns.

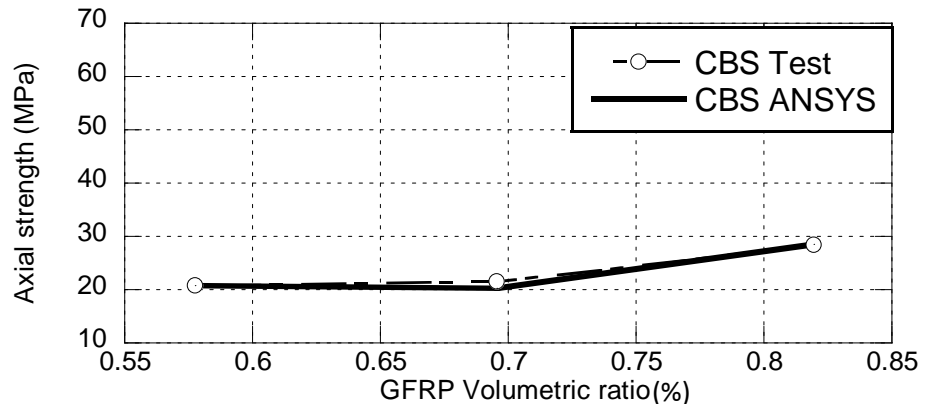


Figure 6.54: Comparisons for effect of volumetric ratio on axial strength between experiment and ANSYS results for brick aggregate GFRP confined square concrete columns.

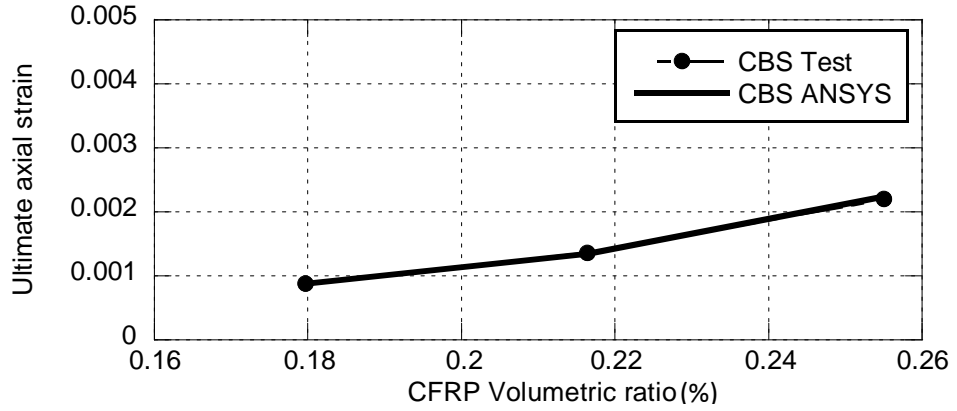


Figure 6.55: Comparisons for effect of volumetric ratio on ultimate axial strain between experiment and ANSYS results for brick aggregate CFRP confined square concrete columns.

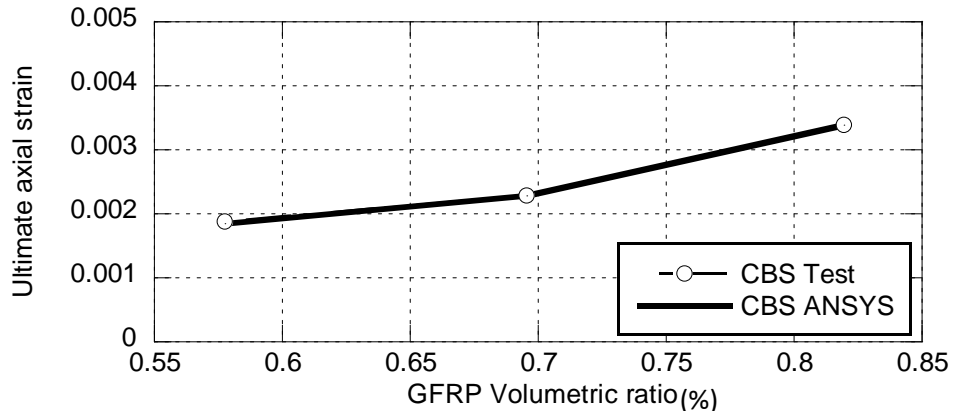


Figure 6.56: Comparisons for effect of volumetric ratio on ultimate axial strain between experiment and ANSYS results for brick aggregate GFRP confined square concrete columns.

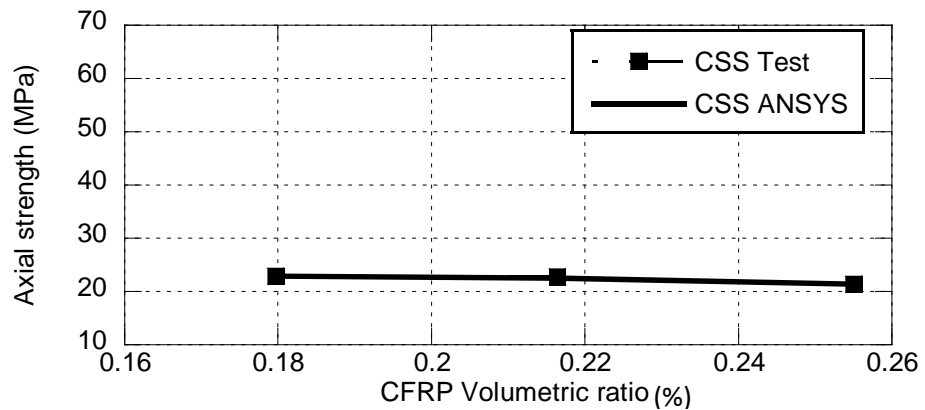


Figure 6.57: Comparisons for effect of volumetric ratio on axial strength between experiment and ANSYS results for stone aggregate CFRP confined square concrete columns.

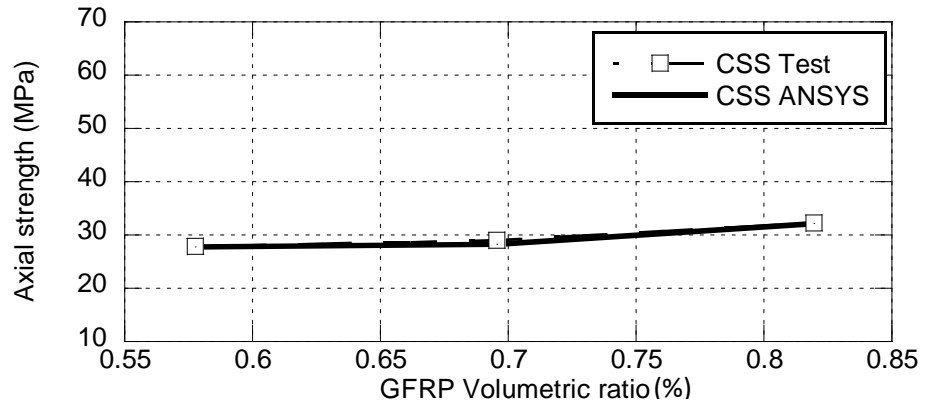


Figure 6.58: Comparisons for effect of volumetric ratio on axial strength between experiment and ANSYS results for stone aggregate GFRP confined square concrete columns.

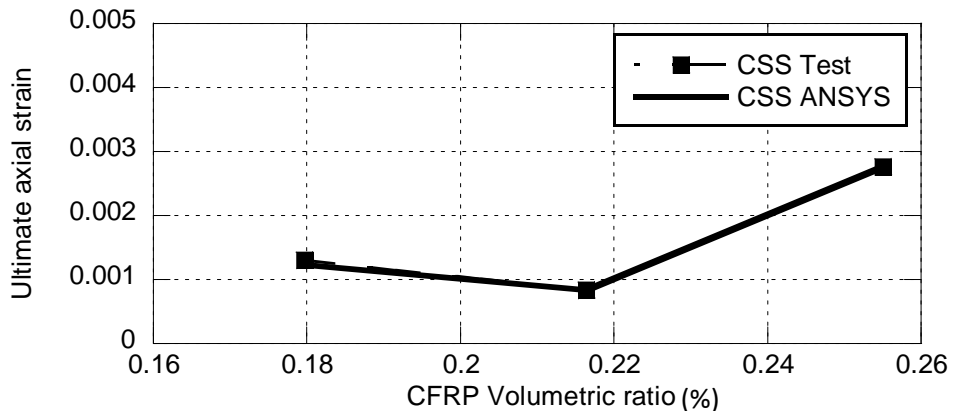


Figure 6.59: Comparisons for effect of volumetric ratio on ultimate axial strain between experiment and ANSYS results for stone aggregate CFRP confined square concrete columns.

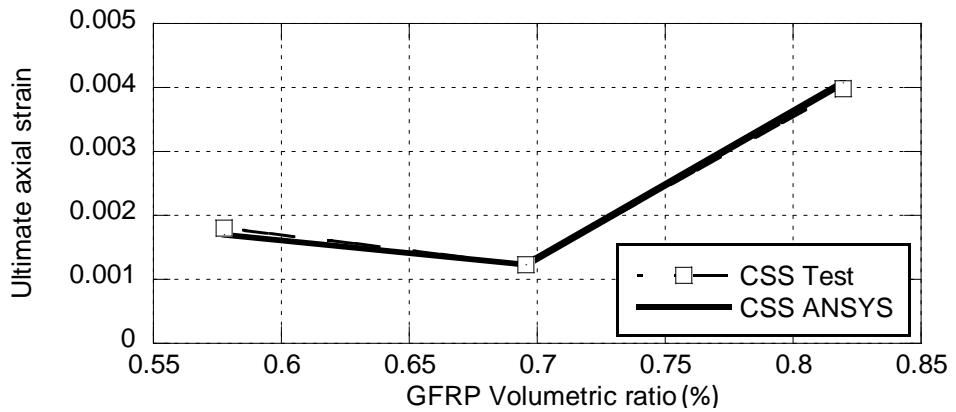


Figure 6.60: Comparisons for effect of volumetric ratio on ultimate axial strain between experiment and ANSYS results for stone aggregate GFRP confined square concrete columns.

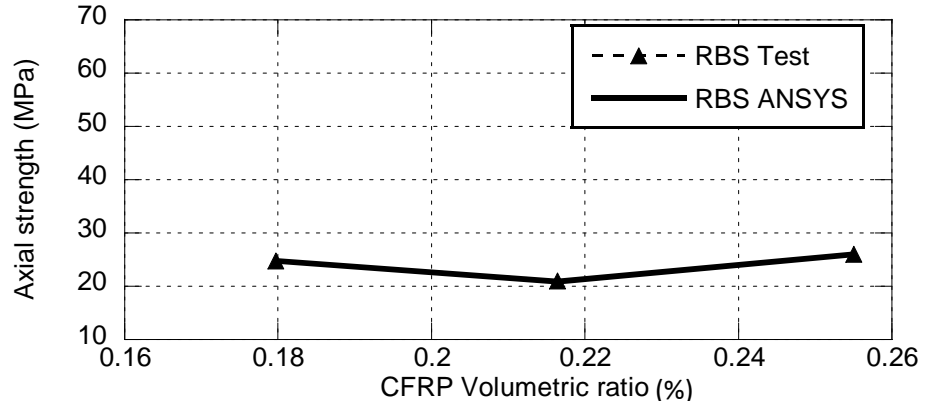


Figure 6.61: Comparisons for effect of volumetric ratio on axial strength between experiment and ANSYS results for recycled brick aggregate CFRP confined square concrete columns.

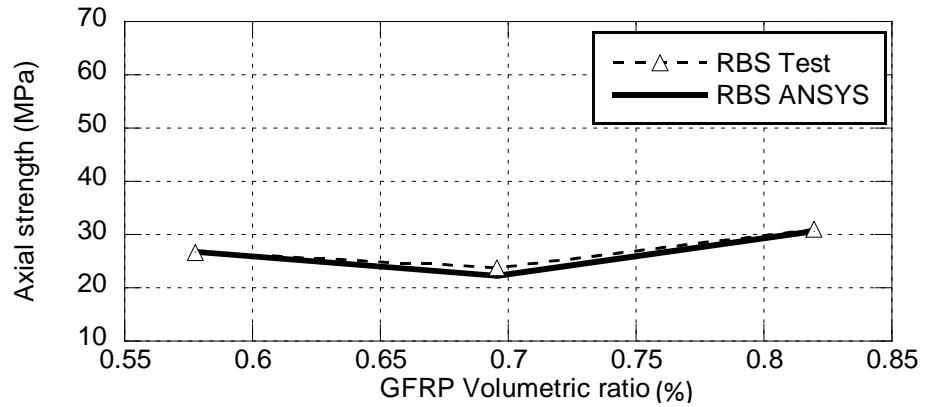


Figure 6.62: Comparisons for effect of volumetric ratio on axial strength between experiment and ANSYS results for recycled brick aggregate GFRP confined square concrete columns.

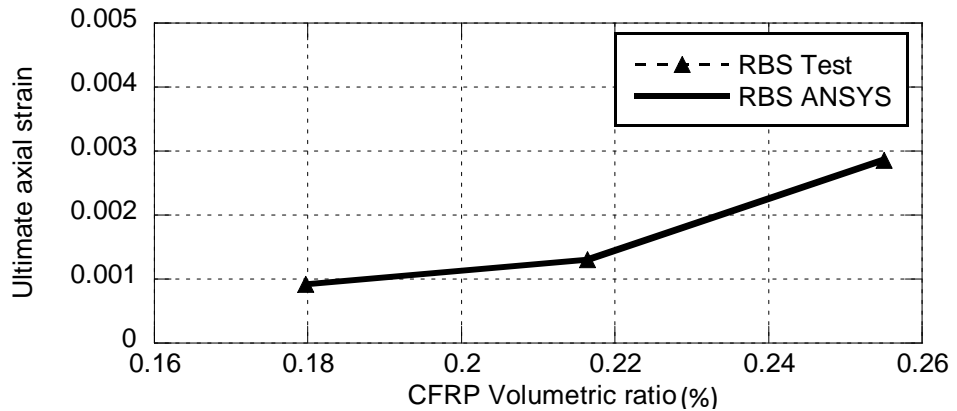


Figure 6.63: Comparisons for effect of volumetric ratio on ultimate axial strain between experiment and ANSYS results for recycled brick CFRP confined square concrete columns.

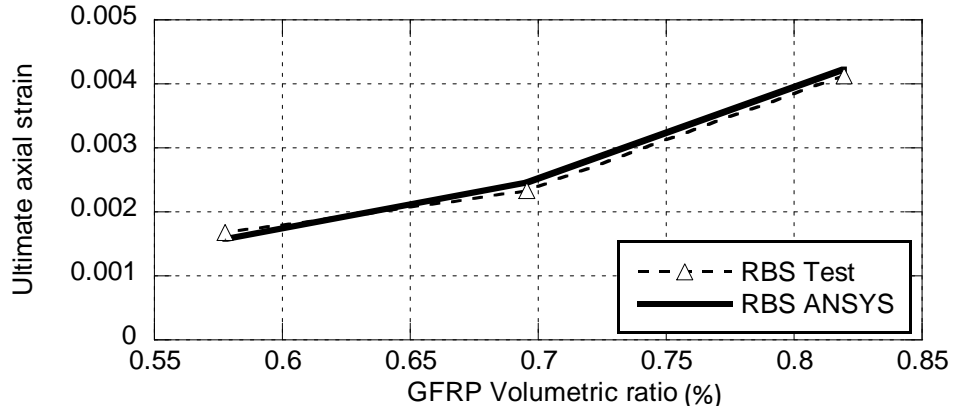


Figure 6.64: Comparisons for effect of volumetric ratio on ultimate axial strain between experiment and ANSYS results for recycled brick aggregate GFRP confined square concrete columns.

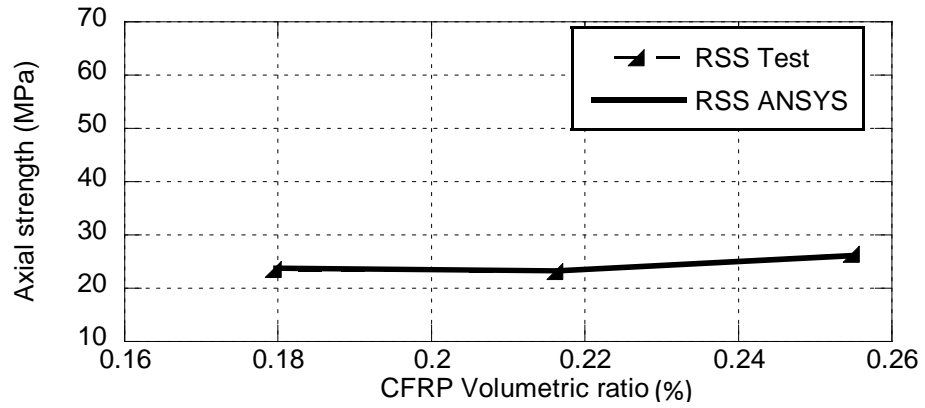


Figure 6.65: Comparisons for effect of volumetric ratio on axial strength between experiment and ANSYS results for recycled stone aggregate CFRP confined square concrete columns.

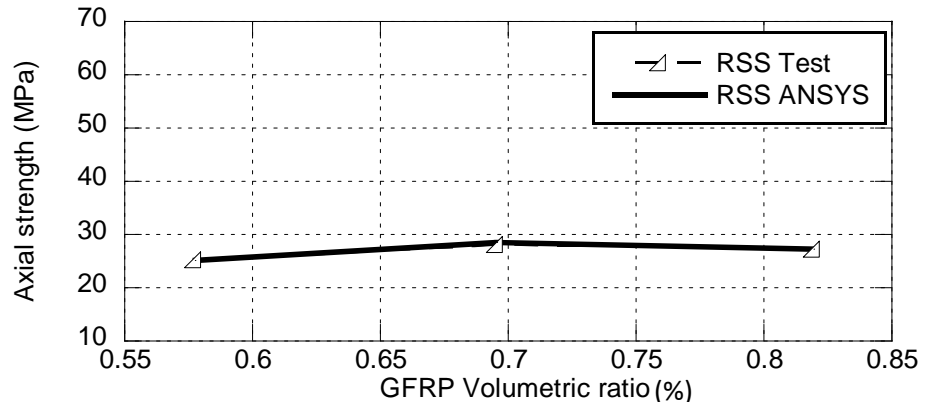


Figure 6.66: Comparisons for effect of volumetric ratio on axial strength between experiment and ANSYS results for recycled stone aggregate GFRP confined square concrete columns.

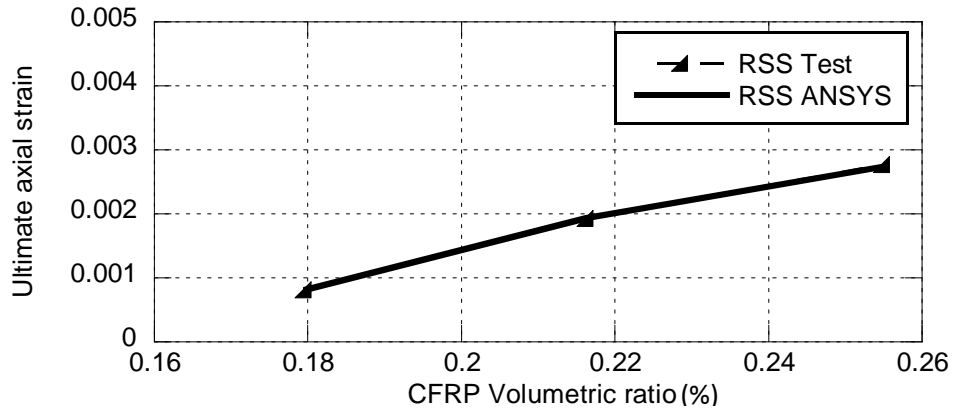


Figure 6.67: Comparisons for effect of volumetric ratio on ultimate axial strain between experiment and ANSYS results for recycled stone aggregate CFRP confined square concrete columns.

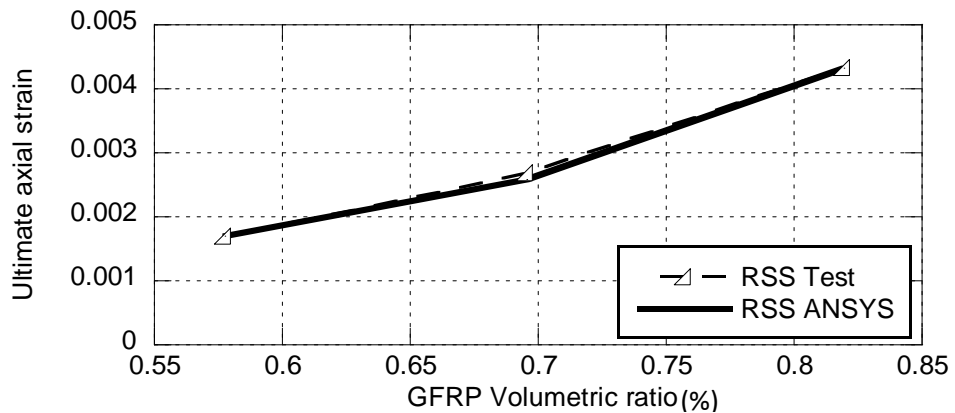
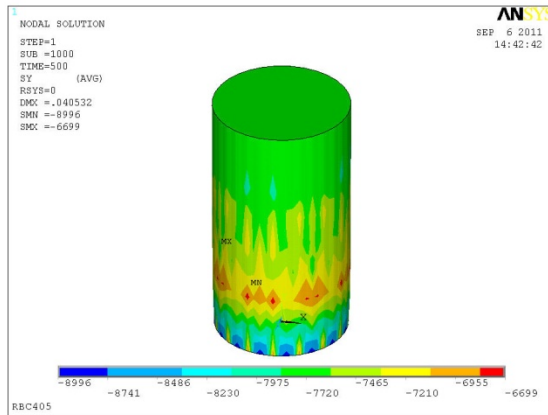


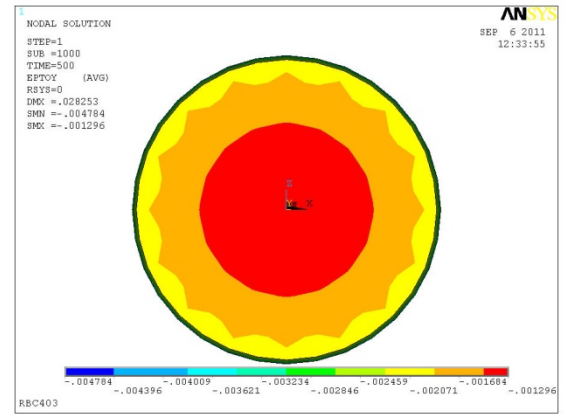
Figure 6.68: Comparisons for effect of volumetric ratio on ultimate axial strain between experiment and ANSYS results for recycled stone aggregate GFRP confined square concrete columns.

### 6.3.7 Stress contours: simulations and experiments

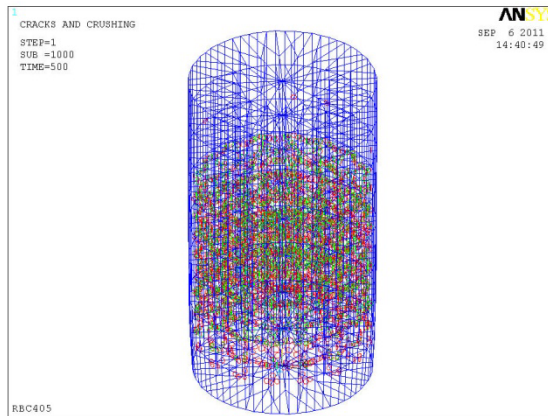
Figures 6.69 and 6.70 show the stress contours and failure pattern from the FE analysis of the short circular and square concrete confined column of three different sizes. As shown in Figures where small red circles are the location of crushing of concrete and green circles are the location of cracking of concrete of the column after FE analysis. The stress contour shows that the stress concentration occurs near mid height of the circular columns and at the corners of the square columns due to dilation of square column is maximum at the corners. The failure location of the FE model is convincingly similar to that of the experiment which validates the loading and boundary condition as well as modeling.



(a)



(b)

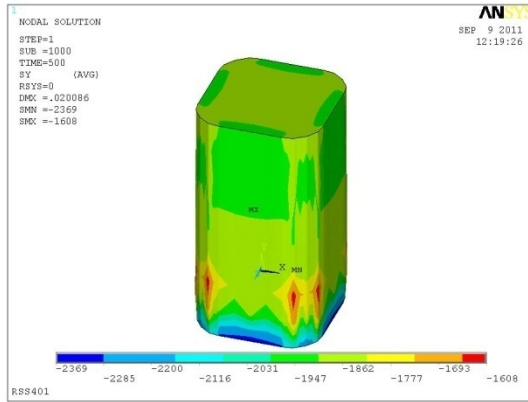


(c)

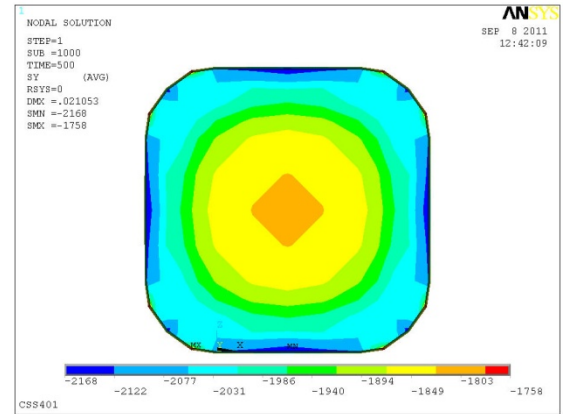


(d)

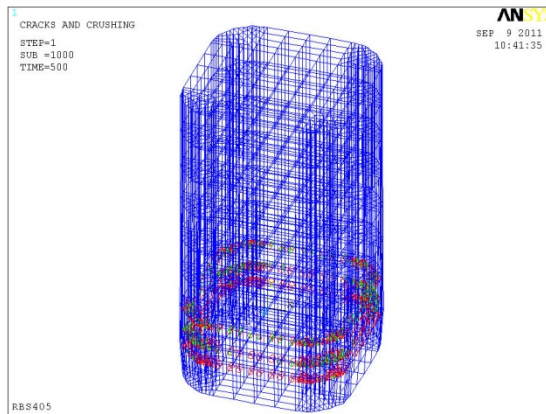
Figure 6.69: Stress contours and crushing pattern (a) stress contours along Y direction (b) bottom view of stress contour of column along Y direction (c) cracks at or near mid height of the column after FE analysis (small red circles are the location of crushing of concrete and green circles are the location of cracking of concrete (d) Crushing of concrete and FRP rupture at the mid height.



(a)



(b)



(c)



(d)

Figure 6.70: Stress contours and crushing pattern (a) stress contours along Y direction (b) bottom view of stress contour of column along Y direction (c) cracks at the bottom of the column after FE analysis (small red circles are the location of crushing of concrete green circles are the location of cracking of concrete (d) Crushing of concrete and FRP rapture at the bottom.



## 7.1 General

With the advancement in the field of fiber reinforced composite materials and their successful application as a strengthening and retrofitting material in structural engineering, engineers need design guidelines and reliable information regarding the behaviour of concrete structures reinforced with fiber reinforced polymers. A considerable amount of experimental and analytical research has been conducted to study the behaviour of FRP-confined concrete columns. However, it is observed that most of the experimental studies involved small-scale specimens. Accordingly, the existing analytical models are calibrated for small-scale specimen's data. Analytical models must be equally applicable to large-scale as well as small-scale specimens before they can be used to develop design guidelines for implementation in the field. In general, the stress-strain responses for FRP-confined concrete columns are bilinear with a sharp softening and a transition zone at approximately the level of corresponding unconfined concrete strength. The first linear zone solely depends on the concrete properties; the slope of stress-strain curve in this zone is same as the slope for unconfined concrete. As the stress level reaches near the unconfined concrete strength, the transition zone to the second portion of the bilinear curve starts. This region represents that the concrete got significantly cracked and the FRP tube started to show its confining characteristics. The slope of the second branch of the stress-strain relationship is mainly related to the stiffness of the confining tube. The second linear branch continues until the peak stress is achieved at the point when FRP ruptures, resulting in the failure of the column. The confined concrete strength is essentially dependent on the maximum confining pressure that the FRP can apply, whereas the slope of the second branch of the stress-strain curve mainly depends on the stiffness of the FRP jacket. For this reason, stress-strain models of different aggregates are developed considering the size of the columns, the Poisson's ratios and dilation characteristics so that these models can be used for predicting confined compressive strength of concrete columns in the design desk.

## 7.2 Models for confined compressive strength of concrete

It is well established that external confinement of a concrete column enhances its strength and ductility. In the past, confinement is usually provided by external jackets or tubes made of metal. Currently, the availability of composite materials with improved physical properties has opened the door of opportunity to rehabilitate concrete structures. In recent years, tests performed by several researchers (Mirmiran and Shahawy 1997a, Chaallal et al. 2006) have confirmed that use of FRP sheets to provide additional confinement to the concrete compression members could be an effective technique to strengthen further their load carrying capacity, or repair deteriorated columns for the designed load considered. As an attempt to the application of composite fabrics where strengthening or retrofitting of structural member is the prime concern, several researchers have proposed models for assessment of gain in strength and ultimate strain of confined concrete. In existing models of FRP confined concrete, it is common to assume that the FRP ruptures when the hoop stress in FRP wrap reaches its tensile strength obtained either from flat coupon test or ring splitting tests (Lam and Teng 2003a, ASTM D3039/D3039M-95, ASTM D2290-92).

In this research the models are prepared to predict the ultimate confined compressive strength of concrete columns  $f'_{cc}$  and ultimate strain  $\epsilon_{cc}$  which is based on the test database of 120 circular and square plain concrete columns of three different sizes. For developing these models, the considered stress-strain curve is the combination of the stress-strain paths of unconfined compressive strength of concrete and confined compressive strength. In this research both the paths are considered to be straight lines as shown in Figure 7.1. As shown in Figure 7.1 it is clear that the first point (point 0) of the curve starts from the origin of the axes of the stress-strain curve. The second point (point 1) of the stress-strain path is the compressive strength  $f'_{c0}$  and maximum axial strain  $\epsilon_{c0}$  of unconfined concrete. The third point (point 2) is the predicted confined compressive strength  $f'_{cc}$  and the ultimate axial strain  $\epsilon_{cc}$  of FRP confined concrete columns. The compressive strength of FRP confined concrete columns  $f'_{cc}$  is related to the confining pressure provided by the FRP wrap to a circular and non-circular section (Lam and Teng, 2003a, b).

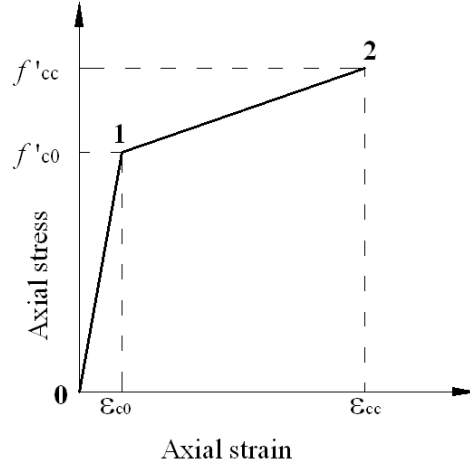


Figure 7.1: Stress-strain Model for confined compressive strength of circular and square concrete columns. Path 0-1 denoted unconfined concrete and Path 1-2 denoted FRP confined concrete.

To study and quantify the behavior of concrete members confined by FRP jacket, the amount of confining pressure (stress) provided by the jacket is needed. Such confining pressure is a function of the column's cross-section, the stiffness of the FRP jacket, and the transverse expansion of the loaded concrete. The lateral confining stress  $f_l$  is produced in the concrete when the confining jacket and the member is loaded such that the concrete starts to dilate and expands laterally. The value of such stress depends on the geometric shape of the member. Several of the existing strength models for FRP-confined concrete take the following form

$$\frac{f'_{cc}}{f'_{co}} = 1 + k_1 \frac{f_l}{f'_{co}} \quad (7.1)$$

where  $f'_{cc}$  and  $f'_{co}$  are the compressive strengths of the confined and the unconfined concrete, respectively,  $f_l$  is the lateral confining pressure, and  $k_1$  is the confinement effectiveness coefficient.

By confining a circular member, the FRP jacket provides a uniform confining stress around the parameter resulting in a great improvement in member's behavior under loading. For application to FRP-confined concrete,  $f_l$  can be related to the amount and strength of the FRP by:

$$f_l = \frac{2f_{frp}t}{D} = \frac{2E_{frp}\epsilon_j t}{D} \quad (7.2)$$

From the test database, the relation between the ratios of the confining pressure  $f_l$  of FRP and unconfined compressive strength  $f'_{co}$  of the circular and square confined concrete column which is termed as actual confining ratio  $f_l / f'_{co}$  with the ratios of confined

compressive strength  $f'_{cc}$  to the unconfined compressive strength  $f'_{c0}$  which is termed as confinement effectiveness or strengthening ratio is through from the regression analysis. In this regression analysis, y axis is denoted by the strengthening ratio and x axis is denoted by actual confining ratio.

Again for developing the equations of ultimate axial strain, the regression analysis of the test database is used. In this regression analysis, the strain enhancement ratio  $\varepsilon_{cc}/\varepsilon_{c0}$  is kept along the y axis and the actual confinement ratio  $f_l/f'_{c0}$  is kept along the x axis. The relation of ultimate axial strain of confined concrete to the actual confinement ratio given by Lam and Teng (2001) is presented in Eq. 7.3.

$$\frac{\varepsilon_{cc}}{\varepsilon_{c0}} = 1 + k_2 \frac{f_l}{f'_{c0}} \quad (7.3)$$

where  $k_2$  is the strain enhancement coefficient which is depends on the type of FRP (Lam and Teng 2001).

The equations for all type of concretes are established with the test results of short circular and square concrete columns of three different sizes. The results of 150 mm x 150 mm x 300 mm sized square columns are taken from Islam (2011) but the data points are used here for making justification of proposed relation. The equations deduced from the regression analysis for the strengths and the deformations are given in the following sections where more precious strain measurement technique is required for better analysis (Figures 7.2-7.17). Better modeling required numerous experimental results.

### 7.2.1 Equation for confined circular concrete columns

#### a) Brick aggregate concrete

For the few test results of this work, the confined compressive strength of concrete column is presented in Eq. 7.4 and Figure 7.2.

$$\frac{f'_{cc}}{f'_{c0}} = 1 + 40.09 \frac{f_l}{f'_{c0}} \quad (7.4)$$

and the ultimate compressive strain of concrete column is presented in Eq. 7.5 and Figure 7.3.

$$\frac{\varepsilon_{cc}}{\varepsilon_{c0}} = 1 + 87.66 \frac{f_l}{f'_{c0}} \quad (7.5)$$

**b) Stone aggregate concrete**

The confined compressive strength of concrete column is presented in Eq. 7.6 and Figure 7.4.

$$\frac{f'_{cc}}{f'_{c0}} = 1 + 64.87 \frac{f_l}{f'_{c0}} \quad (7.6)$$

and the ultimate compressive strain of concrete column is presented in Eq. 7.7 and Figure 7.5.

$$\frac{\varepsilon_{cc}}{\varepsilon_{c0}} = 1 + 113.71 \frac{f_l}{f'_{c0}} \quad (7.7)$$

**c) Recycled brick aggregate concrete**

Eq. 7.8 and Figure 7.6 represents the confined compressive strength of concrete column.

$$\frac{f'_{cc}}{f'_{c0}} = 1 + 32.2 \frac{f_l}{f'_{c0}} \quad (7.8)$$

and Eq. 7.9 and Figure 7.7 represents the ultimate compressive strain of concrete column.

$$\frac{\varepsilon_{cc}}{\varepsilon_{c0}} = 1 + 66.39 \frac{f_l}{f'_{c0}} \quad (7.9)$$

**d) Recycled stone aggregate concrete**

Eq. 7.10 and Figure 7.8 represents the confined compressive strength of concrete column.

$$\frac{f'_{cc}}{f'_{c0}} = 1 + 45.7 \frac{f_l}{f'_{c0}} \quad (7.10)$$

and Eq. 7.11 and Figure 7.9 represents the ultimate compressive strain of concrete column.

$$\frac{\varepsilon_{cc}}{\varepsilon_{c0}} = 1 + 57.25 \frac{f_l}{f'_{c0}} \quad (7.11)$$

Table 7.1 Confinement effectiveness coefficient  $k_1$  for circular columns made of different concretes

Type of concrete	Confinement effectiveness coefficients $k_1$
Brick aggregate concrete	40.09
Stone aggregate concrete	64.87
Recycled brick aggregate concrete	32.2
Recycled stone aggregate concrete	45.7

Table 7.2 Strain enhancement coefficient  $k_2$  for circular columns made of different concretes

Type of concrete	Strain enhancement coefficient $k_2$
Brick aggregate concrete	87.66
Stone aggregate concrete	113.71
Recycled brick aggregate concrete	66.39
Recycled stone aggregate concrete	57.25

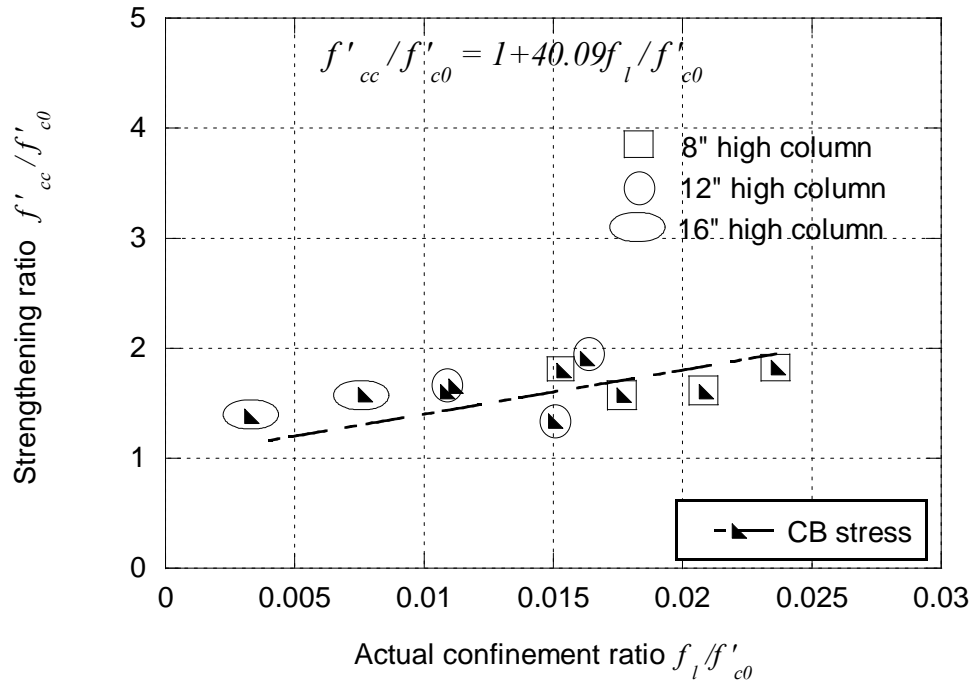


Figure 7.2: Strengthening ratio vs. actual confinement ratio curve for brick aggregate circular concrete columns confined with CFRP and GFRP

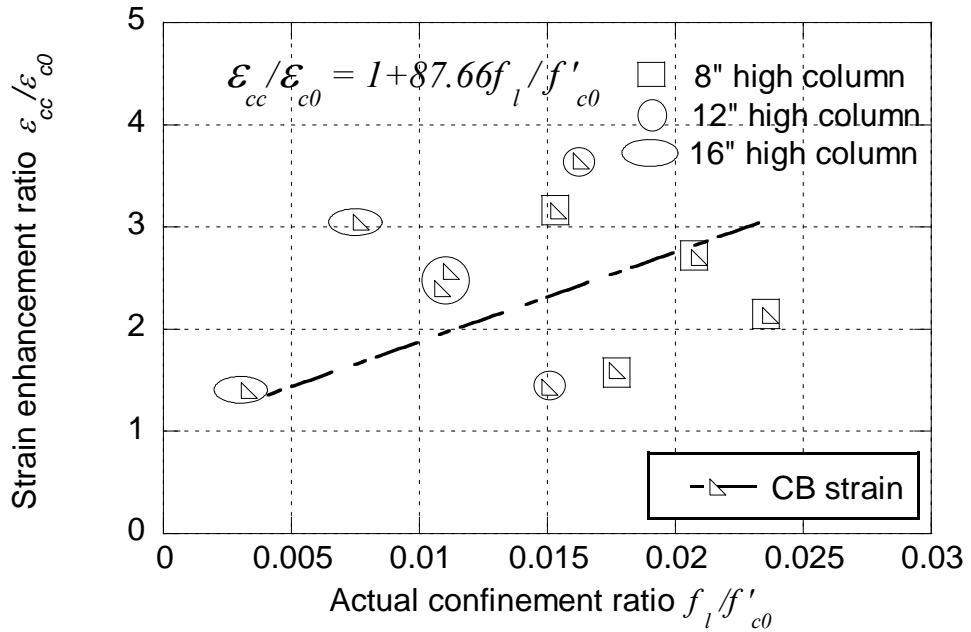


Figure 7.3: Strain enhancement ratio vs. actual confinement ratio curve for brick aggregate circular concrete columns confined with CFRP and GFRP

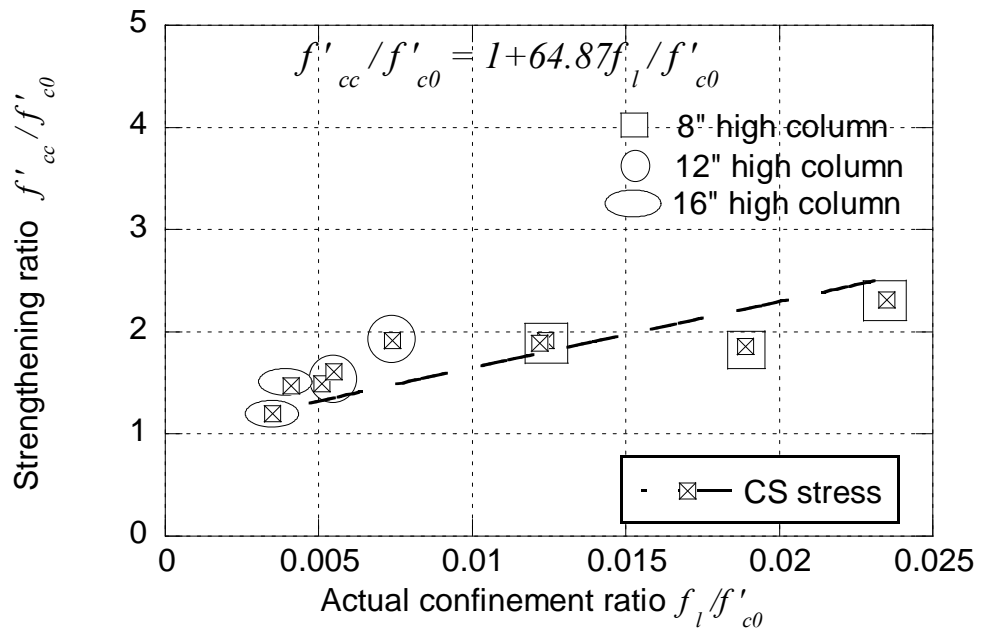


Figure 7.4: Strengthening ratio vs. actual confinement ratio curve for stone aggregate circular concrete columns confined with CFRP and GFRP

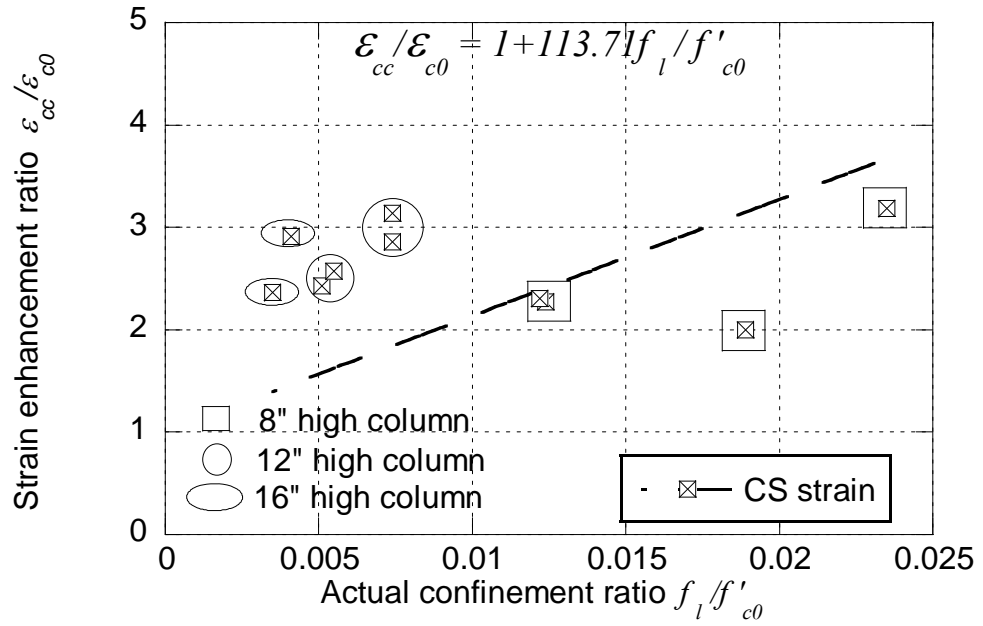


Figure 7.5: Strain enhancement ratio vs. actual confinement ratio curve for stone aggregate circular concrete columns confined with CFRP and GFRP

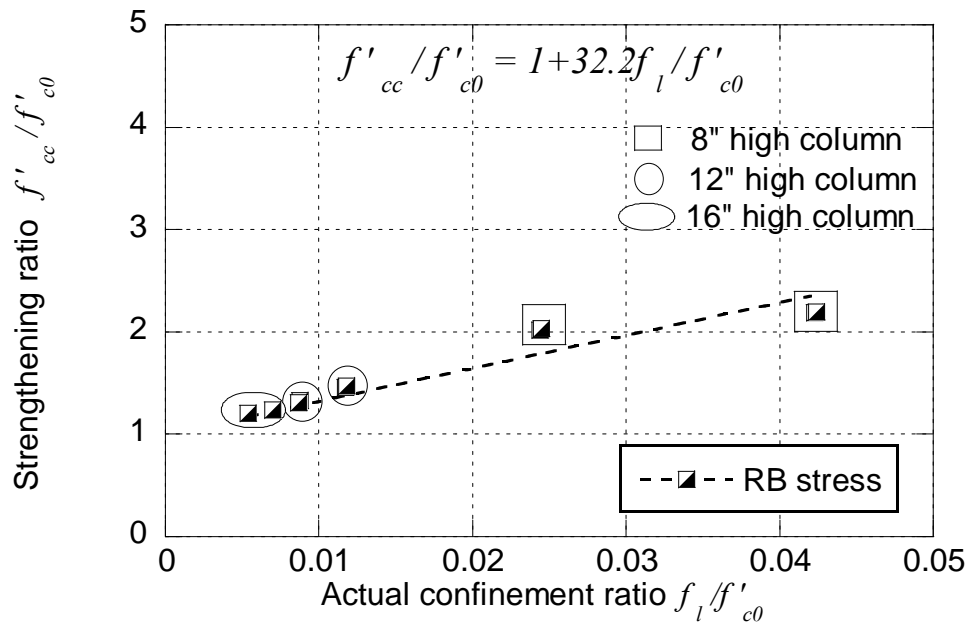


Figure 7.6: Strengthening ratio vs. actual confinement ratio curve for recycled brick aggregate circular concrete columns confined with CFRP and GFRP



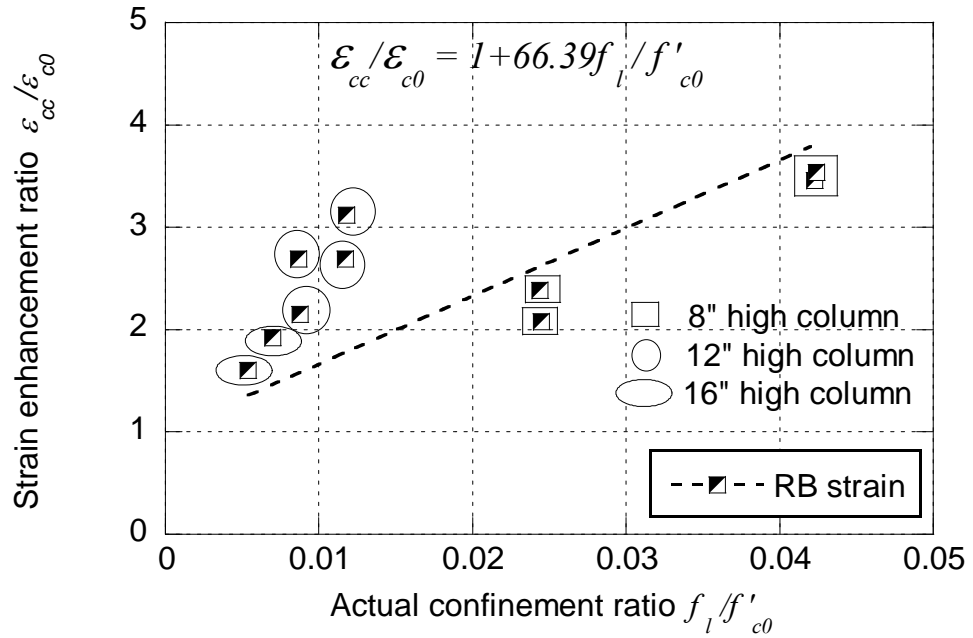


Figure 7.7: Strain enhancement ratio vs. actual confinement ratio curve for recycled brick aggregate circular concrete columns confined with CFRP and GFRP

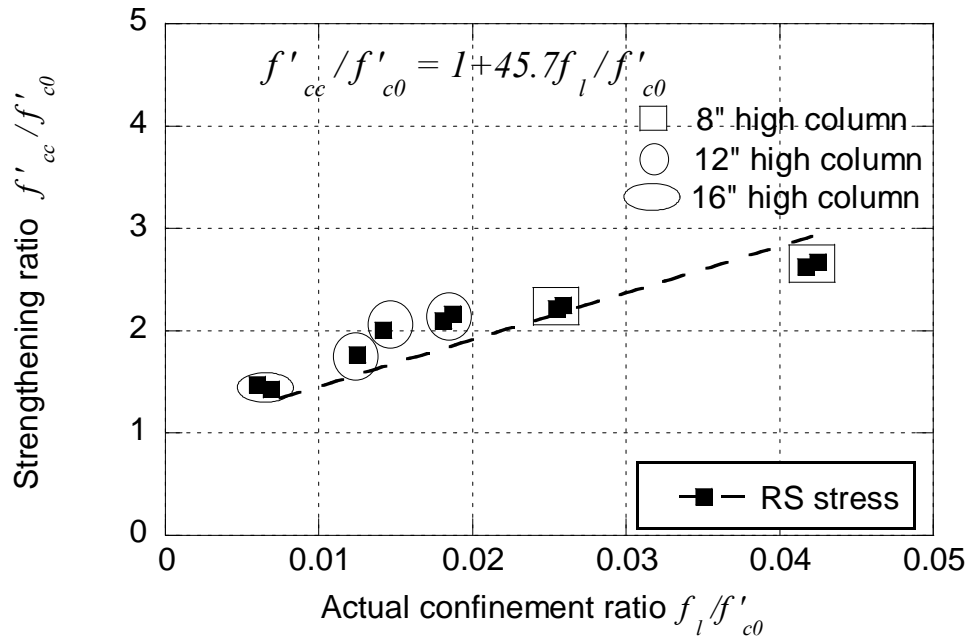


Figure 7.8: Strengthening ratio vs. actual confinement ratio curve for recycled stone aggregate circular concrete columns confined with CFRP and GFRP

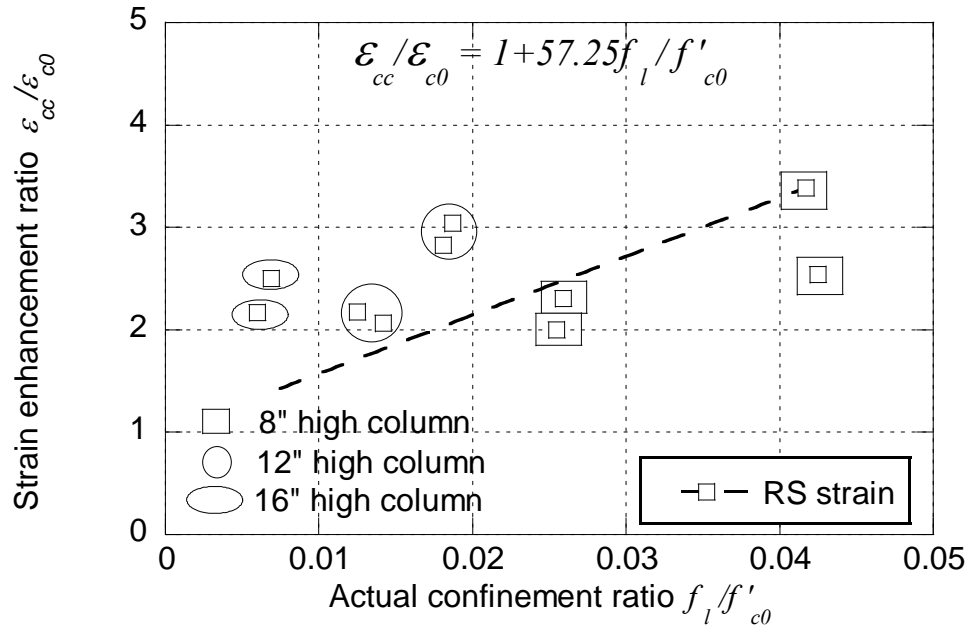


Figure 7.9: Strain enhancement ratio vs. actual confinement ratio curve for recycled stone aggregate circular concrete columns confined with CFRP and GFRP

## 7.2.2 Equation for confined square concrete columns

### a) Brick aggregate concrete

Eq. 7.12 and Figure 7.10 represents the confined compressive strength of concrete column.

$$\frac{f'_{cc}}{f'_{c0}} = 1 + 16.82 \frac{f_l}{f'_{c0}} \quad (7.12)$$

and the ultimate compressive strain of concrete column is presented in Eq. 7.13 and Figure 7.11.

$$\frac{\epsilon_{cc}}{\epsilon_{c0}} = 1 + 10.92 \frac{f_l}{f'_{c0}} \quad (7.13)$$

### b) Stone aggregate concrete

For the few test results of this work, the confined compressive strength of concrete column is presented in Eq. 7.14 and Figure 7.12.

$$\frac{f'_{cc}}{f'_{c0}} = 1 + 26.68 \frac{f_l}{f'_{c0}} \quad (7.14)$$

and Eq. 7.15 and Figure 7.13 represents the ultimate compressive strain of concrete column.

$$\frac{\varepsilon_{cc}}{\varepsilon_{c0}} = 1 + 26.61 \frac{f_l}{f'_{c0}} \quad (7.15)$$

### c) Recycled brick aggregate concrete

The confined compressive strength of concrete column is presented in Eq. 7.16 and Figure 7.14.

$$\frac{f'_{cc}}{f'_{c0}} = 1 + 15.33 \frac{f_l}{f'_{c0}} \quad (7.16)$$

and Eq. 7.17 and Figure 7.15 represents the ultimate compressive strain of concrete column.

$$\frac{\varepsilon_{cc}}{\varepsilon_{c0}} = 1 + 11.15 \frac{f_l}{f'_{c0}} \quad (7.17)$$

### d) Recycled stone aggregate concrete

Eq. 7.18 and Figure 7.16 represents the confined compressive strength of concrete column.

$$\frac{f'_{cc}}{f'_{c0}} = 1 + 8.35 \frac{f_l}{f'_{c0}} \quad (7.18)$$

and the ultimate compressive strain of concrete column is presented in Eq. 7.19 and Figure 7.17.

$$\frac{\varepsilon_{cc}}{\varepsilon_{c0}} = 1 + 15.69 \frac{f_l}{f'_{c0}} \quad (7.19)$$

Table 7.3 Confinement effectiveness coefficient  $k_1$  for square columns made of different concretes

Type of concrete	Confinement effectiveness coefficients $k_1$
Brick aggregate concrete	16.82
Stone aggregate concrete	26.68
Recycled brick aggregate concrete	15.33
Recycled stone aggregate concrete	8.35

Table 7.4 Strain enhancement coefficient  $k_2$  for square columns made of different concretes

Type of concrete	Strain enhancement coefficient $k_2$
Brick aggregate concrete	10.92
Stone aggregate concrete	26.61
Recycled brick aggregate concrete	11.15
Recycled stone aggregate concrete	15.69

The values of confinement effectiveness coefficients  $k_1$  and strain enhancement coefficients  $k_2$  according to Eq. 7.1 and Eq. 7.3 respectively for circular and square concrete columns made of different aggregates are given in Tables 7.1 to 7.4. It is clear from the Tables 7.1 and 7.3 that FRP confinement varies distinctly with the type of concrete. The confinement effectiveness is similar in brick and recycled aggregate concretes. Stone aggregate concrete is not very effective in FRP confinement. From Table 3.2 it is clear that absorption and porosity of stone aggregate is lower and the unit weight and bulk specific gravity is higher than other aggregates. This is why stone aggregate concrete is found to be more effective than other concretes. Again from Tables 7.2 and 7.4 it is clear that the values of  $k_2$  are very close for brick and recycled aggregate concretes. But for the stone aggregate concrete it is found to be higher.

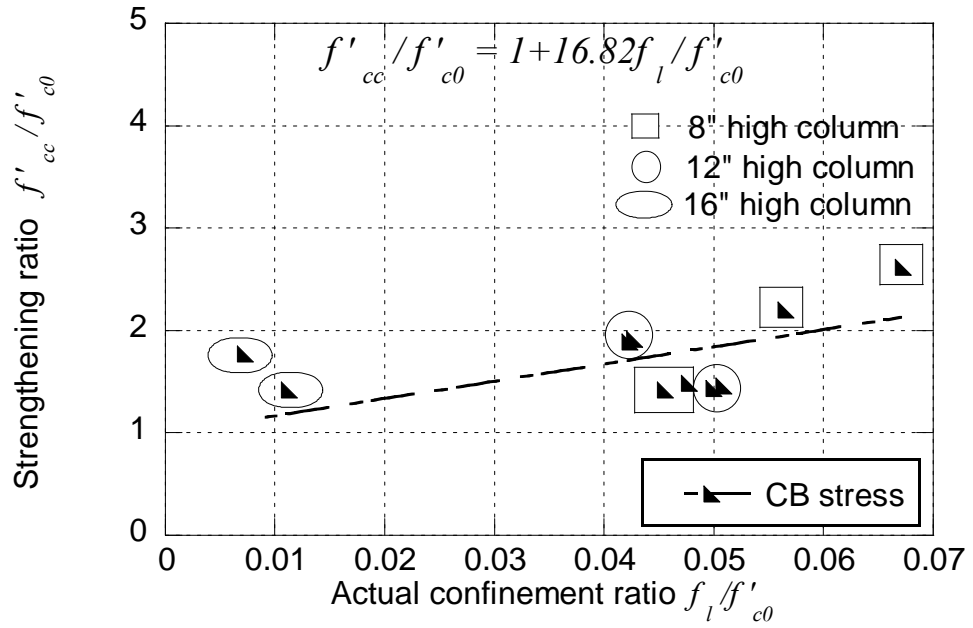


Figure 7.10: Strengthening ratio vs. actual confinement ratio curve for brick aggregate square concrete columns confined with CFRP and GFRP

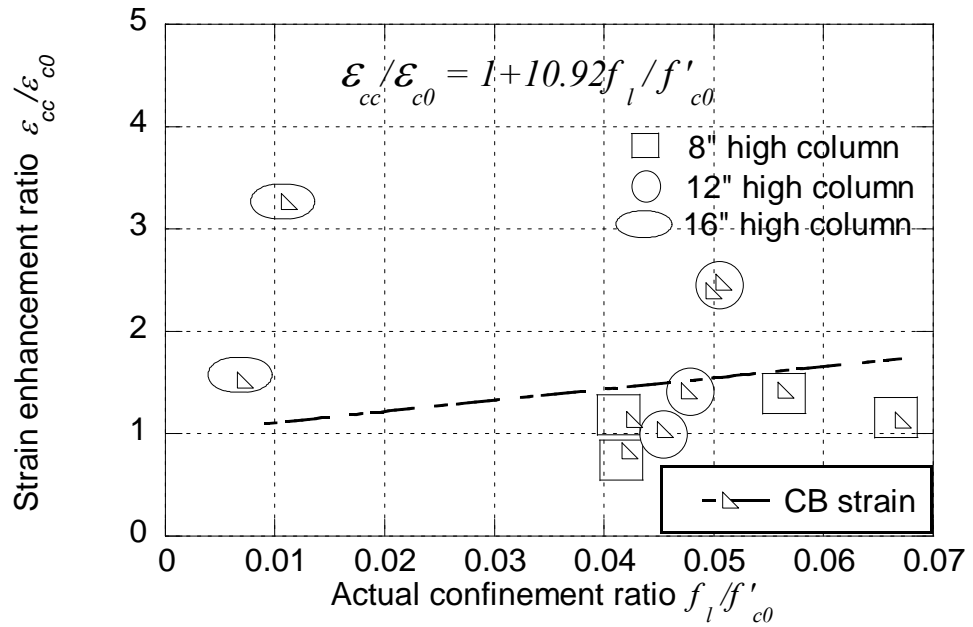


Figure 7.11: Strain enhancement ratio vs. actual confinement ratio curve for brick aggregate square concrete columns confined with CFRP and GFRP

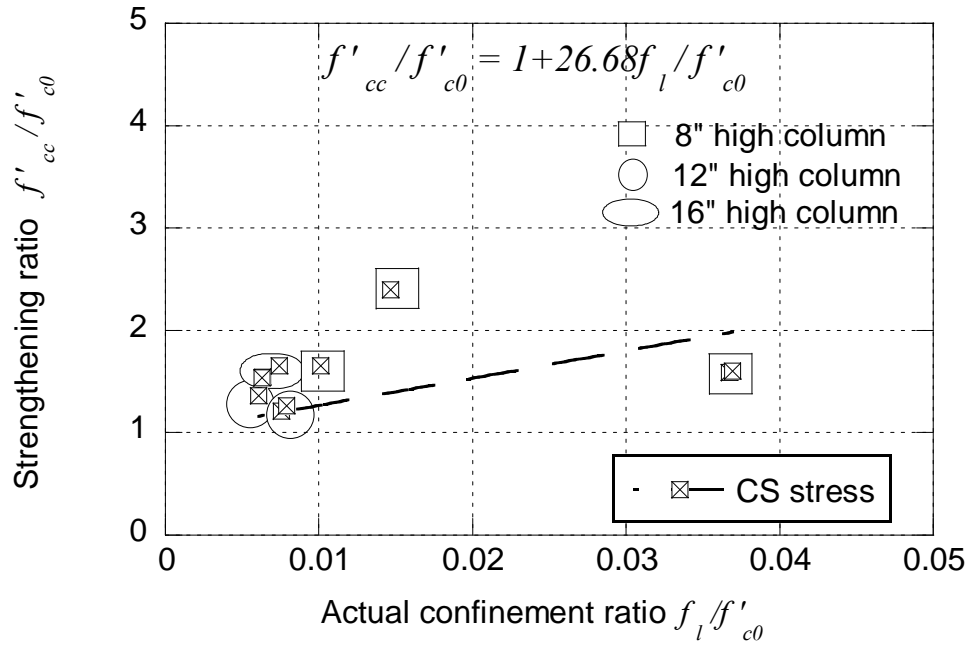


Figure 7.12: Strengthening ratio vs. actual confinement ratio curve for stone aggregate square concrete columns confined with CFRP and GFRP

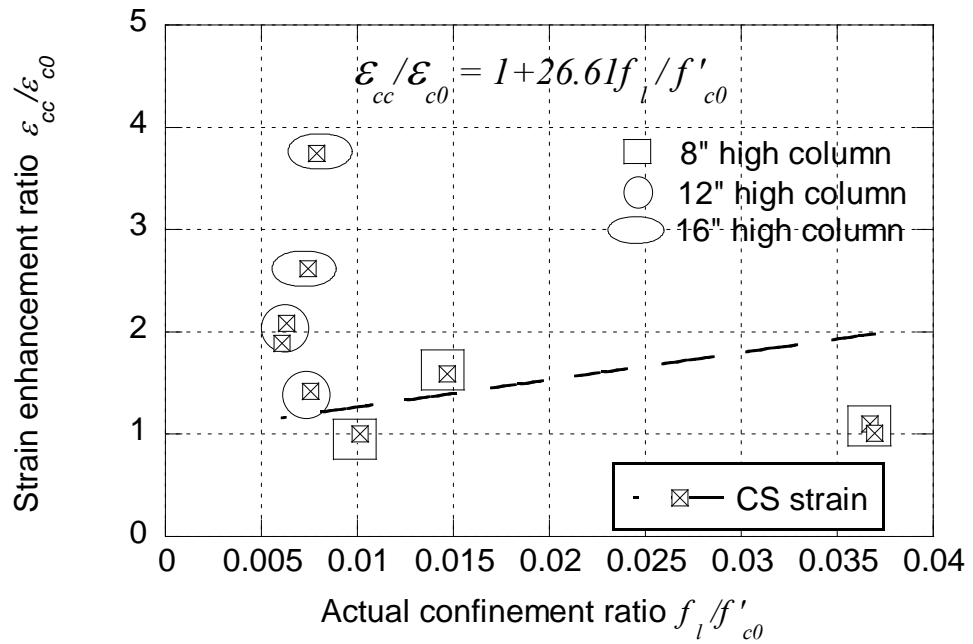


Figure 7.13: Strain enhancement ratio vs. actual confinement ratio curve for stone aggregate square concrete columns confined with CFRP and GFRP

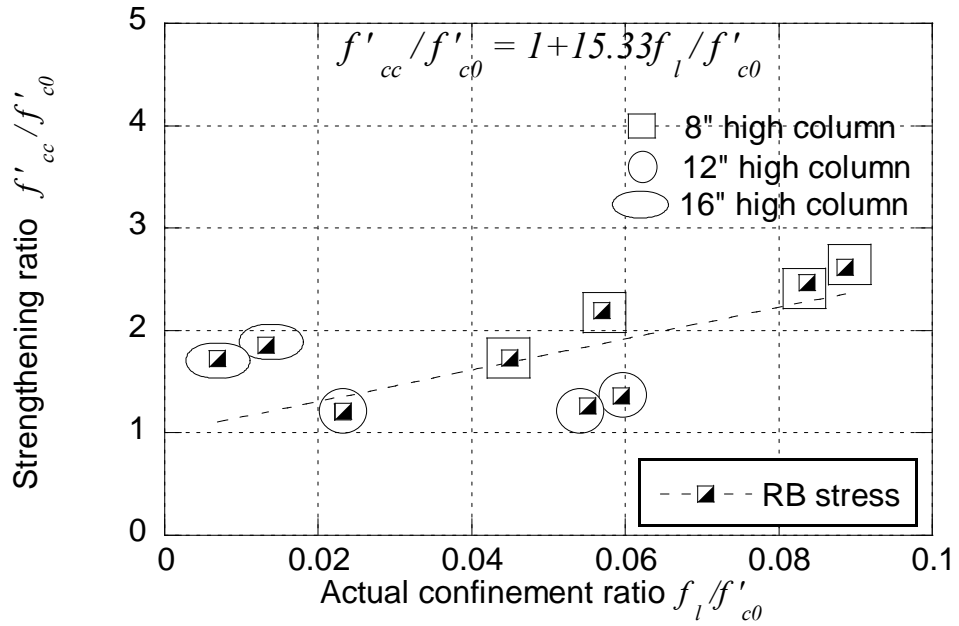


Figure 7.14: Strengthening ratio vs. actual confinement ratio curve for recycled brick aggregate square concrete columns confined with CFRP and GFRP

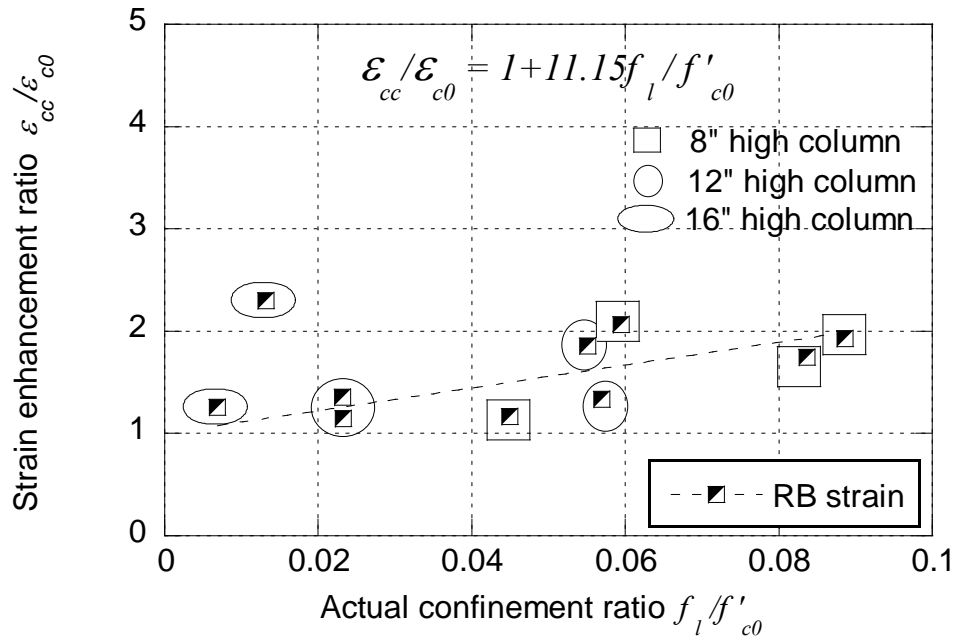


Figure 7.15: Strain enhancement ratio vs. actual confinement ratio curve for recycled brick aggregate square concrete columns confined with CFRP and GFRP

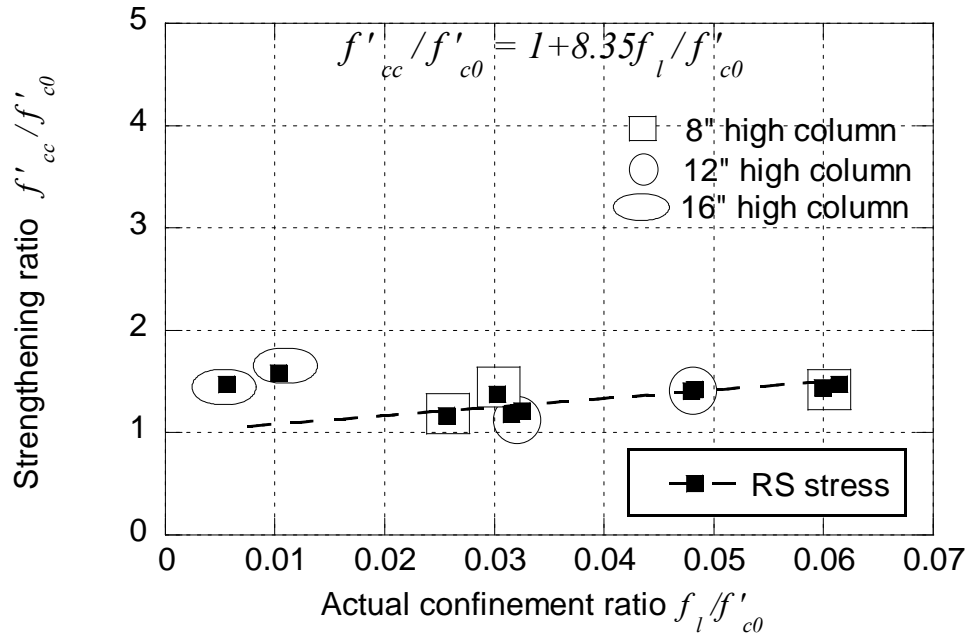


Figure 7.16: Strengthening ratio vs. actual confinement ratio curve for recycled stone aggregate square concrete columns confined with CFRP and GFRP

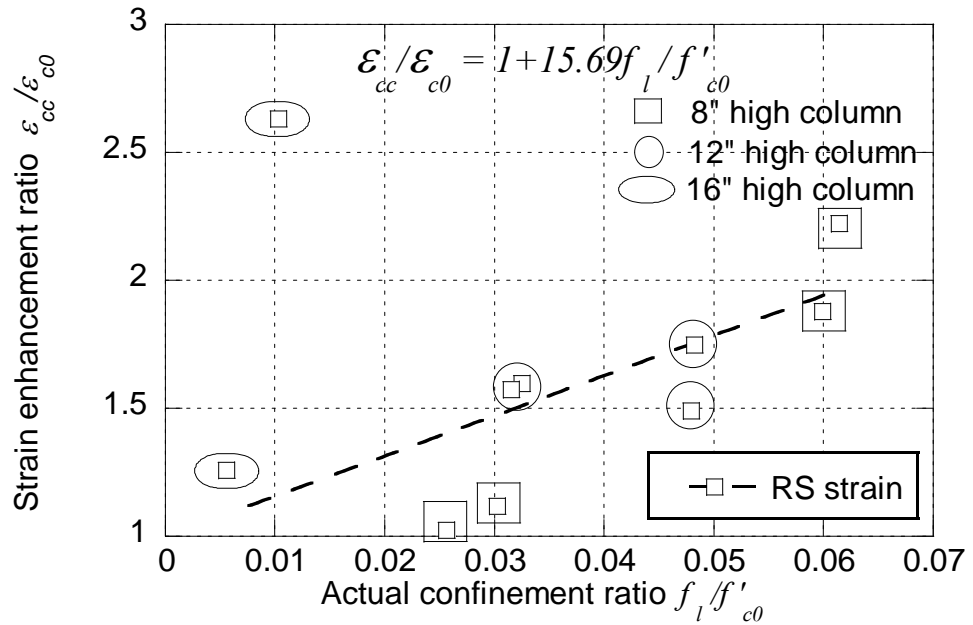


Figure 7.17: Strain enhancement ratio vs. actual confinement ratio curve for recycled stone aggregate square concrete columns confined with CFRP and GFRP



### 7.3 Validation of the models

The proposed stress-strain models of circular and square columns are applied to the 120 columns made of brick, stone, recycled brick and recycled stone aggregate of three different sizes for validation of the models. The typical comparisons of analytical and experimental stress-strain responses of 200 mm high circular and square concrete columns made of brick, stone, recycled brick and recycled stone aggregate are shown in Figures 7.18-7.21 and other 300 mm and 400 mm high circular and square concrete columns are shown in Figures 7.22-7.37 of Appendix C. The proposed model is able to predict the complete stress-strain response of selected specimens with reasonable accuracy. The predicted stress-strain curves have a good agreement with experimental curves in terms of slopes of first and second ascending branches confined concrete strength but the result of corresponding ultimate compressive strain varied due to the limitation of strain measurement technique in some cases. This validates the model for predicting the confined compressive strength  $f'_{cc}$  and confined ultimate compressive strain  $\epsilon_{cc}$  of FRP wrapped circular and square confined concrete columns. These models for stress-strain response of the circular and square confined concrete short columns made of different aggregates are proposed considering the size and curvature of the columns, the Poisson's ratios and dilation characteristics so that these models can be used for predicting confined compressive strength of concrete columns. However further investigation is required to use these model in the design desk. Summary of the test results and output of the models of circular and square concrete columns are shown in Tables 7.5 and 7.6 of Appendix D.1 and D.2.

Comparisons of the existing models of the literature with the experimental results of 200 mm, 300 mm and 400 mm high square and circular concrete columns made of brick, stone, recycled brick and recycled stone aggregate are shown in Figures 7.38-7.49. ACI 440 model (2002), Lam and Teng's model (2003b), Kumutha et al. model (2007) and Wu and Wang model (2009) has a considerable similarities with the test results of 200 mm high CFRP confined square concrete columns made of brick aggregate, stone aggregate, recycled brick aggregate and recycled stone aggregate concrete as shown in Figure 7.38.

For 200 mm high GFRP confined square columns made of brick, stone and recycled stone aggregate concrete, ACI 440 model (2002), Lam and Teng's model (2003b), and Wu and Wang model (2009) has considerable similarities with the test results as shown in Figures 7.39. For recycled brick aggregate concrete columns, ACI 440 model (2002), Lam and Teng's model (2003b) and Kumutha et al. model (2007) showed considerable

similarities with the test results as shown in Figures 7.39. Al-Salloum's model (2007) is found not valid for 200 mm high square columns with corner radius of 25 mm.

For 300 mm high CFRP confined square columns made of stone, recycled brick and recycled stone aggregate concrete, ACI 440 model (2002), Lam and Teng's model (2003b), Kumutha et al. model (2007) and Wu and Wang model (2009) has considerable similarities with the test results as shown in Figures 7.40. But for brick aggregate concrete columns, ACI 440 model (2002) and Al-Salloum's model (2007) showed considerable similarities with the test results as shown in Figures 7.40.

For 300 mm high GFRP confined square columns made of brick, recycled brick and recycled stone aggregate concrete, ACI 440 model (2002), Kumutha et al. model (2007) and Al-Salloum's model (2007) has considerable similarities with the test results as shown in Figures 7.41. But for stone aggregate concrete columns, ACI 440 model (2002), Lam and Teng's model (2003b) and Wu and Wang model (2009) showed considerable similarities with the test results as shown in Figures 7.41.

ACI 440 model (2002), Lam and Teng's model (2003b), Kumutha et al. model (2007), Wu and Wang model (2009) and Shehata et al. model (2002) has considerable similarities with the test results of 400 mm high CFRP confined square concrete columns made of brick aggregate, stone aggregate, recycled brick aggregate and recycled stone aggregate concrete as shown in Figure 7.42.

ACI 440 model (2002), Lam and Teng's model (2003b), Wu and Wang model (2009) and Shehata et al. model (2002) has considerable similarities with the test results of 400 mm high GFRP confined square concrete columns made of brick aggregate, stone aggregate, recycled brick aggregate and recycled stone aggregate concrete as shown in Figure 7.43.

For 200 mm high CFRP confined circular columns made of brick aggregate concrete, Youssef et al. model (2007), Lam and Teng's model (2003a) and Wu and Wang model (2009) has considerable similarities with the test results as shown in Figures 7.44. For stone, recycled brick and recycled stone aggregate concrete columns, ACI 440 model (2002) showed considerable similarities with the test results as shown in Figures 7.44 but regression analysis required more test data to fit the curve for a better model.

For 200 mm high GFRP confined circular columns made of brick aggregate concrete, ACI 440 model (2002) has considerable similarities with the test results as shown in

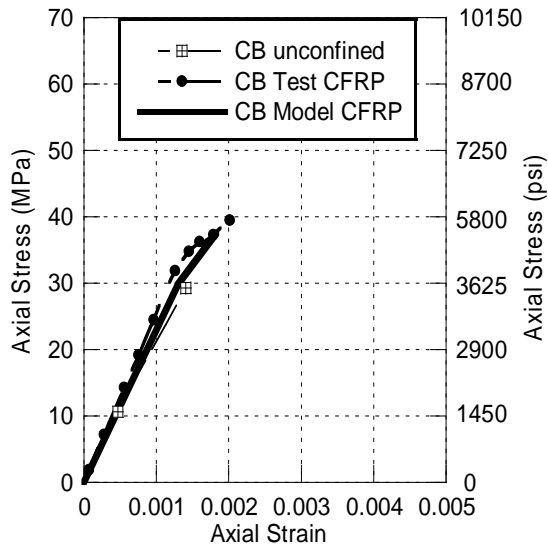
Figures 7.45 but for other aggregate concrete columns, no considerable similarities is found with the test results as shown in Figures 7.45 due to some limitations of regression analysis. Regression analysis required more test data to fit the curve for a better model.

ACI 440 model (2002) has considerable similarities with the experimental results of 300 mm high CFRP and GFRP confined circular concrete columns made of brick aggregate, stone aggregate, recycled brick aggregate and recycled stone aggregate concrete as shown in Figure 7.46-7.47.

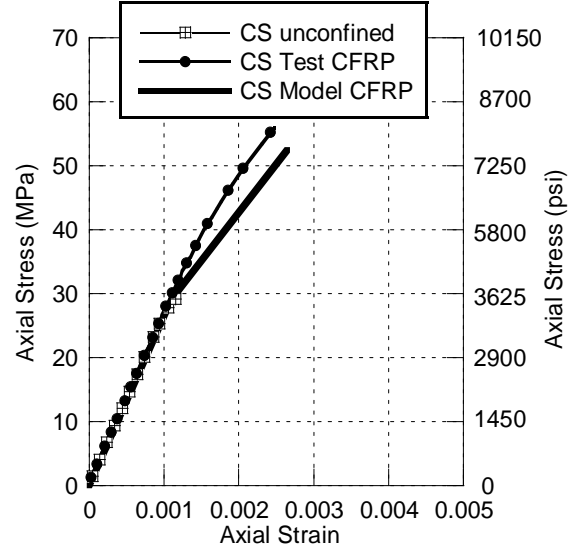
For 400 mm high CFRP confined circular columns made of brick aggregate concrete and recycled brick aggregate concrete, Youssef et al. model (2007), Lam and Teng's model (2003a) and Wu and Wang model (2009) has considerable similarities with the test results as shown in Figures 7.48. For stone and recycled stone aggregate concrete columns, ACI 440 model (2002) showed considerable similarities with the test results as shown in Figures 7.48.

ACI 440 model (2002) has considerable similarities with the experimental results of 400 mm high GFRP confined circular concrete columns made of brick aggregate, stone aggregate, recycled brick aggregate and recycled stone aggregate concrete as shown in Figure 7.49. Mirmiran et al. model (1998) was found to be conservative amongst the models.

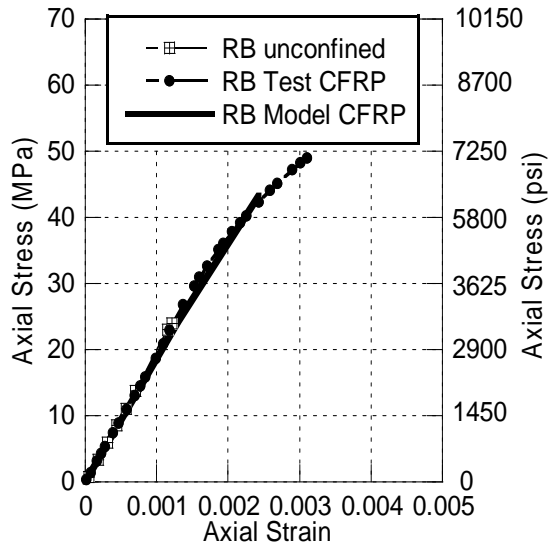
It is concluded that the proposed models predict the stress strain response of different sizes of columns have a reasonable accuracy.



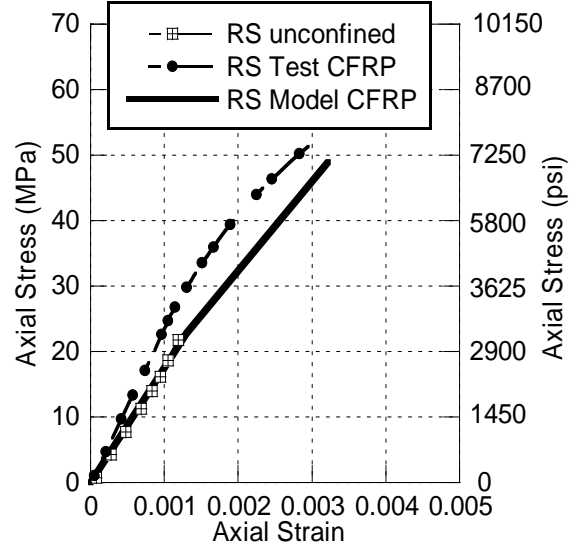
(a)



(b)

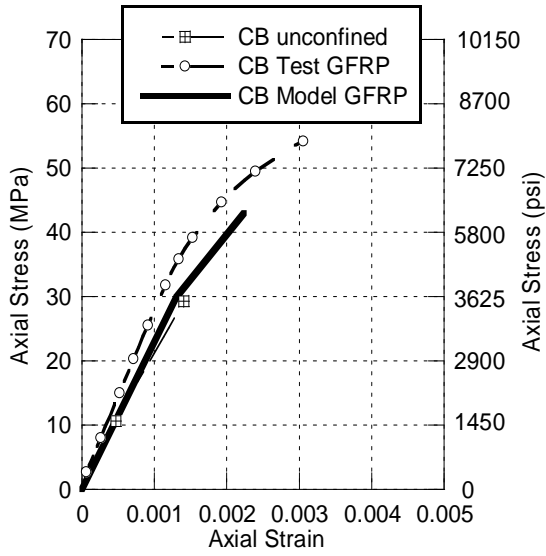


(c)

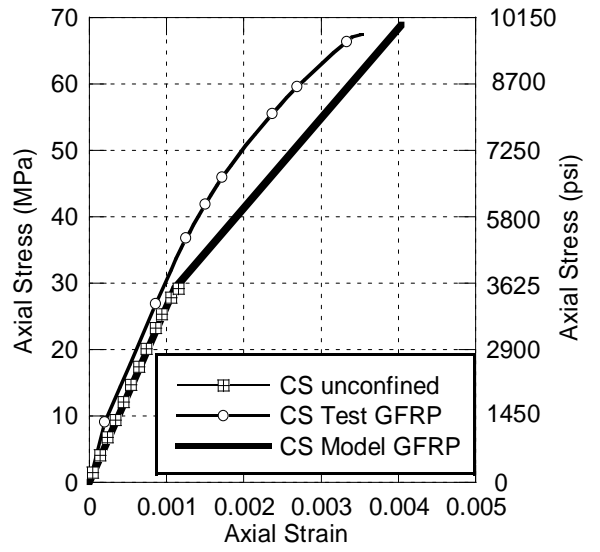


(d)

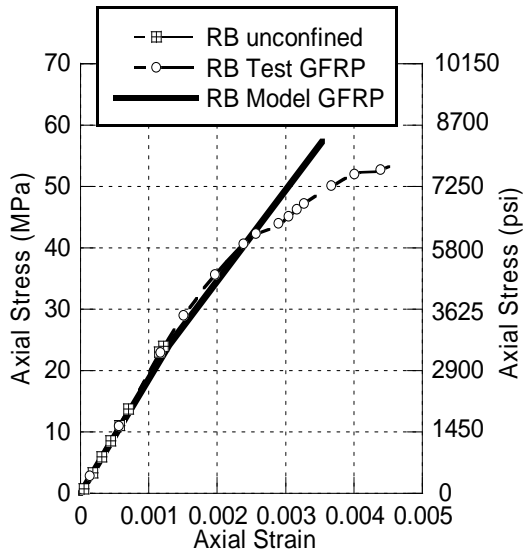
Figure 7.18: Model of 100 mm diameter CFRP confined circular column made of (a) brick aggregate (b) stone aggregate (c) recycled brick aggregate and (d) recycled stone aggregate concrete.



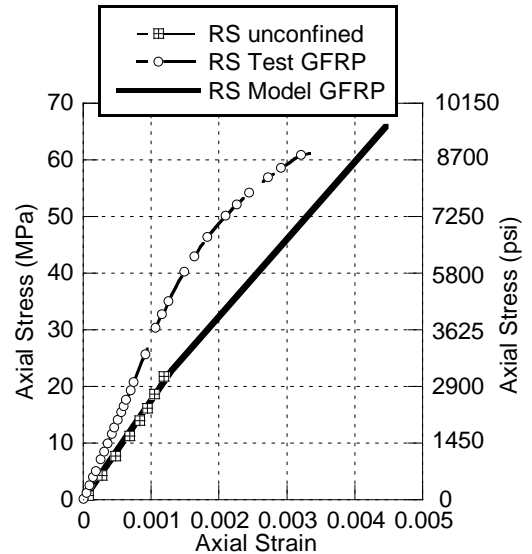
(a)



(b)

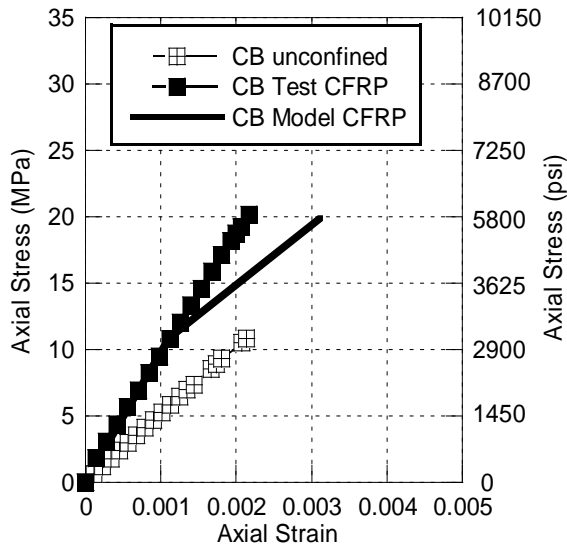


(c)

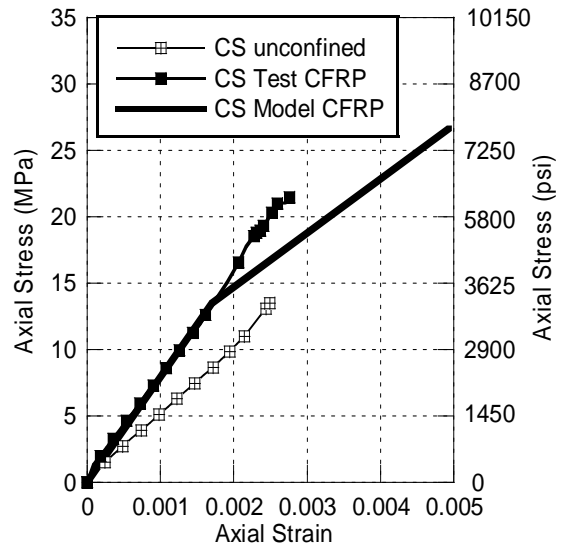


(d)

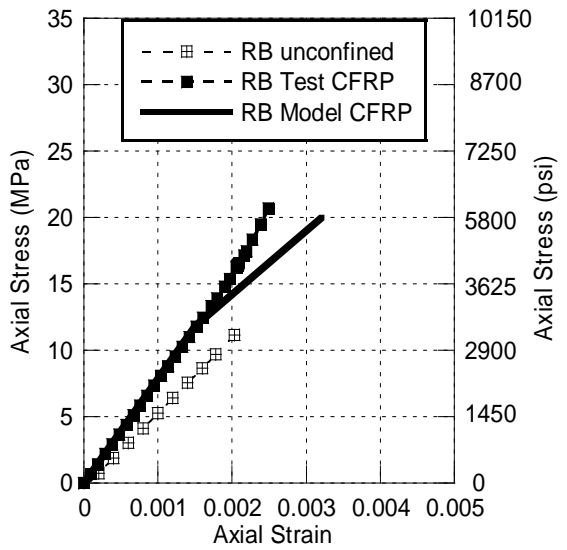
Figure 7.19: Model of 100 mm diameter GFRP confined circular column made of (a) brick aggregate (b) stone aggregate (c) recycled brick aggregate and (d) recycled stone aggregate concrete.



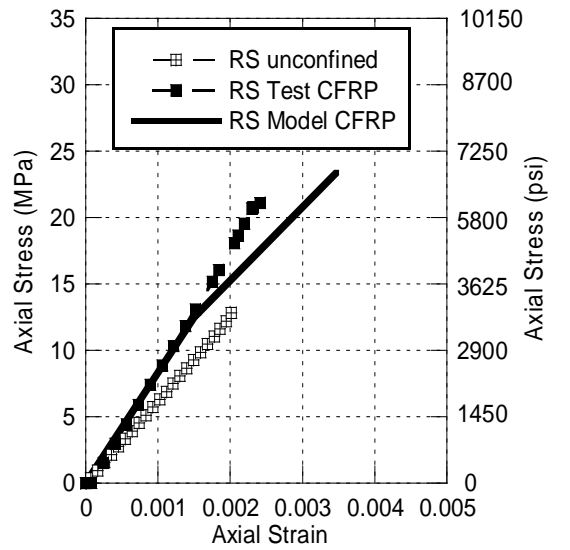
(a)



(b)

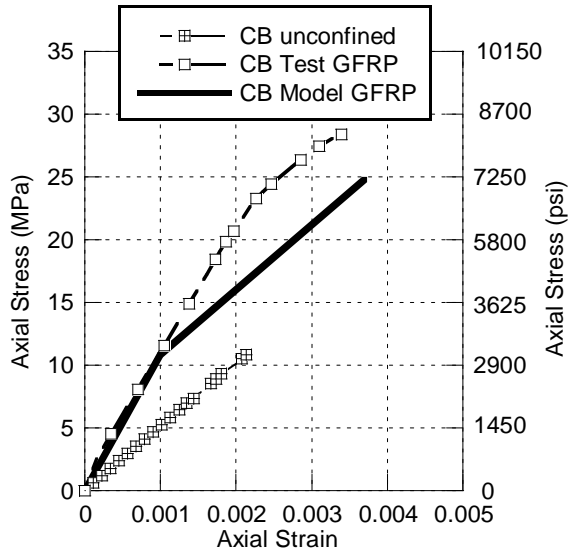


(c)

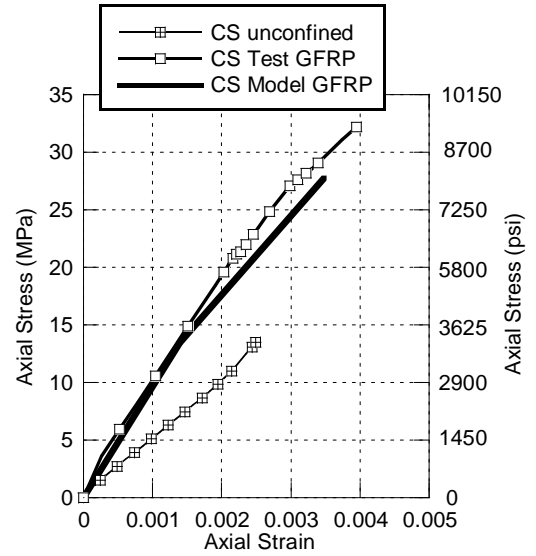


(d)

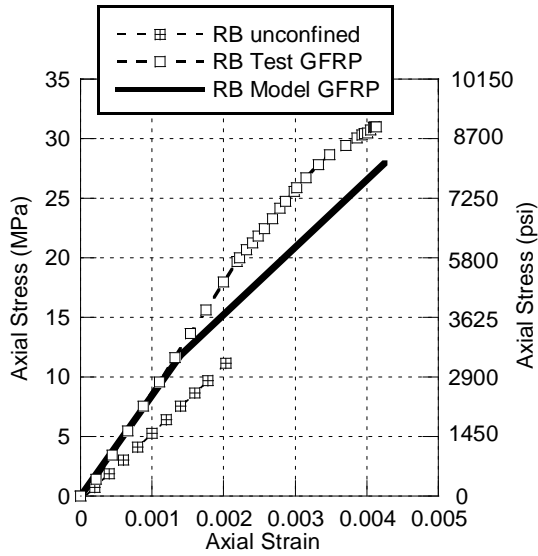
Figure 7.20: Model of 100 mm x 100 mm size CFRP confined square column made of (a) brick aggregate (b) stone aggregate (c) recycled brick aggregate and (d) recycled stone aggregate concrete.



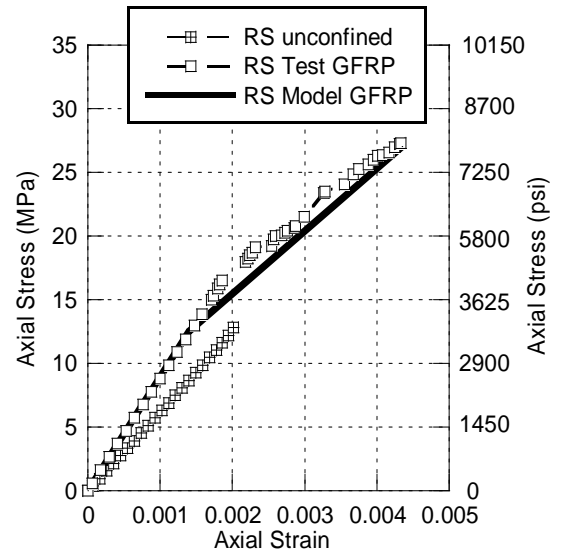
(a)



(b)



(c)



(d)

Figure 7.21: Model of 100 mm x 100 mm size GFRP confined square column made of (a) brick aggregate (b) stone aggregate (c) recycled brick aggregate and (d) recycled stone aggregate concrete.

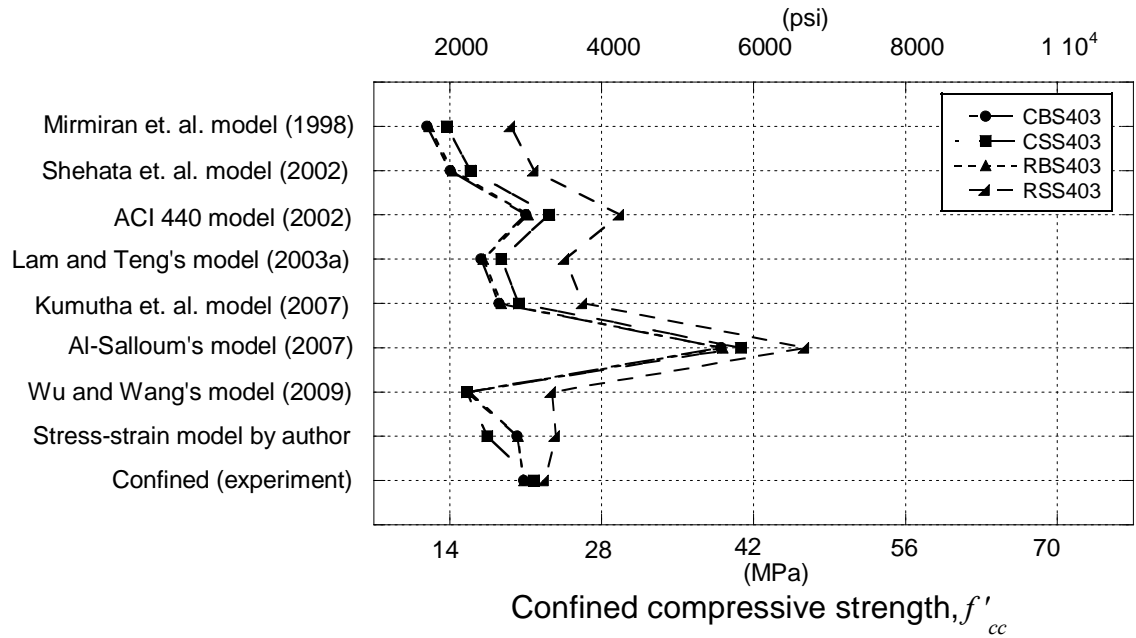


Figure 7.38: Comparison of confined compressive strength of brick, stone, recycled brick and recycled stone aggregate 100mm x 100mm size square concrete column confined by CFRP with existing models.

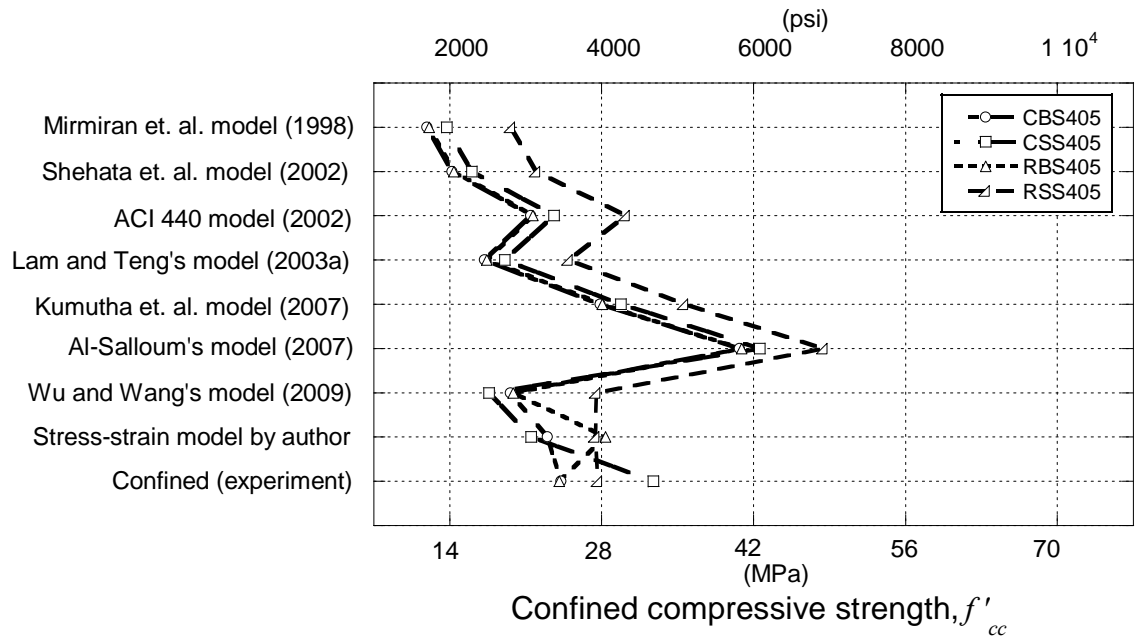


Figure 7.39: Comparison of confined compressive strength of brick, stone, recycled brick and recycled stone aggregate 100mm x 100mm size square concrete column confined by GFRP with existing models.



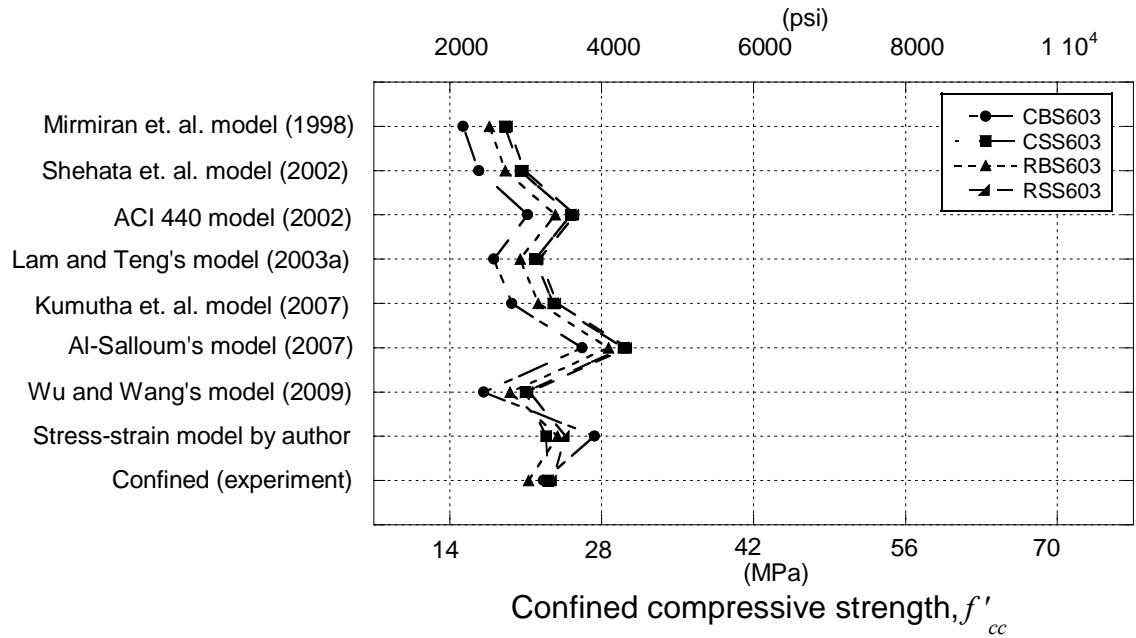


Figure 7.40: Comparison of confined compressive strength of brick, stone, recycled brick and recycled stone aggregate 150mm x 150mm size square concrete column confined by CFRP with existing models.

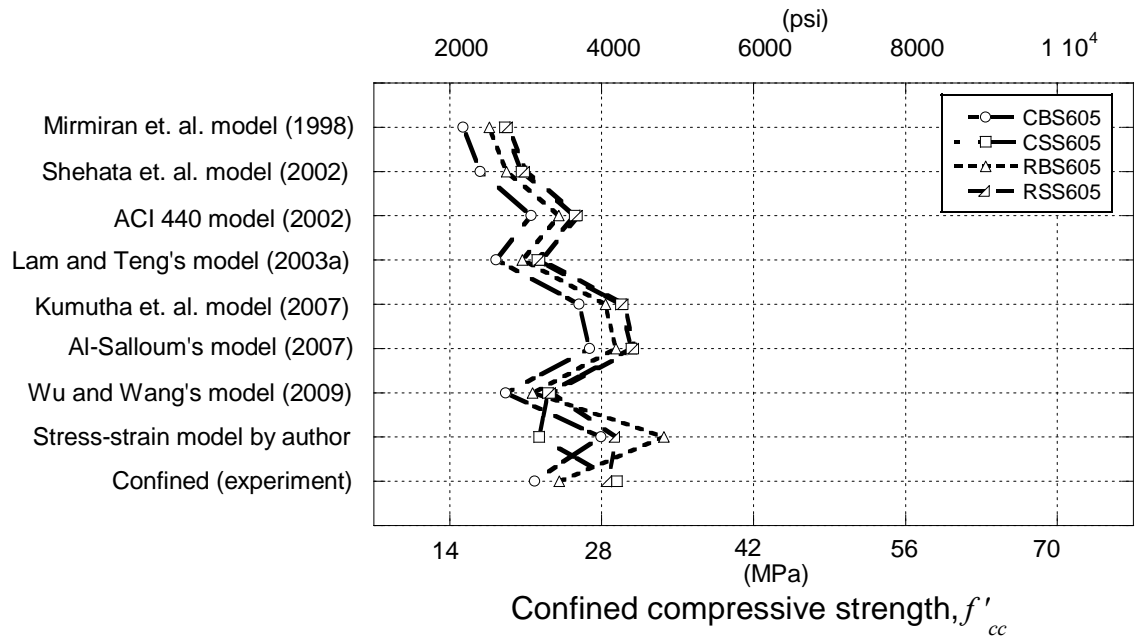


Figure 7.41: Comparison of confined compressive strength of brick, stone, recycled brick and recycled stone aggregate 150mm x 150mm size square concrete column confined by GFRP with existing models.

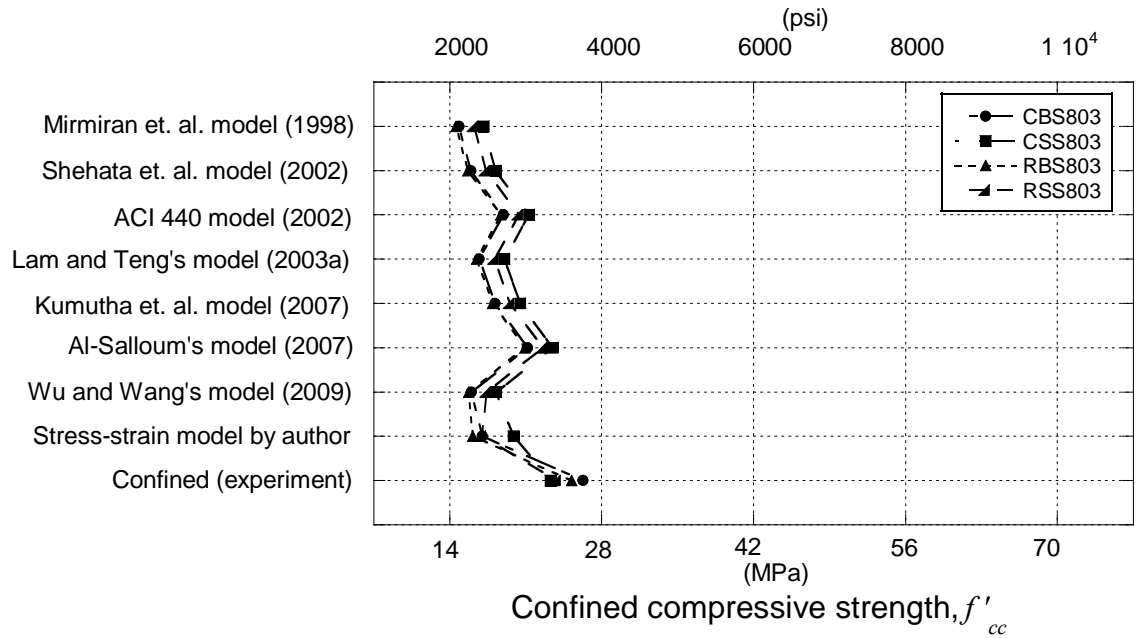


Figure 7.42: Comparison of confined compressive strength of brick, stone, recycled brick and recycled stone aggregate 200mm x 200mm size square concrete column confined by CFRP with existing models.

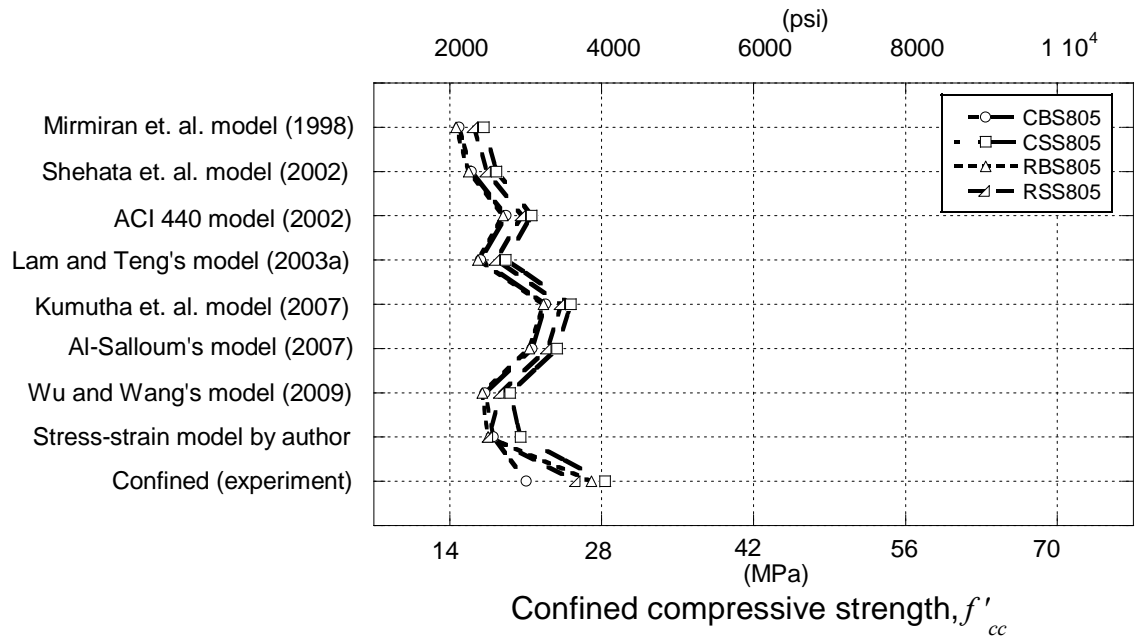


Figure 7.43: Comparison of confined compressive strength of brick, stone, recycled brick and recycled stone aggregate 200mm x 200mm size square concrete column confined by GFRP with existing models.

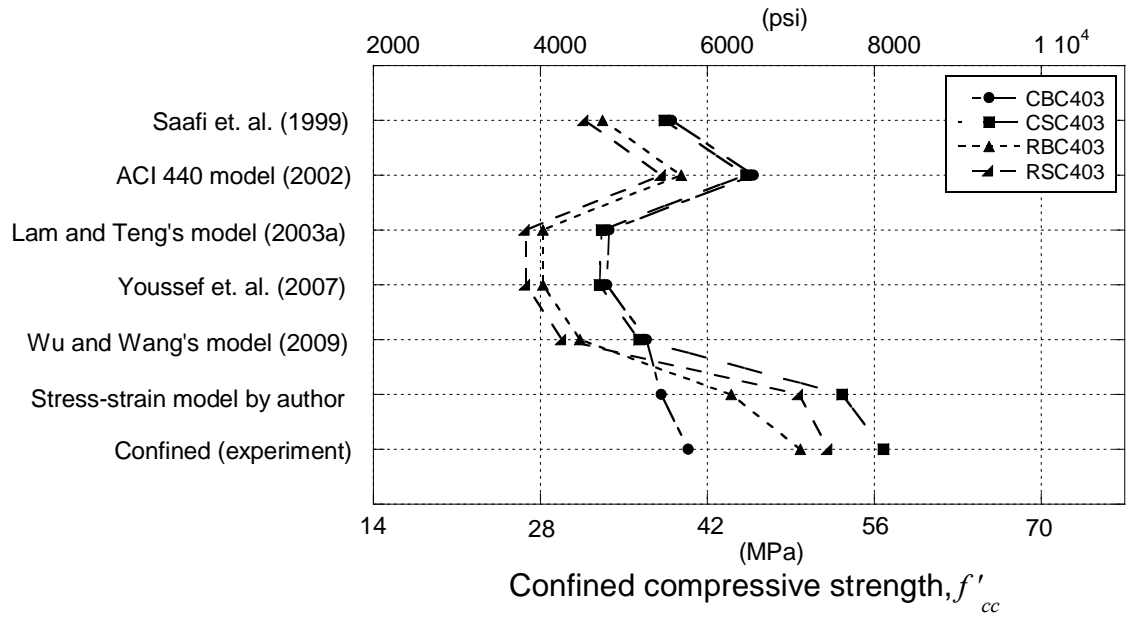


Figure 7.44: Comparison of confined compressive strength of brick, stone, recycled brick and recycled stone aggregate 100mm diameter circular concrete column confined by CFRP with existing models.

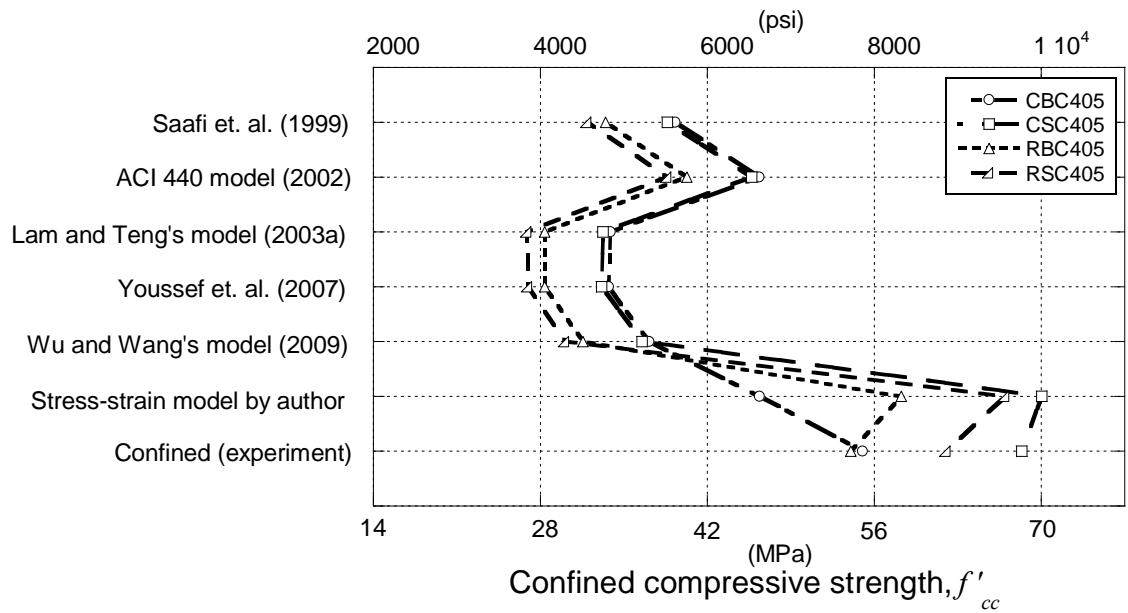


Figure 7.45: Comparison of confined compressive strength of brick, stone, recycled brick and recycled stone aggregate 100mm diameter circular concrete column confined by GFRP with existing models.

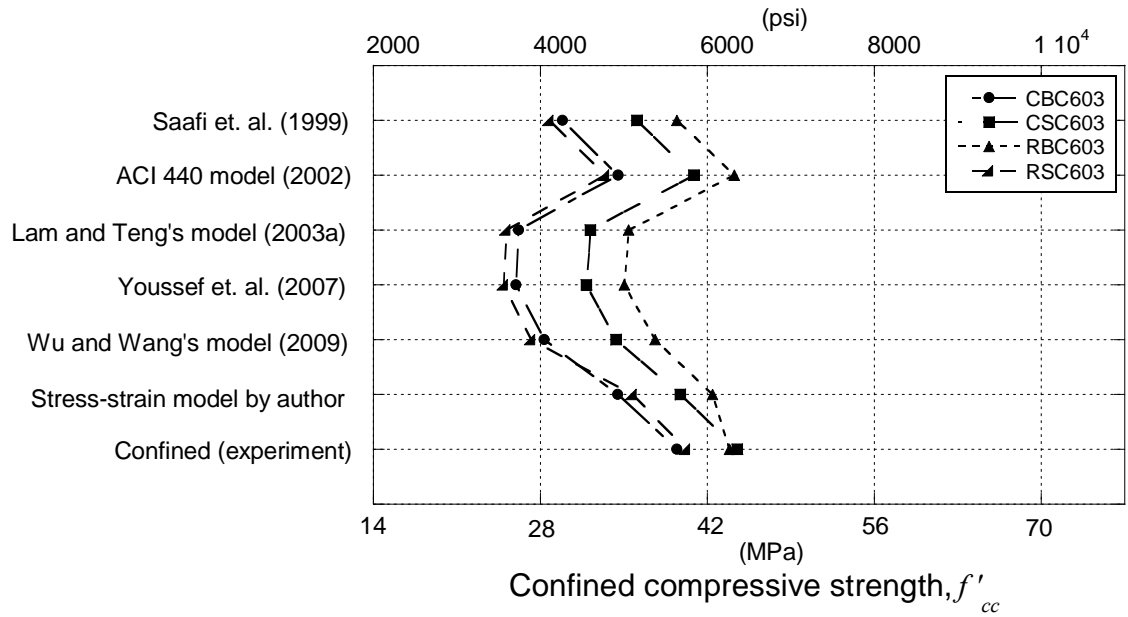


Figure 7.46: Comparison of confined compressive strength of brick, stone, recycled brick and recycled stone aggregate 150mm diameter circular concrete column confined by CFRP with existing models.

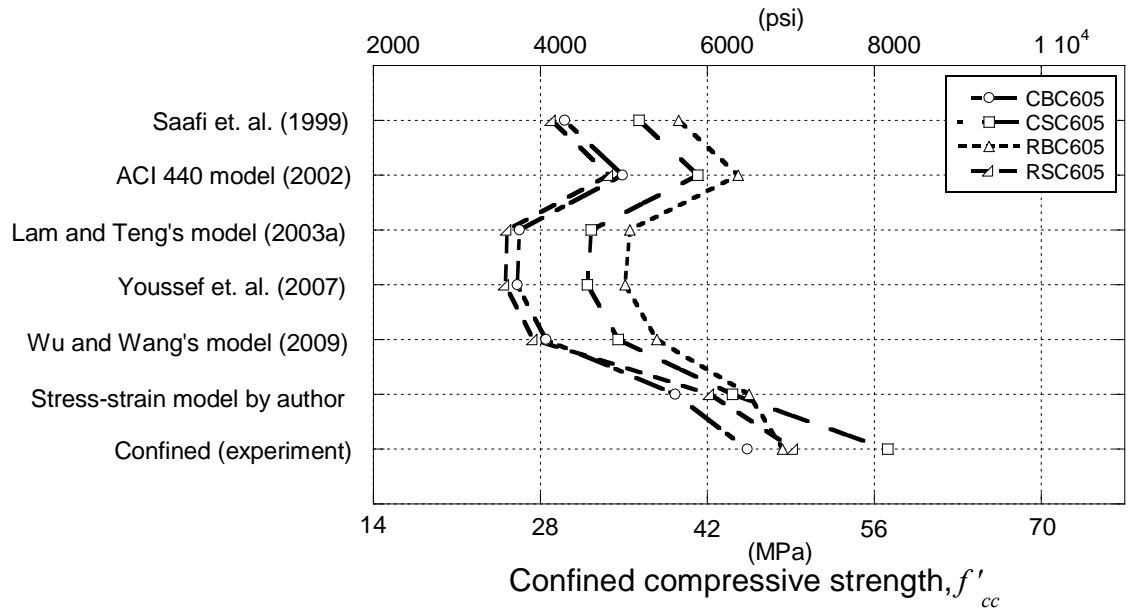


Figure 7.47: Comparison of confined compressive strength of brick, stone, recycled brick and recycled stone aggregate 150mm diameter circular concrete column confined by GFRP with existing models.

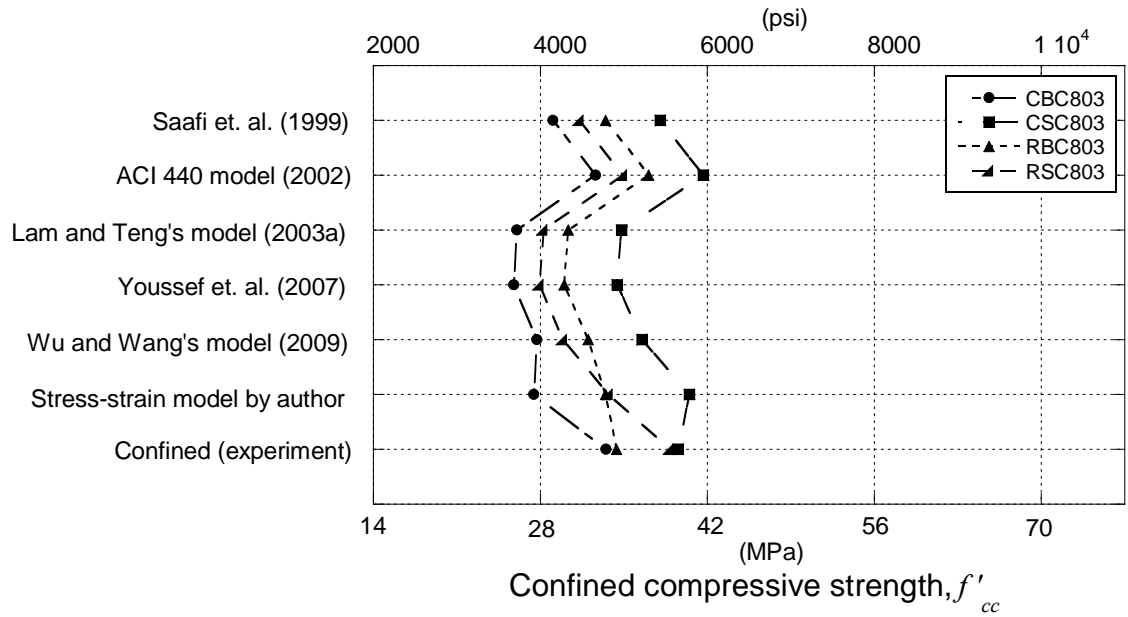


Figure 7.48: Comparison of confined compressive strength of brick, stone, recycled brick and recycled stone aggregate 200mm diameter circular concrete column confined by CFRP with existing models.

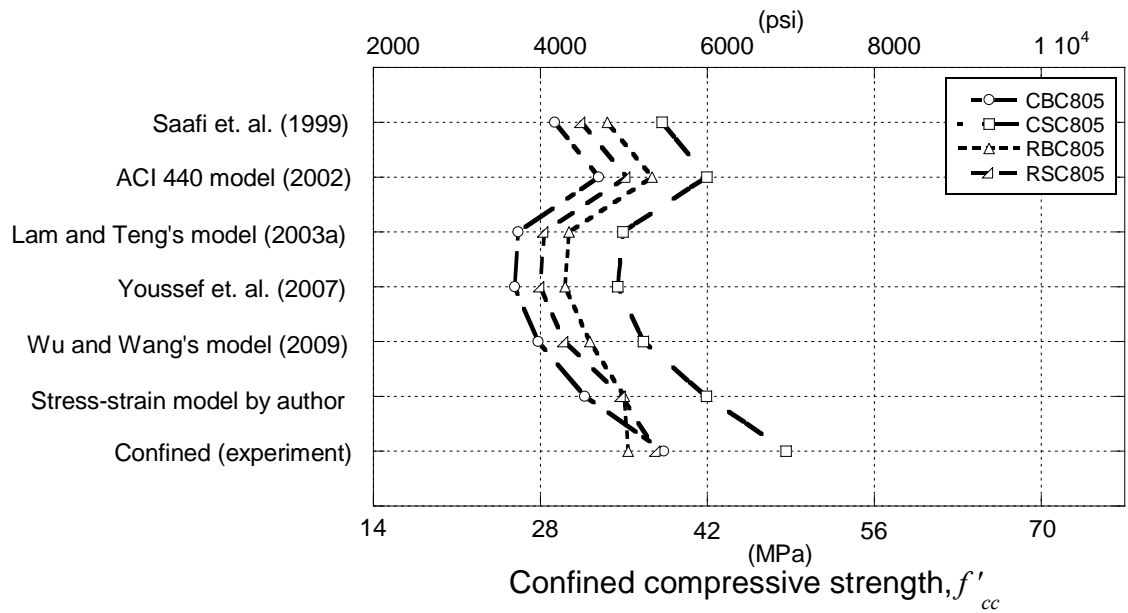


Figure 7.49: Comparison of confined compressive strength of brick, stone, recycled brick and recycled stone aggregate 200mm diameter circular concrete column confined by GFRP with existing models.

## 8.1 General

A large experimental program has been presented to study the behavior of FRP-confined concrete under compressive loads. In the program, the presence of different geometry and columns and different type of fibers are considered. A total of 120 circular and square concrete columns made of four types of coarse aggregate are cast and tested. The obtained results are shown that the efficiency of the confinement is very sensitive to the column cross-section geometry (circular and square) and confining stress. Finally stress-strain models are proposed for the FRP-confined concrete columns to use in the design desk.

## 8.2 Failure patterns

For all circular and square CFRP and GFRP confined columns, collapse is due to fibers rupture and occurred in a sudden and explosive way and is only preceded by some creeping sounds. It occurs prematurely for a stress level appreciably lower than the ultimate strength of the composites. For circular columns, the location of failure is observed mainly in their central zone, sometimes at more than one location, and then delamination spread towards other sections. Regarding confined square concrete columns, most of the failure took place at one of the corners near bottom to mid height of the specimen because of the high stress concentration at these locations. Collapse occurred almost without advance warning by sudden rupture of the composite wrap. However, popping noises are heard during various stages of loading and are attributed to microcracking of the concrete. For all confined concrete columns, delamination is not observed at the overlap location of the jacket, which confirmed the adequate stress transfer over the splice. There is not an obvious size effect on the failure pattern of the CFRP and GFRP confined concrete short columns.

### **8.3 Stress-strain behaviour**

The experimental results clearly demonstrate that composite wrapping of FRP can enhance the structural performance of concrete columns under axial loading, in terms of both maximum strength and strain. The curves of all composite confined concrete specimens are bi-linear with a transition zone. In square cross sections, the stress–strain curve is influenced by the radius to which the corners of the section are rounded off, in order to avoid the breakage of the fibers. The axial stress-strain behavior of confined concrete is significantly affected by the dilation behavior of the concrete. It is observed that the second slope of axial stress- axial strain response is mainly depending on the stiffness of the FRP jacket.

#### **8.3.1 Dilation of concrete**

Confinement of columns by means of FRP jackets is done by containing the dilation of concrete by wrapping of fibers in the hoop direction of concrete columns. In circular columns the confinement due to dilation is uniform throughout the cross section, but for square concrete columns stress concentration at the corners fails to resist further dilation and subsequently larger dilation occurs in the square concrete columns compared to circular columns. The dilation effect mainly depends on the Poisson's ratio of concrete, shape and geometry of the columns.

For all columns, the dilation of square confined concrete columns is found to be higher compared to circular confined columns. For 4 inch high circular and square concrete columns, the dilation of brick, stone, recycled brick and recycled stone aggregate concrete square columns are 47% and 35%, 30% and 17%, 5% and 8%, 113% and 106% higher than circular confined concrete column due to CFRP and GFRP confinement respectively. Again for 6 inch high circular and square concrete columns, the dilation of brick, stone and recycled brick aggregate concrete square column is 114% and 187%, 184% and 156%, 75% and 113% higher than circular confined concrete column due to CFRP and GFRP confinement respectively. The columns made of recycled stone aggregate concrete this value is 281% for CFRP confinement but for GFRP confinement the dilation for both square and circular column is found nearly the same. Again for 8 inch high circular and square concrete columns, the values are 115% and 159%, 21% and 28%, 268% and 201%, 38% and 54. GFRP wraps are able to contain the dilation of

concrete for a longer period which is evident from the axial stress vs. lateral strain diagrams.

### **8.3.2 Axial capacity enhancement**

The gain in compressive strength obtained by the FRP confined concrete depends mainly on the relative stiffness of the FRP jacket to the axial stiffness of the column. It is observed from the axial stress vs. axial strain diagrams that the behavior of CFRP and GFRP wrapped concrete columns are similar to control specimens till the lateral expansion of concrete started. As the concrete starts to dilate, FRP wraps get activated and start containing the specimens from dilating laterally thereby providing passive confinement. The confining pressure provided by the jacket keeps increasing proportional to the applied axial load until failure. As the jacket gets completely activated, the axial stress strain curve starts to flatten and is closer to a straight line in lateral direction until failure. Response of FRP wrapped circular and square columns to axial compression has been found to increase monotonically in a non linear fashion. The elastic response of the specimens is represented by an initial straight portion of the axial stress vs. axial strain curve. This straight portion is followed by a transition stage in which the concrete starts to dilate and FRP wraps start providing confining pressure. This transition stage is then followed by a straight portion which continues till failure as the confining pressure keeps on increasing till failure. Axial stress vs. axial strain curve of FRP wrapped columns does not have any descending branch as the confining pressure keeps increasing until failure.

For 4 inch high concrete columns, the axial strength of brick, stone, recycled brick and recycled stone aggregate concrete circular column is 90% and 93%, 167% and 109%, 133% and 71%, 143% and 126% higher than square confined concrete column due to CFRP and GFRP confinement respectively. Again for 6 inch high concrete columns, 86% and 105%, 91% and 93%, 105% and 100%, 70% and 75% higher than square confined concrete column due to CFRP and GFRP confinement respectively. Similarly for 8 inch high concrete columns, these values are 57% and 46%, 70% and 71%, 42% and 30%, 58% and 48% higher than square confined concrete column due to CFRP and GFRP confinement respectively. The axial load capacity of stone aggregate concrete is found to increase at a rate greater than other concretes for both CFRP and GFRP confinement. It is found that, the increase of axial load capacity of square columns is significantly lower compared to circular columns. Both CFRP and GFRP confinement are very effective for circular concrete columns by significantly increasing the axial strength and ultimate axial



strain. From the experimental results it is clear that GFRP-confined columns can obtain approximately higher increase in axial strength and ultimate axial strain, compared to CFRP-confined columns due to the FRP jacket's thickness.

#### **8.4 Confinement effectiveness affected by geometric parameters**

The main difference between the circular and square shape in terms of confinement is that in the former the lateral pressure is uniformly distributed over the surface of concrete core while in the later it does not. The confinement is effective at the column corner only and the flat sides of square columns remain unconfined. Shape of cross section can directly impact the confinement effectiveness of the jacket. Square sections are less effective than their circular counterparts. The experimental results show that the size of a specimen had a significant effect on the strength of FRP-confined concrete short columns. However, more investigations need to be done to get an accurate result useful in the concrete structures design.

##### **8.4.1 Effect of radius of curvature**

For circular columns, the compressive strength and the ultimate axial strain decreases with increasing radius of curvature for all types of concrete due to the curvature effect. The confinement effectiveness decreases with the increase of radius of curvature and the size effect is more pronounced for circular columns.

##### **8.4.2 Effect of column side to corner radius ratio**

For CFRP and GFRP confined square concrete columns with same corner radius ( $r = 25$  mm), there is no size effect to exist in axial strength but ultimate axial strain decreases with increasing column side to corner radius ratio for all types of concrete. The confinement effectiveness for square columns is much less than that for circular columns due to the presence of corners and sides; the efficiency is reduced due to the corner of the columns.

### **8.4.3 Effect of FRP volumetric ratio**

The compressive strength and ultimate axial strain of the CFRP and GFRP confined circular concrete columns increases as the CFRP and GFRP volumetric ratio increases for all types of concrete. With the same corner radius ( $r = 25\text{mm}$ ), there is no size effect to exist on the axial strength but ultimate axial strain increases with the increase of FRP volumetric ratio of the square concrete columns for all types of concrete.

### **8.4.4 Effect of rigidity ratio**

The compressive strength of the CFRP and GFRP confined circular and square concrete columns clearly depends on the rigidity ratio of the lateral stiffness of the FRP jacket to the axial stiffness of the column rather than solely on the concrete strength. The compressive strength of the CFRP and GFRP confined circular concrete columns increases as the rigidity ratio increases for all types of concrete. But CFRP and GFRP confined square concrete columns with the same corner radius ( $r = 25\text{mm}$ ), there is no size effect to exist on the axial strength for all types of concrete. The experimental results clearly indicate that an increase in confining pressure results in an increase in concrete strength capacities. Since FRP jackets provide passive confining pressure, the jacket stiffness is a critical parameter in determining the confining pressure applied to the confined concrete. FRP with a high modulus of elasticity and a high tensile strength can develop a passive confining pressure leading to a substantial increase of the confined concrete strength.

## **8.5 Finite element modeling**

The finite element modeling has been performed to check mainly the crack pattern evolution, the stress-strain concentrations in the FRP wraps and to validate the experimental data for three different sizes and geometry of columns. For FRP-confined concrete, the resulting stress-strain curves show gradually increasing behavior until the jacket fails. The simulated compressive response of normal-strength concrete confined with FRP has been compared to experimental results on wrapped circular and square columns, showing excellent agreement both in terms of stress-strain behavior and ultimate state of different sizes of columns. The Poisson's ratio of stone aggregate concrete was also evaluated convincingly to be lower than brick aggregate concrete,

recycled stone aggregate concrete and recycled brick aggregate concrete by FE analysis and the values were estimated at 0.25, 0.35, 0.37 and 0.40, respectively. The model has shown the same type of stress concentration around the edges of square sections and middle portion of the circular sections as observed in the experiments. FEA models can be used as templates to further study the FRP-jacketed concrete columns.

## **8.6 Stress-strain models**

Experimental investigations on the compressive strength of FRP confined concrete are expensive in context of Bangladesh. For this reason, stress-strain models are developed for FRP confined concrete made of four different types of aggregate with considering different sizes of columns. The obtained results are shown that the efficiency of the confinement is very sensitive to the column cross section geometry.

On the basis of the obtained results, equations are proposed, for the confined concrete strength and the ultimate confined concrete strain as a function of the confining lateral stress, for each of the cross section geometry used: circular and square. The estimations given by these equations and by formulas found in the literature are compared with the experimental ones from this work. From the comparisons made in this work it is clear that proposed equations to estimate the confined concrete strength should be associated with the cross section shape. In general, the proposed models for square and circular columns are shown a good agreement with experimental results performed by the present study. ACI 440 model (2002), Lam and Teng's model (2003b), Kumutha et al. model (2007) and Wu and Wang model (2009) has considerable similarities with the test results of brick aggregate, stone aggregate, recycled brick aggregate and recycled stone aggregate concrete square columns. Again for circular columns, ACI 440 model (2002) has considerable similarities with the test results of brick aggregate, stone aggregate, recycled brick aggregate and recycled stone aggregate concrete.

The suggested model will be helpful in predicting the compressive strength of concrete confined with FRP composite sheets. The model can also be used in the design equations to predict axial capacity of concrete columns confined with FRP composite sheets.

## **8.8 Scope of future studies**

Based upon the work described in the thesis, some suggestions for future work within this field are noted.

- This research considered the confinement of concrete with single wrap FRP. Behaviour of concrete confined with multilayer FRP wrapping is proposed for future studies.
- FRP wrap is not modeled in the FE model of confined concrete. FE analysis of confined concrete with FRP wrap modeling needs to be studied.
- In this research, columns are unreinforced plain concrete column. Confinement effect of reinforced concrete column is also required to be studied.
- Confinement effects of rectangular columns are also required to be studied.
- Confinement effects in long/slender columns are proposed for future studies.
- Effect of different corner radius of non-circular columns is also required to be studied.

## REFERENCES

---

- ACI 440.2R-02, Guide for the Design and Construction of Externally Bonded FRP Systems for Strengthening Concrete Structures, American Concrete Institute, Reported by ACI Committee 440, 2002.
- ACI 440.2R-08, Guide for the Design and Construction of Externally Bonded FRP Systems for Strengthening Concrete Structures, American Concrete Institute, Reported by ACI Committee 440, 2008.
- Akhtaruzzaman, A. A. and Hasnat, A., Properties of Concrete using Crushed Brick as Aggregate, *Concrete International*, Vol-5, No. 2, pp 58-63, 1983.
- Al-Salloum, Y. A., Influence of Edge Sharpness on the Strength of Square Concrete Columns Confined with FRP Composite Laminates, *Composites, Part B*, Vol-38, pp 640–650, 2007.
- Akogbe, R. K., Liang, M. and Wu, Z., Size Effect of Axial Compressive Strength of CFRP Confined Concrete Cylinders, *International Journal of Concrete Structures and Materials*, Korea Concrete Institute, Vol-5, No.1, pp 49-55, 2011.
- ANSYS, ANSYS Structural Analysis Guide, Version 10.0, ANSYS, Inc., Canonsburg, Pennsylvania, 2005.
- ASTM C 39/C 39M-30, Standard Test Method for Compressive Strength of Cylindrical Concrete Specimens, *Annual Book of ASTM Standards*, 2003:04.02.
- ASTM D 3039/D 3039M-00, Standard Test Method for Tensile Properties of Polymer Matrix Composite Materials, American Society for Testing Materials, 2000.
- ASTM D 2290–92, Standard Test Method for Apparent Tensile Strength of Ring or Tubular Plastics and Reinforced Plastics by Split Disk Method, *Annual Book of ASTM Standards*, 1992:15.03.
- Bank, L. C., *Composites for Construction: Structural Design with FRP Materials*, John Wiley & Sons, Inc., Hoboken, New Jersey, 2006.
- Campione, G., Influence of FRP Wrapping Techniques on the Compressive Behavior of Concrete Prisms, *Cement & Concrete Composites*, Vol-28, pp 497–505, 2006.
- Chaallal, O., Shahawy, M., and Hassan, M., Performance of Axially Loaded Short Rectangular Columns Strengthened with Carbon Fiber-Reinforced Polymer Wrapping, *Journal of Composites for Construction*, ASCE, Vol-7, No. 3, pp 200–208, 2003.

- Chaallal, O., Hassan, M. and LeBlanc, M., Circular Columns Confined with FRP: Experimental versus Predictions of Models and Guidelines, *Journal of Composites for Construction*, ASCE, Vol-10, No. 1, pp 4–12, 2006.
- CSA-S806-02, Design and Construction of Building Components with Fibre-Reinforced Polymers, CSA Rexdale BD, Toronto, 2002.
- Carey, S. A. and Harries, K. A., Axial Behavior and Modeling of Confined Small, Medium, and Large-Scale Circular Sections with Carbon Fiber-Reinforced Polymer Jackets, *ACI Structural Journal*, Vol-102, No.4, pp 596–604, 2005.
- Fardis, M. N. and Khalili, H., FRP-Encased Concrete as a Structural Material, *Magazine of Concrete Research*, Vol-34, No.121, pp 191–202, 1982.
- Gu, X., Li, Y., Zhang, W., and Ouyang, Y., Compressive Stress-Strain Relationship of Concrete Confined by Carbon Fiber Composites Sheets, *Structural Engineering*, Vol-22, No.2, pp 50–56, 2006.
- Hajsadeghi, M. and Alaei, F., Numerical Analysis of Rectangular Reinforced Concrete Columns Confined with FRP Jacket under Eccentric Loading, *Proceedings of the 5th International Conference on FRP Composites in Civil Engineering (CICE)*, Beijing, China, 27-29 September, Paper No. 075, pp 658-661, 2010.
- ISIS M04, Externally Bonded FRP for Strengthening Reinforced Concrete Structures, The Canadian Network of Centres of Excellence on Intelligent Sensing for Innovative Structures, Winnipeg, MB, Canada, 2001.
- Islam, M. M., Interaction Diagrams for Square Concrete Columns Confined with Fiber Reinforced Polymer wraps, M.Sc. Engineering Thesis, Department of Civil Engineering, Bangladesh University of Engineering & Technology, 2011.
- Jia, M. Y. and Cheng, H., Experimental Research of Size Effect of RC Circular Columns Reinforced by CFRP, *Materials and Structures*, Vol-29, No.1, pp 35–36, 2003 .
- Kachlakev, D.I., Miller, T. Yim, S., Chansawat, K., Potisuk, T., Finite Element Modeling of Reinforced Concrete Structures Strengthened with FRP Laminates, California Polytechnic State University, San Luis Obispo, CA and Oregon State University, Corvallis, OR for Oregon Department of Transportation, May. 2001.
- Kumutha, R., Vaidyanathan, R., and Palanichamy, M. S., Behaviour of Reinforced Concrete Rectangular Columns Strengthened using GFRP, *Cement & Concrete Composites*, Vol-29, No. 8, pp 609–615, 2007.
- Karabinis, A. I., Rousakis, T. C. and Manolitsi, G. E., 3D Finite-Element Analysis of Substandard RC Columns Strengthened by Fiber-Reinforced Polymer Sheets, *Journal of Composites for Construction*, ASCE , Vol-12, No. 5, pp 531-540, 2008.
- Lam, L. and Teng, J.G., Strength Models for Fiber-Reinforced-Plastic Confined Concrete, *Journal of Structural Engineering*, ASCE, Vol-128, No. 5, pp 612–623, 2001.

- Lorenzis, L. D., Micelli, F. and Tegola, A. L., Influence of Specimen Size and Resin Type on the Behavior of FRP-Confined Concrete Cylinders, *ACI Materials Journal*, Vol. 99, No. 3, pp46–53, 2002.
- Lam, L. and Teng, J.G., Design-Oriented Stress–Strain Model for FRP-Confined Concrete in Rectangular Columns, *Journal of Reinforced Plastics and Composites*, Vol-22, No.13, pp 1149-1186, 2003a.
- Lam, L. and Teng, J.G., Design-Oriented Stress–Strain Model for FRP-Confined Concrete, *Construction and Building Materials*, Vol-17, pp 471–489, 2003b.
- Lin, C. T. and Li, Y. F., An Effective Peak Stress Formula for Concrete Confined with Carbon Fiber Reinforced Plastics, *Canadian Journal of Civil Engineering*, Vol-30, pp 882–889, 2003.
- Lam, L. and Teng, J.G., Ultimate Condition of Fiber Reinforced Polymer-Confined Concrete, *Journal of Composites for Construction*, ASCE, Vol-8, No. 6, pp 539–548, 2004.
- Lam L., Teng J.G., Cheung C.H., Xiao Y., FRP-Confined Concrete under Axial Cyclic Compression, *Cement & Concrete Composites*, Vol-28, pp 949–958, 2006.
- Luca, A. D., Nardone, F., Matta, F., Nanni, A., Lignola, G. P. and Prota, A., Structural Evaluation of Full-Scale FRP-Confined Reinforced Concrete Columns, *Journal of Composites for Construction*, ASCE, Vol-15, No. 1, pp 112–123, 2011.
- Masia, M. J., Gale, T. N. and Shrive, N. G., Size Effects in Axially Loaded Square-Section Concrete Prisms Strengthened using Carbon Fibre Reinforced Polymer Wrapping, *Canadian Journal of Civil Engineering*, Vol-31, pp 1–13, 2004.
- Mukherjee, A., Boothby, T. E., Bakis, C. E., Joshi, M. V., and Maitra, S. R., Mechanical Behavior of Fiber-Reinforced Polymer-Wrapped Concrete Columns-Complicating Effects.” *Journal of Composites for Construction*, ASCE ,Vol- 8, No.2,pp 97–103, 2004.
- Malvar, L. J., Morrill, K. B. and Crawford, J. E., Numerical Modeling of Concrete Confined by Fiber-Reinforced Composites, *Journal of Composites for Construction*, ASCE, Vol-8, No. 4, pp 315- 322, 2004.
- Maaddawy, T.E., Strengthening of Eccentrically Loaded Reinforced Concrete Columns with Fiber-Reinforced Polymer Wrapping System: Experimental Investigation and Analytical Modeling, *Journal of Composites for Construction*, ASCE, Vol-13, No. 1, pp13-24, 2009.
- Mandal, S., Hoskin, A. and Fam, A., Influence of Concrete Strength on Confinement Effectiveness of Fiber Reinforced Polymer Circular Jackets, *ACI Structural Journal*, Vol-102, No. 3, pp 383–392, 2005.
- Mander, J. B., Priestley, M. J. N. and Park, R., Observed Stress–Strain Behavior of Confined Concrete, *Journal of Structural Engineering*, ASCE, Vol-114, No-8, pp 1827–1849, 1988.
- Matthys, S., Toutanji, H., Taerwe, L., Stress-Strain Behavior of Large-Scale Circular Columns Confined with FRP Composites, *Journal of Structural Engineering*, ASCE, Vol-132, No. 1, pp 123–133, 2006.

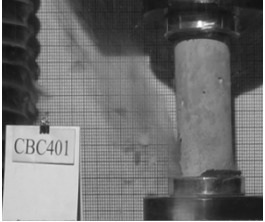
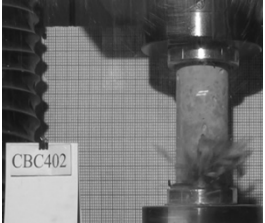
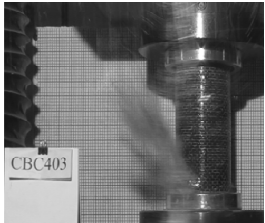



- Mirmiran, A. and Shahawy, M., Dilation Characteristics of Confined Concrete, *Mechanics of Cohesive-Frictional Materials*, Vol-2, pp 237–249, 1997a.
- Mirmiran, A. and Shahawy, M., Behavior of Concrete Columns Confined by Fiber Composites, *ASCE*, Vol-123, No. 5, pp 583–590, 1997b.
- Mirmiran, A., Shahawy, M., Samaan, M., Echary, H. E., Mastrapa, J. C., and Pico, O., Effect of Column Parameters on FRP-Confined Concrete, *Journal of Composites for Construction*, *ASCE*, Vol-2, No. 4, pp 175–185, 1998.
- Mirmiran, A., Zagers, K. and Wenqing, Y., Nonlinear Finite Element Modeling of Concrete Confined by Fiber Composites, *Finite Element Analysis and Design*, *The International Journal of Applied Finite Elements and Computer Aided Engineering*, Vol-35, No.1, pp 79- 96, 2000.
- Mohsen, A.I., Rajai, Z. A. and Moussa, A. I., Experimental and Parametric Study of Circular Short Columns Confined with CFRP Composites, *Journal of Composites for Construction*, *ASCE*, Vol-13, No. 2, pp 135–147, 2009.
- Pessiki, S., Harries, K.A., Kestner, J.T., Sause, R. and Ricles, J.M., Axial Behavior of Reinforced Concrete Columns Confined with FRP Jackets, *Journal of Composites for Construction*, *ASCE*, Vol-5, No. 4, pp 237–245, 2001.
- Parvin, A. and Wang, W., Behavior of FRP Jacketed Concrete Columns under Eccentric Loading, *Journal of Composites for Construction*, *ASCE*, Vol-5, No. 3, pp 146–152, 2001.
- Richart, F. E., Brandtzaeg, A., and Brown, R. L., A Study of the Failure of Concrete under Combined Compressive Stresses, *Engineering Experiment Bulletin No.*, 185, University of Illinois, Urbana, Ill,1928.
- Rochette, P. and Labossiere, Axial Testing of Rectangular Column Models Confined with Composites, *Journal of Composites for Construction*, *ASCE*, Vol-4, No.3,pp 129–136, 2000.
- Samaan, M., Mirmiran, A. and Shahawy, M., Model of Concrete Confined by Fiber Composites, *Journal of Structural Engineering*, *ASCE*, Vol-124, No. 9, pp 1025–1031, 1998.
- Saafi, M., Toutanji, H. A., and Li, Z., Behavior of Concrete Columns Confined with Fiber Reinforced Polymer Tubes, *ACI Structural Journal*, Vol. 96, No.4, pp 500–509, 1999.
- Shahawy, M., Mirmiran, A., Beitelman, A., Test and Modeling of Carbon-Wrapped Concrete Columns, *Composites: Part B*, Vol-31, pp 471–480, 2000.
- Shehata, I. A. E. M., Carneiro, L. A. V. and Shehata, L. C. D., Strength of Short Concrete Columns Confined with CFRP Sheets, *Materials and Structures*, Vol-35: pp 50–58, 2002.
- Spoelstra, M.R. and Monti, G., FRP-Confined Concrete Model, *Journal of Composites for Construction*, *ASCE*, Vol-3, No. 3, pp 143–150, 1999.

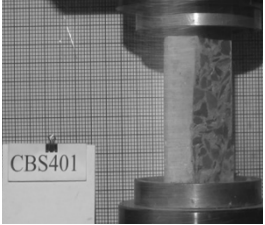
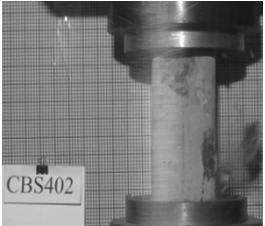
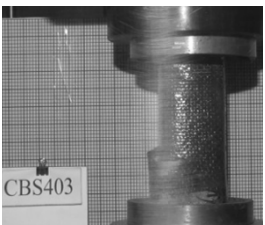
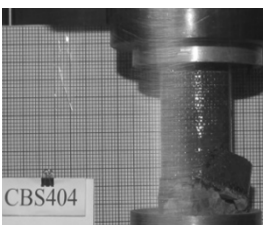
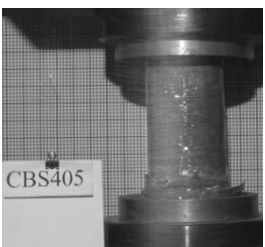
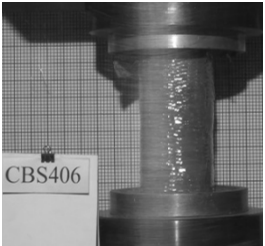


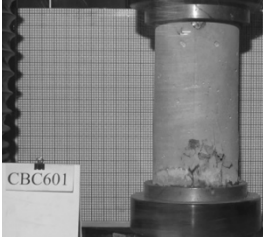
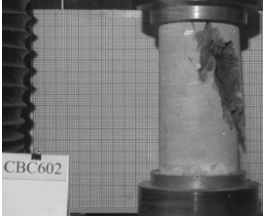
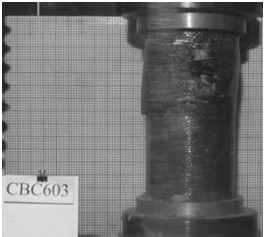
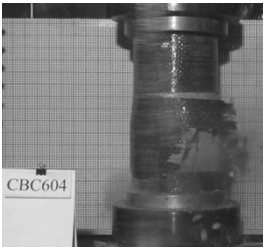


- Silva, M. A. G. and Rodrigues, C. C., Size and Relative Stiffness Effects on Compressive Failure of Concrete Columns Wrapped with Glass FRP, *Journal of Materials in Civil Engineering*, ASCE, Vol-18, No. 3, pp 334–342, 2006.
- Toutanji, H. A., Stress-Strain Characteristics of Concrete Columns Externally Confined with Advanced Fiber Composite Sheets, *ACI Materials Journal*, Vol. 96, No. 3, pp 483–490, 1999.
- Teng J.G., Chen J. F., Smith S. T. and Lam L., *FRP-Strengthened RC Structures*, John Wiley & Sons, Ltd., 2002.
- Thériault, M., Neale, K. W., and Claude, S., Fiber-Reinforced Polymer-Confined Circular Concrete Columns: Investigation of Size and Slenderness Effects, *Journal of Composites for Construction*, ASCE, Vol-8, No. 4, pp. 323-331, 2004.
- Wang, Y. F. and Wu, H. L., Size Effect of Concrete Short Columns Confined with Aramid FRP Jackets, *Journal of Composites for Construction*, ASCE, Vol-14, No. 4, pp 535-544, 2011.
- Wu, Y.F. and Wang, L.M., Unified Strength Model for Square and Circular Concrete Columns Confined by External Jacket, *Journal of Structural Engineering*, ASCE, Vol-135, No. 3, pp 253-261, 2009.
- Wu, H. L., Wang, Z. T., Yu, L. and Li, X. R., Experimental and Computational Studies on High-Strength Concrete Circular Columns Confined by Aramid Fiber-Reinforced Polymer Sheets, *Journal of Composites for Construction*, ASCE, Vol-13, No. 2, pp 125-134, 2009.
- Willam, K. J., and Warnke, E. D., Constitutive Model for the Triaxial Behavior of Concrete, *Proceedings, International Association for Bridge and Structural Engineering*, ISMES, Bergamo, Italy, Vol. 19, pp 1-30, 1975.
- Xiao, Y. and Wu, H., Compressive Behavior of Concrete Confined by Carbon Fiber Composite Jackets, *Journal of Materials in Civil Engineering*, ASCE, Vol-12, No. 2, pp 139–146, 2000.
- Yeh, F. and Chang, K., Size and Shape Effect on FRP Confinements for Rectangular Concrete Columns, 13<sup>th</sup> World Conference on Earthquake Engineering, Vancouver, B.C., Canada, Paper No. 657, 2004.
- Youssef, M. N., Feng, Q., and Mosallam, A. S., Stress-Strain Model for Concrete Confined by FRP Composites, *Composites: Part B*, Vol-38, pp 614–628, 2007.
- Zhu, Z., Ahmad, I., and Mirmiran, A., Effect of Column Parameters on Axial Compression Behavior of Concrete-Filled FRP Tubes, *Advanced Structural Engineering*, Vol-8, No.4, pp 443–449, 2005.

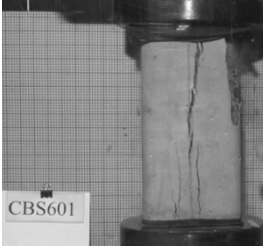

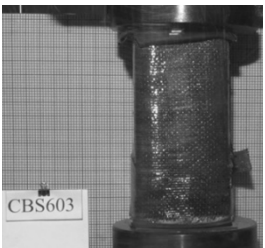
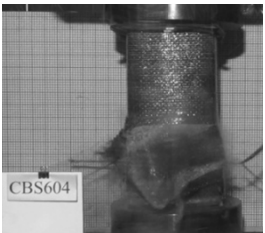
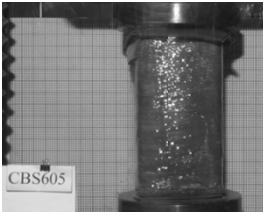
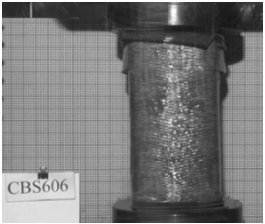
## APPENDIX A.1 Failure patterns of brick aggregate concrete columns

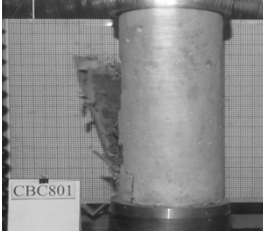
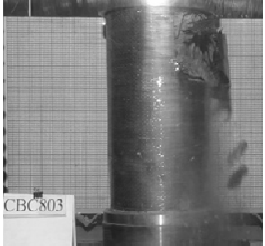

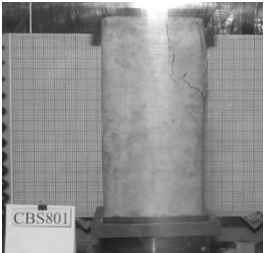
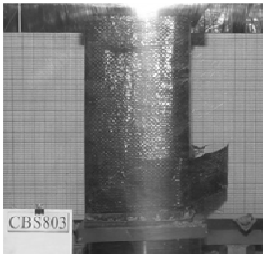

Table 5.1: Failure patterns of brick aggregate concrete columns

Column ID	Type of confinement	Failure location	Failure type	Figure
CBC401	Unconfined	Bottom	Crushing of concrete	
CBC402	Unconfined	Bottom	Crushing of concrete	
CBC403	Confined with CFRP	Bottom	FRP rapture and bursting of concrete	
CBC404	Confined with CFRP	Middle	FRP rapture and bursting of concrete	
CBC405	Confined with GFRP	Middle to bottom	FRP rapture and crushing of concrete	
CBC406	Confined with GFRP	Middle	FRP rapture and crushing of concrete	

Column ID	Type of confinement	Failure location	Failure type	Figure
CBS401	Unconfined	Top to bottom	Split	
CBS402	Unconfined	Top and Bottom corner	Crushing of concrete	
CBS403	Confined with CFRP	Bottom	FRP rapture and crushing of concrete	
CBS404	Confined with CFRP	Bottom	FRP rapture and bursting of concrete	
CBS405	Confined with GFRP	Bottom	FRP rapture and crushing of concrete	
CBS406	Confined with GFRP	Top	FRP rapture and crushing of concrete	

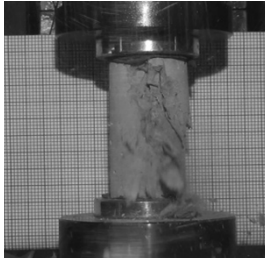
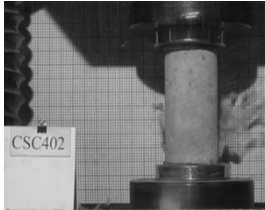
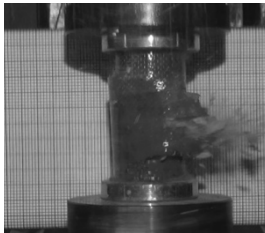
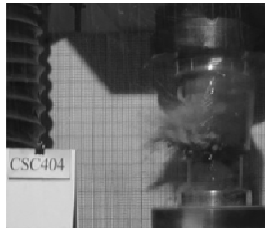
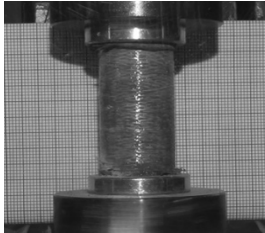
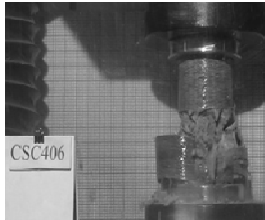
Column ID	Type of confinement	Failure location	Failure type	Figure
CBC601	Unconfined	Bottom	Crushing of concrete	
CBC602	Unconfined	Top to middle	Crushing of concrete	
CBC603	Confined with CFRP	Top to middle	FRP rapture and crushing of concrete	
CBC604	Confined with CFRP	Middle	FRP rapture and bursting of concrete	
CBC605	Confined with GFRP	Middle	FRP rapture and bursting of concrete	
CBC606	Confined with GFRP	Bottom	FRP rapture and crushing of concrete	

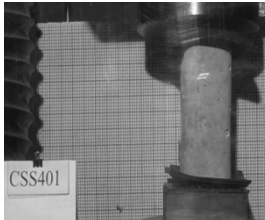

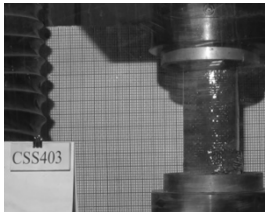
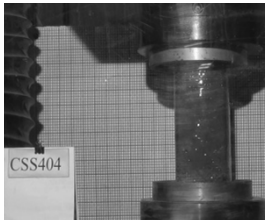


Column ID	Type of confinement	Failure location	Failure type	Figure
CBS601	Unconfined	Top to bottom	Split	
CBS602	Unconfined	Top and Bottom corner	Crushing of concrete	
CBS603	Confined with CFRP	Middle	FRP rapture and crushing of concrete	
CBS604	Confined with CFRP	Middle	FRP rapture and bursting of concrete	
CBS605	Confined with GFRP	Top	FRP rapture and crushing of concrete	
CBS606	Confined with GFRP	Top	FRP rapture and crushing of concrete	

Column ID	Type of confinement	Failure location	Failure type	Figure
CBC801	Unconfined	Middle	Crushing of concrete	
CBC803	Confined with CFRP	Top	FRP rapture and crushing of concrete	
CBC805	Confined with GFRP	Middle	FRP rapture and bursting of concrete	
CBS801	Unconfined	Top	Crushing of concrete	
CBS803	Confined with CFRP	Top and Bottom corner	FRP rapture and crushing of concrete	
CBS805	Confined with GFRP	Top	FRP rapture and crushing of concrete	


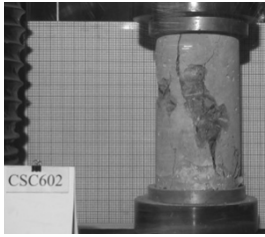
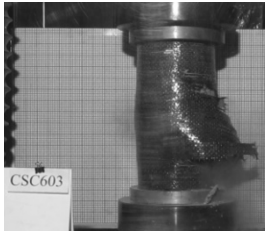
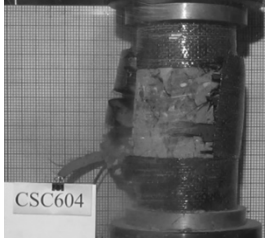
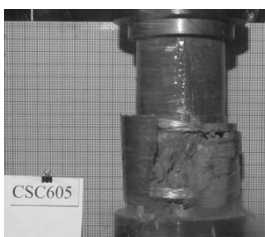
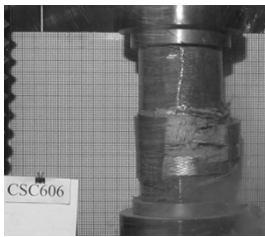
## APPENDIX A.2 Failure patterns of stone aggregate concrete columns


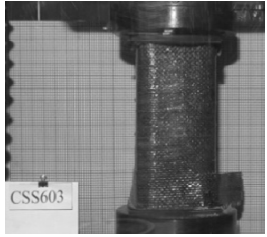
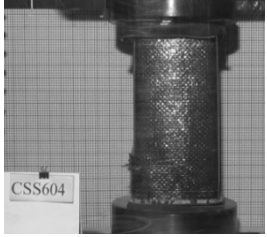
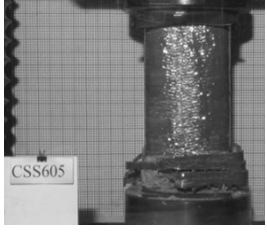

Table 5.2: Failure patterns of stone aggregate concrete columns

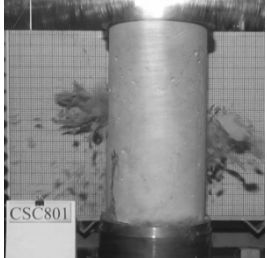

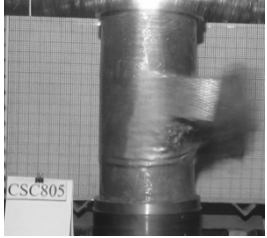
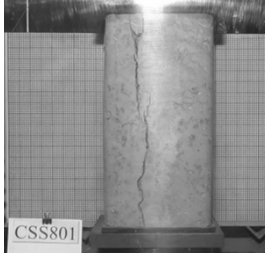
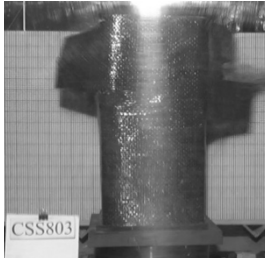
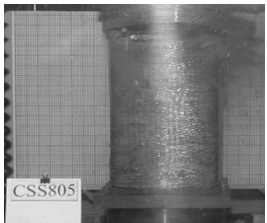
Column ID	Type of confinement	Failure location	Failure type	Figure
CSC401	Unconfined	Top to bottom	Crushing of concrete	
CSC402	Unconfined	Middle	Crushing of concrete	
CSC403	Confined with CFRP	Middle	FRP rapture and bursting of concrete	
CSC404	Confined with CFRP	Middle	FRP rapture and bursting of concrete	
CSC405	Confined with GFRP	Bottom	FRP rapture and crushing of concrete	
CSC406	Confined with GFRP	Bottom	FRP rapture and bursting of concrete	

Column ID	Type of confinement	Failure location	Failure type	Figure
CSS401	Unconfined	Bottom	Crushing of concrete	
CSS402	Unconfined	Bottom	Crushing of concrete	
CSS403	Confined with CFRP	Bottom	FRP rapture and crushing of concrete	
CSS404	Confined with CFRP	Top	FRP rapture and crushing of concrete	
CSS405	Confined with GFRP	Bottom	FRP rapture and crushing of concrete	
CSS406	Confined with GFRP	Bottom	FRP rapture and crushing of concrete	




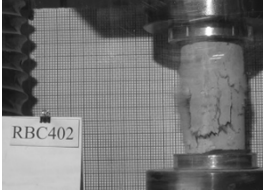
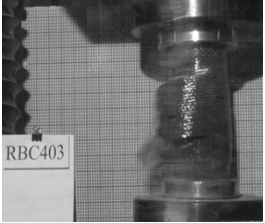
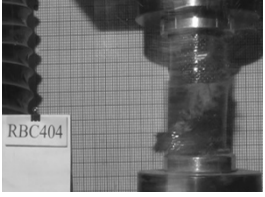
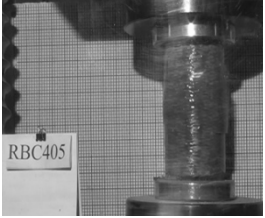
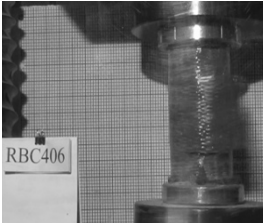
Column ID	Type of confinement	Failure location	Failure type	Figure
CSC601	Unconfined	Top	Crushing of concrete	
CSC602	Unconfined	Middle	Crushing of concrete	
CSC603	Confined with CFRP	Middle	FRP rapture and bursting of concrete	
CSC604	Confined with CFRP	Middle	FRP rapture and bursting of concrete	
CSC605	Confined with GFRP	Bottom	FRP rapture and bursting of concrete	
CSC606	Confined with GFRP	Bottom	FRP rapture and bursting of concrete	

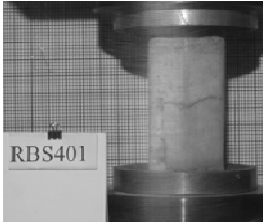
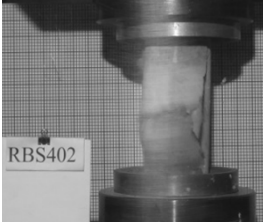
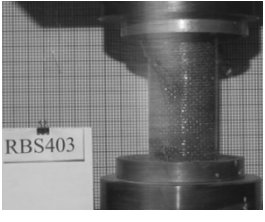
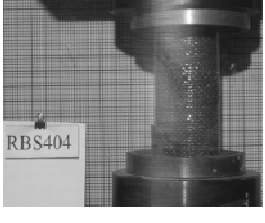
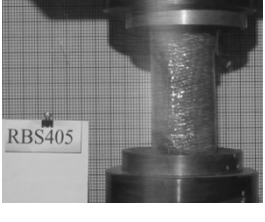
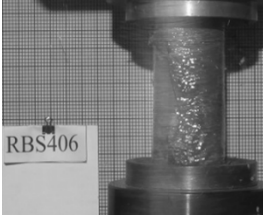
Column ID	Type of confinement	Failure location	Failure type	Figure
CSS601	Unconfined	Top	Concrete crushing	
CSS602	Unconfined	Wasted due to mishandling during testing.		
CSS603	Confined with CFRP	Bottom	FRP rapture and bursting of concrete	
CSS604	Confined with CFRP	Bottom	FRP rapture and crushing of concrete	
CSS605	Confined with GFRP	Bottom	FRP rapture and bursting of concrete	
CSS606	Confined with GFRP	Bottom	FRP rapture and bursting of concrete	

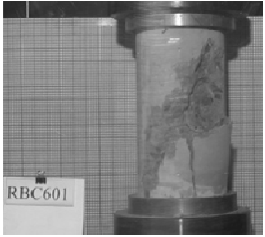

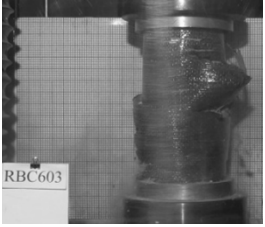
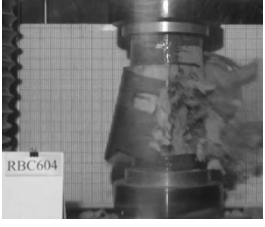
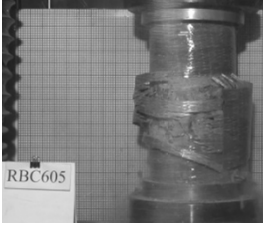

Column ID	Type of confinement	Failure location	Failure type	Figure
CSC801	Unconfined	Middle	Concrete crushing	
CSC803	Confined with CFRP	Middle	FRP rapture and bursting of concrete	
CSC805	Confined with GFRP	Middle	FRP rapture and bursting of concrete	
CSS801	Unconfined	Top to bottom	Split	
CSS803	Confined with CFRP	Top	FRP rapture and bursting of concrete	
CSS805	Confined with GFRP	Top	FRP rapture and crushing of concrete	

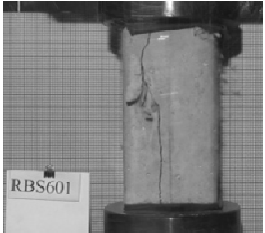
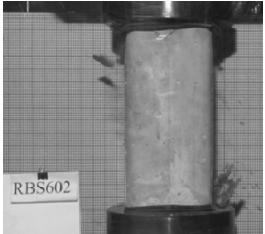
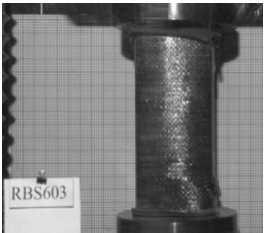
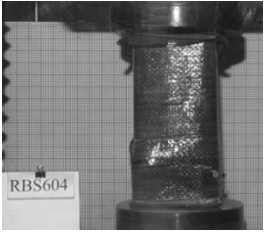
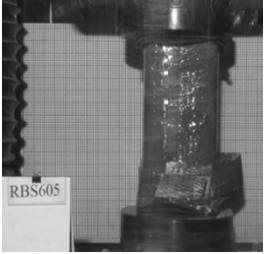

### APPENDIX A.3 Failure patterns of recycled brick aggregate concrete columns

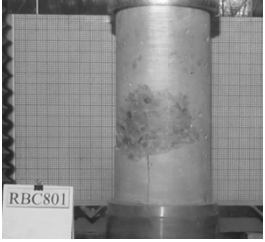


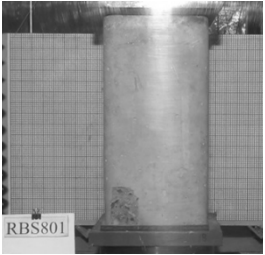
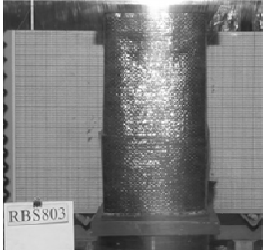

Table 5.3: Failure patterns of recycled brick aggregate concrete columns

Column ID	Type of confinement	Failure location	Failure type	Figure
RBC401	Unconfined	Bottom	Crushing of concrete	
RBC402	Unconfined	Middle	Crushing of concrete	
RBC403	Confined with CFRP	Middle	FRP rapture and bursting of concrete	
RBC404	Confined with CFRP	Middle	FRP rapture and bursting of concrete	
RBC405	Confined with GFRP	Middle	FRP rapture and crushing of concrete	
RBC406	Confined with GFRP	Middle	FRP rapture and crushing of concrete	

Column ID	Type of confinement	Failure location	Failure type	Figure
RBS401	Unconfined	Top to bottom	Split	
RBS402	Unconfined	Top to bottom	Crushing of concrete	
RBS403	Confined with CFRP	Top	FRP rapture and crushing of concrete	
RBS404	Confined with CFRP	Bottom	FRP rapture and crushing of concrete	
RBS405	Confined with GFRP	Top	FRP rapture and crushing of concrete	
RBS406	Confined with GFRP	Top	FRP rapture and crushing of concrete	

Column ID	Type of confinement	Failure location	Failure type	Figure
RBC601	Unconfined	Top to bottom	Crushing of concrete	
RBC602	Unconfined	Middle to bottom	Crushing of concrete	
RBC603	Confined with CFRP	Middle	FRP rapture and bursting of concrete	
RBC604	Confined with CFRP	Middle	FRP rapture and bursting of concrete	
RBC605	Confined with GFRP	Middle	FRP rapture and bursting of concrete	
RBC606	Confined with GFRP	Bottom	FRP rapture and bursting of concrete	

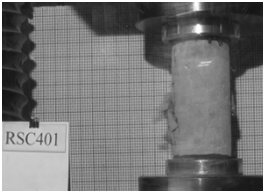
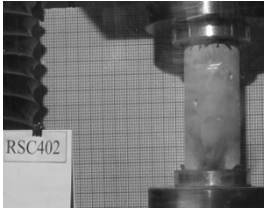
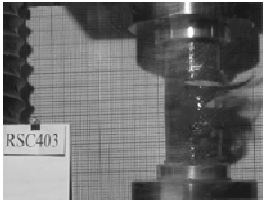
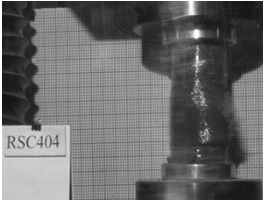
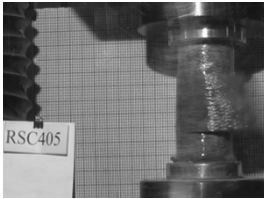
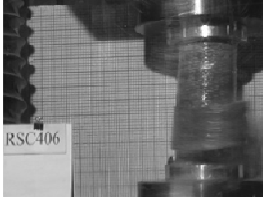
Column ID	Type of confinement	Failure location	Failure type	Figure
RBS601	Unconfined	Top to bottom	Split	
RBS602	Unconfined	Top and bottom corner	Crushing of concrete	
RBS603	Confined with CFRP	Bottom	FRP rapture and crushing of concrete	
RBS604	Confined with CFRP	Middle to bottom	FRP rapture and crushing of concrete	
RBS605	Confined with GFRP	Bottom	FRP rapture and bursting of concrete	
RBS606	Confined with GFRP	Bottom	FRP rapture and crushing of concrete	

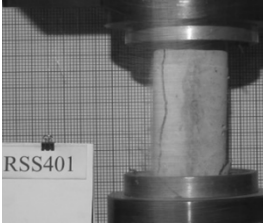

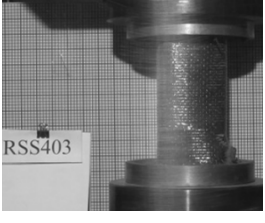
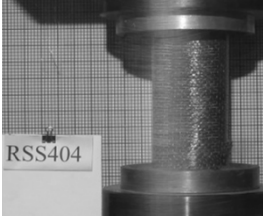
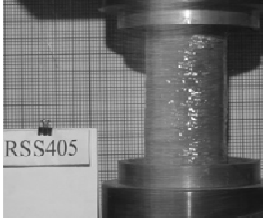
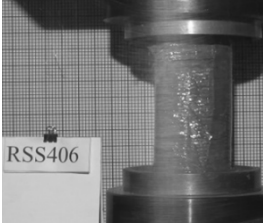
Column ID	Type of confinement	Failure location	Failure type	Figure
RBC801	Unconfined	Middle	Crushing of concrete	
RBC803	Confined with CFRP	Bottom	FRP rapture and crushing of concrete	
RBC805	Confined with GFRP	Top	FRP rapture and crushing of concrete	
RBS801	Unconfined	Bottom corner	Crushing of concrete	
RBS803	Confined with CFRP	Bottom	FRP rapture and crushing of concrete	
RBS805	Confined with GFRP	Top	FRP rapture and bursting of concrete	

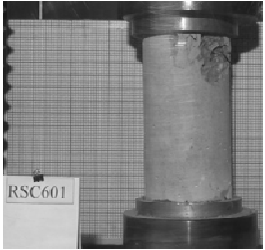


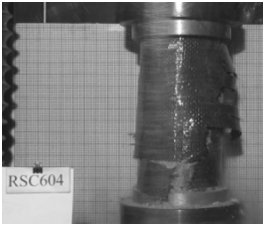
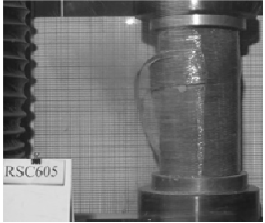
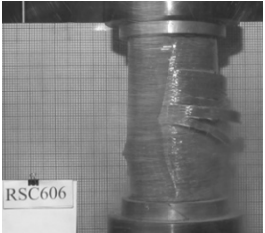




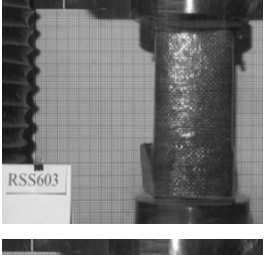
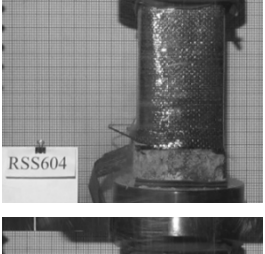
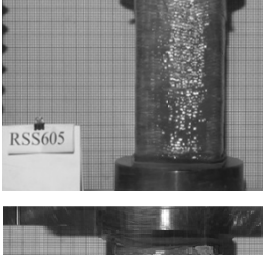

## APPENDIX A.4 Failure patterns of recycled stone aggregate concrete columns




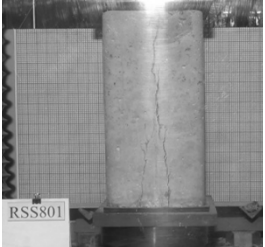
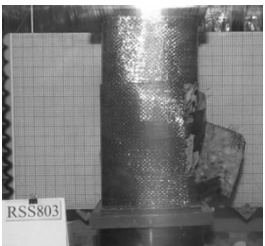
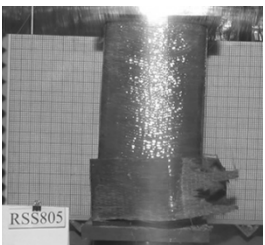
Table 5.4: Failure patterns of recycled stone aggregate concrete columns

Column ID	Type of confinement	Failure location	Failure type	Figure
RSC401	Unconfined	Middle	Crushing of concrete	
RSC402	Unconfined	Bottom	Crushing of concrete	
RSC403	Confined with CFRP	Middle	FRP rapture and bursting of concrete	
RSC404	Confined with CFRP	Middle	FRP rapture and bursting of concrete	
RSC405	Confined with GFRP	Middle	FRP rapture and bursting of concrete	
RSC406	Confined with GFRP	Bottom	FRP rapture and bursting of concrete	

Column ID	Type of confinement	Failure location	Failure type	Figure
RSS401	Unconfined	Top to bottom	Crushing of concrete	
RSS402	Unconfined	Bottom corner	Crushing of concrete	
RSS403	Confined with CFRP	Bottom	FRP rapture and crushing of concrete	
RSS404	Confined with CFRP	Bottom	FRP rapture and crushing of concrete	
RSS405	Confined with GFRP	Bottom	FRP rapture and crushing of concrete	
RSS406	Confined with GFRP	Top	FRP rapture and crushing of concrete	

Column ID	Type of confinement	Failure location	Failure type	Figure
RSC601	Unconfined	Top	Crushing of concrete	
RSC602	Unconfined	Bottom	Crushing of concrete	
RSC603	Confined with CFRP	Top	FRP rapture and crushing of concrete	
RSC604	Confined with CFRP	Middle	FRP rapture and bursting of concrete	
RSC605	Confined with GFRP	Middle	FRP rapture and bursting of concrete	
RSC606	Confined with GFRP	Middle	FRP rapture and bursting of concrete	

Column ID	Type of confinement	Failure location	Failure type	Figure
RSS601	Unconfined	Top to bottom	Split	
RSS602	Unconfined	Top and bottom corner	Crushing of concrete	
RSS603	Confined with CFRP	Bottom	FRP rapture and crushing of concrete	
RSS604	Confined with CFRP	Bottom	FRP rapture and bursting of concrete	
RSS605	Confined with GFRP	Top	FRP rapture and crushing of concrete	
RSS606	Confined with GFRP	Top	FRP rapture and crushing of concrete	

Column ID	Type of confinement	Failure location	Failure type	Figure
RSC801	Unconfined	Top	Crushing of concrete	
RSC803	Confined with CFRP	Middle	FRP rapture and bursting of concrete	
RSC805	Confined with GFRP	Top to middle	FRP rapture and crushing of concrete	
RSS801	Unconfined	Top to bottom	Split	
RSS803	Confined with CFRP	Middle to bottom	FRP rapture and crushing of concrete	
RSS805	Confined with GFRP	Bottom	FRP rapture and crushing of concrete	

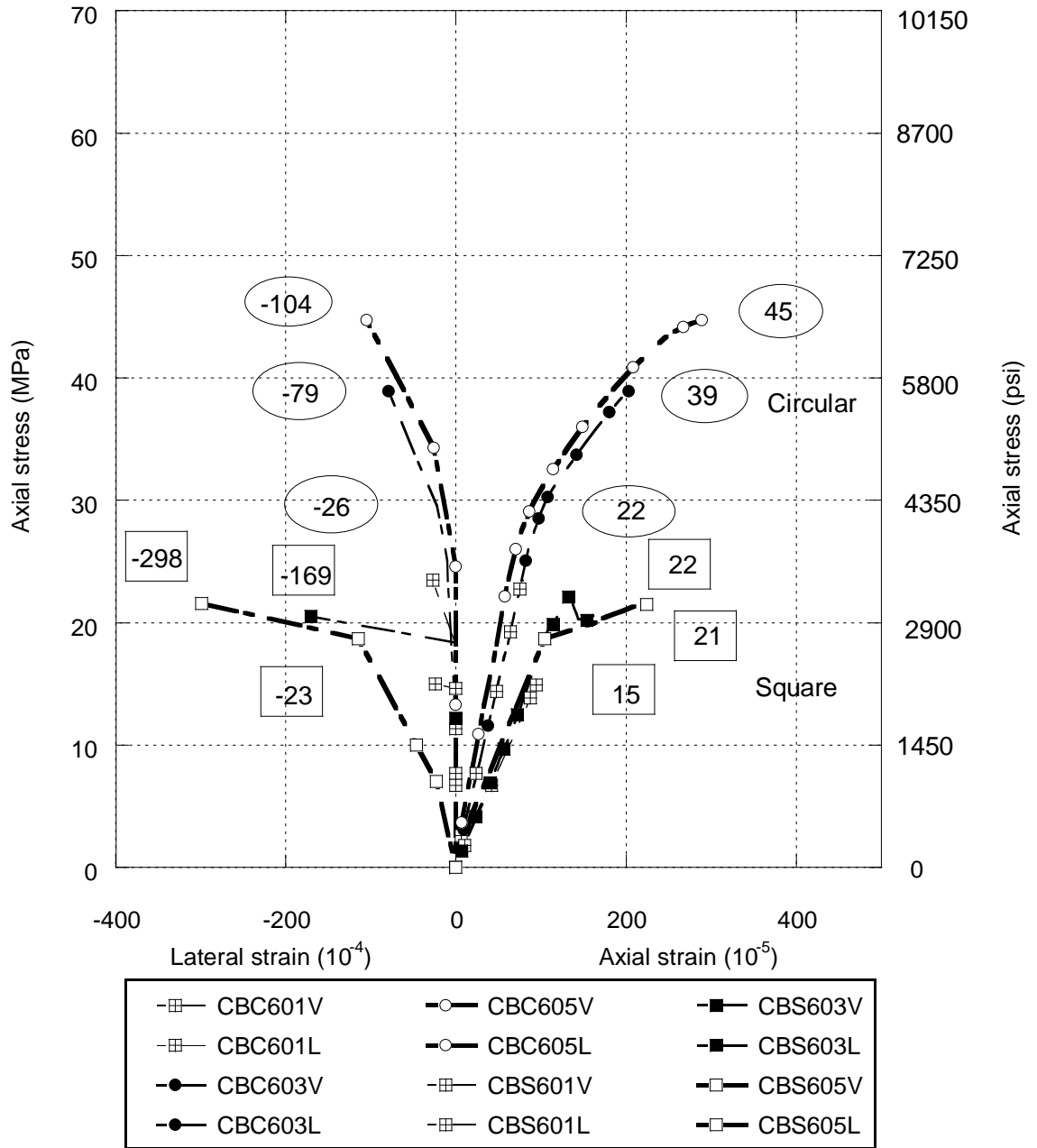


Figure 5.13: Stress-strain behaviours of unconfined and confined circular and square columns made of brick aggregate concrete. Numbers appear in the circles and squares are peak axial stress and peak lateral strain of circular and square columns respectively (MPa).  $\square$  Unconfined column,  $\bullet$  CFRP confined circular column,  $\circ$  GFRP confined circular column,  $\blacksquare$  CFRP confined square column,  $\square$  GFRP confined square column.

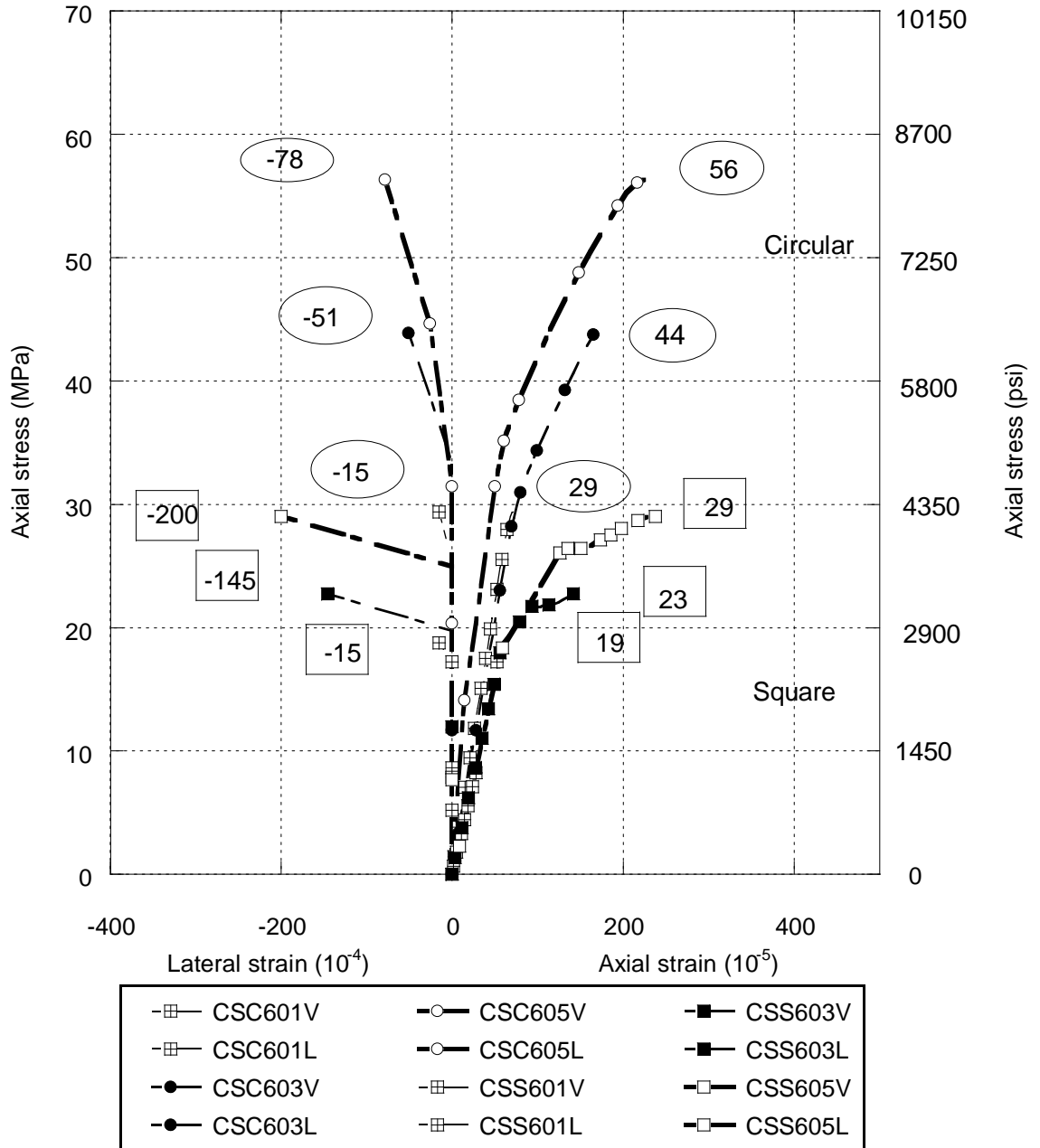


Figure 5.14: Stress-strain behaviours of unconfined and confined circular and square columns made of stone aggregate concrete. Numbers appear in the circles and squares are peak axial stress and peak lateral strain of circular and square columns respectively (MPa).  $\square$  Unconfined column,  $\bullet$  CFRP confined circular column,  $\circ$  GFRP confined circular column,  $\blacksquare$  CFRP confined square column,  $\square$  GFRP confined square column.

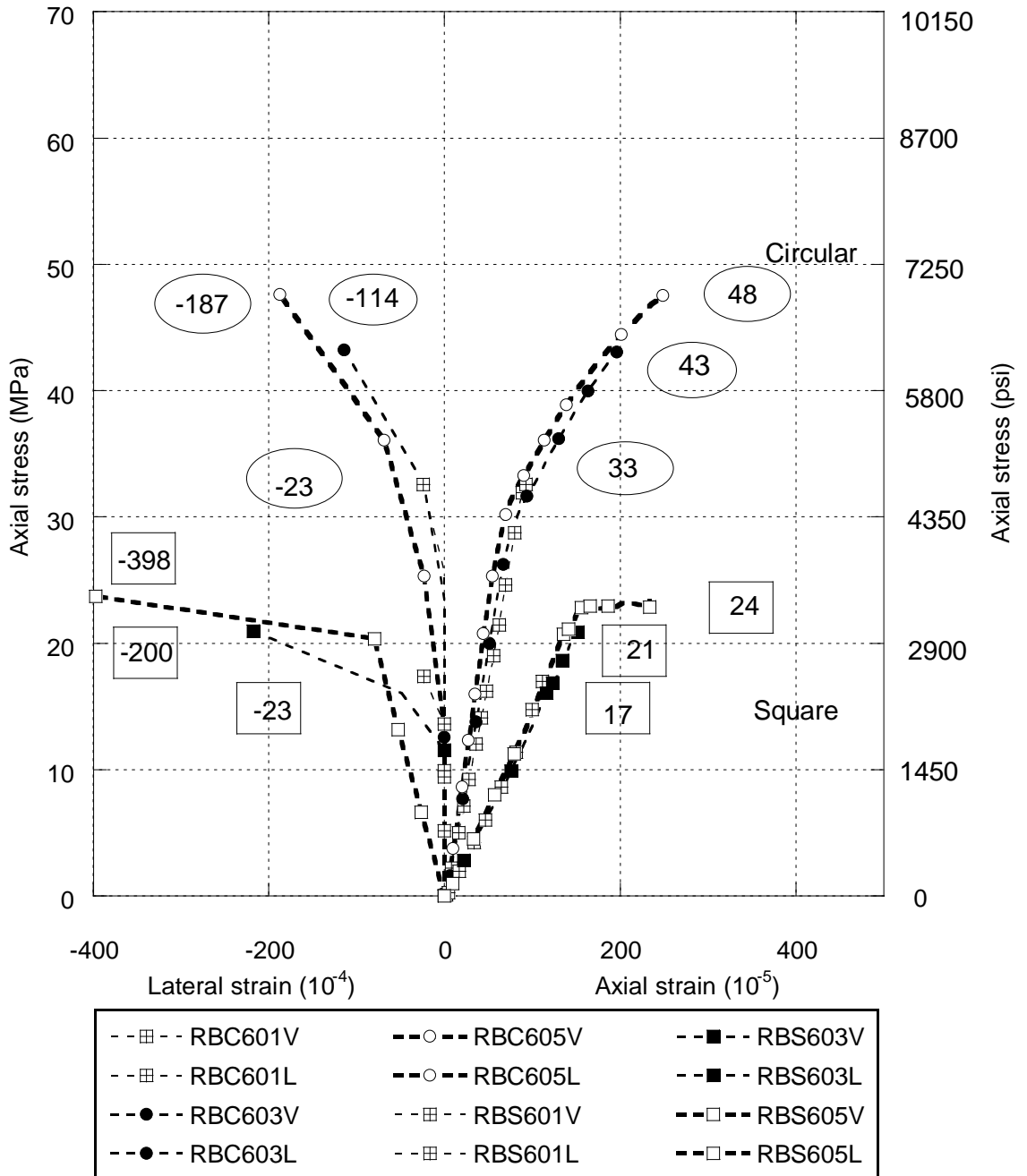


Figure 5.15: Stress-strain behaviours of unconfined and confined circular and square columns made of recycled brick aggregate concrete. Numbers appear in the circles and squares are peak axial stress and peak lateral strain of circular and square columns respectively (MPa)  $\square$  Unconfined column,  $\bullet$  CFRP confined circular column,  $\circ$  GFRP confined circular column,  $\blacksquare$  CFRP confined square column,  $\square$  GFRP confined square column.



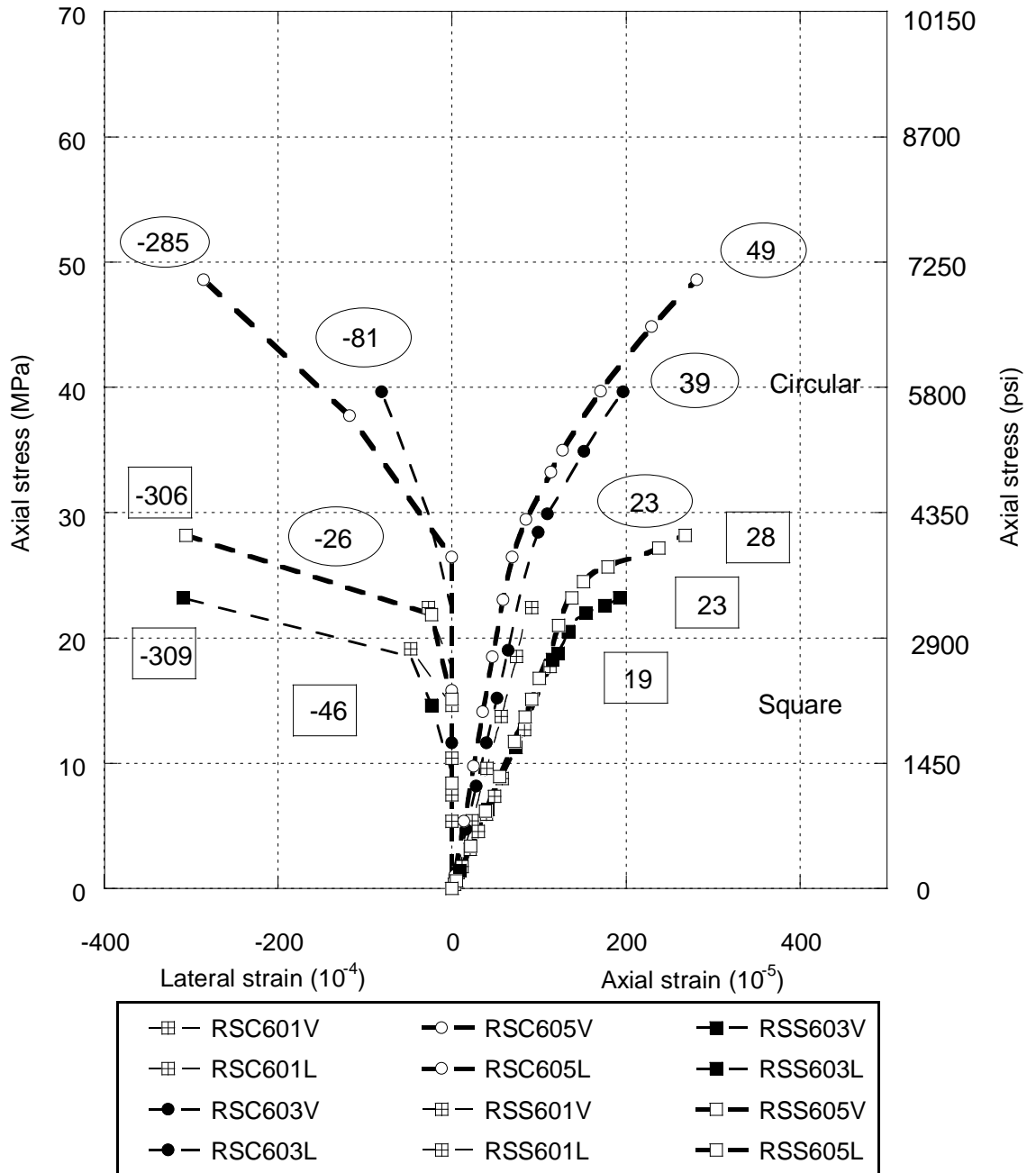


Figure 5.16: Stress-strain behaviours of unconfined and confined circular and square columns made of recycled stone aggregate concrete. Numbers appear in the circles and squares are peak axial stress and peak lateral strain of circular and square columns respectively (MPa).  $\boxplus$  Unconfined column,  $\bullet$  CFRP confined circular column,  $\circ$  GFRP confined circular column,  $\blacksquare$  CFRP confined square column,  $\square$  GFRP confined square column.

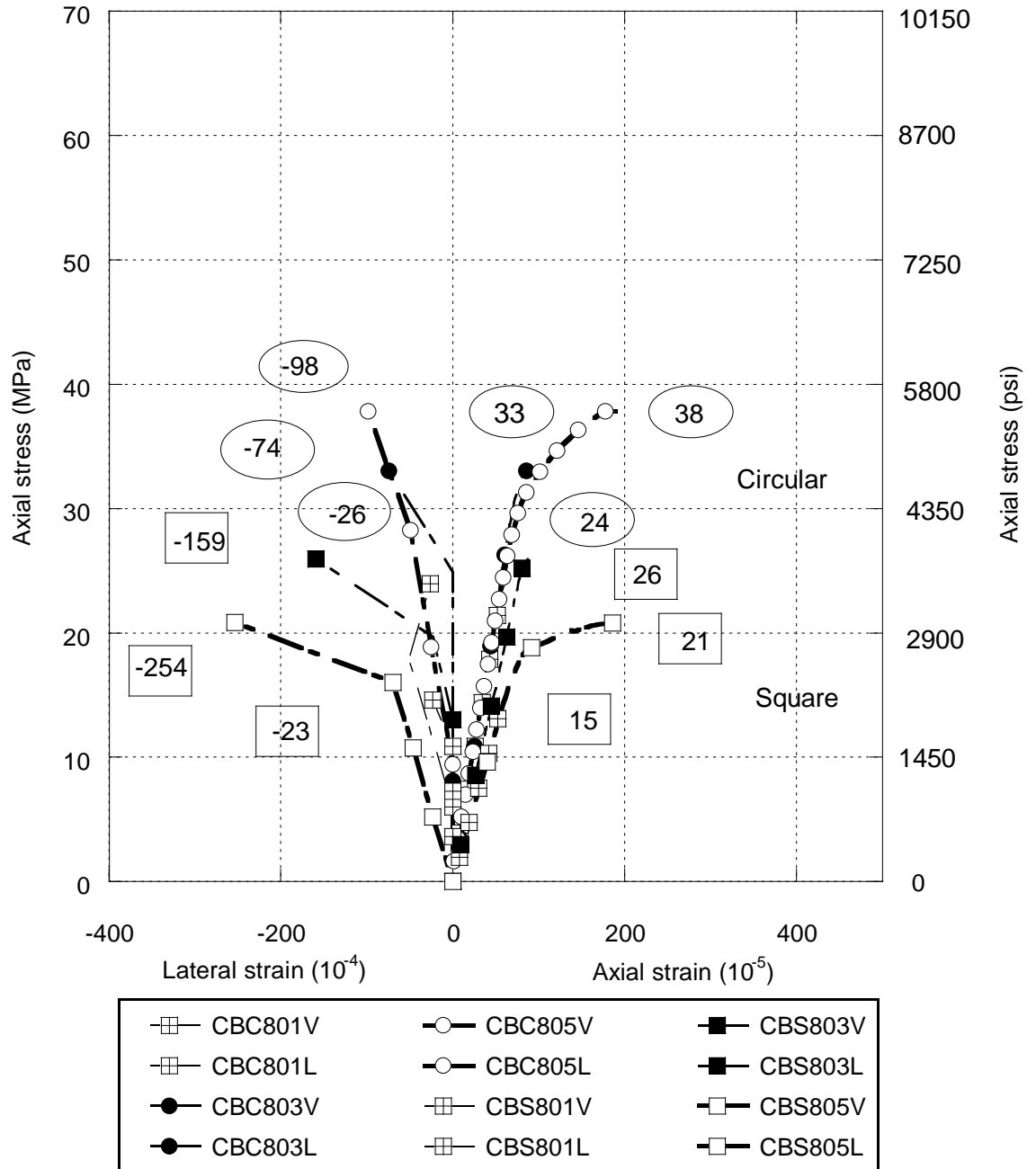


Figure 5.17: Stress-strain behaviours of unconfined and confined circular and square columns made of brick aggregate concrete. Numbers appear in the circles and squares are peak axial stress and peak lateral strain of circular and square columns respectively (MPa). ▣ Unconfined column, ● CFRP confined circular column, ○ GFRP confined circular column, ■ CFRP confined square column, ▣ GFRP confined square column.

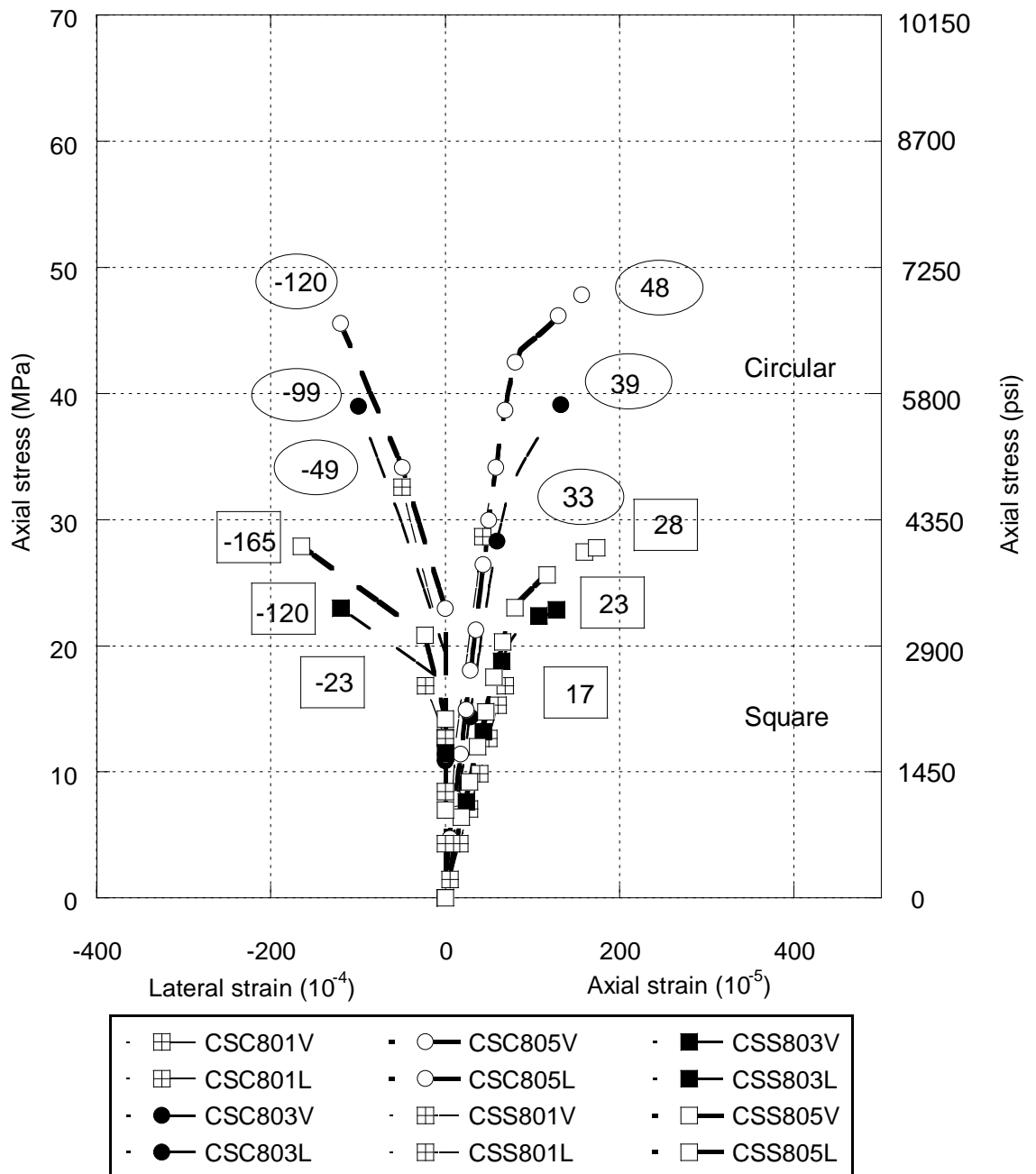


Figure 5.18: Stress-strain behaviours of unconfined and confined circular and square columns made of stone aggregate concrete. Numbers appear in the circles and squares are peak axial stress and peak lateral strain of circular and square columns respectively (MPa). ▣ Unconfined column, ● CFRP confined circular column, ○ GFRP confined circular column, ■ CFRP confined square column, ▣ GFRP confined square column.

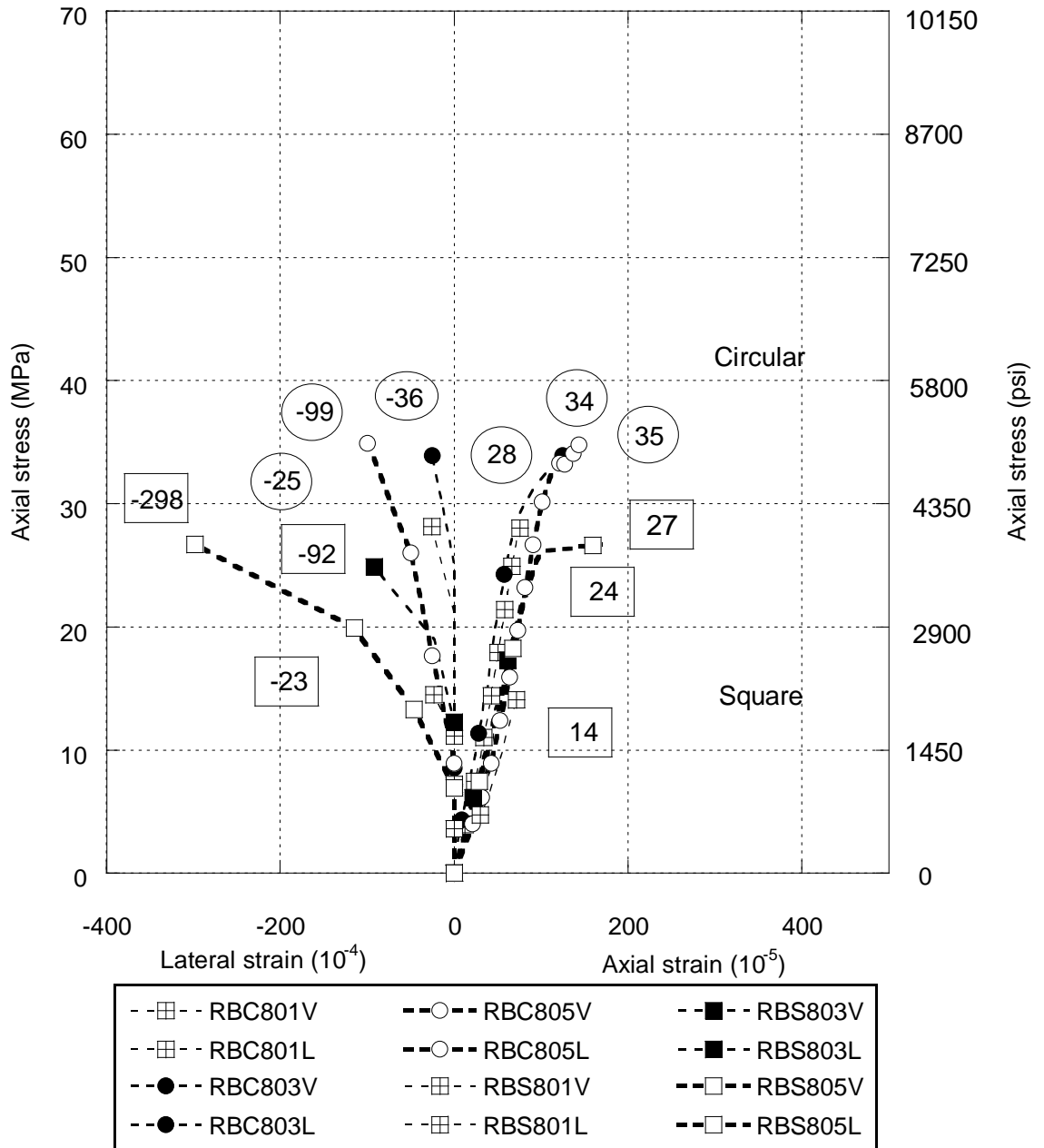


Figure 5.19: Stress-strain behaviours of unconfined and confined circular and square columns made of recycled brick aggregate concrete. Numbers appear in the circles and squares are peak axial stress and peak lateral strain of circular and square columns respectively (MPa).  $\square$  Unconfined column,  $\bullet$  CFRP confined circular column,  $\circ$  GFRP confined circular column,  $\blacksquare$  CFRP confined square column,  $\square$  GFRP confined square column.

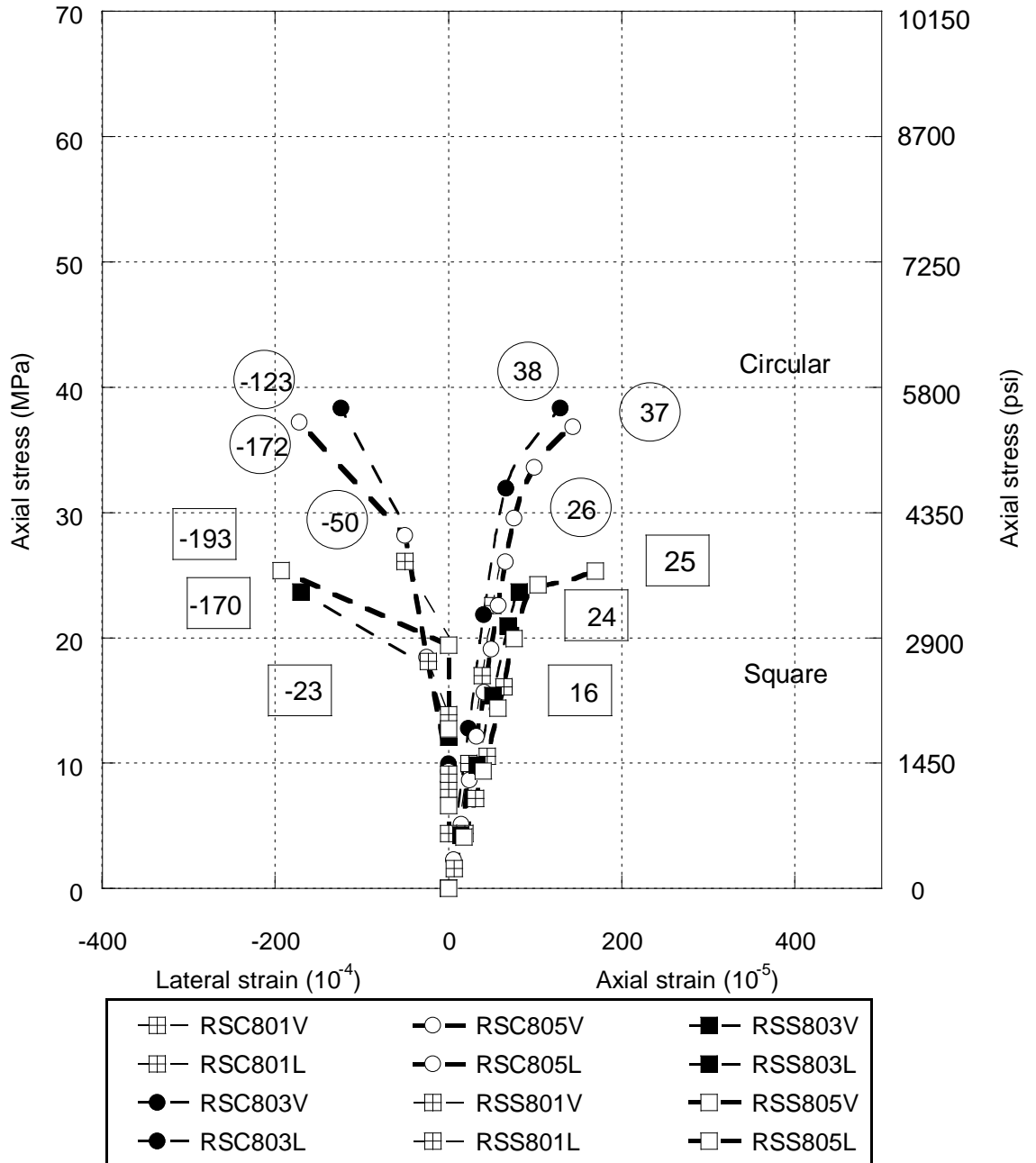
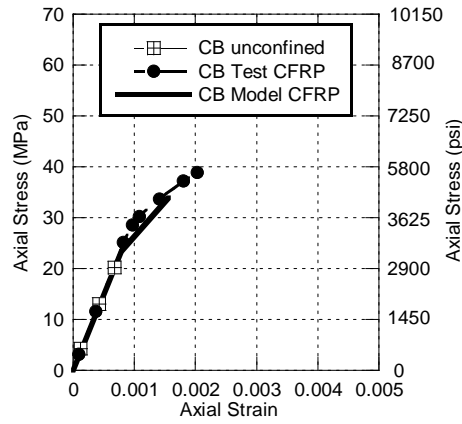
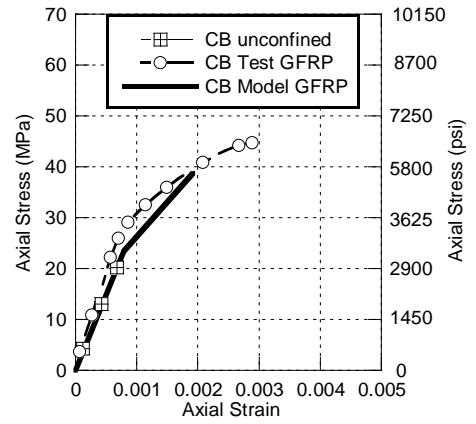


Figure 5.20: Stress-strain behaviours of unconfined and confined circular and square columns made of recycled stone aggregate concrete. Numbers appear in the circles and squares are peak axial stress and peak lateral strain of circular and square columns respectively (MPa). ⊠ Unconfined column, ● CFRP confined circular column, ○ GFRP confined circular column, ■ CFRP confined square column, □ GFRP confined square column.

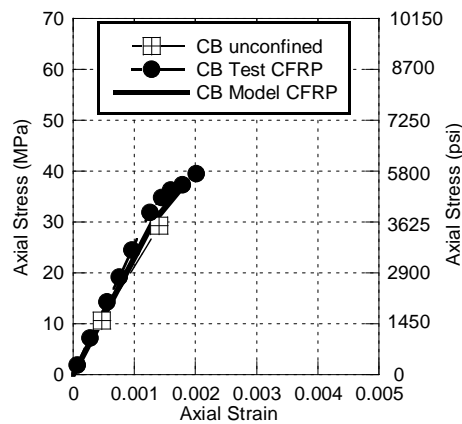


(a)

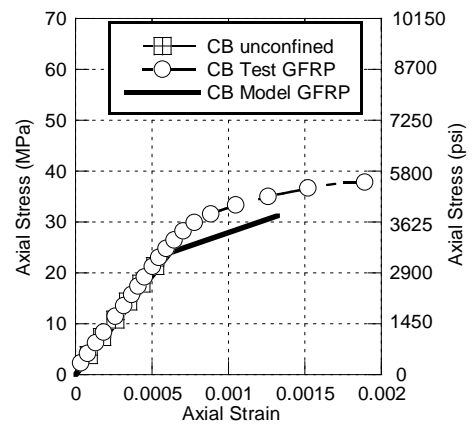


(b)

Figure 7.22: Model of 150 mm diameter circular column made of brick aggregate (a) confined with CFRP (b) confined with GFRP.

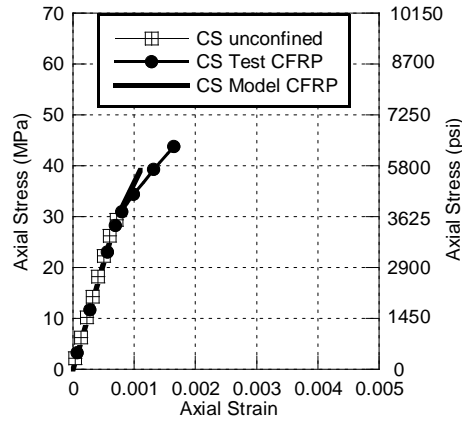


(a)

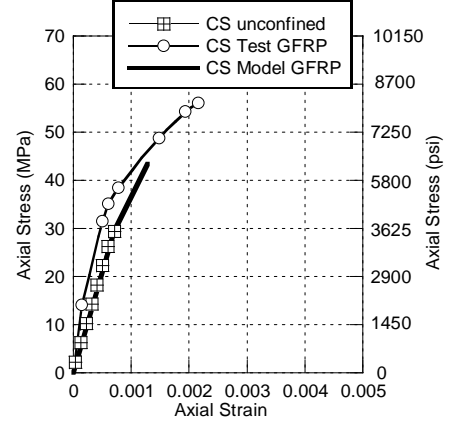


(b)

Figure 7.23: Model of 200 mm diameter circular column made of brick aggregate (a) confined with CFRP (b) confined with GFRP.

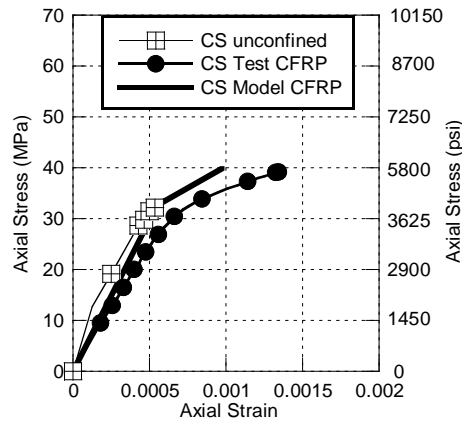


(a)

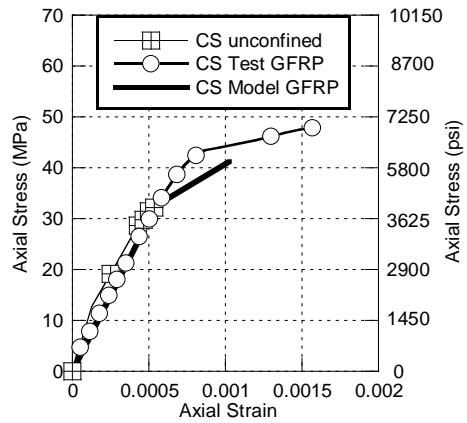


(b)

Figure 7.24: Model of 150 mm diameter circular column made of stone aggregate (a) confined with CFRP (b) confined with GFRP.

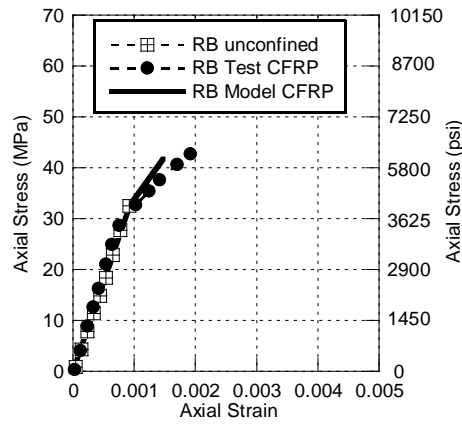


(a)

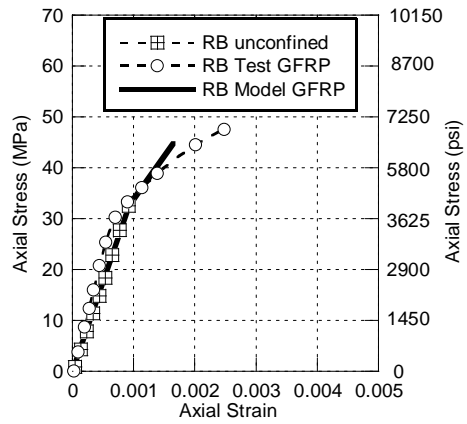


(b)

Figure 7.25: Model of 200 mm diameter circular column made of stone aggregate (a) confined with CFRP (b) confined with GFRP.

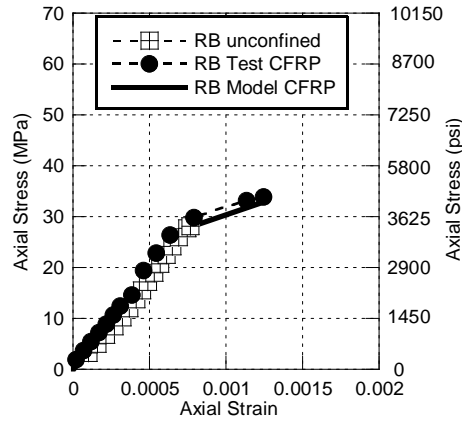


(a)

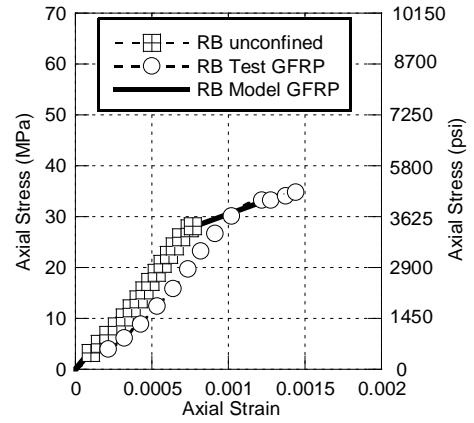


(b)

Figure 7.26: Model of 150 mm diameter circular column made of recycled brick aggregate (a) confined with CFRP (b) confined with GFRP.

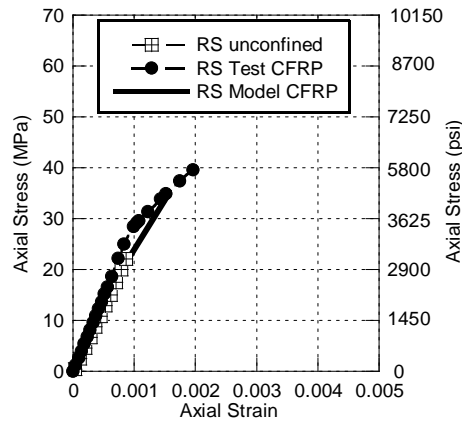


(a)

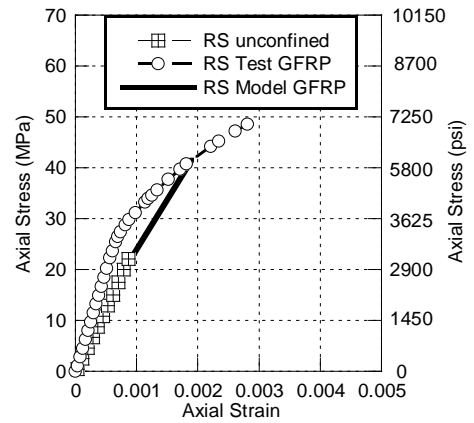


(b)

Figure 7.27: Model of 200 mm diameter circular column made of recycled brick aggregate (a) confined with CFRP (b) confined with GFRP.

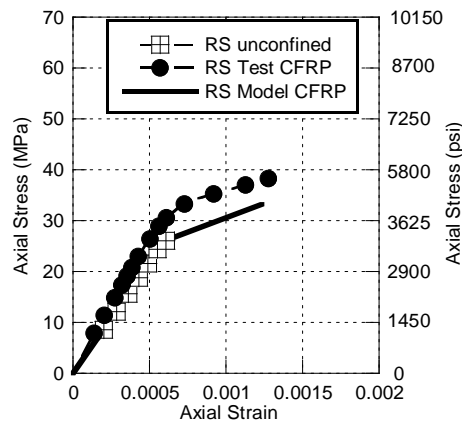


(a)

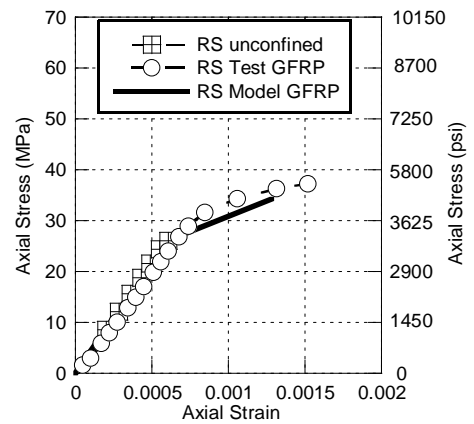


(b)

Figure 7.28: Model of 150 mm diameter circular column made of recycled stone aggregate (a) confined with CFRP (b) confined with GFRP.



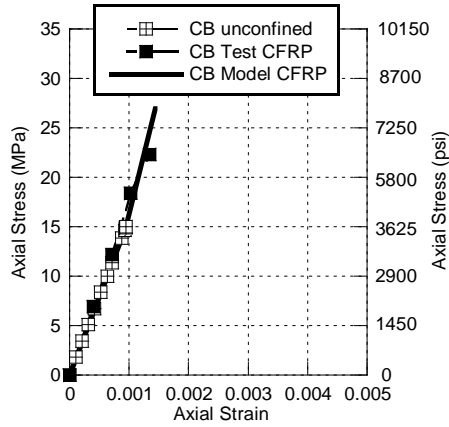
(a)



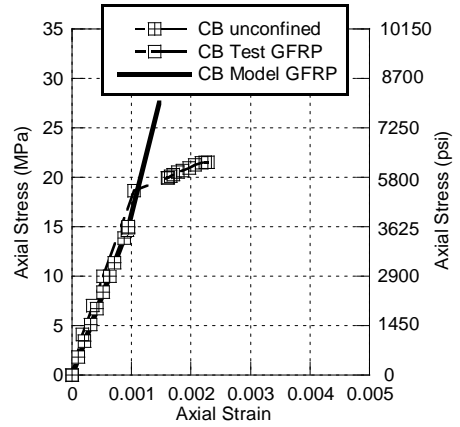
(b)

Figure 7.29: Model of 200 mm diameter circular column made of recycled stone aggregate (a) confined with CFRP (b) confined with GFRP.



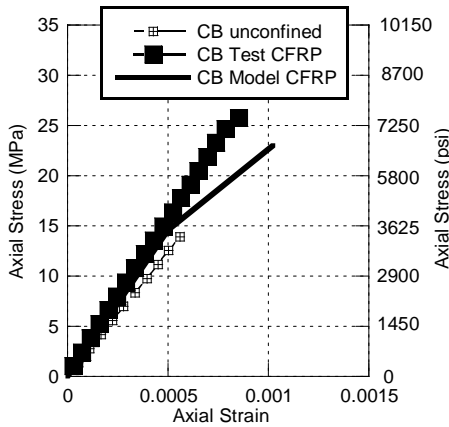


(a)

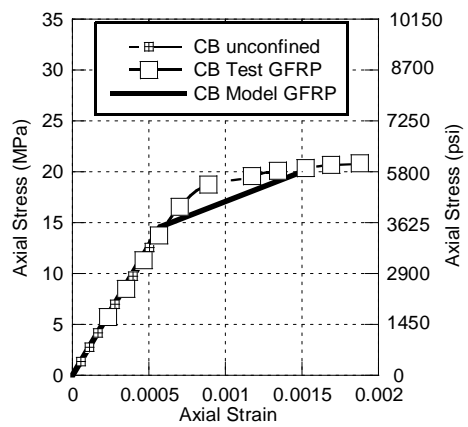


(b)

Figure 7.30: Model of 150 mm x 150 mm size square column made of brick aggregate (a) confined with CFRP (b) confined with GFRP.

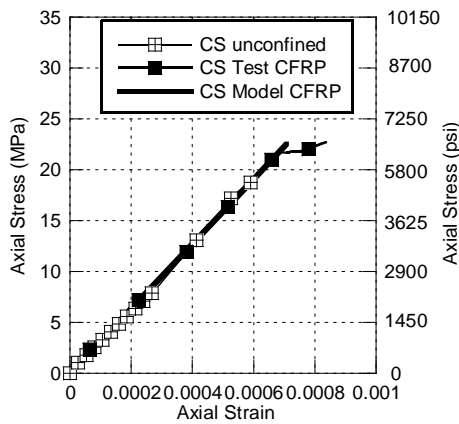


(a)

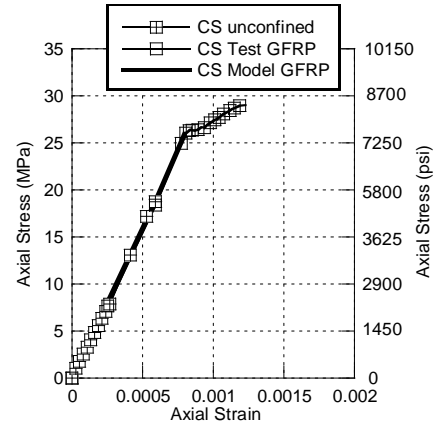


(b)

Figure 7.31: Model of 200 mm x 200 mm size square column made of brick aggregate (a) confined with CFRP (b) confined with GFRP.

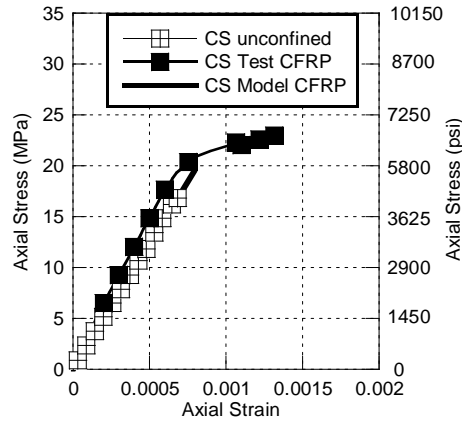


(a)

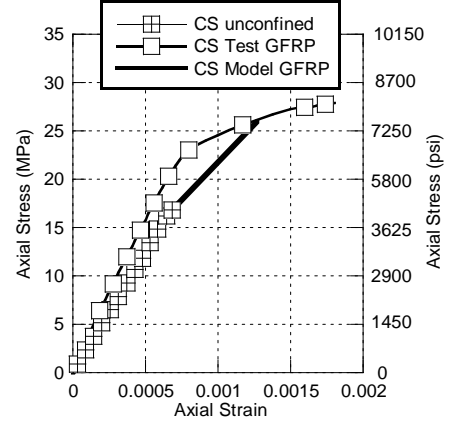


(b)

Figure 7.32: Model of 150 mm x 150 mm size square column made of stone aggregate (a) confined with CFRP (b) confined with GFRP.

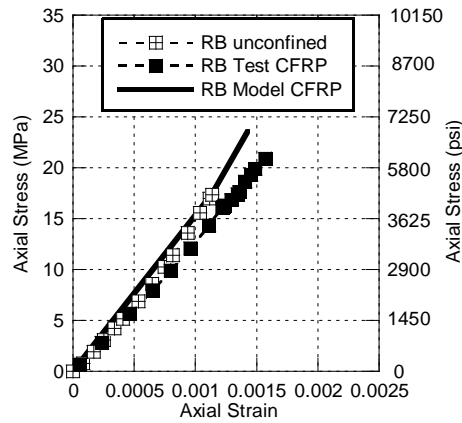


(a)

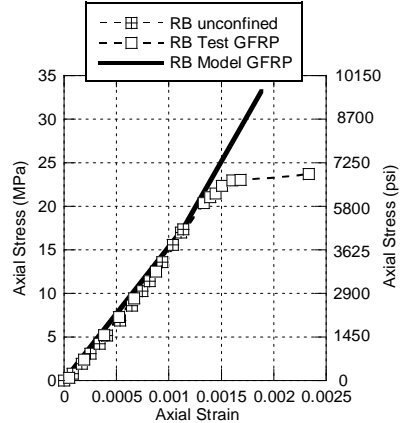


(b)

Figure 7.33: Model of 200 mm x 200 mm size square column made of stone aggregate (a) confined with CFRP (b) confined with GFRP.

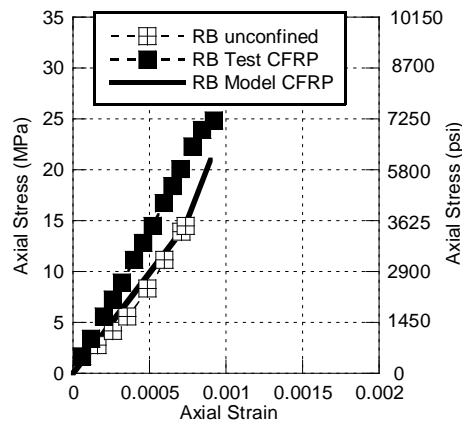


(a)

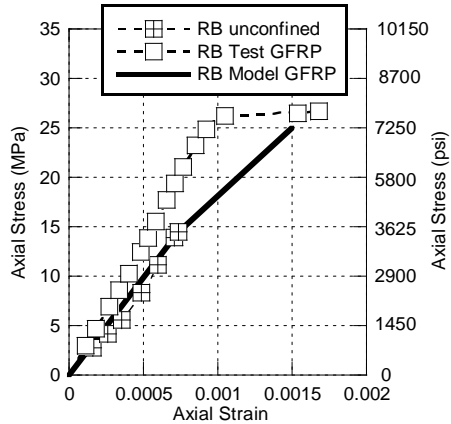


(b)

Figure 7.34: Model of 150 mm x 150 mm size square column made of recycled brick aggregate (a) confined with CFRP (b) confined with GFRP.

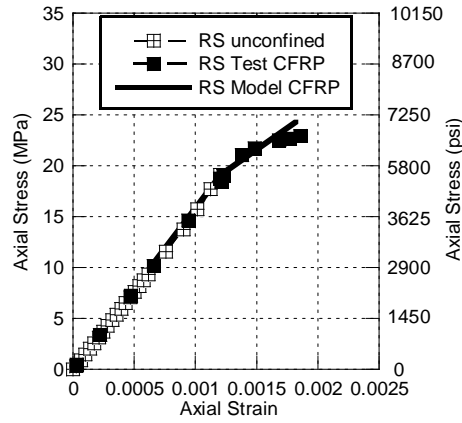


(a)

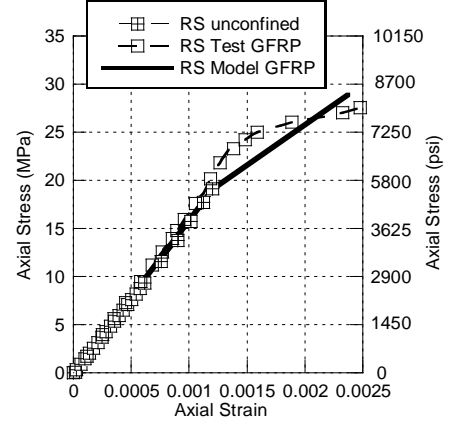


(b)

Figure 7.35: Model of 200 mm x 200 mm size square column made of recycled brick aggregate (a) confined with CFRP (b) confined with GFRP.

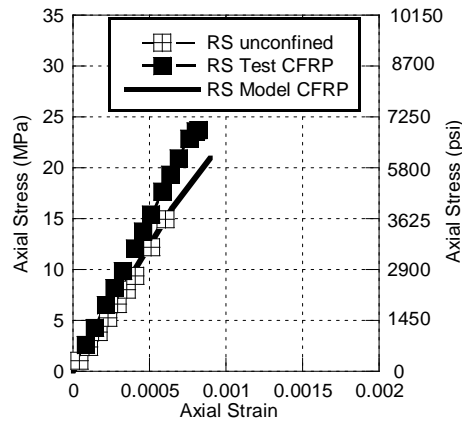


(a)

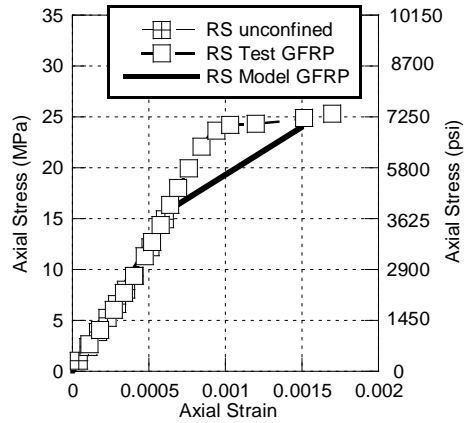


(b)

Figure 7.36: Model of 150 mm x 150 mm size square column made of recycled stone aggregate (a) confined with CFRP (b) confined with GFRP.



(a)



(b)

Figure 7.37: Model of 200 mm x 200 mm size square column made of recycled stone aggregate (a) confined with CFRP (b) confined with GFRP.

## APPENDIX D.1 Test results of circular concrete columns

Table 7.5: Summary of test results of circular unconfined and confined concrete columns

Column ID	$\varepsilon_{c0}$	$\varepsilon_i$	$f'_{cc}$ (MPa)	$f_l$ (MPa)	$\frac{f_l}{f'_{c0}}$	$\frac{f'_{cc}}{f'_{c0}}$	$f'_{cc}$ (MPa) calculated	Error %	$\frac{\varepsilon_{cc}}{\varepsilon_{c0}}$	$\varepsilon_{cc}$ calculated	Error %
CBC401	0.00144	0.00056	29.75	-	-	-	-	-	-	-	-
(unconfined)											
CBC402	0.00130	0.00056	29.90	-	-	-	-	-	-	-	-
(unconfined)											
CBC403	0.00207	0.00083	39.81	0.45	0.0150	1.34	37.60	5.57	1.43	0.00183	11.17
CBC404	0.00230	0.00098	46.77	0.52	0.0176	1.57	40.07	14.34	1.60	0.00202	12.32
CBC405	0.00308	0.00123	54.21	0.70	0.0236	1.82	45.70	15.70	2.14	0.00243	21.11
CBC406	0.00390	0.00108	47.80	0.62	0.0208	1.61	43.07	9.89	2.70	0.00224	42.60
CBC601	0.00079	0.00040	23.47	-	-	-	-	-	-	-	-
(unconfined)											
CBC602	0.00080	0.00043	25.62	-	-	-	-	-	-	-	-
(unconfined)											
CBC603	0.00203	0.00073	38.90	0.26	0.0112	1.66	33.97	12.66	2.56	0.00157	22.79
CBC604	0.00190	0.00071	37.73	0.25	0.0108	1.61	33.66	10.80	2.40	0.00154	18.76
CBC605	0.00289	0.00100	44.70	0.38	0.0162	1.90	38.74	13.32	3.65	0.00192	33.58
CBC606	0.00250	0.00094	42.23	0.36	0.0153	1.80	37.90	10.26	3.16	0.00186	25.72
CBC801	0.00062	0.00024	23.93	-	-	-	-	-	-	-	-
(unconfined)											
CBC803	0.00086	0.00029	33.03	0.08	0.0033	1.38	27.06	18.07	1.40	0.00102	-18.42
CBC805	0.00188	0.00064	37.80	0.18	0.0076	1.58	31.27	17.28	3.05	0.00132	29.47
CSC401	0.00110	0.00043	29.16	-	-	-	-	-	-	-	-
(unconfined)											
CSC402	0.00130	0.00043	28.86	-	-	-	-	-	-	-	-
(unconfined)											
CSC403	0.00250	0.00067	55.94	0.36	0.0124	1.92	52.55	6.05	2.27	0.00265	-5.87
CSC404	0.00253	0.00066	55.05	0.35	0.0122	1.89	52.18	5.21	2.30	0.00262	-3.50
CSC405	0.00350	0.00120	67.37	0.69	0.0235	2.31	73.65	-9.33	3.18	0.00404	-15.48
CSC406	0.00220	0.00097	54.21	0.55	0.0189	1.86	64.96	-19.84	2.00	0.00347	-57.59
CSC601	0.00070	0.00019	29.39	-	-	-	-	-	-	-	-
(unconfined)											
CSC602	0.00074	0.00023	35.21	-	-	-	-	-	-	-	-
(unconfined)											
CSC603	0.00170	0.00042	43.87	0.15	0.0051	1.49	39.17	10.72	2.43	0.00111	34.82
CSC604	0.00180	0.00045	47.33	0.16	0.0055	1.61	39.94	15.62	2.57	0.00114	36.65
CSC605	0.00220	0.00057	56.32	0.22	0.0074	1.92	43.48	22.79	3.14	0.00129	41.45
CSC606	0.00200	0.00057	56.28	0.22	0.0074	1.91	43.47	22.76	2.86	0.00129	35.62
CSC801	0.00055	0.00018	32.59	-	-	-	-	-	-	-	-
(unconfined)											
CSC803	0.00130	0.00042	38.98	0.11	0.0035	1.20	39.92	-2.42	2.36	0.00098	24.92
CSC805	0.00160	0.00047	47.89	0.13	0.0041	1.47	41.30	13.75	2.91	0.00103	35.75
RBC401	0.00130	0.00082	24.31	-	-	-	-	-	-	-	-
(unconfined)											
RBC402	0.00160	0.00091	26.84	-	-	-	-	-	-	-	-
(unconfined)											
RBC403	0.00310	0.00110	49.08	0.59	0.0244	2.02	43.37	11.63	2.38	0.00243	21.50
RBC404	0.00270	0.00111	49.43	0.60	0.0245	2.03	43.51	11.98	2.08	0.00244	9.47
RBC405	0.00450	0.00180	53.23	1.03	0.0423	2.19	57.44	-7.90	3.46	0.00354	21.28
RBC406	0.00460	0.00180	53.31	1.03	0.0424	2.19	57.48	-7.84	3.54	0.00355	22.91
RBC601	0.00093	0.00044	32.58	-	-	-	-	-	-	-	-
(unconfined)											
RBC602	0.00089	0.00040	29.88	-	-	-	-	-	-	-	-
(unconfined)											
RBC603	0.00200	0.00080	43.22	0.29	0.0088	1.33	41.82	3.24	2.15	0.00147	26.30
RBC604	0.00250	0.00079	42.56	0.28	0.0087	1.31	41.68	2.06	2.69	0.00147	41.38
RBC605	0.00250	0.00100	47.60	0.38	0.0117	1.46	44.85	5.78	2.69	0.00165	33.92
RBC606	0.00290	0.00101	47.99	0.38	0.0118	1.47	44.95	6.34	3.12	0.00166	42.83

RBC801	0.00078	0.00042	28.16	-	-	-	-	-	-	-	-
(unconfined)											
RBC803	0.00125	0.00056	33.89	0.15	0.0054	1.20	33.02	2.58	1.60	0.00126	-0.83
RBC805	0.00150	0.00069	34.88	0.20	0.0070	1.24	34.51	1.04	1.92	0.00136	9.18
RSC401	0.00130	0.00080	22.88	-	-	-	-	-	-	-	-
(unconfined)											
RSC402	0.00130	0.00097	27.63	-	-	-	-	-	-	-	-
(unconfined)											
RSC403	0.00300	0.00110	51.36	0.59	0.0259	2.24	48.97	4.65	2.31	0.00323	-7.52
RSC404	0.00260	0.00109	50.68	0.58	0.0255	2.21	48.62	4.06	2.00	0.00320	-23.08
RSC405	0.00330	0.00170	61.18	0.97	0.0425	2.67	65.98	-7.86	2.54	0.00446	-35.16
RSC406	0.00440	0.00167	60.13	0.95	0.0417	2.63	65.24	-8.50	3.38	0.00441	-0.14
RSC601	0.00092	0.00040	22.44	-	-	-	-	-	-	-	-
(unconfined)											
RSC602	0.00110	0.00036	20.18	-	-	-	-	-	-	-	-
(unconfined)											
RSC603	0.00200	0.00078	39.65	0.28	0.0125	1.77	35.23	11.15	2.17	0.00158	21.16
RSC604	0.00190	0.00089	45.08	0.32	0.0142	2.01	36.98	17.96	2.07	0.00167	12.33
RSC605	0.00280	0.00110	48.55	0.42	0.0187	2.16	41.59	14.33	3.04	0.00190	32.01
RSC606	0.00260	0.00107	47.00	0.41	0.0181	2.09	40.98	12.81	2.83	0.00187	27.99
RSC801	0.00060	0.00029	26.10	-	-	-	-	-	-	-	-
(unconfined)											
RSC803	0.00130	0.00058	38.33	0.16	0.0060	1.47	33.23	13.29	2.17	0.00123	5.00
RSC805	0.00150	0.00063	37.19	0.18	0.0069	1.43	34.33	7.71	2.50	0.00128	14.45

## APPENDIX D.2 Test results of square concrete columns

Table 7.6: Summary of test results of square unconfined and confined concrete columns

Column ID	$\epsilon_{c0}$	$\epsilon_j$	$f'_{cc}$ (MPa)	$f_l$ (MPa)	$\frac{f_l}{f'_{c0}}$	$\frac{f'_{cc}}{f'_{c0}}$	$f'_{cc}$ (MPa) calculated	Error %	$\frac{\epsilon_{cc}}{\epsilon_{c0}}$	$\epsilon_{cc}$ calculated	Error %
CBS401 (unconfined)	0.00300	0.00140	11.65	-	-	-	-	-	-	-	-
CBS402 (unconfined)	0.00213	0.00130	10.85	-	-	-	-	-	-	-	-
CBS403	0.00250	0.00120	20.52	0.46	0.0421	1.89	19.90	3.03	0.83	0.00311	-24.54
CBS404	0.00342	0.00121	20.74	0.46	0.0425	1.91	19.99	3.63	1.14	0.00312	8.70
CBS405	0.00427	0.00151	23.88	0.61	0.0564	2.20	22.69	4.97	1.42	0.00345	19.39
CBS406	0.00339	0.00180	28.41	0.73	0.0670	2.62	24.79	12.75	1.13	0.00369	-8.96
CBS601 (unconfined)	0.00095	0.00109	14.99	-	-	-	-	-	-	-	-
CBS602 (unconfined)	0.00149	0.00146	20.08	-	-	-	-	-	-	-	-
CBS603	0.00135	0.00281	22.29	0.71	0.0476	1.49	26.98	-21.05	1.42	0.00144	-6.92
CBS604	0.00099	0.00268	21.25	0.68	0.0453	1.42	26.42	-24.34	1.04	0.00142	-43.69
CBS605	0.00228	0.00277	21.50	0.75	0.0498	1.43	27.54	-28.10	2.40	0.00147	35.66
CBS606	0.00236	0.00282	21.90	0.76	0.0507	1.46	27.78	-26.83	2.48	0.00148	37.34
CBS801 (unconfined)	0.00057	0.00031	14.61	-	-	-	-	-	-	-	-
CBS803	0.00088	0.00054	25.90	0.10	0.0070	1.77	16.76	35.28	1.53	0.00102	-16.91
CBS805	0.00188	0.00080	20.78	0.16	0.0111	1.42	17.78	14.44	3.27	0.00106	43.21
CSS401 (unconfined)	0.00250	0.00100	13.48	-	-	-	-	-	-	-	-
CSS402 (unconfined)	0.00120	0.00082	10.99	-	-	-	-	-	-	-	-
CSS403	0.00276	0.00130	21.45	0.49	0.0367	1.59	26.68	-24.37	1.10	0.00494	-79.26
CSS404	0.00253	0.00131	21.59	0.50	0.0369	1.60	26.76	-23.97	1.01	0.00496	-95.68
CSS405	0.00398	0.00049	32.30	0.20	0.0147	2.40	18.77	41.90	1.59	0.00348	12.51
CSS406	0.00250	0.00034	22.27	0.14	0.0101	1.65	17.12	23.11	1.00	0.00317	-26.97
CSS601 (unconfined)	0.00059	0.00049	18.76	-	-	-	-	-	-	-	-
CSS603	0.00084	0.00056	22.73	0.14	0.0076	1.21	22.55	0.79	1.42	0.00071	15.29
CSS604	0.00221	0.00058	23.66	0.15	0.0079	1.26	22.71	4.04	3.74	0.00071	67.68
CSS605	0.00123	0.00044	28.99	0.12	0.0063	1.55	21.92	24.38	2.08	0.00069	43.88
CSS606	0.00306	0.00044	28.88	0.12	0.0063	1.54	21.91	24.14	5.19	0.00069	77.51
CSS801 (unconfined)	0.00069	0.00031	16.87	-	-	-	-	-	-	-	-
CSS803	0.00130	0.00054	22.96	0.10	0.0061	1.36	19.61	14.59	1.89	0.00080	38.54
CSS805	0.00180	0.00062	27.90	0.13	0.0074	1.65	20.21	27.56	2.62	0.00082	54.26
RBS401 (unconfined)	0.00214	0.00135	11.85	-	-	-	-	-	-	-	-
RBS402 (unconfined)	0.00266	0.00190	16.65	-	-	-	-	-	-	-	-
RBS403	0.00250	0.00140	20.54	0.53	0.0450	1.73	20.01	2.57	1.17	0.00321	-28.45
RBS404	0.00286	0.00177	26.03	0.68	0.0570	2.20	22.19	14.73	1.34	0.00350	-22.25
RBS405	0.00413	0.00260	30.99	1.05	0.0887	2.62	27.95	9.82	1.93	0.00425	-2.97
RBS406	0.00373	0.00245	29.25	0.99	0.0837	2.47	27.04	7.55	1.74	0.00413	-10.78
RBS601 (unconfined)	0.00113	0.00161	17.39	-	-	-	-	-	-	-	-
RBS602 (unconfined)	0.00113	0.00161	17.39	-	-	-	-	-	-	-	-
RBS603	0.00153	0.00159	20.95	0.40	0.0232	1.20	23.57	-12.51	1.35	0.00143	6.98

RBS604	0.00130	0.00160	21.02	0.40	0.0233	1.21	23.59	-12.23	1.15	0.00143	-9.59
RBS605	0.00234	0.00384	23.72	1.03	0.0595	1.36	33.24	-40.14	2.06	0.00188	19.40
RBS606	0.00210	0.00356	21.98	0.96	0.0551	1.26	32.08	-45.94	1.86	0.00183	13.04
RBS801	0.00073	0.00044	14.37	-	-	-	-	-	-	-	-
(unconfined)											
RBS803	0.00092	0.00052	24.84	0.10	0.0069	1.73	15.89	36.05	1.26	0.00078	14.37
RBS805	0.00168	0.00094	26.69	0.19	0.0132	1.86	17.28	35.26	2.30	0.00084	50.13
RSS401	0.00248	0.00189	19.27	-	-	-	-	-	-	-	-
(unconfined)											
RSS402	0.00220	0.00140	14.28	-	-	-	-	-	-	-	-
(unconfined)											
RSS403	0.00254	0.00130	22.43	0.49	0.0257	1.16	23.40	-4.33	1.02	0.00347	-36.88
RSS404	0.00277	0.00153	26.46	0.58	0.0303	1.37	24.15	8.75	1.12	0.00365	-32.03
RSS405	0.00433	0.00230	27.30	0.93	0.0482	1.42	27.03	0.97	1.75	0.00435	-0.45
RSS406	0.00369	0.00229	27.15	0.92	0.0480	1.41	26.99	0.59	1.49	0.00434	-17.63
RSS601	0.00121	0.00099	19.12	-	-	-	-	-	-	-	-
(unconfined)											
RSS602	0.00106	0.00083	15.94	-	-	-	-	-	-	-	-
(unconfined)											
RSS603	0.00193	0.00245	23.17	0.62	0.0325	1.21	24.31	-4.91	1.60	0.00182	5.40
RSS604	0.00190	0.00238	22.50	0.60	0.0316	1.18	24.16	-7.37	1.57	0.00181	4.98
RSS605	0.00268	0.00436	28.17	1.17	0.0614	1.47	28.93	-2.68	2.22	0.00237	11.57
RSS606	0.00227	0.00425	27.47	1.15	0.0599	1.44	28.68	-4.41	1.88	0.00234	-3.29
RSS801	0.00065	0.00035	16.00	-	-	-	-	-	-	-	-
(unconfined)											
RSS803	0.00081	0.00047	23.50	0.09	0.0056	1.47	16.75	28.74	1.26	0.00070	13.55
RSS805	0.00170	0.00082	25.31	0.17	0.0104	1.58	17.38	31.32	2.63	0.00075	55.78